PERFORMANCE-BASED EARTHQUAKE ENGINEERING WITH THE FIRST-ORDER RELIABILITY METHOD

by

SMITHA DEVI KODURU

B.Tech, Sri Venkateswara University, 2000
M.Eng, University of Toronto, 2003

A THESIS SUBMITTED IN PARTIAL FULFILMENT OF

THE REQUIREMENTS FOR THE DEGREE OF

DOCTOR OF PHILOSOPHY

in

THE FACULTY OF GRADUATE STUDIES

(Civil Engineering)

The University of British Columbia

(Vancouver)

June 2008

Abstract

Performance-based earthquake engineering is an emerging field of study which complements the prescriptive methods that the design codes provide to ensure adequate seismic performance of structures. Accounting for uncertainties in the performance assessments forms an important component in this area. In this context, the present study focuses on two broad themes; first, treatment of uncertainties and the application of the first-order reliability method (FORM) in the finite-element reliability analysis, and second, the seismic risk assessment of reinforced concrete structures for performance states such as, collapse, and monetary loss. In the first area, the uncertainties arising from the inherent randomness in nature (aleatory) and due to the lack of knowledge (epistemic) are identified. A framework for the separation of these uncertainties is proposed. Following this, the applicability of FORM to the linear and nonlinear finite-element structural models under static and dynamic loading is investigated. The case studies indicate that FORM is applicable for linear and nonlinear static problems. Strategies are proposed to circumvent and remedy potential challenges to FORM. In the case of dynamic problems, the application of FORM is studied with an emphasis on cumulative response measures. The limit-state surface is shown to have a closed and nonlinear geometric shape. Solution methods are proposed to obtain probability bounds based on the FORM results. In the application-oriented second area of research, at first, the probability of collapse of a reinforced concrete frame is assessed with nonlinear static analysis. By modelling the post-failure behaviour of individual structural members, the global response of the structure is estimated beyond the component failures. The final application is the probabilistic assessment of monetary loss for a high-rise shear wall building due to the seismic hazard in the Cascadia Subduction zone. A 3-dimensional finite-element model of the structure with nonlinear material models is subjected to stochastic ground motions in the reliability analysis. The parameters for stochastic ground motion model are developed for Vancouver, Canada. Monetary losses due to the damage of structural and non-structural components are included.

Table of Contents

Abstract ..... **ii**

Table of Contents ..... **iii**

List of Tables ..... **vi**

List of Figures ..... **viii**

Acknowledgements ..... **xii**

Dedication ..... **xiii**

Co-Authorship Statement ..... **xiv**

Chapter 1. Introduction **1**

1.1. Background 1

1.2. Objectives and Scope 4

1.3. Organization of Chapters 4

1.3.1. Chapter 2: Identification of uncertainties *5*

1.3.2. Chapter 3: Feasibility of FORM – statics *5*

1.3.3. Chapter 4: Feasibility of FORM – dynamics *6*

1.3.4. Chapter 5: Probabilistic evaluation of collapse *6*

1.3.5. Chapter 6: Probabilistic evaluation of loss *7*

1.3.6. Chapter 7: Conclusions and future work *7*

References 7

Chapter 2. Identification of Uncertainties **10**

2.1. Introduction 10

2.2. Epistemic Uncertainty 13

2.3. The Probabilistic Approach 17

2.4. The Fuzzy Randomness Approach 22

2.5. Implementations in OpenSees 26

2.6. Numerical Example 27

2.7. Conclusions 31

References 45

Chapter 3. Feasibility of FORM - Statics 48
3.1. Introduction 48
3.2. Conditions for Applicability of FORM 50
3.3. Limit-state Functions for Static FE Analysis 55
3.3.1. Limit-state functions in traditional engineering; linear FE models 55
3.3.2. Limit-state functions in earthquake engineering; nonlinear FE models 57
3.4. Case Studies 58
3.4.1. Case 1: Linear finite element problems 58
3.4.2. Case 2: Nonlinear finite element problems 59
3.5. Interpretation and Discussion of Results 61
3.5.1. Finding 1: Linear FE models may result in nonlinear limit-state functions 61
3.5.2. Finding 2: The degree of nonlinearity is affected by the model fidelity 62
3.5.3. Finding 3: Limit-state function with maximum response may cause non-convergence 63
3.5.4. Finding 4: Piece-wise linear material models may cause non-convergence 64
3.5.5. Finding 5: Non-convergence of the FE analysis may be detrimental for FORM 65
3.5.6. Finding 6: Numerical noise may impede the convergence 65
3.5.7. Finding 7: The nonlinearity in the limit-state surface is moderate in statics 66
3.6. Concluding Remarks 67
References 84

Chapter 4. Feasibility of FORM – Dynamics 86
4.1. Introduction 86
4.2. Limit-state Functions in Dynamic Analysis 87
4.3. The Time-variant Reliability Problem 89
4.4. Study of FE-Based Reliability Analysis with Cumulative Response 93
4.4.1. Random structural properties 94
4.4.2. Random dynamic loading 101
4.4.3. Random structural properties and loading 104
4.5. Solution Strategies 104
4.5.1. Random structural properties (open limit-state surface) 105
4.5.2. Random dynamic loading (closed limit-state surface) 106
4.6. Concluding Remarks 108
References 129

Chapter 5. Probabilistic Evaluation of Collapse 131

5.1. Introduction 131
5.2. Finite Element Reliability Analysis for Seismic Capacity Evaluations 133
5.3. Implementation of Probabilistic Capacity and Post-failure Response Models 138
5.4. Problems and Remedies in the Convergence of the Reliability Analysis 141
5.5. Numerical Example 144
5.6. Conclusions 147
References 154

Chapter 6. Probabilistic Evaluation of Loss 156
6.1. Introduction 156
6.2. Unified Reliability Analysis 158
6.3. Ground Motion Model 160
6.3.1. Crustal earthquakes 165
6.3.2. Subcrustal earthquakes 167
6.3.3. Subduction earthquakes 168
6.4. Building Model 170
6.5. Damage and Loss Models 173
6.5.1. Structural members 173
6.5.2. Non-structural members 175
6.6. Evaluation of the Total Loss Curve 177
6.7. Analysis and Results 179
6.8. Conclusion 183
References 198

Chapter 7. Conclusions and Future Work 201
7.1. Summary of Research Contributions 201
7.2. Future Research Directions 204
References 207

List of Tables

Table 2.1 Uncertainty modelling of the aleatory random variables of the R.C. structure 34

Table 2.2 Uncertainty modelling of the epistemic random variables 34

Table 2.3: Importance ranking of epistemic random variables 35

Table 2.4: Uncertainty modelling of the fuzzy random variables 36

Table 3.1: Parameters for the linear models 68

Table 3.2: Reliability results of the linear models 68

Table 3.3: Parameters for the nonlinear models 69

Table 3.4: Reliability results of the nonlinear models 69

Table 3.5: Importance ranking for the displacement limit-state function in linear models 70

Table 4.1: Structural parameters of the SDOF-SS and SDOF-RC structures 109

Table 4.2: Structural parameters of MDOF structure 109

Table 4.3: Probability for SDOF-SS with energy limit-state function 109

Table 4.4: Probability for SDOF-RC with energy limit-state function 110

Table 4.5: Probability for MDOF with energy limit-state function 110

Table 4.6: Probability for MDOF with cost limit-state function 110

Table 4.7: Probability for SDOF with energy limit-state function and random load 111

Table 4.8: Probability for MDOF with cost limit-state function and random load 111

Table 5.1: Distribution parameters of probabilistic model coefficients 148

Table 5.2: Uncertainty modeling of the material and geometric parameters 148

Table 5.3: Importance measures and ranking of the parameters 149

Table 6.1: Parameters of modulating functions – Crustal earthquakes 184

Table 6.2: Parameters of modulating functions – Subcrustal earthquakes 184

Table 6.3: Parameters of modulating functions – Subduction earthquakes 184

Table 6.4: Fundamental periods and damping ratios 185

Table 6.5: Distribution parameters of mass and material random variables 185

Table 6.6: Damage ratios for each category of non-structural elements 185

Table 6.7: Total quantity, damage quantity, unit loss ratios for each category of non-structural elements 186

List of Figures

Figure 2.1: (a) Uncertainty in the distribution of x due to uncertain parameters μ and σ; (b) Uncertainty representation of the mean μ and the standard deviation σ; (c) Uncertainty representation of the reliability index β 37

Figure 2.2 : (a) Limit-state surface g=0 for different realizations of an epistemic random variable θ ; (b) Kink in the function β(θ), resulting in discontinuity in the derivative 38

Figure 2.3: Membership function of a fuzzy number 38

Figure 2.4: Fuzzy probability density function 39

Figure 2.5: Fuzzy limit state surface 39

Figure 2.6: Fuzzy reliability index 40

Figure 2.7: Software architecture of the reliability module in OpenSees 40

Figure 2.8: Selected base classes in the framework of reliability analysis tools 41

Figure 2.9: Selected reliability analysis tools utilized in the nested reliability analysis 41

Figure 2.10: Two-storey two-bay reinforced concrete structure. Node numbers and element numbers (in parenthesis) are shown. 42

Figure 2.11: (a) Probability density function for the reliability index; (b) Cumulative distribution function for the reliability index 43

Figure 2.12: Results from sampling analysis 43

Figure 2.13: Membership function for fuzzy numbers versus mean and standard deviation of the corresponding random variable. 44

Figure 2.14: Fuzzy reliability index from analysis of reinforced concrete structure 44

Figure 3.1: Schematic representation of the FE-based FORM analysis 71

Figure 3.2: Criteria for the applicability of FORM 72

Figure 3.3: Structural models. a) Single-degree-of-freedom system; b) Multiple-degree-of-freedom system 73

Figure 3.4: Limit-state function behaviour for linear model of SDOF. Behaviour of displacement limit-state function for the variation of a) cross-section dimension (mm); b) length (mm); Stress limit-state function behaviour for c) cross-section dimension (mm); d) length (mm). 74

Figure 3.5: Displacement limit-state surface behaviour in the standard normal space for linear model of SDOF with random variables as, a) cross-section dimension and material stiffness; b) length and material stiffness; c) cross-section dimension and lateral load; d) length and lateral load 75

Figure 3.6: Limit-state function behaviour for linear model of MDOF. Variation of displacement limit-state function for the variation of a) width of the center column; b) depth of the center column; c) bay-width; d) storey height. The units of all the random variables are in mm 76

Figure 3.7: Displacement limit-state surface behaviour in the standard normal space for linear model of MDOF with random variables as, a) width of the center column and lateral load; b) depth of the center column and lateral load; c) bay-width and lateral load; d) storey height and lateral load 77

Figure 3.8: Stress limit-state surface behaviour in the standard normal space for linear model of MDOF, with random variables as lateral load and gravity load on the center column. 78

Figure 3.9: a) Concrete material model; b) Steel material model 78

Figure 3.10: Behaviour of displacement limit-state function for nonlinear model of SDOF. Variation of limit-state function due to the variation of , a) cross-section dimension (mm); b) length (mm); c) Young's modulus of steel (N/mm^2) and d) yield stress of steel (N/mm^2) 79

Figure 3.11: Behaviour of displacement limit-state function for nonlinear model of MDOF. Variation of limit-state function for the variation of material properties, a) compressive strength of concrete (N/mm^2); b) yield stress of steel (N/mm^2); c) strain in concrete at compressive strength, d) Young's modulus of steel (N/mm^2) 80

Figure 3.12: Behaviour of displacement limit-state function for nonlinear model of MDOF. Variation of limit-state function for the variation of nonlinear static analysis parameters, a) lateral load (N); b) number of fibers in the fiber-discretized cross-section; c) load step size in the nonlinear static analysis, d) numerical limits on convergence tolerances in logarithmic scale 81

Figure 3.13: Behaviour of displacement limit-state surface in the standard normal space for the nonlinear model of MDOF, with random variables as lateral load and a) depth of the center column; b) width of the center column; c) compressive strength of concrete of the center column, d) strain at the compressive strength of the concrete of the center column..... 82

Figure 3.14: Flow chart to check the feasibility of FORM..... 83

Figure 4.1: Schematic representation of the influence of peak response parameters on the behaviour of the limit-state function; a) response, b) limit-state function 112

Figure 4.2: a) Basic single-degree-of-freedom (SDOF) structure; b) Single-degree-of-freedom structure with structural steel (SDOF-SS) and reinforced concrete sections (SDOF-RC); c) Multiple-degree-of-freedom (MDOF) structure with reinforced concrete section 113

Figure 4.3: a) Stress-strain relationship of steel; b) Stress-strain relationship of concrete..... 113

Figure 4.4: Behaviour of energy limit-state function (in Nmm) of the SDOF-SS, for the variation of (a) length (mm) ; (b) cross-section dimension (mm); (c) Young's modulus of steel, (N/mm^2); (d) yield stress of steel (N/mm^2); (e) mass (kg); (f) critical damping ratio 114

Figure 4.5: Behaviour of the energy limit-state surface (in Nmm) of the SDOF-SS in the standard normal space for the variation of the random variables; (a) mass and Young's modulus of steel, (b) mass and length, (c) mass and cross-section dimension, (d) mass and yield stress of steel. 115

Figure 4.6: (a) Ground motion record; (b) Elastic response spectrum with 5% damping 116

Figure 4.7: Behaviour of energy limit-state function (in Nmm) of the SDOF-SS for the ground motion loading, for the variation of (a) length (mm) ; (b) cross-section dimension (mm); (c) Young's modulus of steel, (N/mm^2); (d) yield stress of steel (N/mm^2); (e) mass (kg); (f) critical damping ratio 117

Figure 4.8: Behaviour of energy limit-state function (in Nmm) of the SDOF-RC, for the variation of (a) length (mm) ; (b) cross-section dimension (mm); (c) Young's modulus of steel, (N/mm^2); (d) compressive strength of concrete (N/mm^2); (e) mass (kg); (f) critical damping ratio 118

Figure 4.9: Behaviour of the energy limit-state surface (in Nmm) of the SDOF-RC in the standard normal space for the variation of the random variables; (a) mass and Young's modulus of steel, (b) mass and length, (c) mass and cross-section dimension, (d) mass and compressive strength of concrete..... 119

Figure 4.10: Behaviour of damage index limit-state function of the SDOF-RC, for the variation of (a) length (mm) ; (b) cross-section dimension (mm); (c) Young's modulus of steel, (N/mm^2); (d) compressive strength of concrete (N/mm^2) (e) mass, (kg); (f) damping ratio 120

Figure 4.11: Behaviour of the damage limit-state surface of the SDOF-RC in the standard normal space for the variation of the random variables; (a) mass and Young's modulus of steel, (b) mass and length, (c) mass and cross-section dimension, (d) mass and compressive strength of concrete..... 121

Figure 4.12: Behaviour of energy limit-state function (in Nmm) of the MDOF, for the variation of (a) Young's modulus of steel, (N/mm^2); (b) compressive strength of concrete (N/mm^2); (c) height of the top storey (mm); (d) mass on the center column in bottom storey (kg) 122

Figure 4.13: Behaviour of cost limit-state function (in $) of the MDOF, for the variation of (a) Young's modulus of steel, (N/mm^2); (b) compressive strength of concrete (N/mm^2); (c) height of the top storey (mm); (d) mass on the center column in bottom storey (kg)..... 123

Figure 4.14: Behaviour of energy limit-state surface (in Nmm) of SDOF structure..... 124

Figure 4.15: Variation in the amplitude of excitation with respect to the pulse spacing. Excitations with pulse spacing at 0.02s and 4.0s and a) amplitude of both the pulses 1.0, b) amplitude of the pulses 1.0 and -1.0, respectively. Excitations with pulse spacing at 0.02s and 2.0s with c) amplitude of both the pulses 1.0, and d) amplitude of the pulses 1.0 and -1.0, respectively..... 125

Figure 4.16: Behaviour of the energy limit-state surface (in Nmm) of the SDOF with random pulses in the loading spaced at 0.02s and 2.0s..... 126

Figure 4.17: a) Behaviour of the damage index limit-state surface of the SDOF-RC structure; b) Behaviour of the cost limit-state surface (in $) of the MDOF structure 127

Figure 4.18: Behaviour of the energy limit-state surface (in Nmm) of the SDOF in the standard normal space with the random variables as, a) stiffness and loading pulse, b) yield strength and loading pulse, c) mass and loading pulse, d) damping ratio and loading pulse 128

Figure 5.1: Possible structural events prior to attainment of the target displacement 150

Figure 5.2: Key steps in finite element reliability analysis by FORM (i=1, 2, 3,)..... 151

Figure 5.3: Transition into post-failure response 151

Figure 5.4: Smoothed post-failure response of springs 152

Figure 5.5: Finite element model of the RC frame..... 152

Figure 5.6: Probability curve of the displacement at global collapse..... 153

Figure 6.1: Evaluation of the monetary loss in unified reliability analysis. 187

Figure 6.2: (a) White noise, y_i; (b) White noise filtered with 5Hz filter with 10% damping resulting in stationary process, s_k; (c) Modulated and filtered white noise, z_k 188

Figure 6.3: Parameters of a modulating function..... 189

Figure 6.4: (a) 3D view of the analysis model of the building; (b) finite element model of the building (columns are constrained at each storey with rigid diaphragms). 190

Figure 6.5: Steps involved in the evaluation of the monetary loss due to the damage of non-structural components..... 191

Figure 6.6: Damage quantity – loss relationship..... 191

Figure 6.7: Comparison of hazard curves for spectral frequency of 1Hz..... 192

Figure 6.8: The probability curves of monetary loss conditioned on the occurrence of Crustal, Subcrustal and Subduction earthquakes 193

Figure 6.9: The probability curves for discounted monetary loss, L conditioned on the occurrence of Crustal, Subcrustal and Subduction earthquakes. 194

Figure 6.10: The combined total probability curve of monetary loss conditioned on the occurrence of an earthquake 195

Figure 6.11: Annual probability of exceedance of monetary loss..... 196

Figure 6.12: Probability of exceedance in 50 years of discounted loss..... 197

Acknowledgements

I take this opportunity to thank, first and foremost, my advisor, Dr.Terje Haukaas. I am grateful for his confidence in my potential, generosity with his time, and continuous encouragement to improve my research abilities. It has been a privilege to be his student and be a part of his research vision. I would not have come this far without his support in all my endeavours.

Also, I express gratitude towards my supervisory committee members, Dr.Elwood, Dr.Foschi, and Dr.Sexsmith for their unwavering support throughout my doctoral studies. I am grateful for the exposure to their vast and varied expertise through the reliability seminars. Special thanks to Dr.Ventura for lending structural drawings of an existing high-rise building in Vancouver.

The funding provided by National Science and Engineering Research Council (NSERC) through Canada Graduate Scholarship is gratefully acknowledged.

I would like to thank my fellow graduate students, in particular, Babak, Jose, Kate, Soheil, Martin, Hugon, Freddy, and Armin, for sharing my journey through the graduate studies. I cannot forget to mention Vignesh, Kari, and Chris for the graduate life outside research. Finally, this work would be impossible without the strength and courage of my mother, who encouraged me to pursue Civil Engineering, my sister, and the patience of my husband through the long years of my graduate studies.

Dedication

I dedicate this work to my husband, Venkata. Words can't describe his role in this achievement.

Co-Authorship Statement

Chapters 2-4 and 6 are developed based on the discussions with Dr. Terje Haukaas (Supervisor). The author of this thesis is responsible for the literature review, collection of data, development of input models, performing the case studies, and the interpretation of the results. Chapter 5 is a collaborative effort with Dr. Terje Haukaas and Dr. Kenneth J. Elwood (UBC). The finite-element model developed by Dr. Elwood has been used for the publication in Chapter 5.

The manuscript preparation for the publications in Chapters 2-6 is done in collaboration with the co-authors. The author of this thesis is responsible for the major portion of the writing, performing the analyses, and preparation of the tables and figures, and entirely accountable for any inaccuracies and errors.

Chapter 1. INTRODUCTION

Performance-based earthquake engineering is an emerging area of research which emphasises the seismic performance of the structures for different safety levels. This paradigm signals a move away from the exclusively prescriptive methods of design codes. The codes have traditionally provided the response measures which are to be verified against pre-determined threshold values. In addition to the ‘‘ultimate limit-states’’ and the ‘‘serviceability limit-states’’ pre-defined by the design codes, performance-based earthquake engineering seeks to define limit-states based on additional concerns, such as ‘‘down-time,’’ ‘‘monetary loss,’’ ‘‘repair costs,’’ etc.

The emergence of the performance-based earthquake engineering has necessitated the application of the sophisticated structural analysis methods, such as finite-element analysis, for accurate predictions of the structural response. Furthermore, it has brought the unavoidable uncertainties in the seismic engineering to a sharp focus. Uncertainties exist to a great extent not only in the prediction of the intensity and occurrence of the earthquakes but also in the quantification of the performance measures such as damage and monetary loss. Consequently, the prediction of the structural performance must account for these uncertainties in a rational and consistent manner. Traditional structural reliability methods have provided a practical framework for dealing with uncertainties. However, certain unique challenges exist in the application of the reliability methods in the context of the performance-based earthquake engineering. The presence of large number of random variables to capture the uncertainties in the earthquake ground motions and structural models, and high computational costs associated with the nonlinear time-history analytical methods are distinctive features of rigorous performance-based earthquake engineering. These form the motivation for this study.

1.1. BACKGROUND

The Pacific Earthquake Engineering Research (PEER) center has been prominent in addressing the uncertainties in the context of the performance-based earthquake engineering. The PEER methodology, originally proposed by Cornell and Krawinkler (2000) and presented in detail by Moehle and Deierlein

(2004), and Porter (2003), involves de-aggregation of the performance-based earthquake engineering into four sections; 1) hazard analysis to account for the ground motion intensities, 2) estimating engineering demand parameters which are essentially the outcomes of a structural analysis, 3) identifying the damage state of a structure by employing damage measures, and 4) evaluating the decision variables such as repair cost, downtime, loss of productivity, which are relevant to the stakeholders. The uncertainties are accounted in each section with the development of conditional cumulative probability distributions known as ''fragility curves'' (Moehle and Deierlein 2004).

Several researchers have worked within this paradigm focusing on a single section, such as probabilistic seismic hazard analysis to obtain ground motion intensities by Stewart *et al.* (2001), Baker and Cornell (2005, 2006a, b), the fragility curves for the engineering demand parameters by Krawinkler *et al.* (2003), Taghavi and Miranda (2005), Akkar *et al.* (2005), Ramamoorthy *et al.* (2006), Porter *et al.* (2007), the fragility curves for damage and collapse by Shaikhutdinov (2004), Pagni and Lowes (2006), Brown and Lowes (2007), Badillo-Almaraz *et al.* (2007), Zhu *et al.* (2007), and the fragility curves for loss estimation by Porter *et al.* (2001), Porter *et al.* (2002), Miranda and Aslani (2003), Kircher (2003), Comerio (2006).

Each fragility curve is conditioned on the variable of the section ahead of it. For example, the fragility curves for the engineering demand parameter are conditioned on the intensity measures, the fragility curves for the damage measure are conditioned on the engineering demand parameters and the fragility curves for the decision variables are conditioned on the damage measures. Eventually, the probability distribution for a decision variable is obtained by employing individual fragility curves in a multiple integral. The evaluation of the multiple integral is typically carried out by the simulation methods. Simplified approaches, such as ''Four-way'' graphical method by Mackie and Stojadinovic (2006), are developed for rapid assessment of the performance in lieu of sophisticated methods of structural analysis. More detailed approaches, such as those presented by Moehle *et al.* (2005) and Yang (2006), involve fitting probability distributions to a sample set of structural responses obtained from detailed nonlinear time-history analyses.

Performance assessment by the fragility curve approach imposes certain limitations on the propagation of uncertainty. The uncertainties in the estimation of the intensity measures are not distinguished from the uncertainties in the estimation of damage measures in the probability assessment of the exceedance of the decision variables. Furthermore, it is not possible to discern the uncertainties stemming from the randomness (aleatory) and the lack of knowledge (epistemic) when the fragility curves are developed from sparse experimental or field data. Finally, only the information regarding the second moment statistics is available in the probability distribution obtained for the decision variables.

An alternate approach is to perform a single reliability analysis by employing individual models for the estimation of ground motion intensities, engineering demand parameters, damage measures and decision variables. ‘‘Unified reliability analysis’’ (Haukaas 2007) is one such approach. Employing individual models in a single reliability analysis facilitates the propagation of uncertainties from different sources. However, rigorous performance assessment of complex structures with such an approach involves significant computational effort.

Detailed estimation of the structural damage under earthquake excitation involves modelling of the nonlinear inelastic behaviour of the materials. This compels the utilization of time-stepping methods for the dynamic analysis. Even for a deterministic analysis, estimation of structural response and damage with finite element models and refined nonlinear time-history analysis involves considerable computation time. For example, a single time-history analysis of a 32 storey building with a detailed three dimensional finite element model and nonlinear material models takes about a day on a 2.66GHz processor. In this context, a reliability analysis method such as mean centered Monte Carlo Simulation would increase the computational effort manifold. The presence of several random variables, contributed primarily due to refined ground motion models, discourages the utilization of reliability methods such as response surface methods, which become computationally expensive with the increasing number of random variables.

First-order reliability method (FORM) involves reasonable computational effort when employed in conjunction with ‘‘direct differentiation methods’’ for the gradient computation (Haukaas and Der Kiureghian 2004). Furthermore, importance measures, which rank the influence of the random variables

on the performance measures, are a by-product of this method. However, certain criteria exist for the feasibility of the application of FORM and the accuracy of the probability estimates from this method. This premise motivates the current study.

1.2. OBJECTIVES AND SCOPE

The present study concentrates on the application of FORM to the performance-based earthquake engineering problems. The potential pitfalls and the solution strategies for the applicability of FORM with finite element models are investigated. The objective is to promote the application of the structural reliability methods for the probabilistic assessments of structural performance. Diverse topics are explored within this context and the research is presented in a manuscript-based format. The objectives of each chapter are different and are precisely stated in their introduction.

The scope of the study for the applicability of FORM is limited to the structural models with finite elements. Diverse material models and performance functions are utilized in demonstrating FORM application. However, the example applications in performance assessments are primarily focused on reinforced concrete buildings. In particular, procedures are presented for the probabilistic assessments of performance objectives, such as "monetary loss" and "structural collapse."

1.3. ORGANIZATION OF CHAPTERS

As mentioned above, this study is organized in a manuscript-based format. This implies each of the following chapters, excluding the concluding chapter, are written as individual manuscripts for journal publication. Each chapter has the requisite content to be independent of the preceding chapters. However, Chapters 3 and 4 form the manuscript for a two-part paper. Hence, these two chapters refer to each other.

The study starts with the identification, categorization and separation of the aleatory and epistemic uncertainties arising from various sources in Chapter 2. This is followed by the investigation of the applicability of FORM with finite element structural models. This work is divided into two-parts based on the analysis type; statics in Chapter 3 and dynamics in Chapter 4. The following two chapters are focused

on the practical applications. Chapter 5 is the probabilistic assessment of collapse of a reinforced concrete frame with nonlinear static analysis. Chapter 6 is the probabilistic assessment of monetary loss of a high-rise reinforced concrete shear-wall building with nonlinear dynamic analysis. Chapter 7 presents the concluding remarks. A synopsis of each chapter is presented below.

1.3.1. Chapter 2: Identification of uncertainties

Finite element reliability analysis has been devised to obtain the probability of response events based on random material, geometry and loading parameters. Previously, such analysis has not distinguished between the uncertainties arising from inherent randomness, and from model errors and insufficient knowledge about the probability distribution parameters. In this chapter it is argued that this distinction is imperative for meaningful interpretation of the resulting reliability and to provide confidence in reliability assessments among practicing engineers. To this end, the sources of epistemic uncertainty are identified and explicitly included in the analysis. The quantification, representation, and propagation of epistemic uncertainty by different approaches are presented and compared, including the Bayesian probabilistic approach and the fuzzy randomness approach. Consequently, measures of confidence in the reliability index are obtained. Also, the utilization of importance measures is emphasized in order to identify where data gathering or model improvement has the greatest influence. Another novelty is the implementations in the rapidly advancing OpenSees software. The extended software produces an uncertain reliability index from which point estimates or confidence bounds are extracted. A numerical example involving a nonlinear finite element model of a reinforced concrete building with several hundred random variables is employed to demonstrate the implementations.

1.3.2. Chapter 3: Feasibility of FORM – statics

The intention in this chapter is to expose potential pitfalls and remedies when carrying out reliability computations in conjunction with finite element (FE) analysis. This type of analysis is increasingly being utilized to predict performance probabilities in various civil engineering applications. Emphasis is placed on the FORM due to its appealing computational efficiency; a principal concern in FE-based reliability

analysis. The study demonstrates that certain limit-state functions are fully amenable to FORM, while others carry the potential for difficulties. The limit-state functions and associated issues are categorized and exposed in this work by means of an enumerated list of findings. These findings are intended to guide the practicing engineer who is faced with carrying out a FE-based reliability analysis. This work is accompanied by Chapter 4 that presents developments for the fundamentally different dynamic problem.

1.3.3. Chapter 4: Feasibility of FORM – dynamics

As an extension of Chapter 3, the feasibility of application of the FORM is studied in the context of dynamic analysis. A novel formulation of the limit-state function is considered for utilization in the FE-based reliability analysis with dynamic loading and inelastic material models. This formulation includes cumulative response measures which capture the influence of the dynamic excitation on the structural performance. It is contrasted with the traditional time-variant reliability analysis and the applicability of FORM with cumulative response measures is investigated.

1.3.4. Chapter 5: Probabilistic evaluation of collapse

This chapter addresses the probabilistic seismic capacity evaluation of the existing non-ductile reinforced concrete structures that are vulnerable to shear, and thus axial, failures of their columns. The probability of structural collapse at a target lateral displacement imposed by seismic hazard is estimated by reliability analysis. For this purpose, the prevalent nonlinear static procedure is extended with finite element reliability analysis. The global structural model is enhanced by incorporating probabilistic capacity and post-failure response models of individual columns. The challenges in the detection of collapse and the potential problems and remedies in the reliability analysis due to ‘‘gradient discontinuities’’ are presented. In particular, ‘‘smoothing’’ of the post-failure response models is implemented to represent realistic member behaviour and to avoid non-convergence in the reliability analysis. Finally, parameter importance measures are employed to identify the parameters with the highest contribution to the uncertainty in the structural performance.

1.3.5. Chapter 6: Probabilistic evaluation of loss

This chapter offers a pioneering application of performance-based earthquake engineering. A probability curve for the total seismic loss of a real-world building is obtained by means of state-of-the-art models for the impending ground-motion, the structure, the non-structural content, the damage, and the ensuing losses. The probabilistic nature of the models is emphasized. In particular, the seismic hazard at the building's location (Vancouver, Canada) is described by a comprehensive and novel probabilistic model. It is argued that this ground motion model is particularly advantageous in the probabilistic analysis, compared to the more common utilization of a limited set of ground motions recorded elsewhere. In this study, the probabilistic integrals are carried out by means of a reliability formulation; referred to as unified reliability analysis. Each evaluation of the loss-based limit-state function entails a unique realization of the ground motion and a state-of-the-art inelastic dynamic finite element analysis of the structure. The result is a demonstration of the added-value performance-based engineering that should be part of the future of earthquake engineering; adding to the prescriptive, non-informative design code approach.

1.3.6. Chapter 7: Conclusions and future work

This chapter summarizes the research contributions in this work. The topics for the future research are identified and conclusions are drawn regarding the practical use of the research findings.

REFERENCES

Akkar, S., Sucuoglu, H., and Yakut, A. (2005), "Displacement-based fragility functions for low- And mid-rise ordinary concrete buildings," *Earthquake Spectra*, 21(4), 901-927.

Badillo-Almaraz, H., Whittaker, A. S., and Reinhorn, A. M. (2007), "Seismic fragility of suspended ceiling systems," *Earthquake Spectra*, 23(1), 21-40.

Baker, J. W., and Cornell, C. A. (2006), "Correlation of response spectral values for multicomponent ground motions," *Bulletin of the Seismological Society of America*, 96(1), 215-227.

Baker, J. W., and Cornell, C. A. (2006). "Spectral shape, epsilon and record selection." Earthquake Engineering and Structural Dynamics, 35(9), 1077-1095.

Baker, J. W., and Cornell, C. A. (2005), "A vector-valued ground motion intensity measure consisting of spectral acceleration and epsilon," *Earthquake Engineering and Structural Dynamics*, 34(10), 1193-1217.

Brown, P. C., and Lowes, L. N. (2007), "Fragility functions for modern reinforced-concrete beam-column joints," *Earthquake Spectra*, 23(2), 263-289.

Comerio, M. C. (2006), "Estimating downtime in loss modeling," *Earthquake Spectra*, 22(2), 349-365.

Cornell, C.A. and Krawinkler, H. (2000), Progress and challenges in seismic performance assessment, *PEER Center News*, http://peer.berkeley.edu/news/2000spring.

Haukaas, T. (2007), "Unified reliability and design optimization in earthquake engineering," *Proceedings of the Risk Acceptance and Risk Communication Workshop, Stanford, California, March 26-27.*

Haukaas, T. and Der Kiureghian, A. (2004), *Finite Element Reliability and Sensitivity Methods for Performance-Based Engineering*, Report no. PEER 2003/14, Pacific Earthquake Engineering Research Center, University of California, Berkeley

Kircher, C. A. (2003), "Earthquake loss estimation methods for welded steel moment-frame buildings," *Earthquake Spectra*, 19(2), 365-384.

Krawinkler, H., Medina, R., and Alavi, B. (2003), "Seismic drift and ductility demands and their dependence on ground motions," *Engineering Structures*, 25(5), 637-653.

Mackie, K. R., and Stojadinovic, B. (2006), "Fourway: Graphical tool for performance-based earthquake engineering," *Journal of Structural Engineering*, 132(8), 1274-1283.

Miranda, E., and Aslani, H. (2003), *Probabilistic Response Assessment for Building-Specific Loss Estimation*, Report no. PEER 2003/03, Pacific Earthquake Engineering Research Center, University of California, Berkeley.

Moehle, J., Stojadinovic, B., Der Kiureghian, A. and Yang, T.Y. (2005), *An application of PEER performance-based earthquake engineering methodology*. Research Digest No. 2005-1, Pacific Earthquake Engineering Research Center, University of California, Berkeley, California

Moehle, J., and Deierlein, G.G. (2004), " A framework methodology for performance-based earthquake engineering," *Proceedings of 13th World Conference on Earthquake Engineering, Vancouver, Canada, August 1-6, 2004,* Canadian Association for Earthquake Engineering

Pagni, C. A., and Lowes, L. N. (2006), "Fragility functions for older reinforced concrete beam-column joints," *Earthquake Spectra*, 22(1), 215-238.

Porter, K. A., Kiremidjian, A. S., and LeGrue, J. S. (2001), "Assembly-based vulnerability of buildings and its use in performance evaluation," *Earthquake Spectra*, 17(2), 291-312.

Porter, K. A., Beck, J. L., and Shaikhutdinov, R. V. (2002), "Sensitivity of building loss estimates to major uncertain variables," *Earthquake Spectra*, 18(4), 719-743.

Porter, K.A. (2003), "An overview of PEER's performance-based earthquake engineering methodology," *Proceedings of the Ninth International Conference on Applications of Statistics and Probability in Civil Engineering,ICASP9*, San Francisco, California

Porter, K., Kennedy, R., and Bachman, R. (2007), "Creating fragility functions for performance-based earthquake engineering," *Earthquake Spectra*, 23(2), 471-489.

Ramamoorthy, S.K., Gardoni, P., and Bracci, J.M. (2006), "Probabilistic demand models and fragility curves for reinforced concrete frames," *Journal of Structural Engineering*, 132(10), 1563-1572

Shaikhutdinov, R. (2004), *Structural Damage Evaluation: Theory and Applications to Earthquake Engineering,* Report no. EERL 2004-06, Earthquake Engineering Research Laboratory, California Institute of Technology, Pasadena, California.

Stewart, J., Chiou, S., Bray, J., Graves, R., Somerville, P. and Abrahamson, N. (2001), *Ground Motion Evaluation Procedures for Performance-Based Design*, Report no. PEER 2001/09, Pacific Earthquake Engineering Research Center, University of California, Berkeley.

Taghavi, S., and Miranda, E. (2005), "Approximate floor acceleration demands in multistory buildings. II: Applications," *Journal of Structural Engineering*, 131(2), 212-220.

Yang, T.Y. (2006), *Performance evaluation of innovative steel braced frames,* Ph.D. Dissertation, University of California, Berkeley, California

Zhu, L., Elwood, K.J., and Haukaas, T. (2007), "Classification and seismic safety evaluation of existing reinforced concrete columns," *Journal of Structural Engineering*, 133, 1316-1330.

Chapter 2. IDENTIFICATION OF UNCERTAINTIES[1]

2.1. INTRODUCTION

The advent of performance-based engineering has placed increased emphasis on realistic simulation of structural behaviour under extreme loading. Instead of the traditional prescriptive and non-transparent code rules to ensure life safety, the next-generation codes include additional performance indicators. Examples are amount of damage, monetary loss, and loss of functionality (downtime). Such predictions require comprehensive numerical modelling and realistic representation of nonlinear structural behaviour. Although extensive research is currently being conducted in this area, the response predictions can ultimately only be made in a probabilistic manner. Uncertainty is present in every aspect of the analysis. Hence, the prediction of structural performance must be done within a reliability framework.

Finite element reliability analysis (FERA) has been developed to account for uncertainties in structural analysis. The input parameters of the finite element model are provided as random variables to account for uncertainty in the material, geometry, and loading parameters. Subsequently, the probability of response events is computed. This is achieved by defining limit-state functions (also referred to as performance functions) in terms of response quantities of the finite element analysis. For instance, the probability that the displacement response d from a nonlinear static pushover analysis exceeds a threshold d_0 is addressed by the limit-state function $g = d_0 - d$, where d obviously is a function of the random input variables. Numerical examples involving comprehensive nonlinear finite element models with approximately 500 random variables are presented in Haukaas and Der Kiureghian (2004).

The reliability problem is a multifold integral in the space of random variables. The joint probability density function (PDF) of the random variables is the integration of the failure domain defined by the limit-state function(s). In the case of one limit-state function the problem reads

[1] A version of this chapter has been published. Koduru, S.D. and Haukaas, T. (2006), "Uncertain reliability index in finite element reliability analysis," *International Journal of Safety and Reliability*, 1(1-2), 77-101

$$p_f = \int \cdots \int_{g \le 0} f(\mathbf{x}) \mathrm{d}\mathbf{x} \tag{2-1}$$

where p_f is the sought probability, $\mathbf{x}$ is the vector of random variables, and $f(\mathbf{x})$ is the joint PDF. In the first and second order reliability methods (FORM and SORM) the integration boundary g=0 is approximated by a hyper-plane and a paraboloid, respectively, at the most likely failure point in the transformed space of uncorrelated standard normal random variables $\mathbf{y}$. This point is termed the most probable failure point (MPP). The reliability index β is related to the probability by $\beta = -\Phi^{-1}(p_f)$, where Φ is the standard normal cumulative distribution function (CDF). In FORM analysis the reliability index represents the minimum distance from the origin in the standard normal space to the integration boundary g=0. Upon determining this point, the corresponding failure probability is computed by $p_f = \Phi(-\beta)$. Of particular interest to the developments in this chapter is the availability of importance measures from FORM. This analysis renders available importance vectors that rank the model parameters according to their relative influence on the reliability. Moreover, these vectors contain information to distinguish parameters as "resistance" and "load" variables. Details and numerical examples are presented by Haukaas and Der Kiureghian (2005).

The first coupling between FORM reliability analysis and the finite element method is found in Der Kiureghian and Taylor (1983). A number of contributions have since been presented, including those by Liu and Der Kiureghian (1991), Gutierrez *et al*. (1994), Zhang and Der Kiureghian (1997), Der Kiureghian and Zhang (1999), Sudret and Der Kiureghian (2000), Imai and Frangopol (2000), Haldar and Mahadevan (2000), Frier and Sorensen (2003), and Haukaas and Der Kiureghian (2004). In essence, FERA entails the merger between finite element analysis and reliability methods such as the FORM and SORM, sampling methods, and response surface methods. However, several reliability methods tend to be practically prohibitive due to high computational cost, particularly for problems with hundreds of random variables. Each time the limit-state function is evaluated a finite element analysis is required, which is usually a computationally demanding task. Of particular effectiveness in FERA is the combination of FORM and subsequent importance sampling around the most probable failure point. This

scheme requires only approximately 10 evaluations of the limit-state function (and its gradient with respect to the random variables) to find the approximation point in FORM, followed by efficient importance sampling analysis centred at this point.

An important aspect of the FERA methodology is that probability distributions are prescribed on the *fundamental* parameters of the problem. For instance, the Young's modulus of a material is characterized as a random variable, instead of a global response parameter such as the storey stiffness. This is advantageous because data is available for the fundamental parameters but rarely for the global parameters. The data is typically obtained by performing coupon tests or concrete cylinder tests for small specimens in the laboratory. This remedies the problem that data is unavailable for the response of the entire structure, but it introduces uncertain model errors of the type discussed in this chapter. It is also noted that, in principle, the FERA methodology requires complete knowledge of the probability distribution of all the random variables, as well as information about correlation. In reality, uncertainty exists in the description of the probability distributions and the correlation due to limited availability of data. This adds to the uncertain errors that are present due to the utilization of specimen tests to model complex 3-dimensional structural components, as well as errors in the numerical modelling and analysis procedures. This motivates the present study.

The uncertainty that is reducible by human intervention, for instance by data gathering or by model improvement, is termed "epistemic" uncertainty (Hacking 1975). In this chapter, sources of epistemic uncertainty in finite element reliability analysis are reviewed and accounted. As pointed out by Der Kiureghian (1989), the presence of epistemic uncertainty makes the calculated probability itself a random variable. Explicit representation of this uncertainty by probabilistic or other means results in an uncertain reliability, rather than a scalar value. In this chapter this viewpoint is adopted and different approaches to account for epistemic uncertainty in FERA are explored.

The developments in this chapter are implemented in the OpenSees software. OpenSees (open system for earthquake engineering simulation) is an open-source, object-oriented general-purpose finite element

code written in C++ and specifically developed for earthquake engineering analysis. It is the official computational platform of the Pacific Earthquake Engineering Research (PEER) Center and has recently been adopted as the simulation platform of NEES, the NSF-sponsored George E. Brown Jr. Network for Earthquake Engineering Simulation. OpenSees was extended with reliability and response sensitivity capabilities by Haukaas and Der Kiureghian (2004), thus enabling FERA in OpenSees. Source code, user's guide, and executable files are available at the Internet site http://opensees.berkeley.edu. In this chapter OpenSees is further extended to explicitly account for epistemic uncertainty.

2.2. EPISTEMIC UNCERTAINTY

A number of uncertainties are present in numerical prediction of structural performance. These include uncertain material properties, uncertain geometrical imperfections, and uncertain modelling and analysis errors. These all contribute to the uncertainty in the prediction even under well-defined loading conditions. The different types of uncertainty are commonly classified as being either aleatory or epistemic in nature (Hacking 1975). The aleatory uncertainty is defined as the inherent variability of a phenomenon and is therefore irreducible without changing the phenomenon itself. Conversely, the epistemic uncertainty is due to lack of knowledge and is thereby reducible provided additional information.

It is emphasized that several paradigms and schools of thought exist in the classification and representation of uncertainty. Indeed, one may argue that aleatory uncertainty does not exist in our application. This viewpoint would be supported by the fact that natural phenomena are not uncertain if we fully understand the processes that govern them. If one was able to develop models that described the materials even at the molecular level, then a true representation of nature without aleatory uncertainty could be envisioned. However, this is practically impossible and this viewpoint is rejected. In this chapter a number of *types* of uncertainty are considered that can be classified as being either aleatory or epistemic *in nature*.

In the literature a number of categorizations of types of uncertainty are encountered. O'Hagan and Oakley (2004) categorize the types of uncertainty as parametric uncertainty, model inadequacy, residual variability, and code inadequacy. Der Kiureghian (1989) classifies sources of uncertainty as inherent variability, estimation error, model imperfection, and human error. Parry (1996) employs a briefer categorization of uncertainty as parametric, model, and completeness uncertainty. However, the uncertainties arising from the lack of statistical data to assess the model parameters and the lack of knowledge to obtain a complete and correct model form are distinguished by all the researchers. Winkler (1996) argues that, although the classification of uncertainties is useful from a practical point of view, all categorizations are nonetheless artificial. Hora (1996) agrees that such classifications are difficult to generalize and label as aleatory or epistemic in nature. Ditlevsen (1983) makes the case that all theoretical uncertainty may be modelled as "subjective probabilities," with the exception of gross errors.

It is concluded that a number of types of uncertainty are present, depending on the type of the problem at hand. Moreover, it is argued that for the objectives in this chapter the categorization of types of uncertainty is not essential. Rather, what is essential is to distinguish between the nature of them; aleatory or epistemic. The latter is intuitively most challenging and is not exclusively amenable to probabilistic characterization. Indeed, epistemic uncertainty makes the probability estimates themselves uncertain. It is argued that it is imperative for the future use of FERA to comprehensively identify sources of epistemic uncertainty, and to explicitly include them in the analysis by distinguishing them from aleatory uncertainties. To this end, the following exposition of epistemic uncertainty in probabilistic prediction of structural response is suggested:

Idealization uncertainty: The foundation for structural analysis is the idealization of reality into a mathematical boundary value problem. This entails continuum mechanics assumptions that provide mathematical equations for equilibrium, kinematics, and constitutive behaviour, as well as boundary

conditions. For instance, a common kinematics equation in beam theory neglects shear deformation. Epistemic uncertainty is thereby introduced, due to imperfect model form and/or missing parameters.[2]

Complexity uncertainty: The parameters of an idealized boundary value problem are commonly determined by laboratory tests of small specimens. In the real structure, however, complex multi-axial stress states are present. For instance, the stress paths in a beam-column connection or the bonding between concrete and reinforcement are complicated phenomena for which models and data are limited. Hence, the estimates from simplified laboratory tests carry uncertainty. In this chapter, this is separated from the idealization uncertainty and referred as complexity uncertainty.

Statistical uncertainty: Parameters such as material stiffness and strength are assessed based on available data. Uncertainty arises when the number of observations is too small, which is frequently the case. This leads to uncertainty in the probability distribution parameters of the random variables and is referred to as statistical uncertainty. It is noted that measurement error, which for a given measuring device or procedure is aleatory, adds to the statistical uncertainty to form the total uncertainty in the distribution parameters.

Finite element discretization uncertainty: Structural members such as beams, columns and shear walls are modelled as discrete elements in a finite element analysis. Deficiencies in mesh density and order of the shape functions introduce errors in the structural response predictions. It is debated whether such errors are uncertain, because an "infinitely" refined mesh with convergent elements would lead to a unique result. For a new structure for which such an exercise is practically impossible, it is considered that this error to be epistemically uncertain in nature.

Finite element analysis uncertainty: Approximate numerical analysis techniques are employed to obtain the response in nonlinear and/or dynamic finite element analysis. Examples are the Newton-Raphson procedure to attain equilibrium and the Newmark time-stepping schemes to accommodate time-history

[2] We recognize that, technically, the inherent randomness in omitted random variables is aleatory in nature.

analysis. The presence of errors due to finite tolerances and time increments, as well as computer round-off, signifies reducible, and hence epistemic, uncertainty in the computed response.

Reliability analysis uncertainty: From Eq. (2-1) it is evident that the estimation of the probability of failure requires the evaluation of a multifold integral. This is addressed by inherently approximate reliability methods. Moreover, it is generally not a trivial task to determine what constitutes failure, which leads to uncertainty in the limit-state functions employed to specify the failure criterion. These approximations in the reliability analysis techniques and the performance criteria result in further epistemic uncertainty in the final result; the structural reliability.

In this chapter a *framework* is implemented for accounting for epistemic uncertainty and to compare different techniques. Statistical uncertainty in the material and geometry properties of the finite element model is selected as the primary case for demonstration. Several researchers are working to develop probabilistic models to account for epistemic model uncertainties, including Thacker *et al.* (2001) and Bebamzadeh and Haukaas (2004). From an implementation viewpoint; the statistical uncertainty is most challenging. To account for this uncertainty, distribution parameters for the random variables in FERA, such as means and standard deviations, themselves are allowed to be uncertain. This leads to uncertain probability distributions for the fundamental random variables. Fig. 2-1a indicates the uncertainty in the probability distribution of a random variable x due to the epistemic uncertainty in its distribution parameters; namely, the mean μ and the standard deviation σ. The uncertainty in the mean and the standard deviation may be characterized in different ways as outlined in Fig. 2-1b, where a probabilistic and a fuzzy randomness approach are shown. The epistemic uncertainty in the probability distribution parameters causes the reliability index to be uncertain. As sketched in Fig. 2-1c, a "characterizing function" is obtained that depends on the selected approach, from which point estimates or confidence measures on the reliability may be obtained.

It is stressed that a methodology to account for epistemic uncertainty should result in a reliability measure that (1) provides insight into the relative influence of the various sources of epistemic uncertainty and (2)

provides measures of confidence in the obtained reliability. The first objective is accomplished by exploring importance measures from an epistemic reliability analysis, analogue to the importance measures available from traditional reliability analysis. The second objective is achieved by providing confidence bounds on the reliability, as well as providing distribution functions for the reliability itself. To this end, a number of approaches seem to be available in the literature to address epistemic uncertainties, including those based on probability theory, fuzzy set theory, evidence theory and random set theory. The transferable belief models (Ayyub 2004), imprecise probability methods (Hall and Lawry 2003), coherent lower previsions (de Cooman and Troffeas 2004, Kozine and Utkin 2004), envelope distribution methods (Berleant and Zhang 2004) and the information gap models (Ben-Haim 2004) represent approaches formed by a combination of these theories. In the following two options are explored to compare suitability, efficiency, ease of implementation, and interpretation of results.

2.3. THE PROBABILISTIC APPROACH

A number of researchers consider the probabilistic approach to be supreme in handling any type of uncertainty; aleatory as well as epistemic. In particular, the Bayesian methodology has become a vehicle to incorporate statistical information as well as subjective information, such as engineering judgment. Although the inclusion of this information does not conform to the frequency notion of probability, the result of the reliability analysis is still useful as a measure of "degree of belief" (Vick 2002). The probabilistic approach presented in the following includes the Bayesian option to incorporate information to reduce the epistemic uncertainty.

Consider the case of uncertain distribution parameters. It is denoted by $\mathbf{x}$ the vector of potentially correlated random variables $[x_1, x_2, \ldots x_n]$ that are intended to describe the inherent variability in material, geometry, and load parameters. For instance, one component of $\mathbf{x}$ may be a Young's modulus of one structural member in the finite element model. In this chapter, the parameters of the probability distribution of $\mathbf{x}$ are themselves considered as random variables, collected in the vector $\boldsymbol{\theta} = [\theta_1, \theta_2, \ldots \theta_m]$. One example is a random variable x_1 with an uncertain mean θ_1 as well as an uncertain standard

deviation θ_2. In this paradigm, the random variables $\mathbf{x}$ represent aleatory uncertainty, while $\boldsymbol{\theta}$ are considered to represent epistemic uncertainty.

The Bayesian updating rule is utilized to update the joint PDF for $\boldsymbol{\theta}$ based on available information (Box and Tiao 1973):

$$f''(\boldsymbol{\theta}) = cL(\boldsymbol{\theta}) f'(\boldsymbol{\theta}) \tag{2-2}$$

where $f''(\boldsymbol{\theta})$ is termed the "posterior" joint PDF, c is the normalizing constant, $L(\boldsymbol{\theta})$ is the "likelihood function" for the observed data, and $f'(\boldsymbol{\theta})$ is the "prior" joint PDF. Subjective information is typically incorporated through the prior PDF, while observed data is incorporated as it becomes available through the likelihood function, often with the previous posterior PDF as the prior PDF. In this manner, the posterior distribution $f''(\boldsymbol{\theta})$ is gradually improved by incorporating new information. The reader is referred to Box and Tiao (1973) for further details on Bayesian updating.

The separation of the parameter uncertainty into individual random variables $\boldsymbol{\theta}$ implies that the joint PDF for $\mathbf{x}$ as a function of the distribution parameters is a *conditional* PDF, denoted $f(\mathbf{x}|\boldsymbol{\theta})$. It is noted that the *predictive* PDF of $\mathbf{x}$ that includes the parameter uncertainty is obtained by the rule of total probability in the form of the multifold integral over the outcome space of $\boldsymbol{\theta}$:

$$f(\mathbf{x}) = \int \cdots \int f(\mathbf{x} \mid \boldsymbol{\theta}) f(\boldsymbol{\theta}) \mathrm{d}\boldsymbol{\theta} \tag{2-3}$$

In principle, this joint PDF may then be substituted into Eq. (2-1) to obtain p_f and the corresponding reliability index. This amounts to considering parameters such as the means and standard deviations as random variables themselves in the traditional type reliability analysis. This is conceptually simple to implement. However, this exercise is not useful in our developments because it hinders the separation of aleatory and epistemic uncertainty. Instead, the reliability index is considered to be a function of the random variables $\boldsymbol{\theta}$ and two approaches are explored to explicitly expose the influence of epistemic uncertainty on the reliability index.

First first-order approximations are employed for the statistical moments of functions of random variables, where β is the function and $\boldsymbol{\theta}$ are the random variables. This produces estimates for the mean and the standard deviation of the reliability index. In the second approach the probability distribution for the reliability index is obtained by a nested, parametric reliability analysis. These approaches have in common the need for the reliability index conditioned upon $\boldsymbol{\theta}$. That is, the following form of Eq. (2-1) is evaluated:

$$p_f(\boldsymbol{\theta}) = \int \cdots \int_{g \le 0} f(\mathbf{x} \mid \boldsymbol{\theta}) \mathrm{d}\mathbf{x} \tag{2-4}$$

to obtain the corresponding reliability index $\beta(\boldsymbol{\theta}) = -\Phi^{-1}(p_f(\boldsymbol{\theta}))$.

The question of selecting values for $\boldsymbol{\theta}$ is answered in the first approach by the mean values $\boldsymbol{\mu}_{\boldsymbol{\theta}}$. The mean-value, first-order approximation of the reliability index is obtained by (Ang and Tang 1975)

$$\mu_\beta = \beta(\boldsymbol{\mu}_{\boldsymbol{\theta}}) \tag{2-5}$$

The corresponding first-order approximation of the standard deviation of the reliability index reads

$$\sigma_\beta = \sqrt{\nabla_{\boldsymbol{\theta}} \beta^{\mathrm{T}} \boldsymbol{\Sigma}_{\boldsymbol{\theta}\boldsymbol{\theta}} \nabla_{\boldsymbol{\theta}} \beta} \tag{2-6}$$

where $\nabla_{\boldsymbol{\theta}} \beta$ is the gradient of the reliability index with respect to $\boldsymbol{\theta}$ and $\boldsymbol{\Sigma}_{\boldsymbol{\theta}\boldsymbol{\theta}}$ is the covariance matrix for the random variables $\boldsymbol{\theta}$. When $\boldsymbol{\theta}$ represents parameter uncertainty, specifically the mean and standard deviations of the random variables $\mathbf{x}$, then the gradient of the reliability index from FORM analysis is obtained by the chain rule of differentiation:

$$\nabla_{\boldsymbol{\theta}} \beta = \frac{\partial \beta}{\partial \boldsymbol{\theta}} = \frac{\partial \beta}{\partial \mathbf{y}^*}^{\mathrm{T}} \frac{\partial \mathbf{y}^*}{\partial \boldsymbol{\theta}} \tag{2-7}$$

where $\mathbf{y}^*$ is the coordinates of the MPP in the standard normal space. It is known that $\partial \beta / \partial \mathbf{y}^* = \boldsymbol{\alpha}$ because the reliability index is written $\beta = \boldsymbol{\alpha}^{\mathrm{T}} \mathbf{y}^*$, where $\boldsymbol{\alpha}$ is the negative normalized gradient vector of

the limit-state function in the standard normal space ($\boldsymbol{\alpha} = -\nabla g / \|\nabla g\|$). Moreover, the matrix $\partial \mathbf{y}^* / \partial \boldsymbol{\theta}$ is obtained by differentiation of the probability transformation $\mathbf{y} = T(\mathbf{x})$ at the MPP. For instance, when the well-known Nataf transformation (Liu and Der Kiureghian 1986) is employed then differentiation is performed, for each random variable, the relationship $\mathbf{y} = \mathbf{L}^{-1}\, \Phi^{-1}(\mathrm{F}(x))$ where $\mathbf{L}$ is the lower triangular Cholesky decomposition of the modified correlation matrix and $\mathrm{F}(x)$ is the CDF of the random variable x. In conclusion, this first probabilistic approach renders available a point estimate and a measure of dispersion of the reliability index, provided second-moment information for the "epistemic random variables" $\boldsymbol{\theta}$. It is noted that only one reliability analysis including the computation of the gradient of the reliability index is required to obtain these estimates.

In the second probabilistic approach a probability distribution for β is obtained by a parametric nested reliability analysis with the "outer" limit-state function

$$\tilde{g}(\boldsymbol{\theta}) = \beta(\boldsymbol{\theta}) - \beta_0 \tag{2-8}$$

where the tilde distinguishes it from the limit-state function of the ordinary "inner" limit-state function that is specified by the present performance requirement. By varying the threshold β_0 the CDF $F(\beta_0)$ of the reliability index β is obtained. As pointed out by Der Kiureghian (1989), this is a nested reliability problem, because repeated evaluation of the inner reliability analysis in Eq. (2-4) is required to obtain $\beta(\boldsymbol{\theta})$. The inner problem consists of integrating $f(\mathbf{x} \mid \boldsymbol{\theta})$ in the space of "aleatory random variables" with the integration boundary provided by the user-defined limit-state function, while the outer problem consists of integrating $f(\boldsymbol{\theta})$ in the space of "epistemic random variables" with the integration boundary provided by Eq. (2-8):

$$F(\beta_0) = \int \cdots \int_{\tilde{g} \le 0} f(\boldsymbol{\theta}) \mathrm{d}\boldsymbol{\theta} \tag{2-9}$$

It is noted that an analytical expression is available for the PDF corresponding to this CDF when FORM analysis is employed to solve Eq. (2-9); in this case it is $F(\beta_0) = \Phi(-\tilde{\beta})$ and the chain rule of differentiation yields

$$f(\beta_0) = \frac{\partial F(\beta_0)}{\partial \beta_0} = \frac{\partial F(\beta_0)}{\partial \tilde{\beta}} \frac{\partial \tilde{\beta}}{\partial \beta_0} = -\varphi(\tilde{\beta}) \frac{\partial \tilde{\beta}}{\partial \beta_0} \tag{2-10}$$

where $\tilde{\beta}$ is the reliability index from the outer reliability problem. To evaluate $\partial\tilde{\beta} / \partial\beta_0$ Eq. (2-7) is first invoked, which states that

$$\frac{\partial \tilde{\beta}}{\partial \beta_0} = -\frac{\nabla \tilde{g}^{\mathrm{T}}}{\|\nabla \tilde{g}\|} \frac{\partial \tilde{\mathbf{y}}^*}{\partial \beta_0} \tag{2-11}$$

and then the limit-state function is differentiated, which at the MPP $\tilde{\mathbf{y}}^*$ in the standard normal space of epistemic random variables equals zero. By this it is found (Hohenbichler and Rackwitz 1986, Bjerager and Krenk 1989):

$$\frac{\partial \tilde{\beta}}{\partial \beta_0} = \frac{1}{\|\nabla \tilde{g}\|} \frac{\partial \tilde{g}}{\partial \beta_0}\bigg|_{\tilde{\mathbf{y}}^*} = \frac{1}{\|\nabla \tilde{g}\|} \frac{\partial \tilde{g}}{\partial \beta_0}\bigg|_{\boldsymbol{\theta}^*} = \frac{-1}{\|\nabla \tilde{g}\|} \tag{2-12}$$

where the vertical bar denotes differentiation for fixed $\tilde{\mathbf{y}}^*$-values . This is substituted into Eq. (2-10) to obtain the PDF of the reliability index β. An example is shown in a subsequent section.

A potential problem is noted when FORM analysis is applied to solve Eq. (2-9). In the search for the MPP, $\mathbf{y}^*$, which is the point of approximation in FORM analysis, the gradient of the limit-state function is required to be continuous. In effect, the components of the vector $\partial\beta / \partial\boldsymbol{\theta}$ must be continuous. In rare circumstances this may not be the case because an infinitesimal change in the epistemic random variables $\boldsymbol{\theta}$ may result in a "jump" in the location of $\mathbf{y}^*$. This situation is schematically shown in Fig. 2-2, where the function $\beta(\theta)$ has a "kink" at the value of θ at which the jump to another $\mathbf{y}^*$ location occurs.

Consequently, the gradient is discontinuous and the situation would potentially cause problems in the determination of the MPP in the outer reliability problem. This problem is related to the well-known problem of multiple MPP in FORM analysis. In FERA, where the limit-state function is defined in terms of structural response and is a function of random variables such as material, geometry, and load parameters, such situations are rarely encountered. The use of sampling methods would circumvent the problem. However, this increases the number of inner FORM analyses manifold in order to obtain a point estimate of the reliability index. Furthermore, importance measures to rank the sources of epistemic uncertainty according to relative influence on the reliability are not readily available from sampling analysis. Computational cost comparisons between the different approaches are carried out in a subsequent section.

2.4. THE FUZZY RANDOMNESS APPROACH

An alternative to the probabilistic approach is the fuzzy randomness approach that is summarized in the book by Möller and Beer (2004). In this approach a probabilistic characterization of the aleatory uncertainty is retained, while characterizing the epistemic uncertainty by concepts of fuzzy sets. To explain the concepts of such sets, first consider the classical set that contains a collection of outcomes with so-called "crisp" boundary. That is, if an outcome θ belongs to the set A then it is excluded from belonging to the complement set A^c. A fuzzy set $\widetilde{A}$ differs from a classical set by having a "fuzzy" boundary. Specifically, a fuzzy set assigns varying membership values for an outcome θ to belong to the fuzzy set $\widetilde{A}$. Therefore, the element θ could partially belong to both $\widetilde{A}$ and its complement set $\widetilde{A}^c$. To this end, the fuzzy set is defined as

$$\widetilde{A} = \{\theta, m_A(\theta)\} \tag{2-13}$$

where $m_A(\theta)$ is the membership function defining the degree of belongingness of θ to $\widetilde{A}$. A normalized fuzzy set has the membership values $m_A(\theta) \in [0,1]$. A high value of the membership function indicates a

high degree of belongingness to the set. For a given membership function value, denoted α, a crisp set A_α, is obtained as shown in Fig. 2-3. This is referred to as an "α-level" set and is formulated as

$$A_\alpha = \{\theta \mid m_A(\theta) \geq \alpha\} \tag{2-14}$$

As shown in Fig. 2-3, the α-level set A_α is a connected interval $[\theta_{\alpha L}, \theta_{\alpha U}]$, in which

$$\theta_{\alpha L} = \min[\theta \mid m_A(\theta) \geq \alpha] \tag{2-15}$$

$$\theta_{\alpha U} = \max[\theta \mid m_A(\theta) \geq \alpha] \tag{2-16}$$

Effectively, a fuzzy number may be represented in an interval form at any selected α-level and the interval analysis methods developed by Rao and Berke (1996) are applicable at each α-level (Langley 2000).

In the previous section the distribution parameters of a random variable are considered to be random variables themselves. In this section the distribution parameters are represented by fuzzy numbers for the purpose of comparison with the probabilistic approach. Consider $\mathbf{x}$ to represent the vector of aleatory random variables and $\boldsymbol{\theta}$ to represent the vector of fuzzy numbers that represent epistemic uncertainty in the distribution parameters. In the literature $\mathbf{x}$ are then referred to as "fuzzy random variables" (Möller and Beer 2004, Krätschmer 2001, Körner 1997). A schematic example is shown in Fig. 2-4 for one fuzzy random variable x_i where its mean is a fuzzy number. For α-level 1.0 a crisp PDF for the random variable is obtained (solid line), while other α -levels lead to an interval of possible PDFs. In Fig. 2-4 the boundaries for the PDF obtained at α-level 0.0 is shown. The fuzzy PDF is denoted by $\tilde{f}(x_i)$.

It is stressed that fuzzy numbers may also be considered to represent model errors, in which case they would appear directly as parameters of the model, instead of as parameters of the probability distributions of the random variables. In effect, this will make the limit-state function fuzzy, as indicated in Fig. 2-5. In either case, the analysis approach is the same.

In order to study the effect of the epistemic uncertainty on the reliability index, reliability analyses are carried out at selected α-levels. At each α-level, interval values for the distribution parameters $\boldsymbol{\theta}$ are available and hence, crisp probability distributions for the random variables $\mathbf{x}$. Consequently, an interval for the reliability index, here denoted β_α is obtained. Theoretically, a number of reliability analyses are required at each α-level, each with fixed values for the distribution parameters $\boldsymbol{\theta}$. This is because, in principle, all possible combinations of $\theta_{\alpha L}$ and $\theta_{\alpha U}$ for all components of $\boldsymbol{\theta}$ should be checked. The reliability analyses at each α-level results in a range of values for the reliability index β_α. The maximum and minimum values of the reliability index β_α form the interval of the reliability index [$\beta_{\alpha L}$, $\beta_{\alpha U}$] for that α-level. A fuzzy reliability index $\tilde{\beta}$ is then reconstructed from the intervals of the reliability index over the selected α-levels, as schematically shown in Fig. 2-6. This curve serves a similar purpose as the PDF curve obtained by Eq. (2-9).

The question of selecting $\boldsymbol{\theta}$-values in the reliability analyses at each α-level remains. The total number of possible combinations of lower values $\theta_{\alpha L}$ and upper values $\theta_{\alpha U}$ is equal to 2^m, where m is the number of epistemic random variables, that is, the dimension of $\boldsymbol{\theta}$. Theoretically, this implies that the reliability analysis at each α-level must be repeated 2^m times to obtain all the possible outcomes of β_α, from which the extreme values [$\beta_{\alpha L}$, $\beta_{\alpha U}$] are obtained. The α-level optimization by Möller and Beer (2004) addresses this problem by employing a combination of genetic and gradient-based optimization strategies to obtain the extreme values $\beta_{\alpha L}$ and $\beta_{\alpha U}$. However, these optimization strategies, including those by Elishakoff (1999), Bernardini (1999), and McWilliam (2001), tend to be complex in implementation and computationally expensive.

Instead, in this chapter the use of importance measures from the reliability analysis is explored to obtain the combinations of $\theta_{\alpha L}$ and $\theta_{\alpha U}$ values that will yield the values $\beta_{\alpha L}$ and $\beta_{\alpha U}$. From Hohenbichler and Rackwitz (1986), Bjerager and Krenk (1989), and Haukaas and Der Kiureghian (2005) importance

measures in FERA are available that distinguish resistance variables from load variables. This information is valuable to select combinations of $\theta_{\alpha L}$ and $\theta_{\alpha U}$ values that will give extreme values of β. When the resistance variables are set to their $\theta_{\alpha L}$ values and the load variables are set to their $\theta_{\alpha U}$ values then the lower reliability index $\beta_{\alpha L}$ is obtained. That is, low resistance combined with high load gives a low reliability. Conversely, when the resistance variables are set to their $\theta_{\alpha U}$ values and the load variables are set to their $\theta_{\alpha L}$ values then the upper reliability index $\beta_{\alpha U}$ is obtained.

Two approaches are possible to obtain relevant importance measures for this purpose. First, a single reliability analysis with both $\mathbf{x}$ and $\boldsymbol{\theta}$ as random variables may be performed, as mentioned subsequent to Eq. (2-3). The resulting importance measure, denoted $\boldsymbol{\gamma}$ in Haukaas and Der Kiureghian (2005), provide guidance for selecting $\theta_{\alpha L}$ and $\theta_{\alpha U}$ values. Second, when parameter uncertainty is considered, as in the following numerical example, the reliability sensitivity measures $\partial\beta / \partial\boldsymbol{\mu}$ and $\partial\beta / \partial\boldsymbol{\sigma}$ may instead be employed. However, the selection of values for $\theta_{\alpha L}$ and $\theta_{\alpha U}$ is complicated by the presence of correlation. For instance, if two resistance variables are strongly negatively correlated then it is unlikely that they both take on the value $\theta_{\alpha L}$ (or $\theta_{\alpha U}$) at the same time. By neglecting correlation among $\boldsymbol{\theta}$, the fuzzy variables become "non-interactive." The interval $[\beta_{\alpha L}, \beta_{\alpha U}]$ obtained for the reliability index β with non-interactive fuzzy sets is wider than the true interval when the interaction is considered (Möller and Beer 2004). That is, conservative confidence estimates are obtained. The case is also made that strong negative correlation between the epistemic variables is implausible in the FERA applications under consideration. Furthermore, the effect of strong negative correlation would appear in the importance measure $\boldsymbol{\gamma}$ that are employed to select combinations of $\theta_{\alpha L}$ and $\theta_{\alpha U}$ values, because $\boldsymbol{\gamma}$ includes the effect of correlation between the variables (Haukaas and Der Kiureghian 2005). It is concluded that importance measures from FERA are an efficient and robust approach to select $\theta_{\alpha L}$ and $\theta_{\alpha U}$ values, in lieu of utilizing costly and complex optimization algorithms.

2.5. IMPLEMENTATIONS IN OPENSEES

OpenSees is regarded as a collection of software components rather than a packaged code. This software architecture is facilitated by an object-oriented programming approach. The developer creates objects, or, abstractly, classes, instead of focusing on the procedural attributes of the problem. The objects contain data members and member functions and may interact by calling each other's member functions. The member functions perform operations on the data members of its object, or on data that is passed to the member function at run-time.

Haukaas and Der Kiureghian (2004) extended OpenSees with objects to perform reliability analysis in combination with finite element analysis. The analysis part of these implementations contains a number of analysis tools that are employed in our implementations. Fig. 2-7 shows an overview of the reliability module, where the analysis-domain decomposition is emphasized. The analysis tools are shown with a particular symbol to be data members of the reliability analysis, while the various analysis types are shown to be sub-classes of the generic reliability analysis. The reliability analysis performs operations on the reliability domain, which include random variables, correlation coefficients, and limit-state functions. Eight analysis types that facilitate FOSM, FORM, SORM, sampling analysis, parametric reliability analysis, system reliability analysis, out-crossing analysis, and visualization of the limit-state function were initially available. The analysis type termed EpistemicAnalysis shown in Fig. 2-7 is added in this work.

The developments in this work benefit strongly from the organization of OpenSees into a collection of analysis tools. The existing analysis tools for reliability analysis in OpenSees include probability transformation, determination of search direction and step size in the search for the MPP, search algorithms to determine the MPP, random number generation, etc. These and others are listed in Fig. 2-8, where it is emphasized that they are data members of the reliability analysis, which thereby can make use of them in the analysis. All the tasks required by the methodologies outlined in this chapter are solved by the existing analysis tools, due to the flexibility offered by the object-oriented software architecture in

OpenSees. Consider for example the nested reliability problem posed by Eq. (2-9). Fig. 2-9 shows schematically the interaction between tools of OpenSees when both the inner problem (Eq. (2-4)) and the outer problem (Eq. (2-9)) are addressed by FORM. It is observed that OpenSees allows the outer reliability analysis to use the same reliability analysis tools as the traditional inner analysis. It is stressed that from an implementation viewpoint both the inner and the outer problem can be solved by any of the available algorithms in OpenSees. In the example presented in this chapter FORM is employed to solve the inner problem, for which gradients are then readily available, while FORM and sampling are utilized for the outer problem.

Existing tools in OpenSees are also employed when implementing the fuzzy randomness approach. Our approach consists of providing the upper and lower interval values for the epistemic variables and executing a traditional reliability analysis. This is done at selected α-levels, where the upper and lower values are selected based on information from a prior reliability analysis, as described previously.

2.6. NUMERICAL EXAMPLE

In order to compare the methodologies to account for epistemic uncertainty in FERA, consider the two-storey, two-bay reinforced concrete structure in Fig. 2-10 for reliability analysis. The material properties of the concrete and reinforcement steel, as well as the nodal coordinates and load parameters are modelled as aleatory random variables, as detailed in Table 2-1. These are intended to model the inherent, irreducible uncertainty in the finite element model parameters. A total of 104 aleatory random variables are present.

Consider the limit state function

$$g = 0.015 \times 8300 - u_3 \tag{2-17}$$

where u_3 is the horizontal displacement, in units of mm, of node 3 from a static nonlinear pushover-type analysis. This limit-state function seeks the probability that the horizontal displacement at node 3 exceeds 1.5% of the building height, when uncertain lateral loads are applied to node 2 and 3.

A traditional FERA is performed to determine the ordinary point estimate of the reliability index. A FORM analysis yields $\beta = 2.89$, while an important sampling centred the MPP yields $\beta = 2.84$ with 4% coefficient of variation, which indicates that the limit-state function in Eq. (2-17) is weakly nonlinear. This is a common observation in this type of FERA.

Epistemic uncertainty is now introduced to represent the statistical uncertainty in the distribution parameters of the aleatory random variables. The mean and standard deviation of all the variables $\mathbf{x}$ are collected in the vector $\boldsymbol{\theta}$, according to the previously described methodologies. In the probabilistic approach the mean and standard deviations are considered to be random variables, while in the fuzzy randomness approach they are considered to be fuzzy numbers. Although the application is to parameter uncertainty, it is re-emphasized that the methodology is applicable to represent uncertain model and analysis errors.

In the probabilistic approach, the 58 epistemic random variables are modelled as uncorrelated lognormal random variables with properties shown in Table 2-2. However, all the structure members share the same epistemic random variable to represent the mean or standard deviation of the aleatory random variables for a common parameter. For example, the mean of compressive strength of the cover concrete in all the structural members is represented by a single epistemic random variable. This introduces correlation among the means and standard deviations of the material and load parameters of all the structure members. In this chapter the distribution parameters of these variables are selected by judgment. However, it is emphasized that the probabilistic approach has the advantage that Bayesian updating according to Eq. (2-2) may be used to assess the parameter uncertainty. In this example, the dispersion of the means and standard deviations are selected to reflect the statistical uncertainty due to lack of data, to assess the uncertainty in the material and geometry properties.

First, the second-moments of the reliability index are computed according to Eqs. (2-5) and (2-6). Because the mean of the epistemic random variables $\boldsymbol{\theta}$ are chosen equal to the initial point estimates it is found that the mean of the reliability index is 2.89, as previously reported. The first-order approximation

of the standard deviation is $\sigma_\beta = 0.208$. Hence, it is observed that the reliability index has a coefficient of variation equal to 0.072.

In the more refined probabilistic approach the outer reliability problem in Eq. (2-9) is solved by FORM at selected threshold values β_0. The PDF of the resulting reliability index is shown in Fig. 2-11. It is observed that the peak of the PDF occurs close to the point estimate from the traditional reliability; namely 2.89. Moreover, it is confirmed that the first-order approximation of the standard deviation; namely 0.208, is a reasonable measure of dispersion of the reliability index. However, the PDF of the reliability index provides significantly more information. For instance, from the information in Fig. 2-11a, or more precisely the corresponding CDF in Fig. 2-11b, it is possible to obtain the 95% confidence on the reliability index. Specifically, in this case there is a 0.95 probability that the reliability index is greater than 2.59. These details provide considerably more information than the mere β=2.89 provided by a traditional reliability analysis.

The outer reliability problem in Eq. (2-9) may alternatively be addressed by sampling analysis. However, instead of addressing the limit-state function in Eq. (2-8) outcomes of the vector $\boldsymbol{\theta}$ are sampled and response statistics are performed on the quantity $\beta(\boldsymbol{\theta})$, with a sampling distribution centred at the mean of $\boldsymbol{\theta}$. This approach is conceptually similar to that of Ang (2004). The resulting histogram and the corresponding frequency diagram are shown in Fig. 2-12. As expected, close agreement is found with the PDF curve presented in Fig. 2-11a. It is noted, however, that a high number of samples are required to obtain accuracy in the tail of the distribution of β. To remedy this, importance sampling based on a prior FORM analysis may be performed at a particular threshold level to solve the outer reliability problem. Further comments on computational cost are provided below.

The probabilistic approach has the advantage that importance measures are available to identify the most significant sources of epistemic uncertainty. This information is used to guide the allocation of resources for data gathering and model improvement efforts. When parameter uncertainty is considered, two

measures are available. First, the vectors $\partial\beta/\partial\boldsymbol{\mu}$ and $\partial\beta/\partial\boldsymbol{\sigma}$ from traditional reliability analysis provide insight into the relative influence of each distribution parameter on the reliability. However, the components of these vectors have, in general, different units. Second, the importance vector $\boldsymbol{\gamma}$ from Haukaas and Der Kiureghian (2005) is available when the outer reliability problem is solved by FORM. This renders available a valuable importance measure to directly rank the parameters $\boldsymbol{\theta}$. In this example It is found that the uncertainty in the mean and the standard deviation of the lateral loads rank highest in importance. This indicates that the most contribution to the uncertainty in the reliability index is due to the uncertainty in the lateral loads. The 10 highest ranking epistemic random variables are listed in Table 2-3. It is also observed that the importance ranking is relatively sensitive to the choice of dispersion of the epistemic random variables. For instance, by doubling the coefficient of variation of the mean of the compressive strain of the cover concrete, it is found that this parameter goes from ranking 7 to ranking 5 among the $\boldsymbol{\theta}$-variables.

In the fuzzy randomness approach, the same means and standard deviations that were considered random variables above are considered to be fuzzy numbers, denoted $\boldsymbol{\theta}$. The triangular membership function shown in Fig. 2-13 is selected to represent the epistemic uncertainty in the distribution parameters. The membership functions at α-level 0.0 represent an interval of ± one standard deviation of the random variables employed in the probabilistic analysis. This is a subjective choice that emphasizes both the flexibility in the fuzzy randomness approach, as well as the lack of a well-established methodology, despite the attempts in coupling fuzzy and Bayesian methods (Chou and Yuan 1993, Lee and Park 1997, Taheri and Behboodian 2001). Details are provided in Table 2-4 in terms of values of the distribution parameters at α-levels 1.0 and 0.0. The fuzzy analysis is performed at the three α-levels 0.0, 0.5 and 1.0. The combination of the values $\theta_{\alpha L}$ and $\theta_{\alpha U}$ of each variable in $\boldsymbol{\theta}$ to obtain the extremes $\beta_{\alpha L}$ and $\beta_{\alpha U}$ of the reliability index is found by employing importance measures from the reliability analysis, as previously described. As is commonly the case in FERA, the material parameters are identified as

resistance variables and the nodal loads as load variables. Fig. 2-14 shows the resulting triangular membership function for the reliability index.

It is of significant interest to compare the computational cost between the different approaches to account for epistemic uncertainty. In particular, the number of inner FORM analysis required in each of the approaches indicates the additional computational effort to explicitly represent epistemic uncertainty. The first-order approximation of mean and standard deviation of the reliability index β, are 2.89 and 0.208 respectively. A single FORM analysis with additional computation of reliability sensitivities is sufficient to obtain these results. The nested reliability analysis is performed at 14 selected threshold values β_0 to obtain the PDF of the reliability index in Fig. 2-11. A total of 206 inner reliability analyses were required in this method. Notably, this number of FORM analysis is reduced significantly, to almost a third, if the MPP of the previous analysis is taken as the start point in the nested reliability analysis at the new threshold value. The sampling analysis is done with a total of 1000 FORM analyses to obtain the frequency diagram in Fig. 2-12b. However, the point estimate from this result has a coefficient of variation of 14% at 0.05 probability. Thus, a significantly higher number of FORM analyses are required for the accurate estimation of tail values of β. The fuzzy reliability index $\tilde{\beta}$, in Fig. 2-14 is obtained from a total of 5 FORM analyses at three α-levels, 0.0, 0.5, and 1.0. The triangular fuzzy reliability index is consistent with the PDF in Fig. 2-11; the values at 0.0 α-level, [2.43, 3.36] correspond to the values of the reliability index at ± 2 standard deviations.

2.7. CONCLUSIONS

In this chapter, the quantification and explicit representation of epistemic uncertainty is presented in a finite element reliability framework. The analysis methods in different approaches are developed and implemented. The probabilistic approach and the fuzzy randomness approach, based on the previous work by Der Kiureghian (1989) and Möller and Beer (2004), respectively, are extended to finite element reliability applications.

The probabilistic approach has the advantage of the Bayesian methodology to separate aleatory and epistemic components of the uncertainty and to assess distributions of the epistemic random variables. The confidence intervals on the reliability index are easily available from the probability distribution of β. Particularly, the importance measures obtained from a nested reliability analysis are invaluable in recognizing the highest contributors of the epistemic uncertainty. Such measures provide guidance when seeking additional data and improved models. The first-order estimate on the dispersion of β is available with the modest computational effort.

The fuzzy randomness approach lacks the theoretical background to interpret the fuzzy numbers, as well as established procedures to assess the fuzzy variables from statistical data. In addition, the interval analysis of the discretized fuzzy random variables fails to identify the important sources of epistemic uncertainty. However, the fuzzy randomness method is conceptually simple. Based on assumed membership function it provides an estimate of the dispersion of the reliability index at a lower computational cost than nested reliability analysis or sampling analysis. However, when the inner reliability problem is not amenable to FORM, thus leaving importance ranking of the aleatory random variables unavailable, this approach is limited to a small number of epistemic variables. In such an instance, the computationally costly α-level optimization must be employed to determine the bounds on the reliability index at each α-level.

In the present study, the epistemic analysis options are implemented in the OpenSees software. In the presented numerical example, the first-order second-moment approach, the nested reliability analysis, sampling, and the fuzzy randomness approach are employed to analyse a two-storey two-bay reinforced concrete structure with 104 aleatory and 58 epistemic random variables. The distribution on the reliability index has a mean of 2.89 while the coefficient of variation is 0.072, in a first-order approximation. The fuzzy reliability index is a triangular fuzzy number with characteristic values 2.43, 2.89, and 3.36.

In conclusion, while first-order second-moment approximation is the most computationally efficient method in indicating the dispersion of the reliability index, the nested reliability analysis provides the valuable importance measures and confidence bounds at a reasonable computational effort.

Table 2.1 Uncertainty modelling of the aleatory random variables of the R.C. structure

Parameter	Distribution	Mean	Coefficient of Variation	Correlation
Compressive strength of outer layer of concrete (10 r.v)*	Lognormal	28 N/mm^2	0.15	0.3
Compressive strain of outer layer of concrete (10 r.v.)**	Lognormal	0.002	0.15	0.3
Ultimate strength of outer layer of concrete	Deterministically zero	0.0	0.0	N/A
Ultimate strain of outer layer of concrete (10 r.v.)	Lognormal	0.006	0.15	0.3
Compressive strength of the core concrete (6 r.v.)*	Lognormal	36 N/mm^2	0.15	0.3
Compressive strain of the core concrete (6 r.v.)**	Lognormal	0.005	0.15	0.3
Ultimate strength of the core concrete (6 r.v.)	Lognormal	33 N/mm^2	0.15	0.3
Ultimate strain of the core concrete (6 r.v.)	Lognormal	0.02	0.15	0.3
Tensile strength of the reinforcement steel (10 r.v.)	Lognormal	420 N/mm^2	0.05	0.5
Young's modulus of the reinforcement steel (10 r.v.)	Lognormal	200000 N/mm^2	0.05	0.5
Second slope stiffness ratio of the reinforcement steel (10 r.v.)	Lognormal	0.02	0.10	0.5
Nodal coordinates (18 r.v.)	Normal	As is	σ = 20 mm	0.0
Lateral loads (2 r.v.)	Lognormal	700 KN	0.20	0.6

* Correlated with a coefficient of 0.6
** Correlated with a coefficient of 0.6

Table 2.2 Uncertainty modelling of the epistemic random variables

Parameter	Distribution	Mean	Coefficient of Variation
Mean of compressive strength of outer layer of concrete (1 r.v)	Lognormal	28 N/mm^2	0.04
Standard deviation of compressive strength of outer layer of concrete (1 r.v)	Lognormal	4.2 N/mm^2	0.04
Mean of compressive strain of outer layer of concrete (1 r.v.)	Lognormal	0.002	0.04
Standard deviation of compressive strain of outer layer of concrete (1 r.v.)	Lognormal	0.0003	0.04
Mean of ultimate strain of outer layer of concrete (1 r.v.)	Lognormal	0.006	0.04
Standard deviation of ultimate strain of outer layer of concrete (1 r.v.)	Lognormal	0.0009	0.04

Mean of compressive strength of the core concrete (1 r.v.)	Lognormal	36 N/mm^2	0.04
Standard deviation of compressive strength of the core concrete (1 r.v.)	Lognormal	5.4 N/mm^2	0.04
Mean of compressive strain of the core concrete (1 r.v.)	Lognormal	0.005	0.04
Standard deviation of compressive strain of the core concrete (1 r.v.)	Lognormal	0.00075	0.04
Mean of ultimate strength of the core concrete (1 r.v.)	Lognormal	33 N/mm^2	0.04
Standard deviation of ultimate strength of the core concrete (1 r.v.)	Lognormal	4.95 N/mm^2	0.04
Mean of ultimate strain of the core concrete (1 r.v.)	Lognormal	0.02	0.04
Standard deviation of ultimate strain of the core concrete (1 r.v.)	Lognormal	0.003	0.04
Mean of tensile strength of the reinforcement steel (1 r.v.)	Lognormal	420 N/mm^2	0.01
Standard deviation of tensile strength of the reinforcement steel (1 r.v.)	Lognormal	21 N/mm^2	0.01
Mean of Young's modulus of the reinforcement steel (1 r.v.)	Lognormal	200000 N/mm^2	0.01
Standard deviation of Young's modulus of the reinforcement steel (1 r.v.)	Lognormal	10000 N/mm^2	0.01
Mean of second slope stiffness ratio of the reinforcement steel (1 r.v.)	Lognormal	0.02	0.02
Standard deviation of second slope stiffness ratio of the reinforcement steel (1 r.v.)	Lognormal	0.002	0.02
Mean of nodal coordinates (18 r.v.)	Uniform	As is	σ = 5 mm
Standard deviation of nodal coordinates (18 r.v.)	Uniform	20 mm	σ = 1 mm
Mean of lateral loads (1 r.v.)	Lognormal	700 KN	0.05
Standard deviation of lateral loads (1 r.v.)	Lognormal	140 KN	0.05

Table 2.3: Importance ranking of epistemic random variables

Rank	Epistemic random variable	Importance measure
1	Mean of the lateral loads	0.706635
2	Standard deviation of the lateral loads	0.606378
3	Mean of the compressive stress of the cover concrete	0.314150
4	Mean of the elastic modulus of reinforcement steel	0.117704
5	Mean of the compressive stress of the core concrete	0.079026
6	Mean of the compressive strain of the core concrete	0.058290
7	Mean of the compressive strain of the cover concrete	0.053300
8	Mean of the tensile strength of the reinforcement steel	0.052702
9	Mean of the ultimate compressive strain of the cover concrete	0.034334
10	Mean of the horizontal nodal coordinate of node 4	0.034331

Table 2.4: Uncertainty modelling of the fuzzy random variables

Parameter	α-level		
	1.0	0.0	
Mean of compressive strength of outer layer of concrete (10 r.v)	28 N/mm^2	26.88 N/mm^2	29.12 N/mm^2
Standard deviation of compressive strength of outer layer of concrete (10 r.v)	4.2 N/mm^2	4.03 N/mm^2	4.37 N/mm^2
Mean of compressive strain of outer layer of concrete (10 r.v.)	0.002	1.92 x 10^{-3}	2.08 x 10^{-3}
Standard deviation of compressive strain of outer layer of concrete (10 r.v.)	0.0003	0.29 x 10^{-3}	0.31 x 10^{-3}
Mean of ultimate strain of outer layer of concrete (10 r.v.)	0.006	5.76 x 10^{-3}	6.24 x 10^{-3}
Standard deviation of ultimate strain of outer layer of concrete (10 r.v.)	0.0009	0.86 x 10^{-3}	0.94 x 10^{-3}
Mean of compressive strength of the core concrete (6 r.v.)	36 N/mm^2	34.56 N/mm^2	37.44 N/mm^2
Standard deviation of compressive strength of the core concrete (6 r.v.)	5.4 N/mm^2	5.18 N/mm^2	5.62 N/mm^2
Mean of compressive strain of the core concrete (6 r.v.)	0.005	4.80 x 10^{-3}	5.20 x 10^{-3}
Standard deviation of compressive strain of the core concrete (6 r.v.)	0.00075	0.72 x 10^{-3}	0.78 x 10^{-3}
Mean of ultimate strength of the core concrete (6 r.v.)	33 N/mm^2	31.68 N/mm^2	34.32 N/mm^2
Standard deviation of ultimate strength of the core concrete (6 r.v.)	4.95 N/mm^2	4.75 N/mm^2	5.15 N/mm^2
Mean of ultimate strain of the core concrete (6 r.v.)	0.02	19.2 x 10^{-3}	20.8 x 10^{-3}
Standard deviation of ultimate strain of the core concrete (6 r.v.)	0.003	2.88 x 10^{-3}	3.12 x 10^{-3}
Mean of tensile strength of the reinforcement steel (10 r.v.)	420 N/mm^2	415.80 N/mm^2	424.20 N/mm^2
Standard deviation of tensile strength of the reinforcement steel (10 r.v.)	21 N/mm^2	20.79 N/mm^2	21.21 N/mm^2
Mean of Young's modulus of the reinforcement steel (10 r.v.)	200000 N/mm^2	198000 N/mm^2	202000 N/mm^2
Standard deviation of Young's modulus of the reinforcement steel (10 r.v.)	10000 N/mm^2	9900 N/mm^2	10100 N/mm^2
Mean of second slope stiffness ratio of the reinforcement steel (10 r.v.)	0.02	19.6 x 10^{-3}	20.4 x 10^{-3}
Standard deviation of second slope stiffness ratio of the reinforcement steel (10 r.v.)	0.002	1.96 x 10^{-3}	2.04 x 10^{-3}
Mean of nodal coordinates (18 r.v.)	As is	- 5mm	+5mm
Standard deviation of nodal coordinates (18 r.v.)	20 mm	19 mm	21 mm
Mean of lateral loads (2 r.v.)	700 KN	665 KN	735 KN
Standard deviation of lateral loads (2 r.v.)	140 KN	133 KN	147 KN

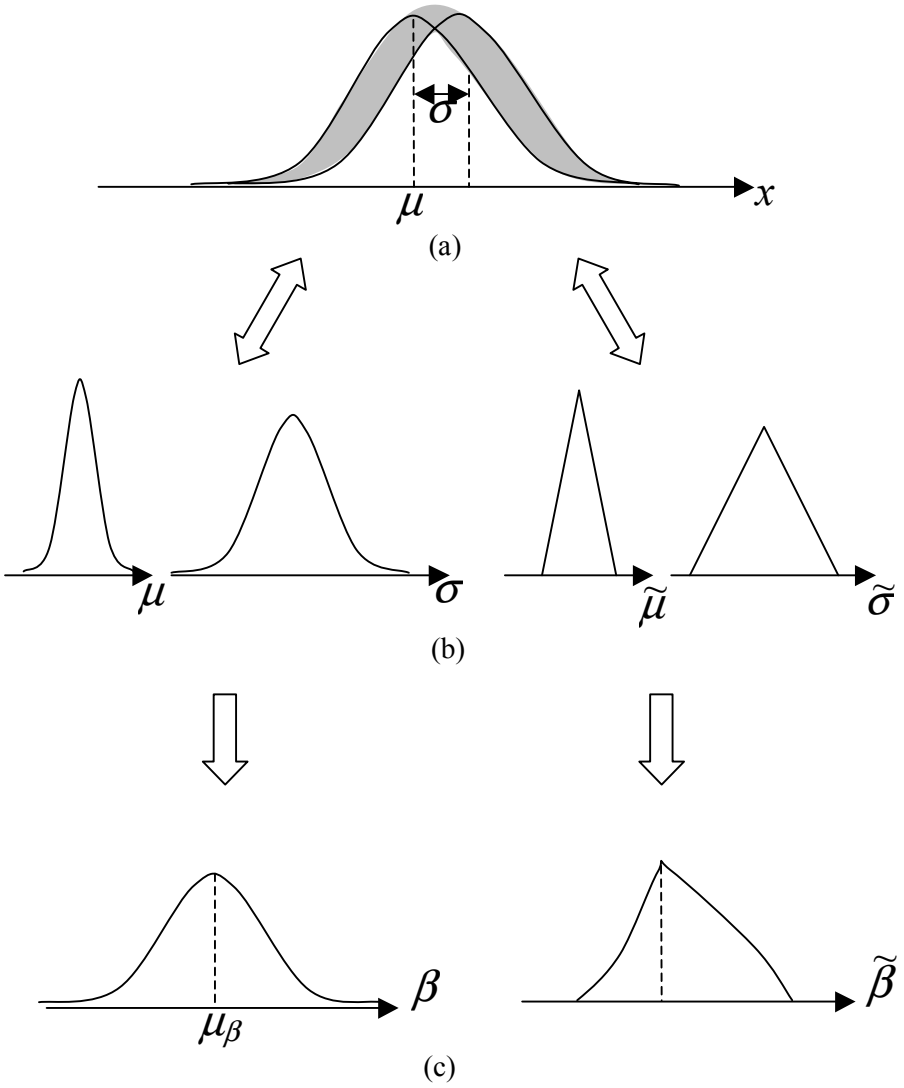

Figure 2.1: (a) Uncertainty in the distribution of x due to uncertain parameters μ and σ; (b) Uncertainty representation of the mean μ and the standard deviation σ; (c) Uncertainty representation of the reliability index β

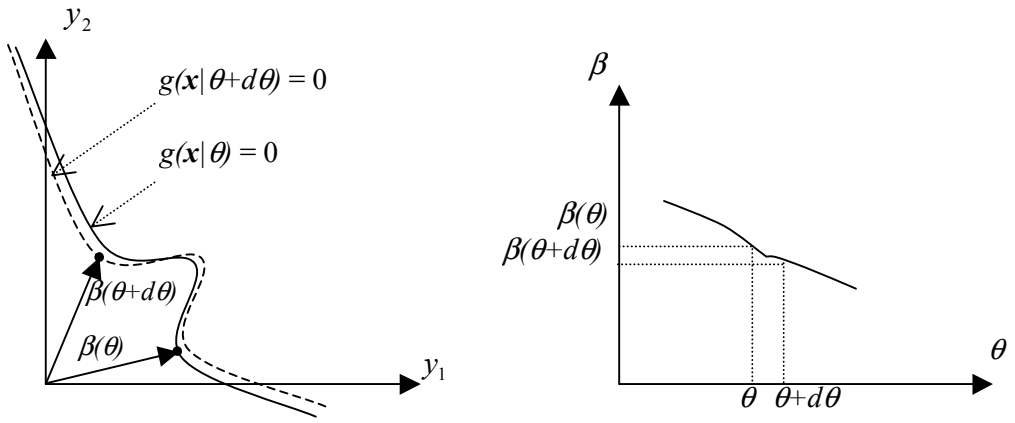

Figure 2.2 : (a) Limit-state surface g=0 for different realizations of an epistemic random variable θ ; (b) Kink in the function β(θ), resulting in discontinuity in the derivative

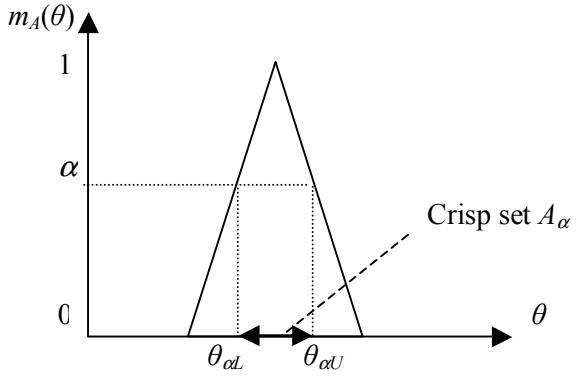

Figure 2.3: Membership function of a fuzzy number

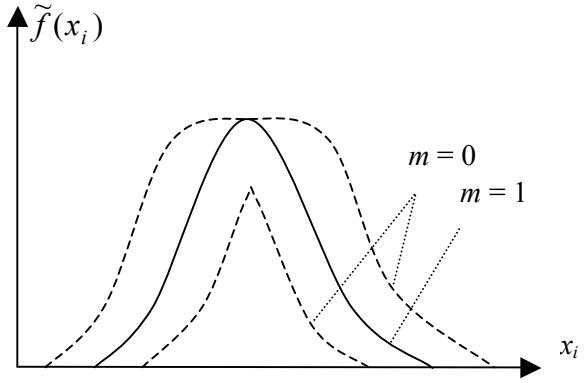

Figure 2.4: Fuzzy probability density function

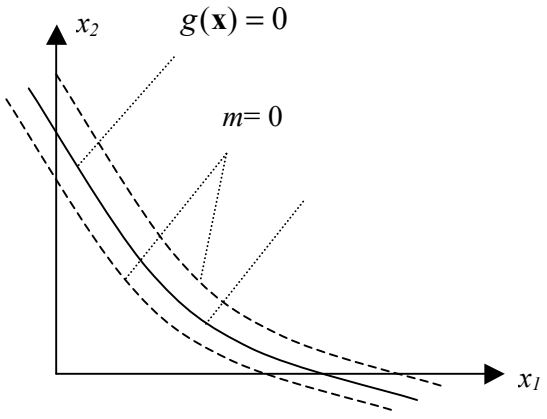

Figure 2.5: Fuzzy limit state surface

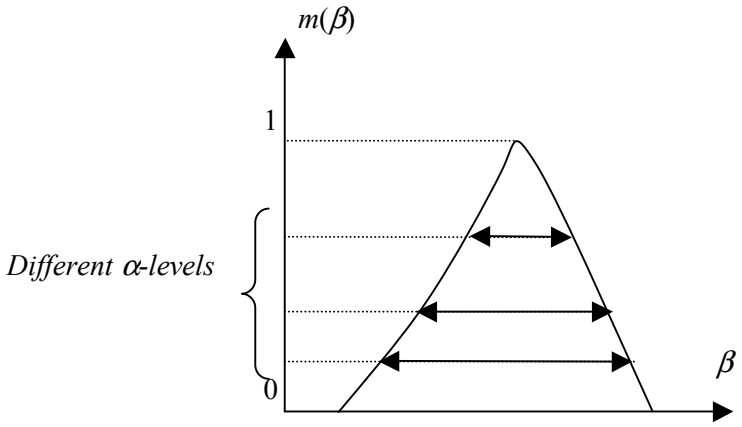

Figure 2.6: Fuzzy reliability index

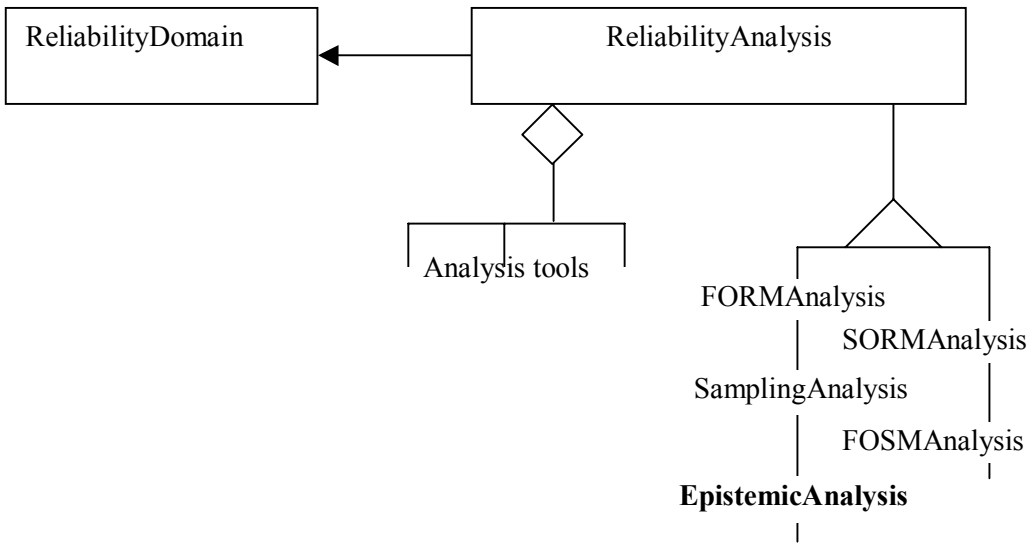

Figure 2.7: Software architecture of the reliability module in OpenSees

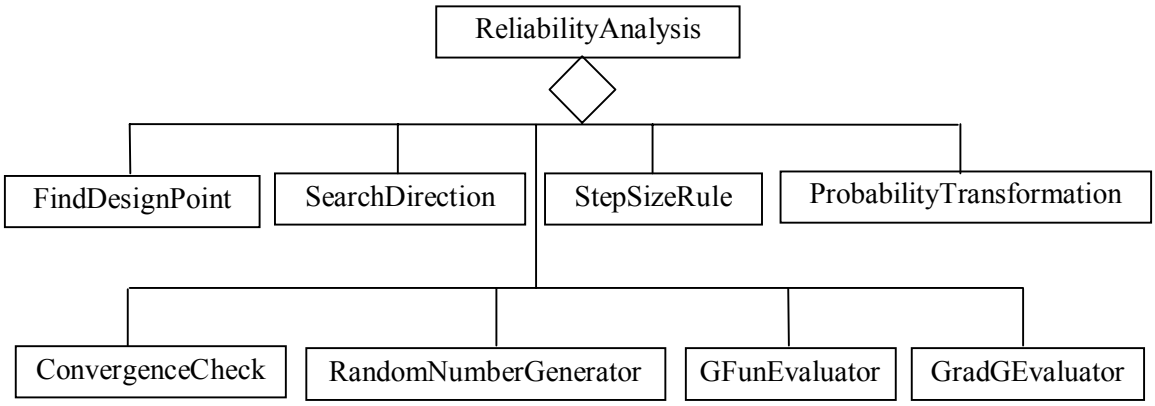

Figure 2.8: Selected base classes in the framework of reliability analysis tools

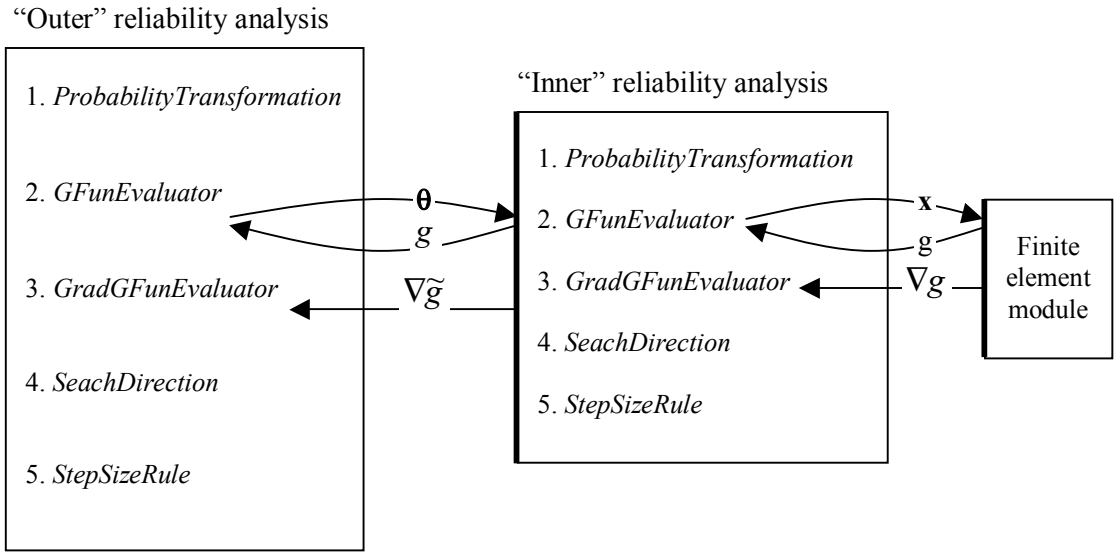

Figure 2.9: Selected reliability analysis tools utilized in the nested reliability analysis

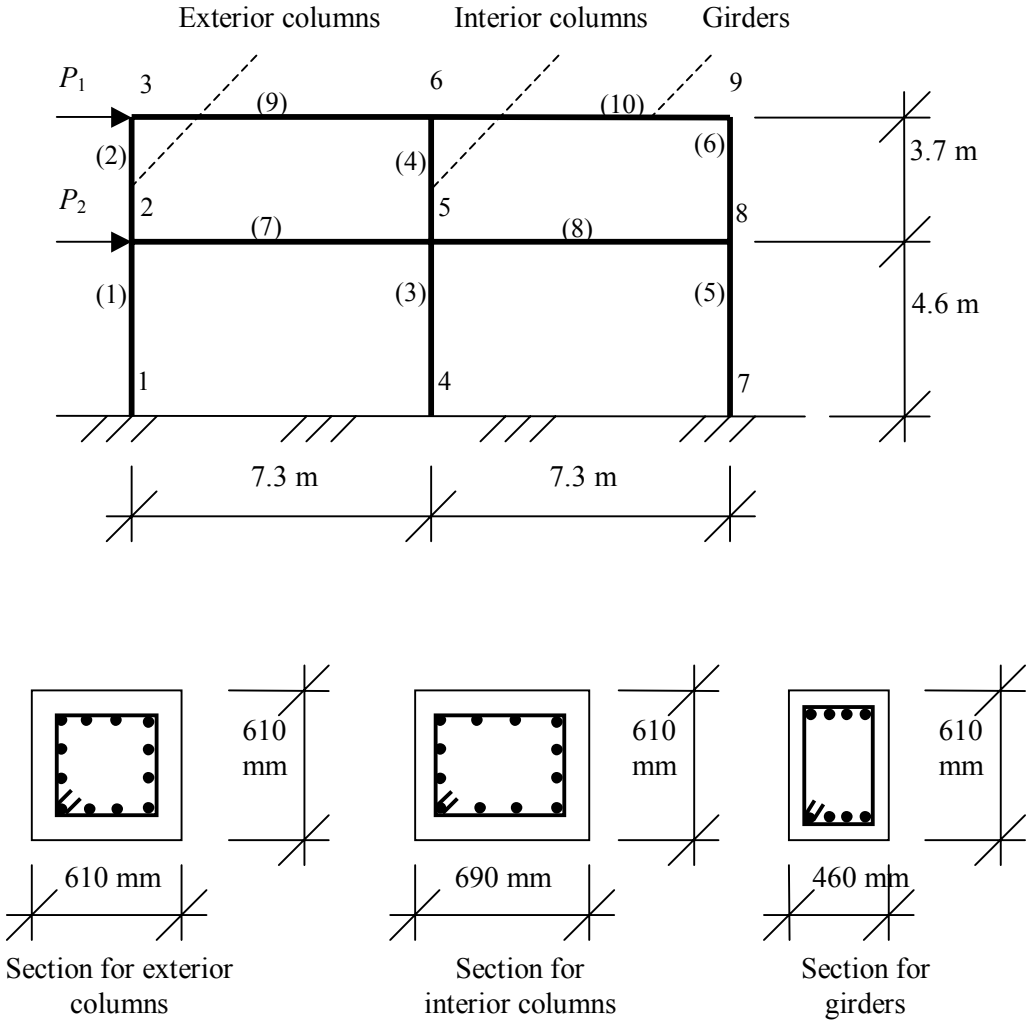

Figure 2.10: Two-storey two-bay reinforced concrete structure. Node numbers and element numbers (in parenthesis) are shown.

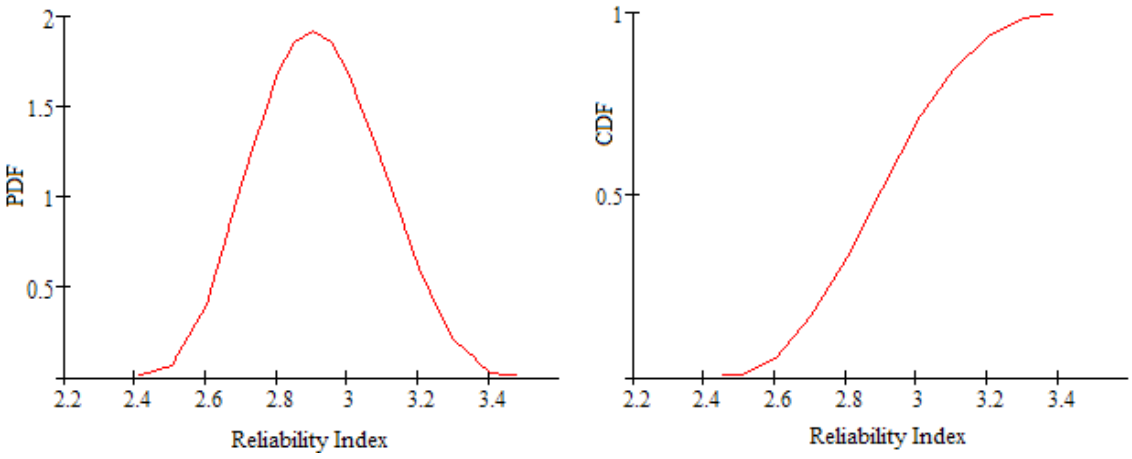

(a) (b)

Figure 2.11: (a) Probability density function for the reliability index; (b) Cumulative distribution function for the reliability index

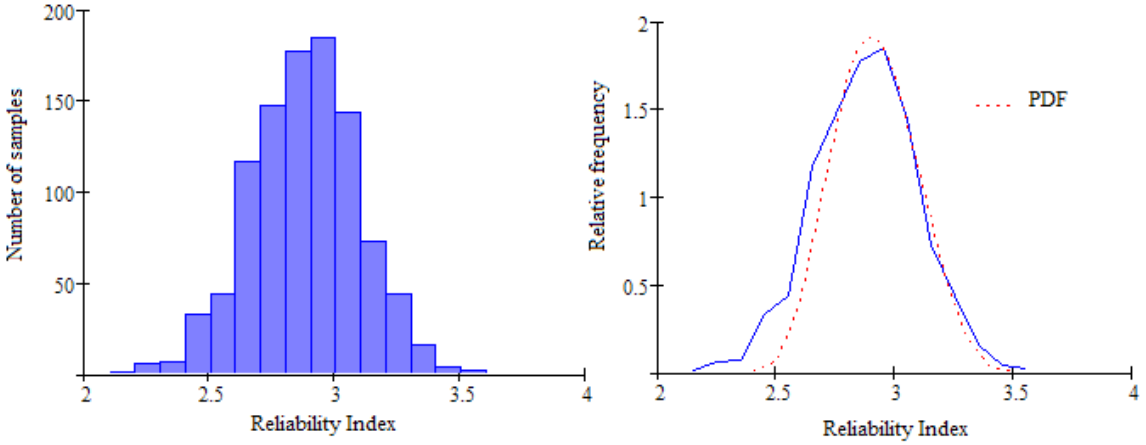

(a) Histogram (b) Relative frequency diagram

Figure 2.12: Results from sampling analysis

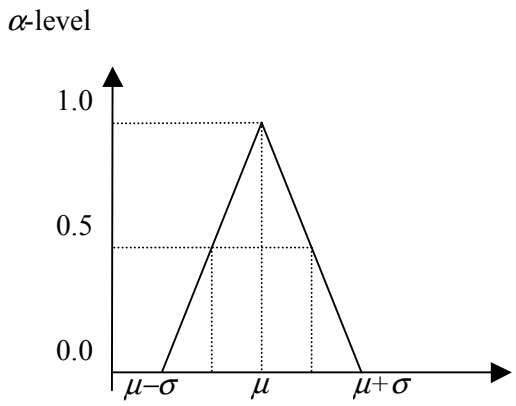

Figure 2.13: Membership function for fuzzy numbers versus mean and standard deviation of the corresponding random variable.

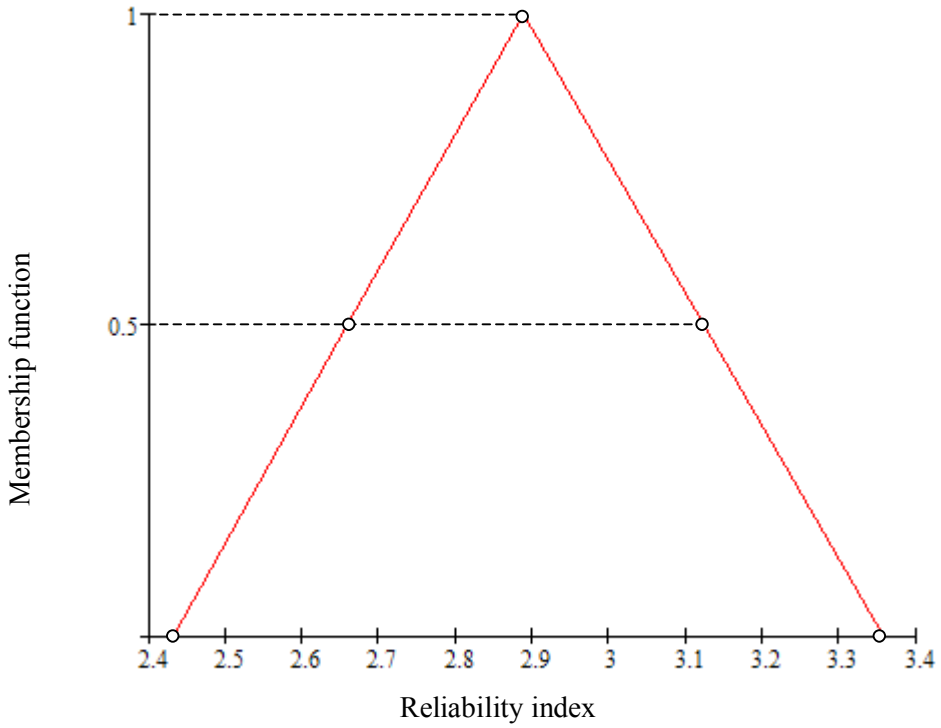

Figure 2.14: Fuzzy reliability index from analysis of reinforced concrete structure

REFERENCES

Ang, A. H-S. (2004), "Modeling and analysis of uncertainties for risk-informed decisions in engineering – with application to bridges," *Proceedings of Second International Conference on Bridge Maintenance, Safety and Management, IABMAS'04*, Kyoto, Japan

Ang, A. H-S. and Tang, W.H. (1975), *Probability concepts in engineering planning and design: vol.1*, Wiley, New York.

Ayyub, B.M. (2004), "From dissecting ignorance to solving algebraic problems," *Reliability Engineering and System Safety*, 85(1-3), 223-238

Bebamzadeh, A. and Haukaas, T. (2004), "Accounting for uncertain model and analysis errors in nonlinear finite element analysis," *Proceedings of Ninth ASCE Specialty Conference on Probabilistic Mechanics and Structural Reliability*, Albuquerque, New Mexico

Berleant, D. and Zhang, J. (2004), "Representation and problem solving with Distribution Envelope Determination (DEnv)," *Reliability Engineering and System Safety*, 85(1-3), 153-168

Bernardini, A. (1999), "What are the Random and Fuzzy Sets and How to Use them for Uncertainty Modelling in Engineering Systems?," *Whys and Hows in Uncertainty Modelling: Probability, Fuzziness and Anti-Optimization*, Ed. I. Elishakoff, Springer Wien New York

Ben-Haim, Y. (2004), "Uncertainty, probability and information-gaps," *Reliability Engineering and System Safety*, 85(1-3), 249-266

Bjerager, P. and Krenk, S. (1989), "Parameter sensitivity in first order reliability theory," *Journal of Engineering Mechanics*, 115(7), 1577-1582

Box, G.E.P. and Tiao, G.C. (1973), *Bayesian Inference in Statistical Analysis*, Wiley, New York

Chou, K.C. and Yuan, J. (1993), "Fuzzy-Bayesian approach to reliability of existing structures," *Journal of Structural Engineering*, 119(11), 3276-3290

de Cooman, G. and Troffaes, M.C.M (2004), "Coherent lower previsions in systems modeling: products and aggregation rules," *Reliability Engineering and System Safety*, 85(1-3), 113-134

Der Kiureghian, A. (1989), "Measures of structural safety under imperfect states of knowledge," *Journal of Structural Engineering*, 115(5), 1119-1140

Der Kiureghian, A. and Taylor, R. L. (1983), "Numerical methods in structural

Reliability," *Proceedings of the Fourth International Conference on Applications of Statistics and Probability in Civil Engineering, ICASP4*, Florence, Italy

Der Kiureghian, A. and Zhang, Y. (1999), "Space-variant finite element reliability analysis," *Computer Methods in Applied Mechanics and Engineering*, 168(1-4), 173-183

Ditlevsen, O. (1983), "Fundamental postulate in structural safety," *Journal of Engineering Mechanics*, 109(4), 1096-1102

Elishakoff, I. (1999), "Are Probabilistic and Anti-Optimization Approaches Compatible?," *Whys and Hows in Uncertainty Modelling: Probability, Fuzziness and Anti-Optimization*, Ed. Elishakoff, Springer Wien New York

Frier, C. and Sorensen, J. (2003), "Stochastic finite element analysis of non-linear structures modelled by plasticity theory," *Proceedings of the Ninth International Conference on Applications of Statistics and Probability in Civil Engineering,ICASP9*, San Francisco, California

Gutierrez, M., Carmeliet, J. and de Borst, R. (1994), "Finite element reliability methods using Diana," *Diana Computational Mechanics 1994*, Eds: G.M.A. Kusters and M.A.N. Hendriks

Hacking, I. (1975), *The Emergence of Probability: A philosophical study of early ideas about probability, induction and statistical inference*, Cambridge University Press, London, New York

Haukaas, T. and Der Kiureghian, A. (2004), *Finite Element Reliability and Sensitivity Methods for Performance-Based Engineering*, Report no. PEER 2003/14, Pacific Earthquake Engineering Research Center, University of California, Berkeley

Haukaas, T. and Der Kiureghian, A. (2005), "Parameter sensitivity and importance measures in nonlinear finite element reliability analysis," *Journal of Engineering Mechanics*, 131(10), 1013-1026

Haldar, A. and Mahadevan, S. (2000), *Reliability Assessment Using Stochastic Finite Element Analysis,* John Wiley and Sons, New York

Hall, J.W. and Lawry, J. (2003), "Fuzzy label methods for constructing imprecise limit state functions," *Structural Safety*, 25(4), 317-341

Hohenbichler, M. and Rackwitz, R. (1986), "Sensitivity and importance measures in structural reliability," *Civil Engineering Systems*, 3(4), 203-209

Hora, S.C. (1996), "Aleatory and epistemic uncertainty in probability elicitation with an example from hazardous waste management," *Reliability Engineering and System Safety*, 54(2-3), 217-223

Imai, K. and Frangopol, D. M. (2000), "Geometrically nonlinear finite element reliability analysis of structural systems, i: theory ii: applications," *Computers and Structures*, 7(6), 677-709

Körner, R. (1997), "On the variance of fuzzy random variables," *Fuzzy Sets and Systems*, 92(1), 83-93

Kozine, I.O. and Utkin, L.V. (2004), "An approach to combining unreliable pieces of evidence and their propagation in system response analysis," *Reliability Engineering and System Safety*, 85(1-3), 103-112

Krätschmer, V. (2001), "A unified approach to fuzzy random variables," *Fuzzy Sets and Systems*, 123(1), 1-9

Langley, R.S. (2000), "Unified approach to probabilistic and possibilistic analysis of uncertain systems," *Journal of Engineering Mechanics*, 126(11), 1163-1172

Lee, C-B. and Park, J-W. (1997), "Reliability analysis based on fuzzy-Bayesian approach," *Seventh International Conference on Computing in Civil and Building Engineering*, Seoul, South Korea.

Liu, P-L. and Der Kiureghian, A. (1986), "Multivariate distribution models with prescribed marginals and covariances," *Probabilistic Engineering Mechanics*, 1(2), 105-112

Liu, P-L. and Der Kiureghian, A. (1991), "Finite element reliability of geometrically nonlinear uncertain structures," *Journal of Engineering Mechanics*, 17(8), 1806-1825

McWilliam, S. (2001), "Anti-optimization of uncertain structures using interval analysis," *Computers and Structures,* 79(4), 421-430

Möller, B. and Beer, M. (2004), *Fuzzy Randomness: Uncertainty in civil engineering and computational mechanics*, Springer, Berlin, New York

O'Hagan, A. and Oakley, J.E. (2004), "Probability is perfect, but we can't elicit it perfectly," *Reliability Engineering and System Safety*, 85(1-3), 239-248

Parry, G.W. (1996), "The characterization of uncertainty in probabilistic risk assessments of complex systems," *Reliability Engineering and System Safety*, 54(2-3), 119-126

Rao, S.S. and Berke, L. (1996), "Analysis of uncertain structural systems using interval analysis," *37th AIAA/ASME/ASCE/AHS/ASC Structures, Structural Dynamics, and Materials Conference: A Collection of Technical Papers*, Salt Lake City, Utah

Sudret, B. and Der Kiureghian, A. (2000), *Stochastic Finite Element Methods and Reliability: A State-of-the-Art Report*, Report No. UCB/SEMM-2000/08, Department of Civil and Environmental Engineering, University of California, Berkeley

Taheri, S.M. and Behboodian, J. (2001), "A Bayesian approach to fuzzy hypothesis testing," *Fuzzy Sets and Systems*, 123(1), 39-48

Thacker, B.H., Riha, D.S., Millwater, H.R. and Enright, M.P. (2001), "Errors and Uncertainties in Probabilistic Engineering Analysis," *American Institute of Aeronautics and Astronautics*, AIAA 123

Vick, S.G. (2002), *Degrees of Belief: Subjective probability and engineering judgment*, ASCE Press, Virginia

Winkler, S.C. (1996), "Uncertainty in probabilistic risk assessment," *Reliability Engineering and System Safety*, 54(2-3), 127-132

Zhang, Y. and Der Kiureghian, A. (1997), *Finite Element Reliability Methods for Inelastic Structures*, Report No. UCB/SEMM-97/05, Department of Civil and Environmental Engineering, University of California, Berkeley

Chapter 3. FEASIBILITY OF FORM - STATICS[1]

3.1. INTRODUCTION

The primary objective in this chapter is to aid the practicing engineer who intends to make reliability assessments based on sophisticated numerical models. An example of this type of analysis is the merger of finite element (FE) analysis and reliability computations to obtain the probability of collapse or damage for structures subjected to extreme loads (e.g., Ching *et al*. 2005). In such applications, limit-states that define the event(s) of interest are cast in terms of response quantities from the FE analysis. Compared with traditional reliability analysis, in which explicit algebraic expressions were utilized to defined failure, this poses unique challenges for the reliability algorithms. A goal in this study is to highlight the acceptable and unacceptable problem formulations and to expose potential pitfalls and remedies. The target audience for the work is the engineer who already utilizes numerical models to predict structural performance, and who now faces the task of accounting for uncertainties. In other words, the study is intended to foster increased and prudent utilization of reliability methods in engineering practice. When merging reliability and FE analysis, it is argued that it is imperative for the analyst to recognize the problem definitions that are either infeasible or have potential for substantial errors.

This work may be viewed as an appraisal of the first-order reliability method (FORM) applied to FE-based limit-state function. The reason for the focus on FORM is its appealing efficiency and accuracy properties. To obtain reasonably accurate probability estimates, FORM requires 5 to 10 evaluations of the limit-state function, and its derivative with respect to the random variables. In fact, it is argued herein that FORM provides the best balance between accuracy and computational cost amongst the many reliability

[1] A version of this chapter has been submitted for publication. Koduru, S.D. and Haukaas, T. "Feasibility of FORM in finite element reliability anlaysis: Part I – Statics."

methods that are available for FE-based applications. The questions related to the accuracy of the results and potential difficulties are addressed by this chapter.

As mentioned above, the feasibility and accuracy of FORM has traditionally been studied in the context of explicit limit-state functions. For example, Fiessler *et al*. (1979) investigated the accuracy of FORM in the presence of nonlinear limit-state surface with explicit limit-state functions. Similar investigations on the accuracy of FORM are found in Ditlevsen and Madsen (1996), Rackwitz (2001) and others. Der Kiureghian and Dakessian (1998) illustrated the methods to identify multiple design points by means of explicit limit-state functions. Zhao and Ono (1999) and Qin *et al*. (2006) explored the effect of probability distribution type, probability transformation methods, and the number of random variables on the accuracy of the FORM by employing explicit limit-state functions. Recently, Yang *et al*. (2006) studied the convergence of FORM analysis in the presence of strong nonlinearities in the limit-state function.

The utilization of FE models in reliability applications has rapidly increased in the academic community in recent decades. A partial list of contributions to the FE-based reliability methods includes those by Der Kiureghian and Taylor (1983), Liu and Der Kiureghian (1991), Gutierrez *et al*. (1994), Zhang and Der Kiureghian (1997), Der Kiureghian and Zhang (1999), Sudret and Der Kiureghian (2000), Imai and Frangopol (2000), Haldar and Mahadevan (2000), Frier and Sorensen (2003), and Haukaas and Der Kiureghian (2004). The term "finite element reliability analysis" is employed to characterize the methodology. The objective in this type of analysis is essentially to compute the probability of rare response events, which are defined in terms of limit-state functions. In contrast, "stochastic finite element methods" focuses on the computation of the probability distribution of the responses, with less focus on the small tail probabilities. Of the two methodologies, only the finite element reliability approach is under consideration in this chapter.

It is noted that the use of FE-based reliability analysis has been mostly limited to the academic community. It is an objective in this work to facilitate an increased use of the methodology in engineering practice by providing a "roadmap" of the various problem formulations. As described in this chapter, the

success of the FORM analysis depends upon several conditions, including a smooth (to be defined shortly) and relatively linear limit-state function. These conditions naturally raise questions for an analyst who is faced with an FE-based reliability analysis. For example, are the limit-state functions associated with linear FE analysis always linear? What is the degree of nonlinearity of the limit-state function for different problem formulations? What is the effect of numerical noise from the FE analysis? Which limit-state function problem formulations are impractical? These and other aspects of FE-based FORM analysis are addressed in this study, for static problems. An important instrument to answer many of these questions is a novel visualization tool that is available in the OpenSees software (McKenna *et al*. 2004) utilized in this study. In particular, the limit-state function in the space of random variables is visualized to reveal potential difficulties. A number of case studies are conducted, in which the FE models vary from simple problems to complex problems that are encountered in "real" applications.

The scope of this study is limited to issues that pertain directly to FE-based analysis. Consequently, the study does not include the effect of the probability transformation when non-normal random variables are utilized. Furthermore, only problems with one limit-state function is considered; not system reliability formulations that are characterized by multiple limit-states. However, this does not exclude the "space variant reliability problem" that appears when the analyst seeks the probability that a response exceed a threshold anywhere in the FE model. The present study is accompanied by Chapter 4 that addresses questions and presents new developments for the fundamentally different dynamic problem. This renders the topic of static cyclic loading outside the scope of the present paper.

3.2. CONDITIONS FOR APPLICABILITY OF FORM

In order to appreciate the potential challenges in the merger of FORM and FE analysis, consider first the fundamental reliability problem with one limit-state function (Ditlevsen and Madsen 1996)

$$p = \int_{g(\mathbf{x})\le 0} \cdots \int f(\mathbf{x})\mathbf{dx} \tag{3-1}$$

where p is the probability of a response event; $\mathbf{x}$ is a vector of random variables that typically include geometry, material and load parameters; $f(\mathbf{x})$ is the joint probability density function for the random variables; and $g(\mathbf{x})$ is the limit-state function, which takes on a negative value for the realizations of $\mathbf{x}$ that result in the response event. Effectively, Eq. (3-1) represents the integration of the probability density $f(\mathbf{x})$ over the domain in the $\mathbf{x}$-space where g is negative. The evaluation of this integral is the primary objective of all structural reliability methods.

The FE analysis enters the reliability problem through the definition of the limit-state function g. A typical, but not all-encompassing, limit-state function is of the form

$$g(\mathbf{x}) = u(\mathbf{x}) - u_o \tag{3-2}$$

where $u(\mathbf{x})$ is a response quantity from FE analysis, which clearly depends upon the realization of the random variables that are input to the analysis, and u_o is a response threshold. Effectively, a reliability analysis with the limit-state function in Eq. (3-2) results in the probability that the response $u(\mathbf{x})$ is less than or equal to the threshold u_o.

The reliability problem in Eq. (3-1) cannot be solved analytically in FE-based reliability analysis, where $u(\mathbf{x})$ is not a simple explicit function of $\mathbf{x}$. A number of reliability methods have been developed to address the problem. These include the first and second-order reliability methods, sampling methods, and response surface methods (Ditlevsen and Madsen 1996). All such reliability methods require repeated evaluation of the limit-state function and thus, repeated FE analyses for different realizations of the random variables $\mathbf{x}$. In view of the computational cost associated with each FE analysis, it is highly beneficial to curtail the number of evaluations of the limit-state function. In fact, this concern renders certain reliability methods unappealing, such as most sampling schemes. An appealing alternative that balances accuracy and computational cost is available in FORM. FORM also produces interesting by-products of the analysis, including the most likely failure scenario and importance-ranking of the random variables.

In FORM, the reliability problem is solved by approximating the integration boundary $g(\mathbf{x})=0$, denoted the "limit-state surface," in Eq. (3-1) by a hyper-plane that is tangential to the limit-state surface at the point on the surface with highest probability density. Importantly, this approximation is made in the transformed space of uncorrelated standard normal random variables, $\mathbf{y}=T(\mathbf{x})$, where T denotes the probability transformation. Due to the rotational symmetry of the joint standard normal probability density function, $f(\mathbf{y})$, the point on the limit-state surface nearest to the origin is the point of highest probability density, known as "most probable failure point" or the "design point" (Ditlevsen and Madsen 1996). From above it is understood that finding the design point poses a constrained optimization problem, which reads

$$\mathbf{y}^* = \arg\min\{\|\mathbf{y}\| \mid g(\mathbf{y}) = 0\} \tag{3-3}$$

The minimum distance between the origin in the standard normal space and the design point is known as the FORM reliability index, β, which relates to the probability by (Hasofer and Lind 1973)

$$p \approx \Phi(-\beta) \tag{3-4}$$

where Φ is the standard normal cumulative distribution function.

The most efficient algorithms to solve Eq. (3-3) are gradient-based and thus, employ the gradient of the limit-state function, $\partial g/\partial \mathbf{y}$ in addition to the value of $g(\mathbf{y}(\mathbf{x}))$ in the search for the design point. Fig. 3-1 illustrates the key steps in this search. It is observed that the reliability module first performs the probability transformation to obtain the realization of the original random variables $\mathbf{x}_i$ from the trial point $\mathbf{y}_i$ in the standard normal space. This facilitates the evaluation of the limit-state function and its gradient. In this phase, the random variables are passed to the FE module, which in turn provides the response quantities, $u(\mathbf{x})$ and the gradient of the response, $\partial u/\partial \mathbf{x}_i$, which enter in the evaluation of the limit-state function $g(\mathbf{y}(\mathbf{x}))$ and its gradient $\partial g/\partial \mathbf{y}$. It is noted that the computation of the response and its derivatives – purposely shown in one box in the FE module in Fig. 3-1 – has been subject to extensive

research in recent decades. The "direct differentiation method" is particularly appealing, whereby response derivatives are computed alongside the ordinary FE response in one analysis (Zhang and Der Kiureghian 1993, Kleiber *et al*. 1997, Haukaas and Scott 2006). Consequently, it is unnecessary to repeat the FE analysis multiple times to obtain gradients by a finite difference formula. In summary, the dashed arrows in Fig. 3-1 illustrate the communication of realizations of the random variables into the FE module and the return of the needed response quantity/quantities. Finally, the reliability algorithm checks for the convergence of the search to the design point and, subsequently, it determines the search direction **d** and search step size *s*, unless convergence was achieved.

The potential difficulties with FORM that are addressed in this chapter for FE-based reliability analysis are divided into two categories. First, the execution of the algorithm in Fig. 3-1 may be hampered. Certain properties of FE-based limit-state functions may cause such problems, as described in the following. Second, even if a unique design point exists and is found, the approximation of the limit-state surface by a hyper-plane at this location, implied by Eq. (3-4), may be called into question. The left column in Fig. 3-2 displays the two criteria that must be satisfied to avoid difficulties on either of these two counts.

The first criterion is that the limit-state function is continuously differentiable; implying that the derivative with respect to all random variables must be continuous in the space of random variables. This is sometimes referred to as the smoothness criterion. A smooth limit-state function is necessary for the gradient-based search algorithms to succeed. When the limit-state function is formulated as an explicit algebraic expression in terms of the random variables, the potential presence of gradient discontinuity is readily detected by analytical differentiation. In the case of FE-based limit-state functions it may not be immediately obvious whether gradient discontinuities exist. There are several potential causes for violation of this criterion.

In the middle column of Fig. 3-2 the violations of the first criterion are separated into three groups; sudden yielding events in the material models, formulation of limit-state functions with maximum responses, and numerical noise from the FE analysis. The first of these is a common occurrence: many

material models for steel and concrete have a non-smooth force-deformation relationship. As demonstrated in the following, caution must be exercised when utilizing such constitutive relationships. The second violation of the smoothness criterion appears when the analyst inadvertently includes, e.g., the maximum stress anywhere in the FE model, in the limit-state function. The problem is that, for different realizations of the random variables the location of the maximum stress may jump to a different location. This sudden shift in the location causes gradient discontinuity. As mentioned before, this is termed the space-variant reliability problem. The third violation; numerical noise, can either be caused by too low tolerance limits in a nonlinear FE analysis or by round-off errors in the evaluation of the limit-state function. The aforementioned violations of the first criterion may lead to non-convergence when solving Eq. (3-3), as specified in the right column in Fig. 3-2. This is further visualized in the following case studies.

The second criterion for the applicability of FORM, listed in the left column in Fig. 3-2, is that the limit-state surface is linear or approximately linear. This is necessary to satisfy the hyper-plane assumptions inherent in Eq. (3-4). Formally, if the limit-state surface is not linear, the evaluation of Eq. (3-4) is an approximation. However, some nonlinearity is acceptable and will still yield excellent estimates of the probability. This is due to the exponential decay of the probability density away from the design point. On the other hand, dramatic nonlinearity in the limit-state surface is detrimental to the result. The middle column in Fig. 3-2 classifies three possible characteristics of the limit-state surface that violate the condition of approximate linearity. A limit-state surface may exhibit severe nonlinearity but may still be "well-behaved." For example, the limit-state surface may be approximately quadratic. Although this would facilitate the application of the second-order reliability method, a strong nonlinearity would lead to inaccurate probability estimates with FORM. This is indicated in the right column in Fig. 3-2. In contrast, the nonlinearity of the limit-state function may appear in the form of highly irregular shapes such as "waves" and "islands," as classified in the two lower boxes in the middle column of Fig. 3-2. Such behaviour of the limit-state surface could lead to convergence of the search algorithm to a local minimum

instead of the global design point implied by Eq. (3-3), as listed in the right column of Fig. 3-2. Under special circumstances, such as a symmetric limit-state surface, several global minima may be present. Clearly, this will lead to an inaccurate probability estimate from FORM.

For an analyst, it may be difficult to ascertain whether a limit-state function formulation satisfies the criteria discussed above. For this purpose, a combination of static and dynamic FE analysis with linear and nonlinear FE models is considered in this chapter and Chapter 4. Visualization of the limit-state function and the limit-state surface is carried out for a number of cases. At the end, a flow chart is provided to guide the analyst in the assessment of the feasibility of FORM.

3.3. LIMIT-STATE FUNCTIONS FOR STATIC FE ANALYSIS

Enumeration of all possible FE-based limit-state functions poses a challenging task. A pragmatic approach is adopted in this work, in which two viewpoints merged. The first viewpoint is that of an engineer who abide by the current code-oriented state-of-practice. From this viewpoint, particular limit-state functions are of interest, while others are impractical. Another viewpoint focuses on the responses and analysis types that are available from a state-of-the-art FE analysis. In the following, various limit-state functions are discussed and categorized with these two viewpoints in mind. Questions regarding the viability of the associated FORM reliability analysis are raised for each limit-state formulation. Subsequently, the questions are answered on the basis of detailed studies and enumerated findings presented later in this chapter.

3.3.1. Limit-state functions in traditional engineering; linear FE models

Consider traditional structural engineering, in which two issues are of primary concern: First, the capacity of the structural members is checked by determining the internal forces (e.g., stresses, bending moments). Second, the serviceability is checked by determining deformations (displacements and rotations). For the most common types of loading the structural analysis in this paradigm is carried out by means of linear models. That is, a proportional relationship exists between the external forces and any response quantity.

The utilization of reliability analysis under these circumstances implies an extension of the prescriptive code-oriented approach. While the code prescribes safety coefficients, a reliability analysis includes the actual probability distributions for loads and structural properties. Typical examples of limit-state function are

$$g(\mathbf{x}) = \frac{M(\mathbf{x})}{M_r} + \frac{P(\mathbf{x})}{P_r} - 1 \tag{3-5}$$

$$g(\mathbf{x}) = V(\mathbf{x}) - 0.1\lambda\phi_c\sqrt{f'_c}\,b_w d \tag{3-6}$$

$$g(\mathbf{x}) = u(\mathbf{x}) - \frac{l_n}{360} \tag{3-7}$$

Eq. (3-5) addresses the interaction of the axial tension and the bending moment of a structural steel column as specified by the Canadian steel design code (CISC-ICCA 2006). Effectively, this limit-state function provides the probability that the code criterion is satisfied. M_r and P_r are the moment resistance and the axial tensile resistance of the steel member, $M(\mathbf{x})$ and $P(\mathbf{x})$ represent the moments and the axial tensile forces on the member due to the applied loads. The limit-state function in Eq. (3-6) contains the shear resistance of a concrete section without the shear reinforcement, as specified by the Canadian concrete design code (CAC 2006). $V(\mathbf{x})$ denotes the shear force at a section due to the applied loads, λ and ϕ_c represent the resistance factors, f'_c represents the compressive strength of concrete, b_w and d represent the section dimensions of the member. Eq. (3-7) is a serviceability limit-state function that provides the probability that the short-term deflection of a flexural element, $u(\mathbf{x})$ is less than or equal a threshold value based on the member length, l_n as specified by the Canadian concrete design code (CAC 2006).

The viability of the above limit-state functions is now questioned along the previously established criteria in Fig. 3-2 for applicability of FORM. Is the limit-state function smooth? Is there detrimental numerical noise from the FE analysis? Is the limit-state surface linear? These questions are addressed in a detailed fashion in the subsequent case studies in this chapter. The case studies are performed with generic

displacement and stress limit-state functions to address the concerns that generally appear with the type of serviceability and ultimate limit-state functions that are exemplified in Eqs. (3-5), (3-6), and (3-7).

3.3.2. Limit-state functions in earthquake engineering; nonlinear FE models

An area of structural engineering in which sophisticated FE analyses has rapidly gained ground is earthquake engineering. Due to the expected nonlinear behaviour of the structure when subjected to strong ground motions, the traditional linear structural analysis is inadequate. It is now common for practicing engineers to carry out static FE analysis with both material nonlinearity and geometrical stiffness effects included. These are often referred to as pushover analysis, in which several objectives may be pursued. For example, in a displacement-control push-over analysis, the objectives of a designer may be to investigate a) the lateral load demands on particular members, b) inelastic deformations at particular sections, and c) lateral stability of the entire structure for a target lateral displacement. Examples of corresponding limit-state functions are

$$g(\mathbf{x}) = V(\mathbf{x}) - V_o \tag{3-8}$$

$$g(\mathbf{x}) = \theta(\mathbf{x}) - \theta_o \tag{3-9}$$

$$g(\mathbf{x}) = \delta(\mathbf{x}) - \delta_o \tag{3-10}$$

Eq. (3-8) is a limit-state function that seeks the probability that the shear force on a member, $V(\mathbf{x})$ is less than a threshold value of a pre-determined ultimate shear strength V_o. The limit-state function in Eq. (3-9) seeks the probability that the plastic rotation $\theta(\mathbf{x})$ of a specified member is less than the ultimate rotational capacity θ_o. Similarly, Eq. (3-10) is specified in terms of the global drift ratio $\delta(\mathbf{x})$, with threshold δ_o. Such global response measures are commonly employed as performance criteria for existing structures under earthquake loads (FEMA-356 2000).

A number of limit-state functions in the form of Eqs. (3-8), (3-9) and (3-10) are possible. Some are amenable to FORM, while others are not. To provide general observations, the following case studies are carried out with limit-state functions with generic displacement and stress responses.

3.4. CASE STUDIES

To expose the potential difficulties in FE-based FORM analysis, two FE models are utilized in this study. These are shown in Fig. 3-3. The single-degree-of-freedom (SDOF) model in Fig. 3-3a provides a simple problem that facilitates an isolated study of certain effects. Specifically, this model is a single structural element, thus avoiding any influence from global structural effects. As shown in Fig. 3-3a, only lateral loads are considered on this model. The other model is the two-bay, two-storey structure in Fig. 3-3b. This is a multi-degree-of-freedom (MDOF) system that includes effects in full-scale FE models. The loading includes gravity loads and lateral loads as shown in Fig. 3-3b. The characteristics of limit-state functions that contain responses from these FE models are subsequently presented, with both linear and nonlinear material models.

In the following, a number of analyses are carried out. The ensuing reliability results are presented in tables and the limit-state surfaces are visualized in plots. However, the interpretation and discussion of the results are not presented in this section. Instead, the significance of the observations is compiled in a subsequent section; categorized as practical findings.

3.4.1. Case 1: Linear finite element problems

Linear static analysis represents the conceptually simplest FE problems in which a linear system of equations is solved to obtain the structural response. Linear FE models are developed for the structures in Fig. 3-3 with elastic beam-column elements and linear elastic material models. The values of the input parameters and the random variables are presented in Table 3-1. All random variables are considered to be uncorrelated. Limit-state functions of the form in Eq. (3-2) are considered; that is, with a response and an associated threshold. As mentioned above, displacement and stress responses are considered. To

distinguish these two types of limit-state functions, the following notation is necessary: The generic displacement response is denoted u, while the generic stress response is denoted f. Then, for convenience, the associated limit-state functions are denoted $g(u)$ and $g(f)$, respectively.

For the SDOF case in Fig. 3-3a, the threshold values in the limit-state functions are 100 mm in $g(u)$ and 500 N/mm^2 in $g(f)$. In Fig. 3-4 the variation of both limit-state functions with respect to h and L is visualized. Next, an analysis is carried out to visualize the limit-state surface for $g(u)$ in the standard normal space. The combinations of P and E with L and h are considered for this visualization; see Fig. 3-5. Finally, reliability analyses are performed with FORM and mean-centered Monte Carlo sampling (MCS) for both limit-state functions. Table 3-2 summarizes the reliability results.

In the MDOF case, the response parameters in the limit-state functions are lateral displacement at the roof and the maximum axial stress in any member. The threshold value is 9 mm for the displacement and 700 N/mm^2 for the stress. The function $g(u)$ is visualized in Fig. 3-6 for variation of H_s, W, b_c and h_c. Visualization of the limit-state surface for $g(u)$ is carried out for h_c, b_c, H_s, and W in combination with the lateral load P, as shown in Fig. 3-7. In the case of $g(f)$, the limit-state surface is visualized for the combination of gravity load, G and lateral load P, as shown in Fig. 3-8. Similar to the SDOF case, reliability analyses are performed with FORM and MCS for both limit-state functions. The results are summarized in Table 3-2.

3.4.2. Case 2: Nonlinear finite element problems

Nonlinear static analysis is routinely performed in the context of performance based earthquake engineering. In this case, the material models include nonlinear stress-strain relationships which introduce nonlinearity in the load-deformation relationship of the structure. As the relationship between the applied loads and the structural response ceases to be linear, iterative algorithms are employed to solve for the nonlinear response. Fig. 3-9 shows the material models considered for the steel and concrete materials in this study. The concrete material has a parabolic stress-strain relationship until the stress reaches the compressive strength, f'_c. The loss of stiffness in the concrete beyond the maximum stress is modelled to

be piece-wise linear. The steel material model is considered to be bilinear. The material stiffness transitions from E to a fraction α of E when the stress increases beyond the yield stress, σ_y.

The reinforced concrete (RC) sections in this chapter are modelled as fibre-discretized cross-sections, which include individual uniaxial material models for confined concrete, unconfined concrete, and reinforcement steel fibre. This modelling captures the interaction between moment-curvature and axial stress-strain behaviour of the cross-section. The MDOF structure is modeled with RC sections, whereas the SDOF case is modeled with a steel section. The values of the input parameters and the random variables are presented in Table 3-3. Again, all random variables are considered to be uncorrelated.

For the SDOF case, the limit-state function is considered with lateral displacement and a threshold value of 100 mm. This limit-state function is visualized for variation in the geometry and material properties, as shown in Fig. 3-10. Subsequently, reliability analyses are performed with FORM and MCS, with results as shown in Table 3-4.

For the MDOF case, two limit-state functions are considered with lateral displacement at the roof and maximum axial stress, as in the linear case. The threshold values are 9 mm and 30 N/mm^2, respectively. It is selected to visualize the variation in $g(u)$ with respect to the material properties, as shown in Fig. 3-11. In Fig. 3-12, the behaviour of $g(u)$ is examined for variation in four parameters: the lateral load; the size of the load step; the value of the tolerance limits for convergence of the nonlinear analysis; and the number of fibres in the RC section of the center column of the bottom storey.

For the case of $g(f)$, the limit-state surface behaviour in the standard normal space is shown in Fig. 3-13. The limit-state surface is visualized for the combination of lateral load and the parameters b_c, h_c, f'_c, and ε_c. Reliability analyses are performed with FORM and MCS for the displacement limit-state function. The analysis parameters are considered at the values presented in Table 3-3. The reliability results are presented in Table 3-4.

3.5. INTERPRETATION AND DISCUSSION OF RESULTS

Previously in this chapter, questions have been raised regarding the applicability of FORM for several FE-based limit-state functions, and subsequently a number of analyses were carried out. In this section the analysis results are utilized to address the questions. Observations are drawn from the visualization plots of the limit-state functions/surfaces, and categorized into enumerated "findings." These findings may be employed by the analyst to judge whether a particular limit-state formulation carry the potential for difficulties or inaccuracies. Subsequently in this chapter, a flow chart is presented that allows the analyst to utilize the findings in a systematic manner to determine the feasibility of FORM. In the following, both potential pitfalls and possible solution strategies are discussed.

3.5.1. Finding 1: Linear FE models may result in nonlinear limit-state functions

It is observed in Fig. 3-4 that nonlinearity appears in the limit-state functions even when the FE model is linear. The reason is that the nonlinearity in the limit-state function is dependent on the relationship between the random variables and the response, rather than the load-displacement relationship of the FE model. In particular, for the SDOF case considered in Fig. 3-4, the stiffness is equal to $3EI/L^3$, where $I = h^4/12$. Hence, the relationship between the response and both h and L is nonlinear. This is what is observed in Figs. 3-4a and 3-4b. Conversely, the maximum axial stress in the cross-section is $6PL/h^3$. Hence, the nonlinear behaviour of $g(f)$ is seen for variation in h, in Fig. 3-4c. However, as expected, the limit-state function, $g(f)$, remains linear for variation in L, as observed in Fig. 3-4d.

The nonlinearity that is observed in Fig. 3-4 manifests itself also in the limit-state surface in Fig. 3-5. To further explain this nonlinearity, consider the limit-state surface: $3Eh^4/12L^3 = P/100$, for the displacement threshold 100 mm. The nonlinear relationship among the random variables explains the nonlinearity observed in the limit-state surface for the random variables P and h, and P and L, as seen in Figs. 3-5c and 3-5d. However, the nonlinearity of the limit-state surface is insignificant for the random variables E and h, and E and L as seen in Figs. 3-5a and 3-5b, although they exhibit nonlinear relationship above. Possible nonlinearity in this type of plots may become more pronounced if a different portion of the standard

normal space is considered. In other words, a greater standard deviation of the random variable could lead to lead to more visible nonlinearity within the selected plot boundaries. Such issues related to the probability transformation are, however, outside the scope of this chapter. It is concluded that even linear FE models may be associated with nonlinear limit-state surfaces, but that the degree of nonlinearity is typically not detrimental for the application of the FORM. This conclusion is further substantiated in the following.

3.5.2. Finding 2: The degree of nonlinearity is affected by the model fidelity

The interesting observation is now made that the nonlinearities observed above for the SDOF problem practically vanishes for the MDOF structure. Consider a comparison of the displacement limit-state function for the linear model of SDOF and MDOF. Fig. 3-4a shows the variation of $g(u)$ with respect to the cross-sectional dimension h for the SDOF case, while Figs. 3-6a and 3-6b shows the variation of $g(u)$ with respect to the cross-sectional dimensions b_c and h_c of the centre column of the MDOF structure. It is observed that the nonlinearity for the MDOF structure is significantly less than for the SDOF case. In fact, for the MDOF, the limit-state function is practically linear for the variation of the cross-section dimensions of the center column; see Figs. 3-6a and 3-6b. The comparison of the limit-state surface in the standard normal space in Fig. 3-5c for the SDOF with Figs. 3-7a and 3-7b for the MDOF structure confirms that the SDOF case suffers from a higher degree of nonlinearity.

The reason for the different behaviour of the SDOF and MDOF cases is the fact that the influence of the center column on the roof displacement is limited by the presence of other elements in the MDOF case. In effect, the limit-state function is fairly linear despite the nonlinear relationship between the depth of column and displacement response. One way to understand and detect this phenomenon is to consider the sensitivity of the response with respect to the random variables. The SDOF response is highly sensitive to the random variable h, as indicated in the importance ranking in Table 3-5. In contrast, the global MDOF response is less sensitive to the random variables b_c and h_c.

From the discussion in this subsection it is clear that the analyst can influence the degree of nonlinearity in the limit-state surface. Specifically, by increasing the model fidelity; e.g., refining the element mesh and employing different random variables in each element. The nonlinearity along each random variable axis will then be reduced. However, it is recognized that these random variables must be correlated, which would re-introduce the nonlinearity. It may also increase the computational cost.

3.5.3. Finding 3: Limit-state function with maximum response may cause non-convergence

The formulation of the limit-state function with envelope response parameters, such as the maximum response at any location in the structure, may result in non-convergence of the FORM analysis. As mentioned earlier, this is the space-variant reliability problem, wherein the location of the maximum response is unknown *a priori*. The non-convergence of the FORM analysis in space-variant problems is due to gradient discontinuities appearing in the limit-state function when the location of the maximum response suddenly shifts.

Consider Fig. 3-8 where the response parameter in the limit-state function is the maximum stress. For the linear MDOF model with the lateral and gravity loads as random variables, the stress is monitored in all the columns. At the mean values of the loads, the maximum stress occurs in the center column in the bottom storey. However, for a certain realization of lateral and gravity loads, the outer left column experiences the maximum stress among all the elements. The sudden change in the location of the maximum stress from the center column to the outer column causes a discontinuity in the gradient of the limit-state surface, as shown in Fig. 3-8. Similarly, consider Fig. 3-13 where the response parameter is the maximum stress in the nonlinear MDOF model. The limit-state surface in the standard normal space exhibits gradient discontinuity when the location of the maximum stress abruptly changes from the center column to the outer column, as shown in Figs. 3-13a, 3-13c, and 3-13d. Notably, the change in location of the maximum stress is due to the change in the realization of the material and the section properties. As the stiffness of the center column varies, the distribution of lateral load changes, which in turn causes the variation in the maximum stress location. It is concluded that the formulation of limit-state functions with

maximum responses may cause gradient discontinuities in the limit-state surface. Under these circumstances, the FORM analysis may not converge, especially when the gradient discontinuity occurs near the design point. Thus, the analyst must ensure that the formulation of the limit-state function does not include any envelope response parameters, to facilitate a successful FORM analysis.

3.5.4. Finding 4: Piece-wise linear material models may cause non-convergence

The material models that are shown in Fig. 3-9 have potential to cause non-convergence of the FORM analysis. When the material stiffness changes abruptly at the yield stress of the steel, and the compressive strength of the concrete, the gradient of the limit-state function may also experience an abrupt change. This is observed in Fig. 3-11b for the nonlinear model of MDOF. The displacement limit-state function is non-smooth at the yield stress of the reinforcement steel equal; namely at σ_y = 150 N/mm^2. For realizations of the yield stress less than 150 N/mm^2, the steel reinforcement yields due to the applied loads. As the yield stress value increases beyond 150 N/mm^2, the reinforcement steel ceases to yield. However, the non-smooth transition of the material state from the pre-yield state to the post-yield state causes the non-smoothness in the limit-state function. Hence, the limit-state function exhibits gradient discontinuity at the realization of the yield stress at 150 N/mm^2.

Interestingly, the displacement limit-state function for the nonlinear SDOF model in Fig. 3-10d does not exhibit gradient continuity for the variation of the yield stress. This is due to the fact that the steel cross-section of the SDOF model is discretized into 20 fibres. Because all the material fibres do not yield at the same load step, the abrupt transition between the pre-yield and the post-yield state is not observed in the displacement response. The yielding of each fibre contributes only to a minor change in the displacement response and hence, the resultant limit-state function is approximately smooth. Similarly, the discretization of the concrete into several fibres in the RC cross-section of the MDOF structure results in an approximately smooth limit-state function, as shown in Figs. 3-11a and 3-11c. Hence, employing fibre-discretized cross-sections with several fibres prevents problems with gradient discontinuity in the limit-state function and facilitates the convergence of the FORM analysis. Alternatively, material models with

smooth transitions between material states remedy the problem. "Smoothing" strategies for this purpose are developed by Haukaas and Der Kiureghian (2006).

3.5.5. Finding 5: Non-convergence of the FE analysis may be detrimental for FORM

As shown earlier, each iteration in the FORM algorithm requires the evaluation of the limit-state function and its gradient (see Fig. 3-1). If the FE analysis fails during the evaluation of the limit-state function, it leads to the failure of the FORM analysis to converge at design point. For a well-designed structure with a robust FE model, the FE analysis is expected to converge when the realizations of the random variables are near the mean values. However, for extreme realizations of the random variables; which is typical for failure scenarios, the structure may become unstable resulting in the non-convergence of the FE analysis. As shown in Fig. 3-12a, the MDOF structure loses its structural integrity when the lateral load exceeds 1800 kN. Beyond this load value a jagged behaviour of the limit-state function is observed; this is the response at the last converged step of the FE analysis. Consequently, the FORM analysis may fail to converge in this case for threshold values in the order of 100 mm.

In cases where the probability of collapse is being investigated, the FORM search algorithm may frequently enter such regions of non-convergence of the FE analysis. Thus, the analyst must exercise caution while employing FORM for the reliability analysis of such problem formulations.

3.5.6. Finding 6: Numerical noise may impede the convergence

The response gradient of the limit-state function determines the search direction for the design point in the FORM reliability analysis. When a finite difference method is employed to determine the response gradient, the limit-state function is evaluated for a small perturbation in the value of the random variables. However, the response gradients obtained in this method will be erroneous if the numerical noise is present in the limit-state function.

The numerical noise is primarily caused due to lax tolerance limits in the nonlinear FE analysis. In the presence of lenient tolerance limits, the change in the response due to the perturbation of random

variables may be inaccurately estimated. Inaccuracies may also be introduced if sufficient significant digits are not considered in the numerical values of the response. Furthermore, the use of an insufficient number of fibres in fibre-discretized cross-sections may cause gradient discontinuities in order of magnitude of numerical noise. In the authors' experience, the combination of a low number of fibres together with large load steps causes difficulties in the FORM analysis. The effect of the number of fibres and load step size on the limit-state function is shown in Figs. 3-12b and 3-12c, respectively. These figures are not explicitly showing the numerical noise; rather, they indicate the values of the number of fibres and size of the load step at which the limit-state function is insensitive.

From above it is concluded that the difficulties in FORM due to numerical noise are largely prevented if rigorous tolerance limits are used in the FE analysis, reasonable number of fibres are employed in the cross-section, and reasonably small load steps are utilized in the FE analysis. However, caution must be exercised when tightening the tolerance limits in the FE analysis. As shown in Fig. 3-12d for the displacement limit-state function of the nonlinear MDOF structure, convergence tolerance values less than 10^{-12} results in non-convergence of the FE analysis. This is indicated in the figure by a sudden change in the limit-state function value; the analyses to the left of 10^{-12} did not converge. Furthermore, attempts to remedy noise by increasing the number of fibres and decreasing the load step size may significantly increase the computational cost of the FE analysis. It noted that under conditions of numerical noise, an alternative remedy is to employ the direct differentiation approach to obtain the gradients or to increase the perturbation in the finite different procedure.

3.5.7. Finding 7: The nonlinearity in the limit-state surface is moderate in statics

Although some nonlinearity is observed in the limit-state surfaces for both linear and nonlinear problem above, it is found that this is not detrimental for the accuracy of FORM. Consider the comparison of the reliability indices from FORM and the MCS in Tables 3-2 and 3-4. MCS is feasible for the applications under consideration due to the low computational cost of the FE analysis. MCS is here considered to provide the most accurate estimate of the probability because it is not influenced by nonlinearity in the

limit-state surface. It is observed that the FORM analysis yields accurate estimates of the reliability index for all the problems under consideration. The reliability indices from the FORM vary in the second or the third decimal place compared to the reliability estimates from the MCS. Thus, the FORM provides satisfactory results with static analysis, particularly when applied to well-designed structures and for low probability values that are typical for structural reliability problems.

3.6. CONCLUDING REMARKS

In this study, the feasibility of the FORM application in FE-based analysis is investigated. A flow chart for an analyst to gage the applicability of FORM is provided in Fig. 3-14. As shown, a smooth limit-state function, absence of detrimental numerical noise, and an approximately linear limit-state surface are pre-requisites for accurate estimates of the probability with FORM. The findings from the case studies presented above reveal potential pitfalls and some remedies for the application of FORM. Specifically, Findings 3 – 5 address the issue of gradient discontinuity, while the issue of numerical noise is addressed by Finding 6. The potential nonlinearity of the limit-state surface is addressed by Findings 1, 2 and 7. In conclusion, FORM in conjunction with static FE analysis is feasible for a wide range of applications and provides accurate estimates of rare response events.

Table 3.1: Parameters for the linear models

Parameter	Mean	Standard Deviation	Distribution
SDOF			
Section dimension (h)	100 mm	10 mm	Lognormal
Length of the column (L)	3000 mm	166.67 mm	Normal
Lateral load (P)	50000 N	10000 N	Lognormal
Material stiffness (E)	200000 N/mm^2	20000 N/mm^2	Lognormal
MDOF			
Depth of girders (h_g)	610 mm	Deterministic*	Deterministic
Width of girders (b_g)	460 mm	Deterministic	Deterministic
Depth of outer columns (h_o)	610 mm	Deterministic	Deterministic
Depth of center column (h_c)	610 mm	20 mm	Lognormal
Width of center column (b_c)	690 mm	20 mm	Lognormal
Bay-width (W)	7300 mm	200 mm	Lognormal
Top storey height (H_s)	3700 mm	200 mm	Lognormal
Bottom storey height (H_L)	4600 mm	Deterministic	Deterministic
Left bay-width (W_L)	7300 mm	Deterministic	Deterministic
Material stiffness (E_c)	14400 N/mm^2	Deterministic	Deterministic
Lateral load (P)	140 KN	28 KN	Lognormal
Gravity load (G)	1700 KN	340 KN	Lognormal
Gravity load (G_1)	850 KN	170 KN	Lognormal
Gravity load (G_2)	430 KN	86 KN	Lognormal

*Deterministic implies that the parameter is not considered as a random variable in the analysis

Table 3.2: Reliability results of the linear models

Structure type	SDOF		MDOF	
Limit-state function type	Displacement	Stress	Displacement	Stress
Threshold value	100 mm	500 MPa	9 mm	700 MPa
Reliability index (FORM)	2.0497	2.7568	2.7234	2.7380
Reliability index (MCS)	2.0525	2.7575	2.7545	2.7630
Coefficient of variation (MCS)	5%	6.80%	6.84%	7%
Number of samples	19036	100000	100000	100000
Probability	2.02%	0.29%	0.32%	0.31%

Table 3.3: Parameters for the nonlinear models

Parameter	Mean	Standard Deviation	Distribution
SDOF			
Section dimension (h)	100 mm	10 mm	Lognormal
Length of the column (L)	3000 mm	166.67 mm	Normal
Lateral load (P)	50000 N	10000 N	Lognormal
Material stiffness (E)	200000 N/mm^2	20000 N/mm^2	Lognormal
Yield stress (σ_y)	500 N/mm^2	75 N/mm^2	Lognormal
Ratio of post-yield stiffness (α)	0.02	Deterministic*	Deterministic
Number of fibres	20	Deterministic	Deterministic
Convergence tolerance	10^{-6}	Deterministic	Deterministic
Load step size	2500 N	Deterministic	Deterministic
MDOF			
Depth of girders (h_g)	610 mm	Deterministic	Deterministic
Width of girders (b_g)	460 mm	Deterministic	Deterministic
Depth of outer columns (h_o)	610 mm	Deterministic	Deterministic
Depth of center column (h_c)	610 mm	20 mm	Lognormal
Width of center column (b_c)	690 mm	20 mm	Lognormal
Bay-width (W)	7300 mm	200 mm	Lognormal
Top storey height (H_s)	3700 mm	200 mm	Lognormal
Bottom storey height (H_L)	4600 mm	Deterministic	Deterministic
Left bay-width (W_L)	7300 mm	Deterministic	Deterministic
Ratio of post-yield stiffness (α)	0.02	Deterministic	Deterministic
Young's modulus of steel (E)	200000 N/mm^2	20000 N/mm^2	Lognormal
Yield stress of steel (σ_y)	420 N/mm^2	63 N/mm^2	Lognormal
Compressive strength of concrete (f'_c)	28 N/mm^2	4.20 N/mm^2	Lognormal
Yield strain of concrete (ε_c)	0.002	0.0003	Lognormal
Lateral load (P)	140 KN	28 KN	Lognormal
Gravity load (G)	1700 KN	Deterministic	Deterministic
Gravity load (G_1)	850 KN	Deterministic	Deterministic
Gravity load (G_2)	430 KN	Deterministic	Deterministic
Number of fibres	12	Deterministic	Deterministic
Convergence tolerance	10^{-6}	Deterministic	Deterministic
Load step size	2.80 KN	Deterministic	Deterministic

*Deterministic implies that the parameter is not considered as a random variable in the analysis

Table 3.4: Reliability results of the nonlinear models

Structure type	SDOF	MDOF	
Limit-state function type	Displacement	Displacement	Stress
Threshold value	100 mm	9 mm	30 MPa
Reliability index (FORM)	2.0505	2.0571	1.8394
Reliability index (MCS)	2.0363	2.0408	1.8458
Coefficient of variation (MCS)	5%	5%	5%
Number of samples	19128	24482	12810
Probability	2.02%	1.98%	3.29%

Table 3.5: Importance ranking for the displacement limit-state function in linear models

Parameter	Importance measure	Rank
SDOF		
Section dimension (h)	0.81688	1
Lateral load (P)	-0.40554	2
Length of the column (L)	-0.35571	3
Material stiffness (E)	0.20424	4
MDOF		
Lateral load (P)	-0.96991	1
Top storey height (H_s)	-0.22430	2
Width of center column (b_c)	0.08015	3
Bay-width (W)	-0.04040	4
Depth of center column (h_c)	0.02997	5
Gravity load (G)	-0.00153	6
Gravity load (G_2)	0.00065	7
Gravity load (G_1)	-0.00026	8

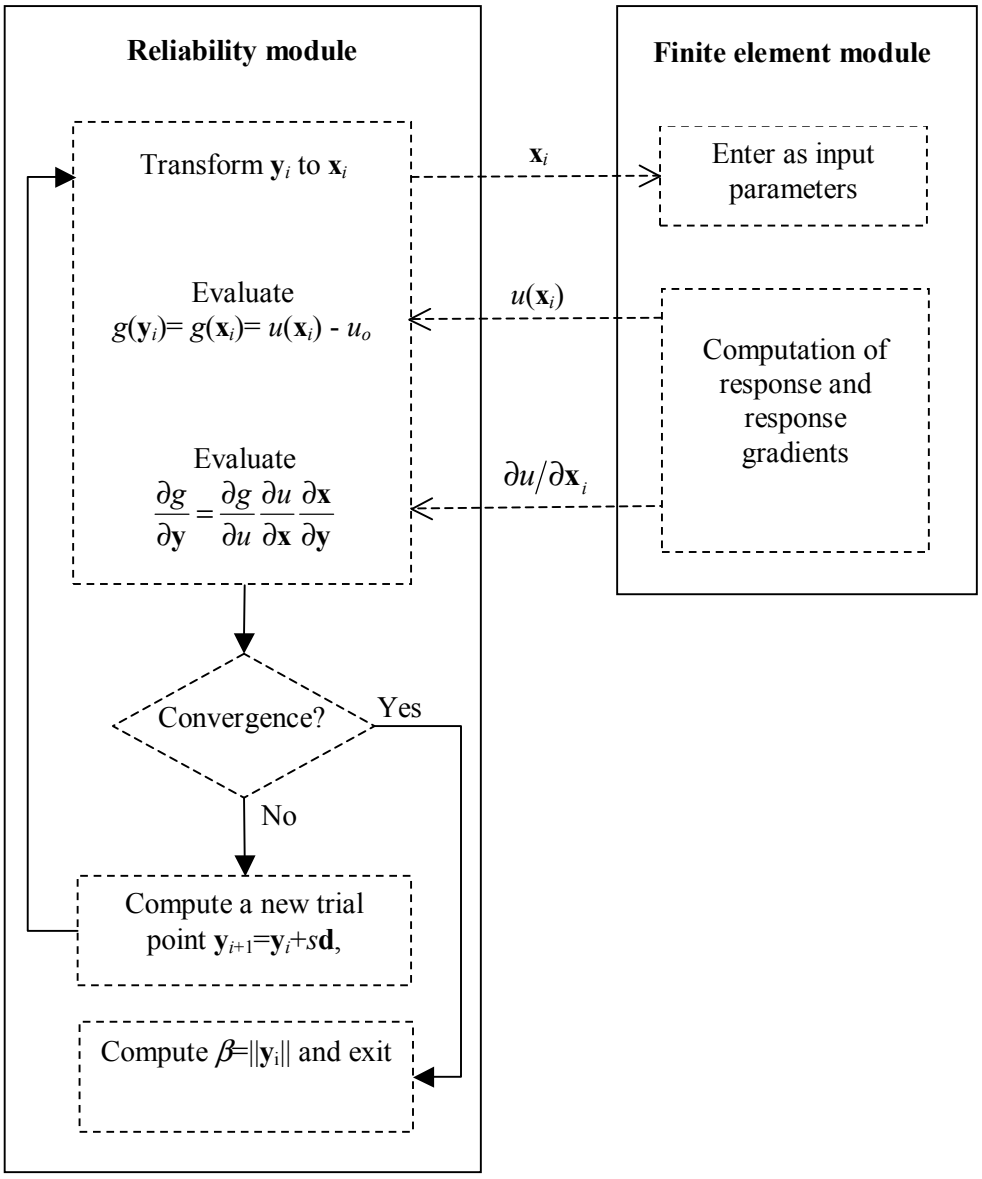

Figure 3.1: Schematic representation of the FE-based FORM analysis

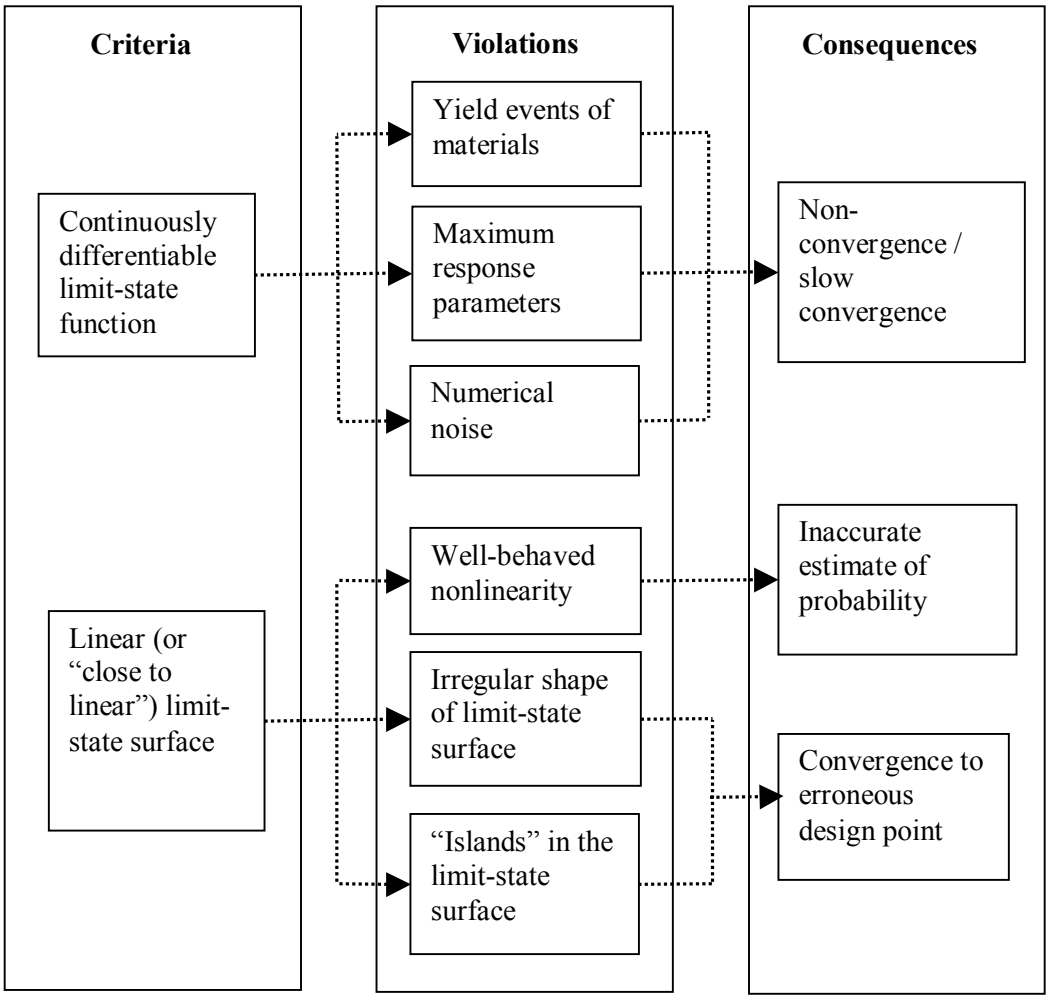

Figure 3.2: Criteria for the applicability of FORM

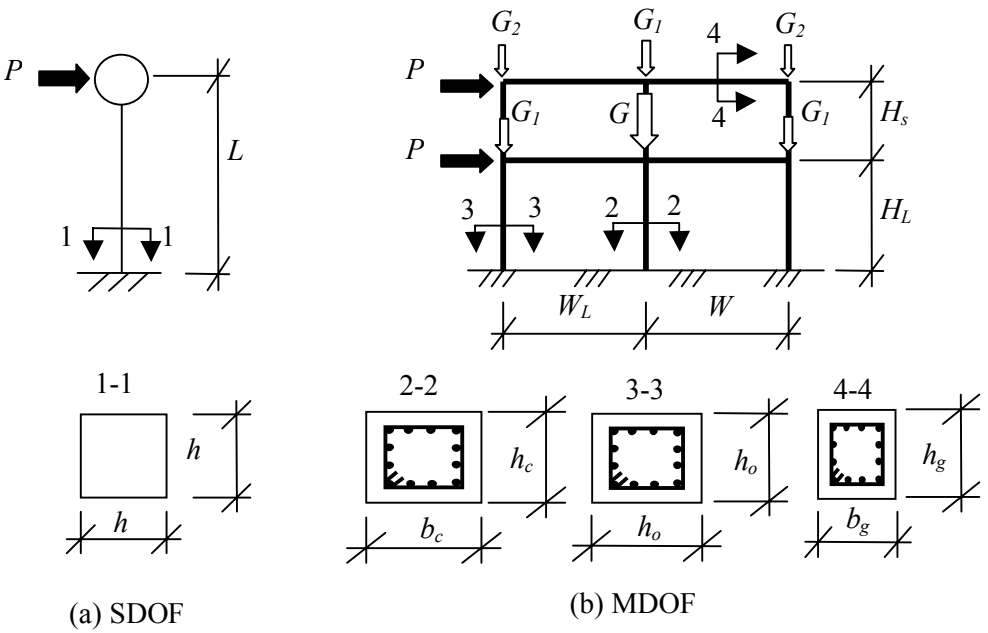

Figure 3.3: Structural models. a) Single-degree-of-freedom system; b) Multiple-degree-of-freedom system

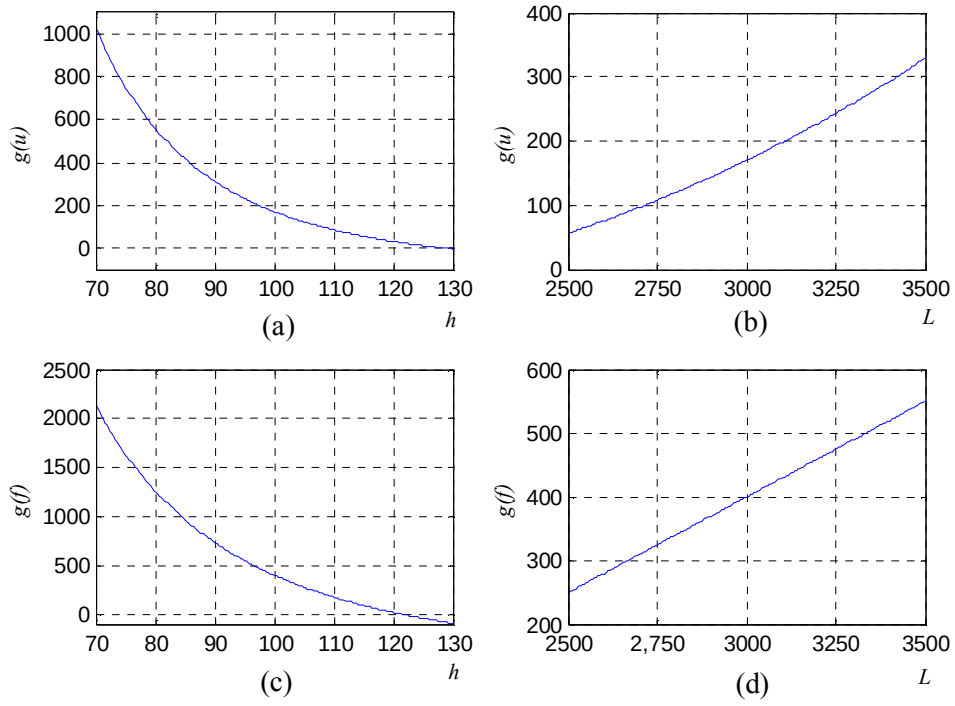

Figure 3.4: Limit-state function behaviour for linear model of SDOF. Behaviour of displacement limit-state function for the variation of a) cross-section dimension (mm); b) length (mm); Stress limit-state function behaviour for c) cross-section dimension (mm); d) length (mm).

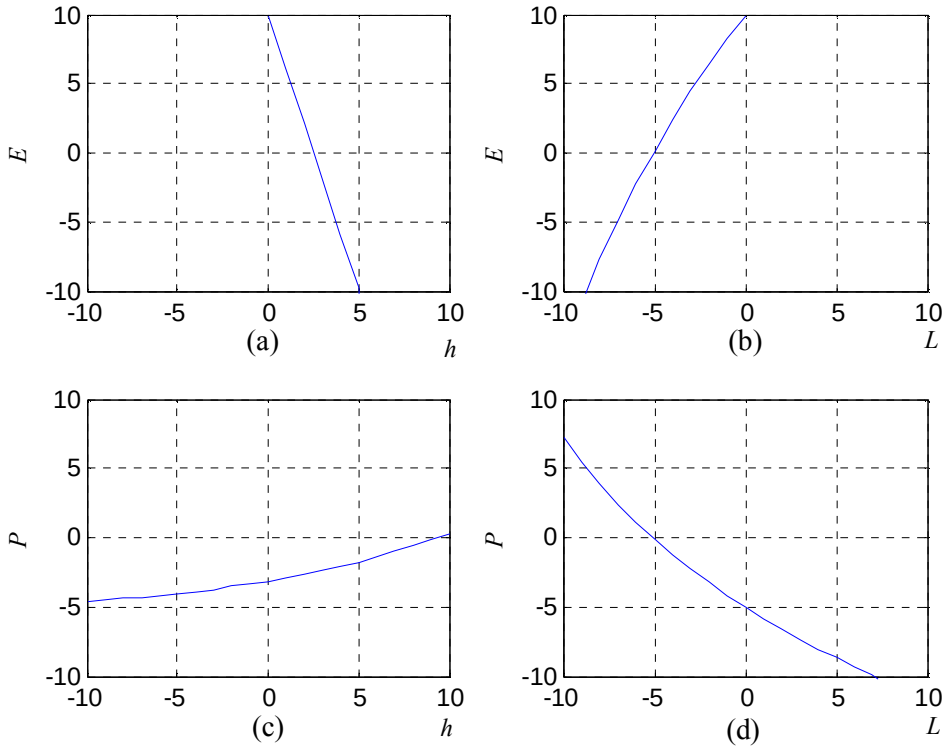

Figure 3.5: Displacement limit-state surface behaviour in the standard normal space for linear model of SDOF with random variables as, a) cross-section dimension and material stiffness; b) length and material stiffness; c) cross-section dimension and lateral load; d) length and lateral load

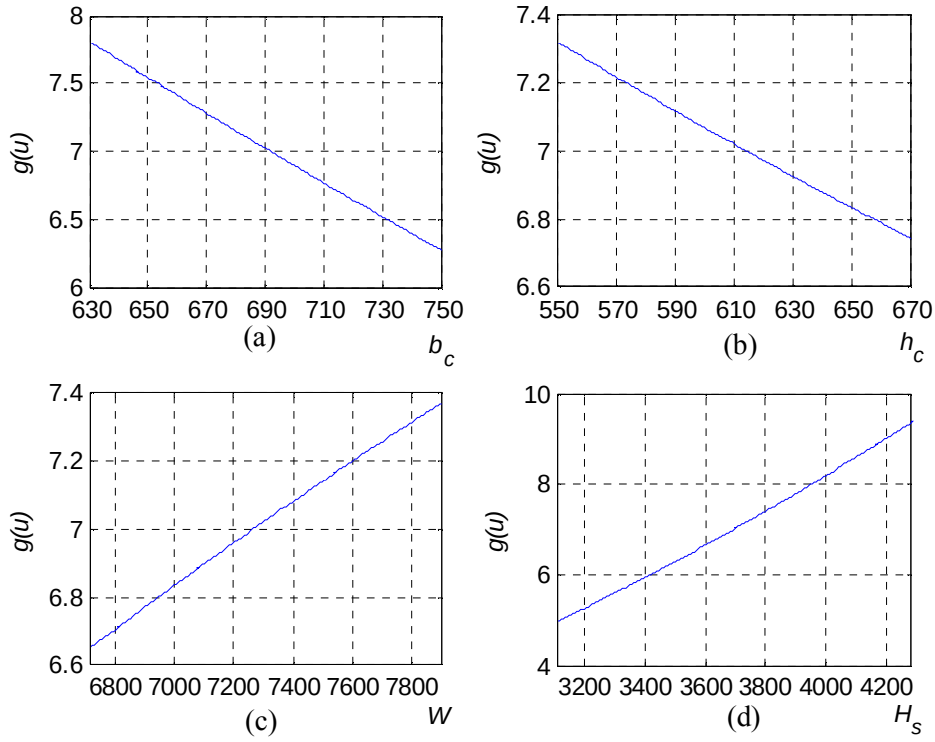

Figure 3.6: Limit-state function behaviour for linear model of MDOF. Variation of displacement limit-state function for the variation of a) width of the center column; b) depth of the center column; c) bay-width; d) storey height. The units of all the random variables are in mm

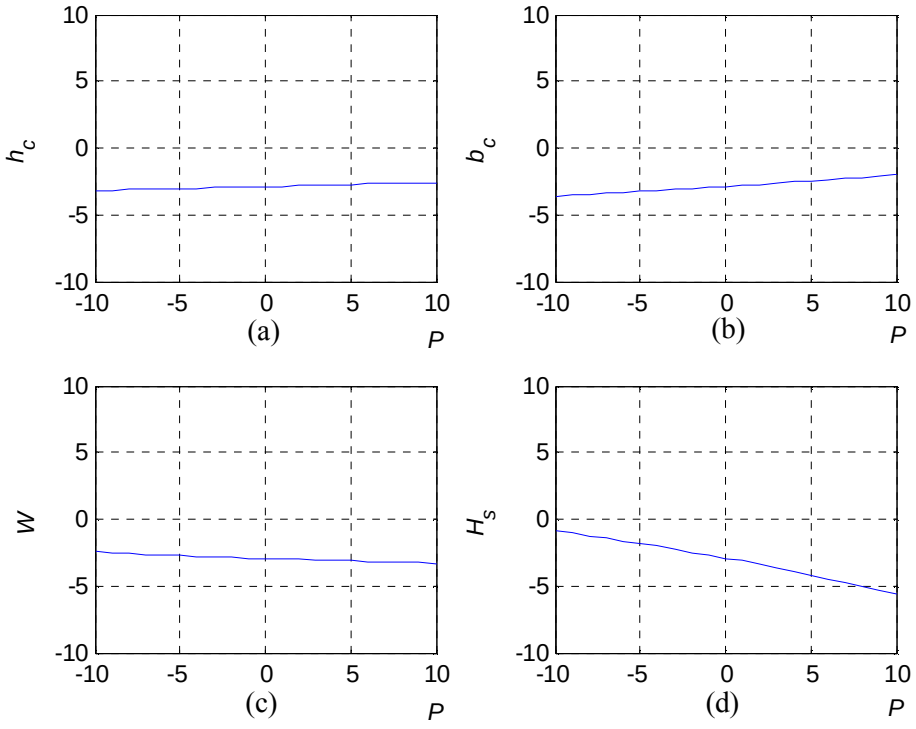

Figure 3.7: Displacement limit-state surface behaviour in the standard normal space for linear model of MDOF with random variables as, a) width of the center column and lateral load; b) depth of the center column and lateral load; c) bay-width and lateral load; d) storey height and lateral load

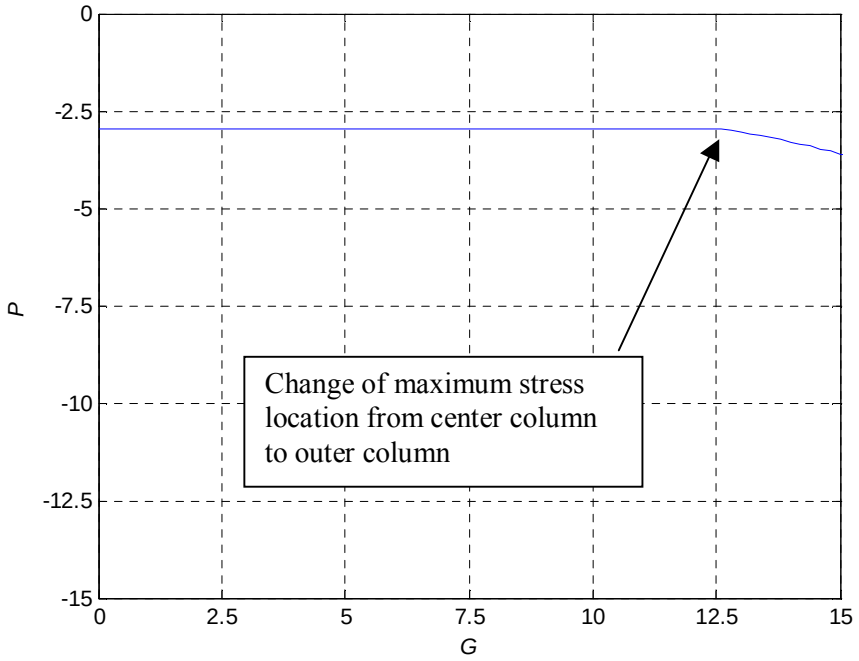

Figure 3.8: Stress limit-state surface behaviour in the standard normal space for linear model of MDOF, with random variables as lateral load and gravity load on the center column.

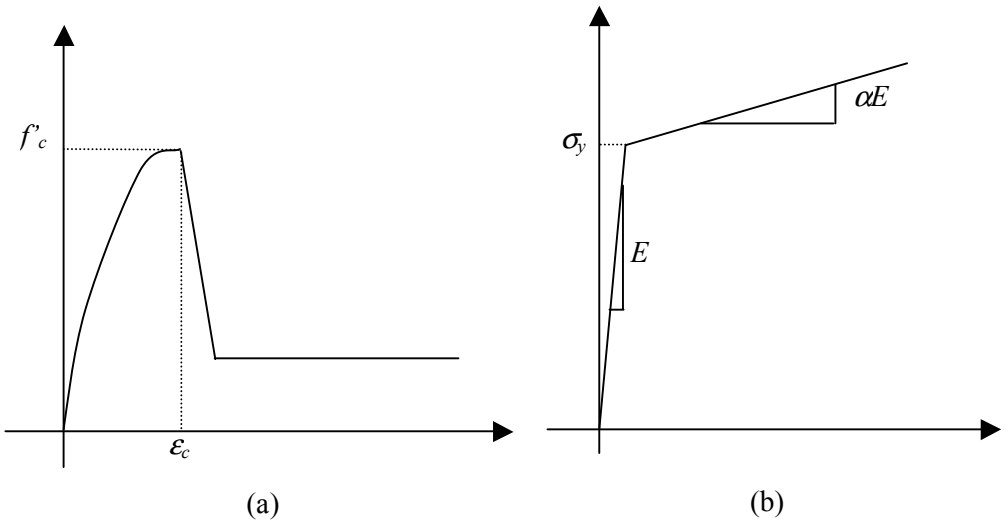

Figure 3.9: a) Concrete material model; b) Steel material model

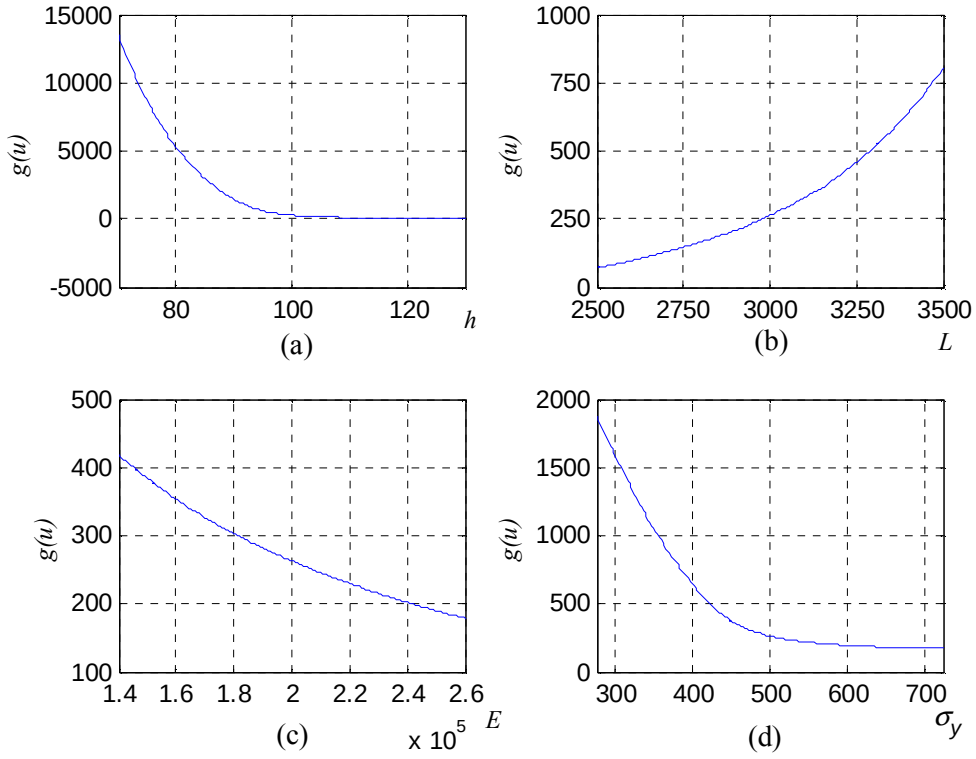

Figure 3.10: Behaviour of displacement limit-state function for nonlinear model of SDOF. Variation of limit-state function due to the variation of , a) cross-section dimension (mm); b) length (mm); c) Young's modulus of steel (N/mm^2) and d) yield stress of steel (N/mm^2)

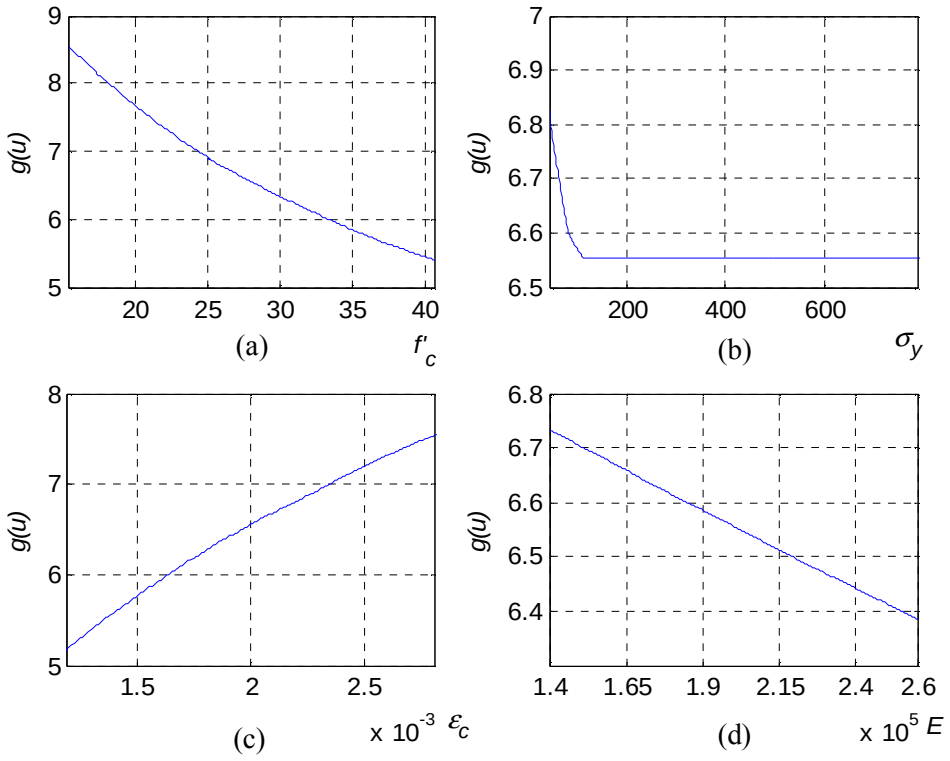

Figure 3.11: Behaviour of displacement limit-state function for nonlinear model of MDOF. Variation of limit-state function for the variation of material properties, a) compressive strength of concrete (N/mm^2); b) yield stress of steel (N/mm^2); c) strain in concrete at compressive strength, d) Young's modulus of steel (N/mm^2)

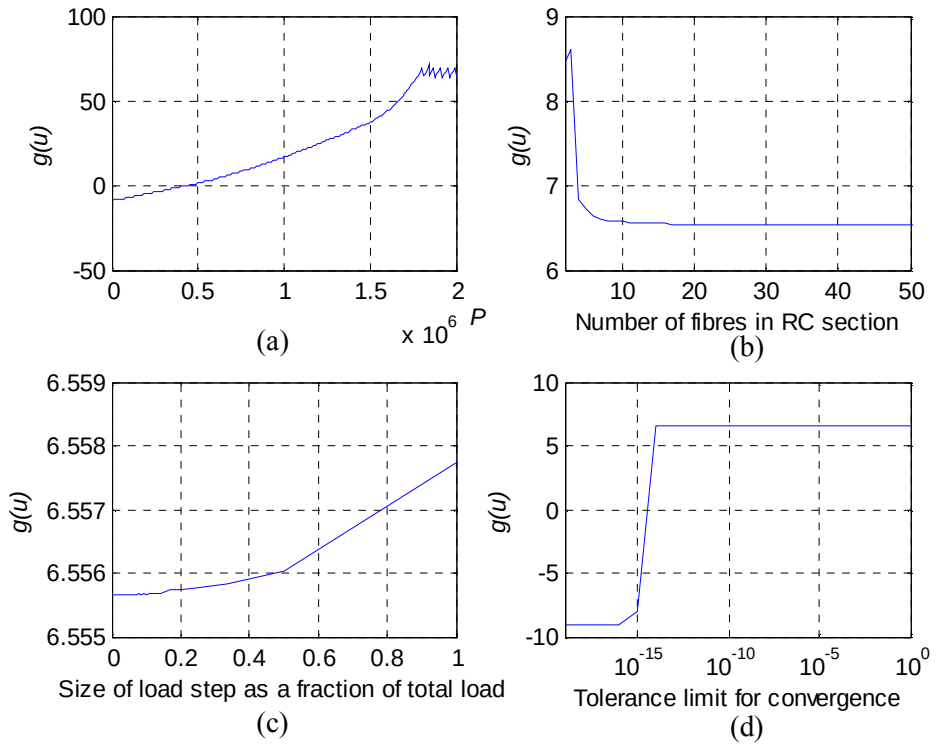

Figure 3.12: Behaviour of displacement limit-state function for nonlinear model of MDOF. Variation of limit-state function for the variation of nonlinear static analysis parameters, a) lateral load (N); b) number of fibers in the fiber-discretized cross-section; c) load step size in the nonlinear static analysis, d) numerical limits on convergence tolerances in logarithmic scale

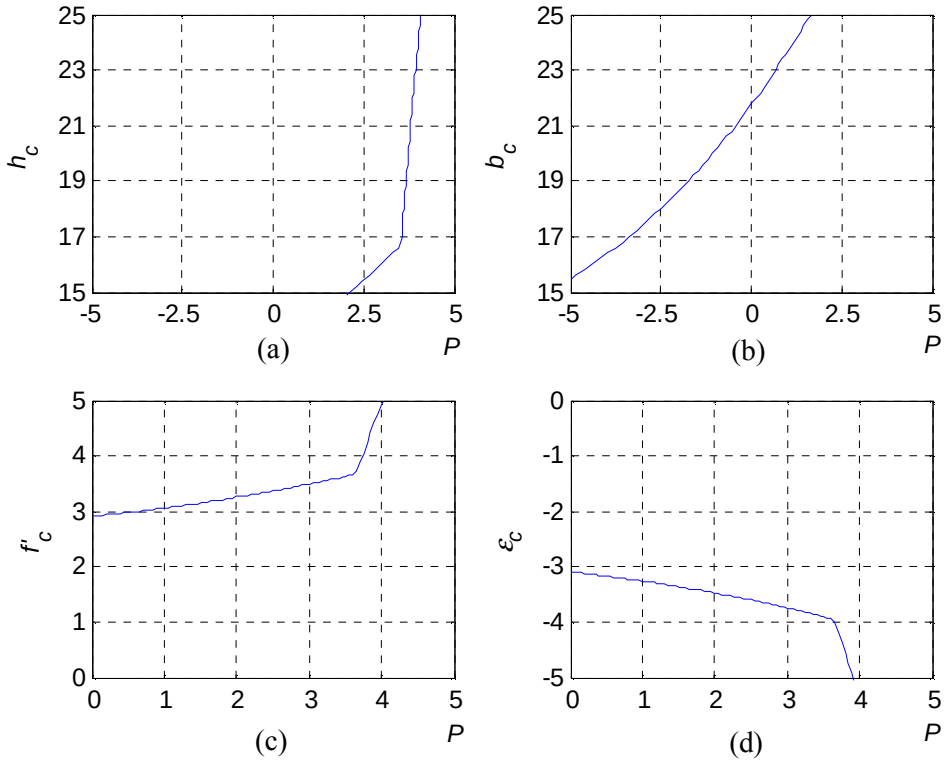

Figure 3.13: Behaviour of stress limit-state surface in the standard normal space for the nonlinear model of MDOF, with random variables as lateral load and a) depth of the center column; b) width of the center column; c) compressive strength of concrete of the center column, d) strain at the compressive strength of the concrete of the center column

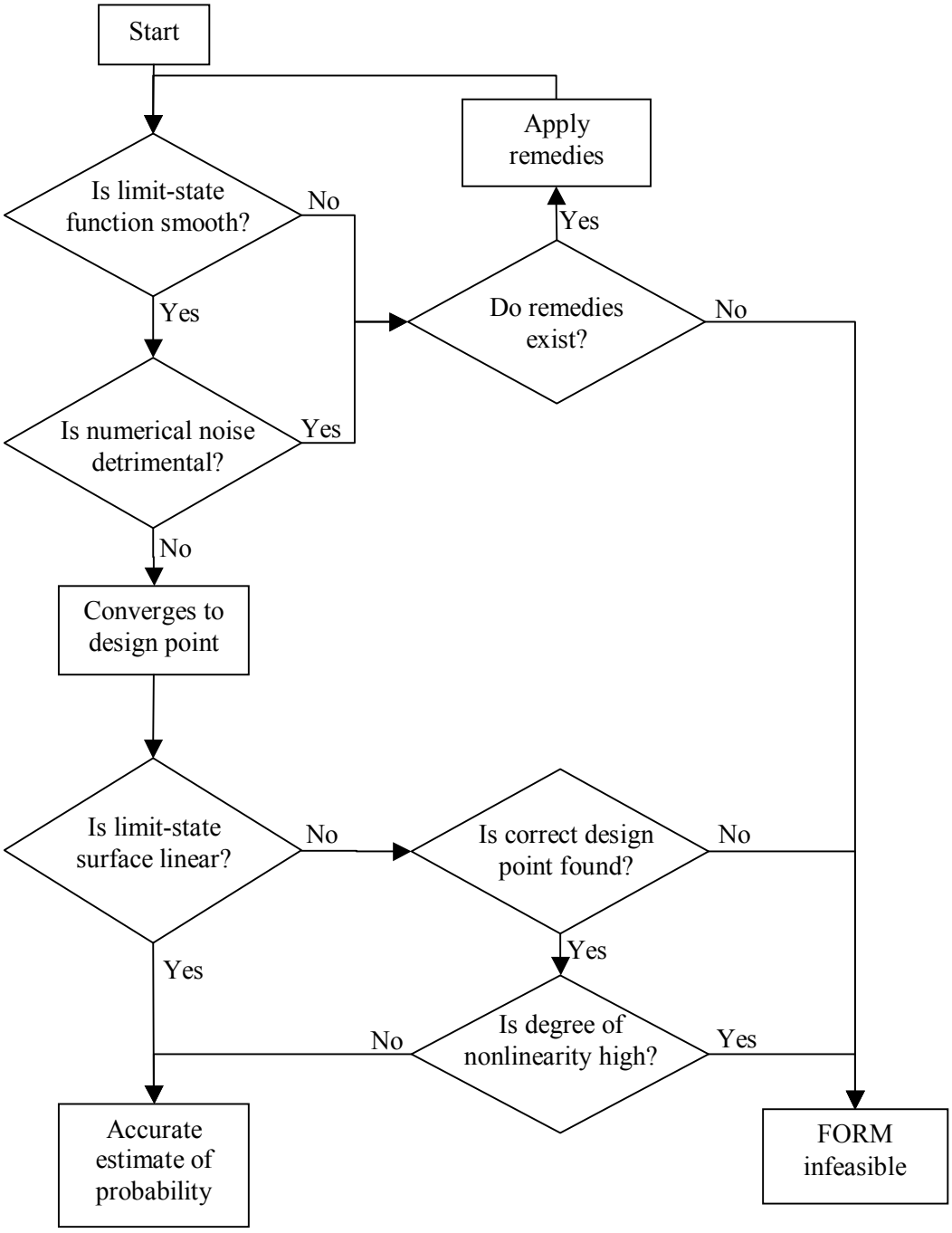

Figure 3.14: Flow chart to check the feasibility of FORM

REFERENCES

Cement Association of Canada (CAC) (2006), *Concrete Design Handbook: Third Edition*. Ottawa: Cement Association of Canada.

Ching, J., Beck, J.L. and Au, S.K. (2005), "Hybrid subset simulation method for reliability estimation of dynamical systems subjected to stochastic excitation," *Probabilistic Engineering Mechanics*, 20 (3), 199-214

Canadian Institute of Steel Construction (CISC-ICCA) (2006), *Handbook of Steel Construction: Ninth Edition*, Willowdale: Canada

Der Kiureghian, A. and Taylor, R. L. (1983), "Numerical methods in structural reliability," *Proceedings of the Fourth International Conference on Applications of Statistics and Probability in Civil Engineering, ICASP4, Florence, Italy*

Der Kiureghian, A. and Dakessian, T. (1998), "Multiple design points in first and second-order reliability," *Structural Safety*, 20, 37-49

Der Kiureghian, A. and Zhang, Y. (1999), "Space-variant finite element reliability analysis," *Computer Methods in Applied Mechanics and Engineering*, 168(1-4), 173-183

Ditlevsen, O., and Madsen, H.O. (1996), *Structural Reliability Methods*, Wiley, Chichester, New York, NY

FEMA-356 (Federal Emergency Management Agency) (2000), *Prestandard and Commentary for the Seismic Rehabilitation of Buildings*, ASCE, Federal Emergency Management Agency, Washington, D.C.

Fiessler, B., Neumann, H.-J. and Rackwitz, R. (1979), "Quadratic limit-state in structural reliability," *Journal of Engineering Mechanics Division*, 105 (EM4), 661-676

Frier, C. and Sorensen, J. (2003), "Stochastic finite element analysis of non-linear structures modelled by plasticity theory," *Proceedings of the Ninth International Conference on Applications of Statistics and Probability in Civil Engineering,ICASP9*, San Francisco, California

Gutierrez, M., Carmeliet, J. and de Borst, R. (1994), "Finite element reliability methods using Diana," *Diana Computational Mechanics 1994*, Eds: G.M.A. Kusters and M.A.N. Hendriks

Haldar, A. and Mahadevan, S. (2000), *Reliability Assessment Using Stochastic Finite Element Analysis,* John Wiley and Sons, New York

Hasofer, A. M. and Lind, N.C. (1973), "An exact and invariant first-order reliability format," *Paper No. 119, Solid Mechanics Division*, University of Waterloo, Canada

Haukaas, T. and Der Kiureghian, A. (2004), *Finite Element Reliability and Sensitivity Methods for Performance-Based Engineering*, Report no. PEER 2003/14, Pacific Earthquake Engineering Research Center, University of California, Berkeley

Haukaas, T. and Der Kiureghian, A. (2006), "Strategies for finding the design point in non-linear finite element reliability analysis," *Probabilistic Engineering Mechanics*, 21 (2), 133-147

Haukaas, T. and Scott, M. H. (2006), "Shape sensitivities in the reliability analysis of nonlinear frame structures," *Computers and Structures*, 84 (15-16), 964-977

Imai, K. and Frangopol, D. M. (2000), "Geometrically nonlinear finite element reliability analysis of structural systems, i: theory ii: applications," *Computers and Structures*, 7(6), 677-709

Kleiber, M., Antunez, H., Hien, T. and Kowalczyk, P. (1997), *Parameter Sensitivity in Nonlinear Mechanics*, John Wiley and Sons Ltd. West Sussex, UK

Liu, P-L. and Der Kiureghian, A. (1991), "Finite element reliability of geometrically nonlinear uncertain structures," *Journal of Engineering Mechanics*, 17(8), 1806-1825

McKenna, F., Fenves, G.L., and Scott, M.H. (2004), *OpenSees*: *Open system for earthquake engineering simulation*. Pacific Earthquake Engineering Research Center, University of California, Berkeley, CA

Qin, Q., Lin, D., Mei, G. and Chen, H. (2006), "Effects of variable transformations on errors in FORM results," *Reliability Engineering and System Safety*, 91(1): 112-118

Rackwitz, R. (2001), "Reliability analysis – a review and some perspectives," *Structural Safety*, 23, 365-395

Sudret, B. and Der Kiureghian, A. (2000), *Stochastic Finite Element Methods and Reliability: A State-of-the-Art Report*, Report No. UCB/SEMM-2000/08, Department of Civil and Environmental Engineering, University of California, Berkeley

Yang, D., Li, G. and Cheng, G. (2006), "Convergence analysis of the first-order reliability method using chaos theory," *Computers and Structures*, 83, 563-571

Zhao, Y.-G. and Ono, T. (1999), "A general procedure for first/second-order reliability method (FORM/SORM)," *Structural Safety*, 21, 95-112

Zhang, Y. and Der Kiureghian, A. (1993), "Dynamic response sensitivity of inelastic structures," *Computer Methods in Applied Science and Engineering*, 108, 23-36

Zhang, Y. and Der Kiureghian, A. (1997), *Finite Element Reliability Methods for Inelastic Structures*, Report No. UCB/SEMM-97/05, Department of Civil and Environmental Engineering, University of California, Berkeley

Chapter 4. FEASIBILITY OF FORM – DYNAMICS[1]

4.1. INTRODUCTION

The primary objective in this chapter is to facilitate reliability analysis that uses sophisticated numerical models. In the context of structural engineering, simulation of response by means of dynamic finite element (FE) analysis has not traditionally been part of mainstream practice. However, special areas such as offshore and earthquake engineering represent a growing number of exceptions. In particular, the recent trend towards "performance-based earthquake engineering," in which simulation of structural performance is a key ingredient, motivates dynamic analysis. In this context, the desire to simulate structural performance during extreme loading events necessitates treatment of uncertainties. This motivates the present study, in which the feasibility of reliability analysis in conjunction with FE analysis to obtain performance probabilities is explored.

The first issue that is encountered in dynamic FE analysis with time-stepping methods, regardless of the inclusion of reliability analysis, is computational cost. Even after decades of growth in computer power it is still an arduous task to embark on a dynamic time-history analysis with a sophisticated model of a real-world building. The time required to run one FE analysis for some realistic time-varying loading may be in the order of hours. This places strict constraints on the feasibility of various reliability methods. Sampling methods are typically infeasible, while FORM presents a promising balance of accuracy and computational efficiency. This inspires the present study of the feasibility of FORM for computation of performance probabilities by means of advanced dynamic FE analysis. Novel developments to foster such analysis in future engineering practice are emphasized. These efforts build upon Chapter 3, which describes the FE-based FORM methodology and exposes the advantages and pitfalls with static FE-based reliability analysis.

[1] A version of this chapter has been submitted for publication. Koduru, S.D. and Haukaas, T. "Feasibility of FORM in finite element reliability analysis: Part II – Dynamics."

The scope of the present study is limited to FE-based analyses. This is emphasized to avoid unnecessary overlap with the vast field of traditional random vibrations. Several of the problems discussed in this study, such as that of calculating the probability that a response exceeds a threshold during a time period, have earlier been subjected to extensive research. However, the majority of earlier studies have not dealt with the challenges that are particular to FE-based applications. Focus in this chapter is on the extension of the existing field of knowledge to FE-based applications. However, it is noted that some of the points brought to attention of the FE reliability analyst in this chapter are noted in classical studies. For example, a common mistake made by the novice FE-based reliability analyst is to attempt to apply FORM to compute the probability that a response exceeds a threshold during the analysis. This may be a highly non-trivial problem, referred to as time-variant reliability, regardless of whether a FE model is involved.

As noted earlier, FORM provides reasonably accurate estimates of the probability for lesser computational costs compared to many reliability methods in FE-based applications. However, the convergence and the accuracy of FORM are critically dependent on the characteristics of the limit-state function. The conditions for the applicability of FORM and the factors leading to the violations of these conditions are presented in detail in the accompanying Chapter 3 of this study. Specifically, the challenges in the application of FORM stem from potential discontinuities in the gradient of the limit-state functions and the nonlinearity of the limit-state surfaces. This motivates the study of the characteristics of the limit-state function and the limit-state surface to discern the applicability of FORM. This is carried out by performing FE analyses to visualize and study the characteristics of the limit-state functions that are commonly employed in performance-based earthquake engineering. A visualization tool available in the OpenSees software (McKenna *et al*. 2004) is employed.

4.2. LIMIT-STATE FUNCTIONS IN DYNAMIC ANALYSIS

The list of relevant limit-state functions is generated in a different manner in this chapter compared to Chapter 3. While static FE analysis lends itself to limit-state functions based on design criteria in current engineering practice, dynamic time-history analysis is currently more academic in nature. To approach

the matter of possible limit-state functions, consider the responses that are available from a dynamic FE analysis; linear or nonlinear. These include: nodal response parameters such as displacements, velocities, and accelerations; stresses or stress resultants within elements; plastic strain or rotations in elements; and cumulative energy or damage measures. In theory, limit-state functions could be defined in terms of any of these measures, or combinations thereof. Additional options are introduced by considering responses at a particular time instant, or at the final analysis time-step, or at an uncertain time when the response exceeds some threshold.

In this chapter an important distinction – described below – is made to address the multitude of conceivable limit-state functions. The distinction will in turn lead to a novel development for reliability analysis in conjunction with inelastic dynamic FE models. The backdrop for the classification is a growing vision for the future of structural engineering. It may be referred to as "added-value" engineering, which goes beyond the classical code-oriented approach. The idea is to provide the client with more information than mere code compliance; but in fact about actual performance of the structure at hand. This motivates the classification of limit-state functions. It is argued in this chapter that the primary interest, from a future-looking perspective, is not the computation of the probability that a response, e.g., a nodal displacement, exceed a threshold. Of greater interest in performance-based engineering are quantities such as "amount of damage," "repair cost," and "down-time." For a number of stakeholders, including owners, municipalities, and the public, these are more useful in decision making than, say, the maximum displacement response. In fact, this forms the principal motivation for the simulation-based and performance-based engineering paradigms.

Now observe that the practically useful responses are typically cumulative during the FE analysis. Accumulated damage, e.g., in the form of dissipated energy, is one example. To this end, this study categorizes the limit-state functions in dynamic reliability analysis into those that are cumulative during the FE-analysis, and those that are not. Interestingly, the cumulative nature of these practically oriented limit-state functions has implications for the feasibility of the reliability analysis.

In the literature, several cumulative damage measures are developed. A convenient metric to measure damage has been "damage indices," wherein the damage is quantified to be a numerical value between 0 and 1. These numerical values are in turn assigned to a damage state, which includes qualitative assessments of damage. The damage indices are typically dependent on deformations, such as plastic rotations, inter-storey drift ratios, and peak lateral deformations, as well as hysteretic energy, loss of strength, strain, and a combination of the above (Williams and Sexsmith 1995). For example, the Park-Ang damage index (Park and Ang 1985) employs the peak displacement response and the dissipated energy in order to assess the damage state. Bracci *et al*. (1989) proposed a damage index that is monotonically increasing with dynamic loading, based on the strength degradation and ductility of a cross-section. Kratzig *et al*. (1989) developed a damage index that quantifies the accumulated damage, based on the hysteretic energy. More recently, Mehanny and Deierlein (2000) proposed a damage index based on cumulative plastic deformations. The repair costs are typically related to the damage states. Hence, the repair costs increase with increasing damage.

The studies and developments related to cumulative limit-state functions represent key contributions in this chapter. Effectively, this forms a methodology to address the time-variant reliability problem. In the following section, this approach will – conceptually – be contrasted with classical approaches to address time-variant reliability.

4.3. THE TIME-VARIANT RELIABILITY PROBLEM

When dynamic FE analysis is extended with the reliability analysis, the analysts have a tendency to prescribe peak response in the limit-state functions. This is considered as a natural extension from the static case wherein the maximum displacements and stresses are utilized. However, peak responses cause gradient discontinuity in the limit-state function leading to the failure of gradient-based search algorithms. In order to understand this effect conceptually, consider Fig. 4-1. Fig. 4-1a illustrates the displacement response of a structure, u, which is a function of the random variable, x. Consider the peak displacement response in the limit-state function, g. Fig. 4-1b schematically represents the variation of the limit-state

function, with respect to x. For a small perturbation, dx, of the random variable, the amplitude and location of the peak displacement along the time axis may suddenly shift as indicated by the dotted line in Fig. 4-1a. This results in a non-smooth limit-state function as illustrated in Fig. 4-1b. In turn, this violates the continuous gradient criterion for the applicability of FORM.

The uncertainty in the time instant at which a response reaches its peak value, is a key feature hindering the utilization of peak responses in FORM. This uncertainty in the time instant increases when the structural response is a stochastic process. In this context, the reliability problem is traditionally cast as a time-variant reliability problem.

Time-variant reliability analysis aims to find the probability that a stochastic process exceeds a threshold at least once within the duration of interest. The probability is calculated as the first passage of a stochastic process through the limit state surface. It is formally represented as (Li and Der Kiureghian 1995)

$$p_f = P(\min_{t \in T} g(u(t, \mathbf{x})) \leq 0) \tag{4-1}$$

where p_f is the probability of failure within a time period T, and u is the response as a function of time, t and the vector of random variables $\mathbf{x}$. The problem is also known as the "first-excursion" problem or the "first-passage" problem. Eq. (4-1) is also cast as

$$p_f = P(\bigcup_{i}^{n} g(u(t_i, \mathbf{x})) \leq 0) \tag{4-2}$$

where the time period T is discretized into n time instants. Eq. (4-2) transforms the original time-variant problem into a time-invariant system reliability problem with n limit-state functions.

Considerable literature exists to solve Eq. (4-1) for linear dynamic problems with the theory of random vibrations (Lutes and Sarkani 2004). Some key contributions in the field include those by Yang and Shinozuka (1971), Vanmarcke (1975), Mason and Iwan (1983), Naess (1990), Zhang and Der Kiureghian (1994), Li and Der Kiureghian (1995), and Der Kiureghian (2000). The more challenging nonlinear

problem may be addressed by transforming it into a linear problem by means of "equivalent linearization," in order to maintain the applicability of the random vibrations approach (Caughey 1963, Wen 1980). However, in the context of earthquake engineering, Koo and Der Kiureghian (2003), Koo *et al*. (2005), and Fujimura and Der Kiureghian (2007) developed novel methods to address nonlinear random vibrations, which deviate from the equivalent linearization approach. Common to the aforementioned approaches is the "crossing rate" that is employed as a central quantity. An alternative to this strategy is to employ sampling methods, such as importance sampling (Au and Beck 2001), subset simulation (Au and Beck 2003, Ching *et al*. 2005, Katafygiotis *et al*. 2007), and response surface methods, e.g., Yao and Wen (1996), Zhang and Foschi (2004), to solve Eq. (4-2). These methods are applicable to linear and nonlinear dynamic problems. However, the computational efficiency is dependent on several factors, such as the number of intervening random variables and the complexity of the structure.

In the approaches that utilize the crossing rate, Eq. (4-1) is solved by assuming independent crossings of the response, u, into the failure region and that the crossing events are Poisson distributed. Hence, (Vanmarcke 1975)

$$p_f = 1 - \exp\left(\int_0^T \nu(t)dt\right) \tag{4-3}$$

where $\nu(t)$ is the mean out-crossing rate, which is the expected number of crossings of u into the failure region during a unit time. There are several methods to obtain $\nu(t)$. A generally applicable method is to numerically evaluate the temporal distribution of $\nu(t)$ by discretization of T into several time instants. At a given time instant, t_n, the mean out-crossing rate is estimated as (Hagen and Tvedt 1991),

$$\nu(t_n) = \lim_{\delta t \to 0} \frac{P[g(u(t_n, \mathrm{x})) > 0 \cap g(u(t_n + \delta t, \mathrm{x})) \le 0]}{\delta t} \tag{4-4}$$

where δt is a small but finite time interval after the time instant t_n. The parallel system reliability problem in the numerator of Eq. (4-4) is solved with FORM by Koo *et al*. (2005), such that for a small value of δt

$$P[g(u(t_n, \mathbf{x})) > 0 \cap g(u(t_n + \delta t, \mathbf{x})) \leq 0] \cong \Phi(-\beta_1, -\beta_2, \rho) \tag{4-5}$$

where Φ is a bi-variate standard normal distribution, $\beta_2 \approx -\beta_1 = \beta$, where β is the reliability index of the limit-state function $g(u(t_n,\mathbf{x}))$, and ρ is close to -1. Koo *et al*. (2005) discovered that the design point excitation for a single-degree-of-freedom system is the one that yields the mirror image of the free-vibration response for the system released from the threshold displacement. Later, this discovery is utilized by Fujimura and Der Kiureghian (2007) to develop a "tail-equivalent linearization method" to address the nonlinear dynamic problems with multi-degree-of-freedom structures. They also developed an algorithm to determine a sequence of design points for various time instants and threshold values.

The contributions of Koo *et al*. (2005), and Fujimura and Der Kiureghian (2007); namely, the utilization of design points, can be employed to solve the time-variant reliability problem in two ways; 1) numerically estimating $\nu(t)$ and subsequently evaluating Eq. (4-3); and 2) importance sampling around the design point and utilization of the system reliability formulation in Eq. (4-2). The latter approach is explored by Au and Beck (2001) who developed efficient sampling methods to solve the time-variant reliability problem.

Contrary to the response considered above, cumulative responses exceed a threshold value only once during the time period of interest due to their monotonically increasing nature. Therefore, the random vibrations approach with mean out-crossing rate is circumvented with these responses in the limit-state function. Furthermore, cumulative response is always measured at the final analysis load step; thus removing the time-variant uncertainty. Consequently, the system reliability problem in Eq. (4-2), with limit-state functions at several time instants, reduces into a fundamental reliability problem with a single limit-state function at a single time instant. It is therefore of significant interest in this study to explore the characteristics of limit-state functions with cumulative response and assess the feasibility of FORM. In

the following section, the limit-state functions with cumulative response are evaluated numerically for specific SDOF and MDOF systems to explore the applicability of FORM.

4.4. STUDY OF FE-BASED RELIABILITY ANALYSIS WITH CUMULATIVE RESPONSE

The study with cumulative responses is carried out in three parts; first considering randomness only in the structural parameters; then considering randomness only in the dynamic loading; and finally a comprehensive case with randomness in both structural and loading parameters. This categorization facilitates the separation of structural modelling effects and load modelling effects on the feasibility of FORM. The factors that are affecting FORM due to structural modelling, such as aspects of the material models, finite-elements, cross-sectional properties, and geometry, are different from those due to load modelling, such as load amplitude, and frequency. In each category, case studies are presented with the structural models illustrated in Fig. 4-2.

Fig. 4-2a illustrates a basic single-degree-of-freedom (SDOF) system defined by mass, M = 100 kg, damping C = 5%, stiffness K = 4000 N/mm and yield strength P_y = 196.2 N. The post-yield stiffness is considered as 2% of the initial stiffness K. The bilinear material model of this structure facilitates the study without the influence of cross-section modelling. The second structure, shown in Fig. 4-2b, is also a SDOF system modelled as a nonlinear beam-column element. This structural model includes the influence of the material and cross-section models in contrast to the structural model in Fig. 4-2a. The cross-section is modelled as a fibre-discretized section. Two types of materials - structural steel (SS) and reinforced concrete (RC) - are considered. This structure is termed “SDOF-SS” and “SDOF-RC” to represent the structural steel and reinforced concrete cross-sections, respectively. This terminology differentiates the structure in Fig. 4-2b from the basic single-degree-of-freedom system in Fig. 4-2a. The numerical values of the model parameters for SDOF-SS and SDOF-RC are presented in Table 4-1.

A two-storey two-bay structure shown in Fig. 4-2c is considered to represent a multiple-degree-of-freedom (MDOF) system. The MDOF system is a reinforced concrete structure modelled with nonlinear

beam-column elements and fibre-discretized cross-sections with individual fibres representing concrete and reinforcing steel materials. Table 4-2 presents a partial list of the structural parameters relevant to the case studies in this chapter. Further details of the geometry and cross-section properties are found in Chapter 3.

Cumulative responses are dependent on the cyclic force-deformation relationship of material models. Hence, the hysteretic behaviour of material models plays a significant role when cumulative responses enter the limit-state functions. In the present study, the hysteretic behaviour of steel and concrete are based on "*Steel01*" and "*Concrete01*" material models, respectively, in OpenSees (McKenna *et al*. 2004). Figs. 4-3a and 4-3b conceptually illustrate the material models for structural steel and concrete. The reinforcement steel in RC cross-section is also modelled with the material model in Fig. 4-3a.

4.4.1. Random structural properties

The structural models, SDOF-SS, SDOF-RC and MDOF are considered for study in this section. These case studies isolate the effects of the structural properties on the behaviour of the limit-state function, due to the fact that only the structural parameters are considered as random variables. A sine wave of 0.8s period and duration of 8s is considered as the deterministic dynamic load. Hysteretic energy is considered as the cumulative response for all the cases. The energy limit-state function is denoted as $g(e)$ for convenience of notation.

4.4.1.1. SDOF-SS Structure

Fig. 4-4 shows the variation of $g(e)$ for the SDOF-SS model. Figs. 4-4b and 4-4e show significant nonlinearity in the limit-state function due to the variation of h and M, respectively. It is observed that $g(e)$ is reasonably linear for the variation of L, E, σ_y, and C. The dramatic nonlinearity of $g(e)$ in Figs. 4-4b and 4-4e is due to the effect of h and M on the period of the structure. The period varies between 1.63-0.47s for the variation of h from 70 mm to 130 mm, and 0.51-1.01s for the variation of M from 1200 kg to 4800 kg. The highest nonlinearity of $g(e)$ is observed in the period range of 0.55-0.61s due to the

transition of structure from elastic to inelastic behaviour within this period range. In Figs. 4-4a and 4-4c corresponding to the variation of L and E, respectively, the period varies between 0.61-1.0s for the variation of L from 2500 mm to 3500 mm, and 0.96-0.70s for the variation of E from 140×10^3 N/mm^2 to 260×10^3 N/mm^2. This implies that the variation of L and E has not significantly influenced the structural period to cause the transition between the elastic and inelastic behaviour. Therefore, the variation of L and E results in a fairly linear $g(e)$. The variation of σ_y has no effect on the period of the structure. However, yielding of the structure, and in turn, dissipation of hysteretic energy depends on σ_y. Fig. 4-4d exhibits a linear variation of $g(e)$ for the variation of σ_y. In Fig. 4-4f, the variation of C has insignificant effect on the variation of $g(e)$. This is due to the fact that C has practically no influence on the structural period for the range of values 2-5%, typically considered in the civil engineering structures. Additionally, when the structure yields, hysteretic energy forms a dominant part of energy dissipation as opposed to the viscous damping. This observation implies that cumulative responses are fairly insensitive to the uncertainty present in the estimation of viscous damping. In summary, the observations in Fig. 4-4 indicate certain degree of nonlinearity in the limit-state function but not gradient discontinuities and detrimental numerical noise.

The application of FORM depends on the degree of nonlinearity of the limit-state surface, not the limit-state function itself. Fig. 4-5 illustrates the behaviour of the limit-state surface for several threshold values of the hysteretic energy. The random variables, probability distribution types, and the distribution parameters are as listed in Table 4-1. The limit-state surface is examined for the combination of variables E and M, L and M, h and M, and σ_y and M in the standard normal space. The limit-state surface exhibits significant nonlinearity for all the combinations of random variables in Fig. 4-5.

Certain degree of nonlinearity is expected in the limit-state surface based on the observations in Fig. 4-4. However, the degree of nonlinearity observed in the behaviour of the limit-state surface for the combination of h and M, and σ_y and M implies that the application of the FORM may not be feasible. However, it is noted that the nonlinearities are only due to the variation of h and M as observed with Figs.

4-4b and 4-4e. If the sensitivity of the limit-state surface to these random variables is insignificant, then the nonlinearity may not be detrimental for the application of FORM. Therefore, reliability analysis is performed with FORM and mean-centered Monte Carlo sampling (MCS) to ascertain the degree of nonlinearity of the limit-state surface in the presence of *all* the random variables. A range of threshold values are considered from 1.0×10^6 Nmm to 7.0×10^6 Nmm and the results are listed in Table 4-3. The reliability analyses confirm that the limit-state surface is significantly nonlinear. For example, the reliability analyses with the threshold value of 2.0×10^6 Nmm results in a probability value of 0.42% from the FORM while the probability value from the MCS is 9.92% with 5% coefficient of variation. The difference in the probability estimates from FORM and MCS is in the order of 10%. Thus, the nonlinearity of the limit-state surface is detrimental to the application of FORM in this case. Also, the reliability analyses confirm that the limit-state surface is sensitive to the variation of h and M. This implies that the nonlinearity of the limit-state function observed in Figs. 4-4b and 4-4e indicates a highly nonlinear limit-state surface near the design point.

In order to ascertain that the observations from Figs. 4-4 and 4-5 hold valid for more realistic loading scenarios, a recorded ground motion is now considered. Fig. 4-6 shows the acceleration record of the ground motion and the elastic response spectrum with 5% damping in the units of acceleration due to gravity, g_a. Fig. 4-6b shows that the large amplitudes are at shorter periods, which is a typical observation in response spectra of design codes. Fig. 4-7 shows the variation of $g(e)$ for the variation of structural parameters of SDOF-SS model. Again, Figs. 4-7b and 4-7e exhibit significant nonlinearities for the variation of h and M respectively. This observation confirms that the nonlinearity of $g(e)$ is due to the sensitivity of the structural period to the variation of h and M. Specifically, when the structural period moves closer to the dominant frequencies in the loading, it initiates the yielding and the dissipation of hysteretic energy.

4.4.1.2. SDOF-RC Structure

Consider Fig. 4-8 where the variation of $g(e)$ is sought for the SDOF-RC model for the sine wave loading. The behaviour of the limit-state function is similar to the SDOF-SS case in Fig. 4-4. In particular, the energy limit-state function, $g(e)$, is severely nonlinear for variation of the mass as shown in Fig. 4-8e. Additionally, in Fig. 4-8e, the limit-state function is sensitive to the size of the time step in the dynamic analysis and exhibits numerical noise for larger Δt. Δt affects the hysteretic energy in two ways: 1) the hysteretic energy is evaluated by linearizing the force-deformation relationship between the analysis steps. Consequently, when the force-deformation relationship of RC cross-section is highly nonlinear, the linearization becomes invalid as the analysis time step size increases. 2) When a large analysis time step is applied, the noisy behaviour of the limit-state function is triggered by sudden yielding of more than one concrete fibre in a single time step. In case of a smaller time step, individual fibres yield in a single time step and result in a smoother force-deformation relationship and consequently, a numerically well-behaved limit-state function. In view of this sensitivity of the limit-state function, the analyst must employ an appropriately small time step when utilizing advanced material models with nonlinear and non-smooth force-deformation relationship, such as Concrete01, in the structural model.

Similar to the SDOF-SS case, the behaviour of the limit-state surface is examined in the standard normal space. For this purpose, the combination of the variables E and M, L and M, h_{RC} and M, and σ_y and M, is considered, as shown in Fig. 4-9. As observed in the previous case, the behaviour of the limit-state surface is significantly nonlinear. Furthermore, the limit-state surface exhibits noisy behaviour due to the Concrete01 material, as discussed above. It is apparent that the application of FORM may not be feasible. Nevertheless, significant nonlinearity is observed only for the variation of M in Fig. 4-8e. The presence of several random variables may alleviate the nonlinearity in the limit-state surface near the design point. In order to investigate the effect of random variables other than M, reliability analyses are performed with FORM and MCS considering all the random variables in Table 4-1. The threshold value in $g(e)$ is varied from 0.10×10^6 Nmm to 0.50×10^6 Nmm and the results are tabulated in Table 4-4. A comparison of the

FORM results with those of the MCS indicates that the degree of nonlinearity in the limit-state surface is indeed significant for threshold values below 0.20×10^6 Nmm. The linearization of the limit-state surface in the FORM analysis leads to inaccurate estimation of probability for the threshold values 0.10×10^6 Nmm and 0.15×10^6 Nmm. However, the FORM results are fairly accurate for threshold values above 0.20×10^6 Nmm. This improvement in the accuracy of FORM is because *M* is the sole contributor to the nonlinearity of limit-state surface; as observed in Fig. 4-8e the nonlinearity in the limit-state function *g(e)* with respect to the variation of *M* vanishes beyond the values of 0.20×10^6 Nmm.

Now, consider the SDOF-RC system with a damage index (*DI*) as the cumulative response measure. In the present study, the damage index based on cumulative inelastic deformations, developed by Mehanny and Deierlein (2000), is employed. The damage index value varies from 0.0 to 1.0, representing zero damage to complete damage. The damage index is estimated as

$$DI = \sqrt[\gamma]{(D_\theta^+)^\gamma + (D_\theta^-)^\gamma} \tag{4-6}$$

where D_θ^+ is the positive damage index evaluated as

$$D_\theta^+ = \frac{(\theta_p^+ |_{\text{PHC}})^\alpha + (\sum_i^{n+} \theta_p^+ |_{\text{FHC},i})^\beta}{(\theta_{pu}^+)^\alpha + (\sum_i^{n+} \theta_p^+ |_{\text{FHC},i})^\beta} \tag{4-7}$$

where θ_p^+ is some inelastic deformation in the positive loading direction, θ_{pu}^+ is the ultimate inelastic deformation capacity under monotonic loading in the positive direction. PHC refers to the primary half cycle, which implies that the amplitude in this load cycle exceeds the amplitude of all the previous load cycles. FHC refers to the follower half cycle wherein the amplitude is less than the previous PHC and *n*+ is the total number of FHCs in the positive load direction. Similarly, D_θ^- is the negative damage index evaluated as Eq. (4-7) with the inelastic deformations in the negative loading direction. α, β, and γ are the

calibrated parameters to an experimental database with the values as 1.00, 1.50, and 6.00, respectively, for reinforced concrete columns.

The variation of the damage limit-state function, denoted *g(DI)*, with the variation of the material parameters, such as E and f'_c, the geometry parameters, L and h_{RC}, and the dynamic properties, M and C, is evaluated as shown in Fig. 4-10. It is noted that the input parameters of the damage index are based on the ultimate cross-section deformation at failure. However, as the properties of the cross-section are varied, the input parameters of the damage index may vary. In the present study, the damage indices are considered to indicate a normalized variation of the response and hence, the input parameters are not varied with the variation of the material parameters. The behaviour of $g(DI)$ in Fig. 4-10 is similar to the behaviour of the energy limit-state function in Fig. 4-8. Furthermore, the numerical noise and the degree of nonlinearity in the damage index limit-state surface observed in Fig. 4-11 are similar in nature to energy limit-state surface in Fig. 4-9. Hence, the accuracy of FORM with $g(DI)$ is assumed to be similar to that of $g(e)$ and the reliability analyses are not conducted for this case.

4.4.1.3. MDOF Structure

For the MDOF system with sine wave loading, the limit-state function initially contains hysteretic energy dissipated by the center column in the bottom storey. Fig. 4-12 illustrates the behaviour of the limit-state function for the variation of mass M_1, material properties, such as f'_c and E, and the height of the top storey, H_s. Similar to the case of SDOF-RC, energy limit-state function, $g(e)$ exhibits sensitivity to the size of time step in dynamic analysis as observed in Fig. 4-12d. However, the limit-state function does not exhibit significant nonlinearities compared to Figs. 4-4 and 4-8. Thus, the limit-state surface may not exhibit significant nonlinearity.

In order to ascertain the degree of nonlinearity in the limit-state surface, the reliability analyses are performed with all the random variables presented in Table 4-2. The reliability analyses with the FORM and the MCS are conducted for a range of threshold values and the results are listed in Table 4-5. A comparison of the FORM and the MCS results indicates that the approximation of the limit-state surface

with a hyper-plane is reasonable. The absence of nonlinearity in the limit-state surface is a result of the fundamental period of the MDOF. The variation in the structural parameters has caused the fundamental period of MDOF vary between a range 0.3-0.6s, which is farther away from the period of the excitation at 0.8s. The higher modes of MDOF will have periods lesser that the fundamental period. This implies that the structure did not experience resonance, and the consequent dramatic nonlinearity of the limit-state surface, in any of its modes for the range of threshold values considered. Therefore, the FORM results are accurate for this case in contrast to the SDOF-SS and SDOF-RC. It is emphasised here that the linearity in the limit-state surface is mainly due to the variation of period and is independent of the number of degrees-of-freedom of the structure. However, analogous to the static case, the stiffness of MDOF, and hence the structural period, are less sensitive to the variation of structural parameters of a single element. The presence of multiple elements reduces the sensitivity of the structural period to the variation of parameters of a single element and consequently, reduces dramatic nonlinearities in the limit-state surface.

The hysteretic energy considered for the MDOF system is not a global structural response measure. Hence, the total repair cost, R_t, is considered as the cumulative global response measure. It is calculated as a summation of the cost of repair for each structural member. In turn, the cost of repair is estimated based on the damage index of each member. The cost of repair of each structural member is evaluated such that

$$R = 0.5(1 + \sin(\pi(DI - 0.5)))V \tag{4-8}$$

where R is the repair cost, DI is the damage index based on cumulative plastic deformations in Eq. (4-6) and V is the replacement value of the structural member. Eq. (4-8) is obtained heuristically. To make this cost model amenable to FORM a continuous function is assumed that models the increase in repair cost with increasing damage. The replacement value for columns in bottom storey are considered as \$9300, for the columns in top storey is considered as \$7100 and for the beams as \$10000.

Fig. 4-13 illustrates the behaviour of the total cost limit-state function, $g(R_t)$, for the variation of mass M_1, material properties, such as f'_c and E, and the height of the top storey, H_s. The limit-state function exhibits

significant numerical noise. However, the nonlinearity of the limit-state function appears to be insignificant. In order to ascertain the detrimental effects of the degree of nonlinearity in the limit-state surface, the reliability analyses with FORM and MCS are performed considering all the random variables in Table 4-2. Table 4-6 presents the reliability analyses results for a range of threshold values of the total cost from \$60 to \$140. The probability is consistently over-estimated by FORM in comparison to MCS. However, the accuracy of FORM results is primarily affected by the numerical noise rather than the nonlinearity in the limit-state surface.

4.4.2. Random dynamic loading

Modelling of dynamic load processes, such as winds and earthquakes, include uncertainties in the amplitudes, duration and other load characteristics. From a practical viewpoint, modelling these loads as stochastic processes allows the inclusion of uncertainties in their characteristics. Moreover, the uncertainties in these stochastic processes are often greater than those in structural parameters. This motivates the consideration of the case when the material and geometry parameters of a structure are deterministic while the dynamic loading is random. This case isolates the effects of the probabilistic modelling of the dynamic load on limit-state functions. The structural models, SDOF, SDOF-RC and MDOF are considered for study in this section.

In the present study, the loading is modelled as a discretized random process developed by Li and Der Kiureghian (1995). A Gaussian process is considered such that,

$$s(t) = \sum_{i=1}^{N} y_i h(t - t_i) \tag{4-9}$$

where y_i represent a train of equally spaced random pulses along time axis that are modelled as standard normal random variables, and $h(t\text{-}t_i)$ represents a filter modelled as an impulse response function with a specific period and damping ratio. Eq. (4-9) may represent an earthquake ground motion where pulses are considered the ruptures of a fault that are filtered through a soil medium. Modulating functions are applied to Eq. (4-9) to introduce the nonstationarity, which is the temporal variation in the ground motion

amplitude. In this study, the filter period is considered to be 0.8s with a damping ratio of 5%. Similar to the deterministic loading case, the duration of loading is considered as 8s. A stationary process is considered without the application of modulating functions. In order to study the characteristics of the limit-state surface for this type of loading, the visualization is carried out with two random pulses. These are located at 0.02 s and 4.0 s respectively.

4.4.2.1. SDOF Structure

Fig. 4-14 shows the limit-state surface for the hysteretic energy in the standard normal space for the SDOF system. The threshold values range from 500 Nmm to 1500 Nmm. It is apparent that the limit-state surface has a closed shape, and is point symmetric with respect to the origin. That is, if a realization of **y** is on the limit-state surface, then –**y** is also on the surface. The symmetry of the limit-state surface is due to two reasons; 1) symmetry in the probability distributions of the pulses; and 2) symmetry in the cross-section and geometry parameters of the structure. Consider that the positive realizations of pulses result in a ground motion arriving at the structure in a particular direction, then the negative realizations imply that the ground motion is in the opposite direction. As the dissipated energy is a scalar unit, a symmetric structure dissipates same amount of energy for the ground motion in either direction. Owing to this symmetry, the limit-state surface would have a minimum of two design points.

The shape of the limit-state surface also depends on the spacing of the pulses. If two pulses are sufficiently far apart, the superposition of the pulses does not significantly influence the peak amplitudes. For example, the peak amplitude of the excitation shows minor variation for the pulse spacing at 0.02 s and 4.0 s in Figs. 4-15a and 4-15b. Hence, the energy dissipated by the structure would be nearly twice the energy dissipated by a single pulse irrespective of the positive or negative realizations of the pulses. This results in the limit-state surface as seen in Fig. 4-14.

Conversely, consider the case when two pulses are closely spaced. In this case, when both pulses have realizations in same direction, the peak amplitude of loading will be twice that of a single pulse. Consequently, the limit-state surface is closer to the origin in the standard normal space. However, when

the realizations are in opposite direction, they effectively nullify each other resulting in a significant reduction in the amplitude of loading. Thus, the structure does not dissipate sufficient energy to reach the limit-state threshold and the limit-state surface moves farther away from the origin. Hence, the limit-state surface transforms into an elliptical shape as the spacing between the pulses decreases. The amplitude of the excitation is distinctly influence by the direction of the pulse at 2.0 s in Figs. 4-15c and 4-15d. Fig. 4-16 shows the limit-state surface for two pulses at 0.02 s and 2.0 s respectively. In comparison of Figs. 4-14 and 4-16, it is evident that a reduction in the spacing between pulses varies the shape of limit-state surface.

In addition to the pulse spacing, the application of modulating functions influences the shape of the limit-state surface. The modulating functions magnify the amplitude of pulses at certain time instants while reducing the amplitudes of pulses over the rest of the loading duration. Therefore, the de-amplified pulses cause an elongation in the limit-state surface.

4.4.2.2. SDOF-RC and MDOF structures

As a novel finding in this chapter, it is demonstrated in Fig. 4-17 that the limit-state surface has a closed shape in the standard normal space irrespective of the cumulative response measure and the structural model under consideration. Fig. 4-17a shows the limit-state surface with the damage index of SDOF-RC model for the two pulses spaced at 0.02 s and 4.0 s. In Fig. 4-17b, the structural model is MDOF, while the cumulative response considered is the total repair cost. The total cost limit-state surface is also a closed shape which exhibits symmetry in the standard normal space.

It is noted that the total cost limit-state surface may not maintain gradient continuity as the structure undergoes extreme damage. This is due to the fact that the behaviour of the limit-state surface is related to the effect of the damage concentration within a MDOF structure. For example, if the damage is concentrated in the bottom storey columns, the repair cost of the members will be equal to their full replacement value. An increase in the amplitude of loading does not significantly increase the total repair cost. However, consider that the damage is distributed among the top storey and the bottom storey

columns, but with the total repair cost equal to the previous case. This implies that all the members have suffered only a moderate damage. In this scenario, an increase in the amplitude of loading would increase the damage in each member and consequently, the total repair cost. Therefore, the limit-state surface with total repair cost exhibits the gradient discontinuity based on the distribution of damage to a combination of loading pulses.

4.4.3. Random structural properties and loading

Consider the comprehensive case when the structural properties are random in addition to the loading. Fig. 4-18 shows the limit-state surface in the standard normal space for the random pulse at 0.02s, and the structural properties of SDOF with $g(e)$ as limit-state function. The distributions of yield strength, stiffness, mass and damping ratio are considered as lognormal with the coefficient of variations as 15%, 10%, 20%, and 20%, respectively. As expected, the limit-state surface is symmetric about the random variable axis representing the pulse, while it is "open" along the axis that represents the structural property. Similar behaviour is expected from the SDOF-SS, SDOF-RC and MDOF models for the combination of structural and loading random variables.

4.5. SOLUTION STRATEGIES

In this chapter it is shown that, for cumulative response measures, 1) the limit-state surface is an open and highly nonlinear function when the random variables are structural parameters, and 2) the limit-state surface is a closed and symmetric function when the random variables are loading pulses. In the first case, the limit-state surface is possibly a hyper-paraboloid in the standard normal space. In the second case, the limit-state surface can be approximated by a hyper-ellipsoid in the standard normal space, with the axis of symmetry passing through the origin. When the structural parameters and the loading pulses are considered as random variables, the limit-state surface is a nonlinear function with a combination of quadratic and linear terms. Therefore, it is evident that the application of FORM, which requires an open and approximately linear limit-state surface, is not feasible for the dynamic reliability problems with cumulative responses. However, the application of alternative methods, such as approximation of the

limit-state surface with paraboloids or ellipses may be practical given the insight into the limit-state surface provided in this chapter. This is explored in the following.

4.5.1. Random structural properties (open limit-state surface)

Consider the case where the structural parameters are random variables and the loading is deterministic. As observed in Figs. 4-5, 4-9 and 4-11, the limit-state surface for SDOF-SS and SDOF-RC are approximately quadratic. Therefore, the estimation of the probability by fitting a hyper-paraboloid is considered. For this purpose, the efficient algorithm developed by Der Kiureghian and De Stefano (1991) is employed in order to estimate the principal curvatures. This algorithm estimates the first principal curvature from the same computations employed in the search for the design point, **y*** in the FORM. The probability is then evaluated with the approximate formulation by Breitung (1984)

$$p_p \approx \Phi(-\beta)\prod_{i=1}^{n-1}(1+\beta\kappa_i)^{-1/2} \tag{4-10}$$

where p_p is the probability content of the paraboloid, Φ is the standard normal distribution, β is the reliability index from the FORM analysis, and κ_i is the i^{th} curvature of the hyper-paraboloid of n random variables. In the present study, only the first principal curvature is considered.

The SORM analyses are performed for the SDOF-SS model with energy limit-state function for a range of threshold values. Table 4-3 shows the probability values from FORM, SORM and MCS. SORM provides similar estimates of the probability as that of FORM. This implies that all the curvatures of the paraboloid must be considered for an improvement in the probability estimate. Furthermore, SDOF-RC model is analysed with SORM with energy as the cumulative response in the limit-state function. This case includes the effect of noise due to RC cross-sections. The SORM results presented along with the probability values from FORM and MCS in Table 4-4. Similar to the previous case, the SORM results with the first principal curvature do not show significant improvement over to the FORM results.

4.5.2. Random dynamic loading (closed limit-state surface)

Consider the case where the loading pulses alone are random variables. As stated earlier, the limit-state surface could potentially be approximated by a hyper-ellipsoid based on the behaviour of the limit-state surface observed in Figs. 4-14, 4-16, and 4-17. The probability content of a hyper-ellipsoid in the standard normal space is obtained by considering an infinite linear combination of central or non-central Chi-square distributions (Ruben 1962, Fiessler *et al*. 1979). However, the evaluation of the probability content involves the evaluation of eigenvalues and the curvatures of the hyper-ellipsoid. These evaluations increase the computation cost of the reliability analyses in a high-dimensional standard normal space due to the large number of random variables involved in stochastic ground motion models.

An estimate of the probability is obtained by approximating a spheroid with center at the origin in the standard normal space and the radius equal to the reliability index, β, i.e. distance to a design point, **y***. The probability is estimated such that (Fiessler *et al*. 1979)

$$p_s = \chi_n^{\,2}(\beta^2) \tag{4-11}$$

where p_s is the probability content of the spheroid and χ_n^2 is the central Chi-square distribution with n degrees of freedom, where n is equal to the number of random variables. This estimate provides a lower bound of the probability of survival if the origin lies in the safe domain. An upper bound estimate of the required probability is obtained by approximating the probability content bounded by hyper-planes at the design point, **y*** and its symmetric point –**y***. The upper bound probability is evaluate such that,

$$p_u = 1 - 2 \cdot \Phi(-\beta) \tag{4-12}$$

where p_u is the probability content bounded by the hyper-planes, Φ is the cumulative standard normal distribution and β is the reliability index. This result is identical to that of Eq. (4-11) if the Chi-square distribution is considered with one degree of freedom.

To validate the proposed solution strategies, a random excitation is applied to the SDOF structure and MCS is performed for the energy limit-state function. The excitation is modelled based on Eq. (4-9). The

number of random pulses in the excitation is taken to be 400, which results in pulse spacing of 0.02s over the 8s duration of the loading. Table 4-7 lists the probability values obtained for a range of threshold values of energy from 0.10×10^6 Nmm to 0.50×10^6 Nmm. The coefficient of variation of the probability values from MCS is restricted to be less than 1%. Furthermore, the upper bound and lower bound of the probability are estimated based on Eqs. (4-11) and (4-12) and presented in Table 4-7. The upper bound values present a reasonable estimate of the probability. This implies that the limit-state hyper-ellipsoid has a dominant principal axis, which is substantially longer than the rest of the axes. On the other hand, the lower bound approximation by a hyper-spheroid fails to produce reasonable estimates of the probability. In fact, the estimates are zero irrespective of the value of reliability index. This result is due to the nature of high-dimensional standard normal space, which increases the number of degrees of freedom of Chi-square distribution and dilutes the probability density.

Similarly, the excitation with 400 random pulses over the duration of 8s is applied to the MDOF structure with limit-state function, $g(R_t)$, in order to perform a reliability analyses. A gradient-based search algorithm is employed to estimate the design points for a range of threshold values from \$5 to \$60. Based on the reliability index obtained from these analyses, the upper and lower bound estimates of the probability are calculated as shown in Table 4-8. Furthermore, the reliability analyses are performed with MCS to estimate the probability content and the results are presented in Table 4-8. In MCS, the coefficient of variation of probability values is limited to be below 1%. The lower and upper bound values of the probability in this case are too wide for a meaningful estimation. The lower bound values are zero due to the high-dimensionality of the standard normal space in the presence of large number of random variables. The upper bound values over-estimate the probability, which indicates that the limit-state hyper-ellipsoid has several principal axes with similar lengths.

An alternative strategy to improve the probability bounds is to search for the limit-state surface along each random variable axis and estimate the probability by "multi-point" FORM (Ditlevsen and Madsen 1996). The multi-point FORM is a parallel system reliability formulation. It involves approximating with

a plane at several points on the limit-state surface, which in effect results in a polyhedral approximation of the probability content. However, the search along each random variable axis may be computationally expensive in a high-dimensional standard normal space typical for dynamic problems with stochastic load processes. It is noted that a polyhedral approximation can also be performed with a single design point by assuming a hyper-cube. Further research is required in order to improve the accuracy and efficiency of the probability estimation.

4.6. CONCLUDING REMARKS

The applicability of FORM for the estimation of structural reliability with FE models and nonlinear time-history analysis is explored. The limit-state functions are formulated in the context of performance-based earthquake engineering. In particular, cumulative responses, such as hysteretic energy, damage index, and repair cost, are considered in the limit-state functions. Case studies are conducted with various SDOF and MDOF structures. Following the methodology in Chapter 3 for feasibility assessment, the results indicate that:

1. The gradient discontinuity in the limit-state function is not a significant concern with the cumulative response.
2. The presence of numerical noise is dependent on the analysis parameters such as dynamic analysis load step, material models, and certain cumulative responses such as repair cost.
3. The limit-state surface is a significantly nonlinear function but well-behaved to be approximated by quadratic functions; such as paraboloids or ellipsoids.

The solution strategies are proposed separately for the cases with the random structural properties and random dynamic loading. The approximation of the limit-state surface with a hyper-paraboloid is proposed when only the structural properties are random. In the second case, methods to estimate the probability bounds are presented. The results indicate that further research is required to develop the techniques which improve the accuracy of the probability estimates with reasonable computation cost.

Table 4.1: Structural parameters of the SDOF-SS and SDOF-RC structures

Parameter	Mean	Standard Deviation	Distribution
Mass (M)	3000 kg	600 kg	Lognormal
Damping ration (C)	0.05	Deterministic*	Deterministic
Length of the column (L)	3000 mm	166.67 mm	Normal
Number of fibres	20	Deterministic	Deterministic
Structural Steel (SDOF-SS)			
Cross-section dimension (h)	100 mm	10 mm	Lognormal
Young's modulus (E)	200000 N/mm^2	20000 N/mm^2	Lognormal
Yield stress (σ_y)	500 N/mm^2	75 N/mm^2	Lognormal
Ratio of post-yield stiffness (α)	0.05	Deterministic	Deterministic
Size of dynamic analysis time step (Δt)	0.01s	Deterministic	Deterministic
Reinforced Concrete (SDOF-RC)			
Section dimension (h_{RC})	200 mm	10 mm	Lognormal
Young's modulus of steel (E)	200000 N/mm^2	20000 N/mm^2	Lognormal
Yield stress of steel (σ_y)	500 N/mm^2	75 N/mm^2	Lognormal
Ratio of post-yield stiffness of steel (α)	0.05	Deterministic	Deterministic
Compressive strength of concrete (f'_c)	28 N/mm^2	4.20 N/mm^2	Lognormal
Strain of concrete at f'_c (ε_c)	0.002	0.0003	Lognormal
Size of dynamic analysis time step (Δt)	0.005s	Deterministic	Deterministic

*Deterministic implies that the parameter is not considered as a random variable in the analysis

Table 4.2: Structural parameters of MDOF structure

Parameter	Mean	Standard Deviation	Distribution
Depth of center column (h_c)	610 mm	20 mm	Lognormal
Width of center column (b_c)	690 mm	20 mm	Lognormal
Top storey height (H_s)	3700 mm	200 mm	Lognormal
Ratio of post-yield stiffness of steel (α)	0.02	Deterministic*	Deterministic
Young's modulus of steel (E)	200000 N/mm^2	20000 N/mm^2	Lognormal
Yield stress of steel (σ_y)	420 N/mm^2	63 N/mm^2	Lognormal
Compressive strength of concrete (f'_c)	28 N/mm^2	4.20 N/mm^2	Lognormal
Strain of concrete at f'_c (ε_c)	0.002	0.0003	Lognormal
Mass (M_1)	173.29x10^3 kg	34.66x10^3 kg	Lognormal
Mass (M_2)	86.65x10^3 kg	17.33x10^3 kg	Lognormal
Mass (M_3)	43.83x10^3 kg	8.77x10^3 kg	Lognormal
Number of fibres	12	Deterministic	Deterministic
Damping ration (C)	0.05	Deterministic	Deterministic
Size of dynamic analysis time step (Δt)	0.005s	Deterministic	Deterministic

*Deterministic implies that the parameter is not considered as a random variable in the analysis

Table 4.3: Probability for SDOF-SS with energy limit-state function

Threshold	FORM	SORM	MCS	Difference	Coefficient of Variation
$1.0x10^6$ Nmm	$3.415x10^{-6}$	$3.355x10^{-6}$	0.079592	0.079	5%
$2.0x10^6$ Nmm	0.004208	0.003402	0.099276	0.095	5%
$3.0x10^6$ Nmm	0.060253	0.048653	0.17404	0.114	5%
$4.0x10^6$ Nmm	0.22283	0.18553	0.36440	0.142	5%
$5.0x10^6$ Nmm	0.46134	0.45588	0.63234	0.171	5%
$6.0x10^6$ Nmm	0.71186	0.95502	0.83894	0.128	5%
$7.0x10^6$ Nmm	0.88848	0.99589	0.95041	0.062	5%

Table 4.4: Probability for SDOF-RC with energy limit-state function

Threshold	FORM	SORM	MCS	Coefficient of Variation
$0.10x10^6$ Nmm	$0.72972x10^{-3}$	$0.20063 x10^{-3}$	0.07640	1%
$0.15x10^6$ Nmm	0.12234	0.090521	0.24176	<1%
$0.20x10^6$ Nmm	0.61592	0.61037	0.73542	1%
$0.25x10^6$ Nmm	0.93836	0.99350	0.95820	<1%
$0.30x10^6$ Nmm	0.99517	0.99480	0.99666	<1%

Table 4.5: Probability for MDOF with energy limit-state function

Threshold	FORM	MCS	Coefficient of Variation
500 Nmm	0.12741	0.1298	<1%
1000 Nmm	0.65053	0.6597	<1%
1500 Nmm	0.89554	0.9027	<1%
2000 Nmm	0.95314	0.9611	<1%
2500 Nmm	0.97999	0.9846	<1%

Table 4.6: Probability for MDOF with cost limit-state function

Threshold	FORM	MCS	Coefficient of Variation
$60	0.04558	0.0194	<1%
$80	0.29714	0.1745	<1%
$100	0.64367	0.5208	<1%
$120	0.89875	0.8292	<1%
$140	0.98554	0.9608	<1%

Table 4.7: Probability for SDOF with energy limit-state function and random load

Threshold	Reliability index	Lower bound	Upper bound	MCS	Coefficient of Variation
0.10×10^6 Nmm	0.90844	0	0.63636	0.3702	<1%
0.20×10^6 Nmm	1.2749	0	0.79766	0.6986	<1%
0.30×10^6 Nmm	1.5617	0	0.88164	0.8303	<1%
0.40×10^6 Nmm	1.8031	0	0.92860	0.9003	<1%
0.50×10^6 Nmm	2.0171	0	0.95632	0.9390	<1%

Table 4.8: Probability for MDOF with cost limit-state function and random load

Threshold	Reliability index	Lower bound	Upper bound	MCS	Coefficient of Variation
\$5	1.171	0	0.7584	1.9027×10^{-3}	<1%
\$10	1.6479	0	0.9006	0.04704	<1%
\$20	2.3286	0	0.9806	0.3798	<1%
\$40	3.2615	0	0.9989	0.8358	<1%
\$60	3.6106	0	0.9997	0.9528	<1%

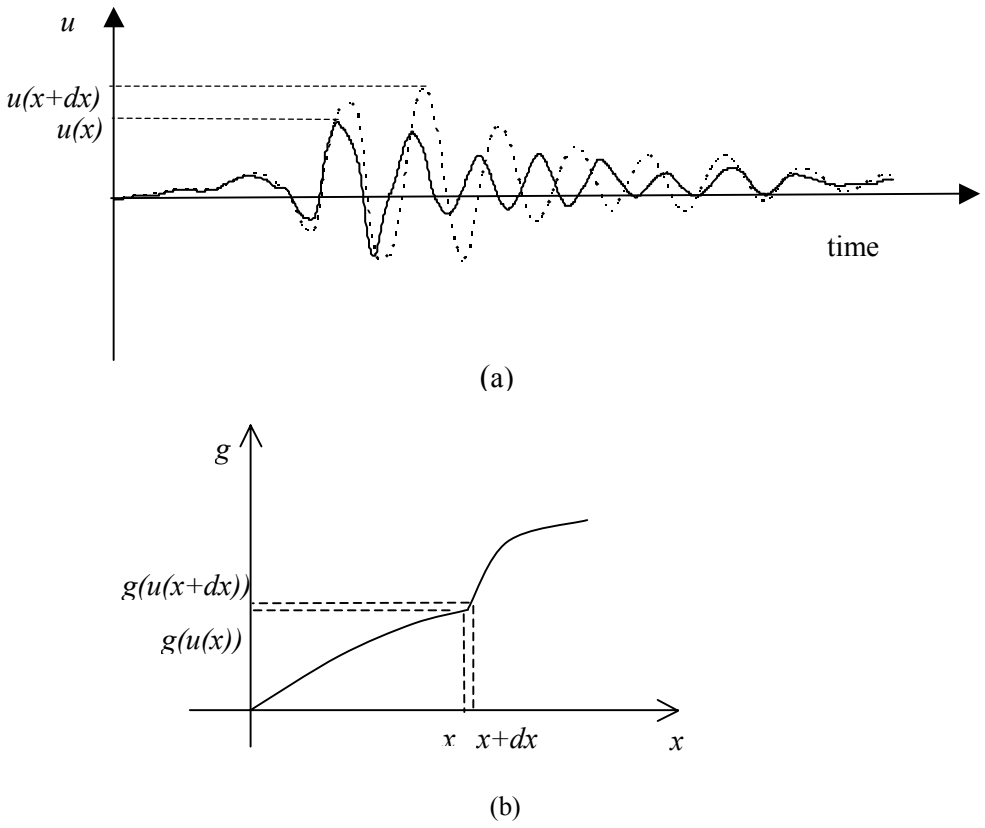

Figure 4.1: Schematic representation of the influence of peak response parameters on the behaviour of the limit-state function; a) response, b) limit-state function

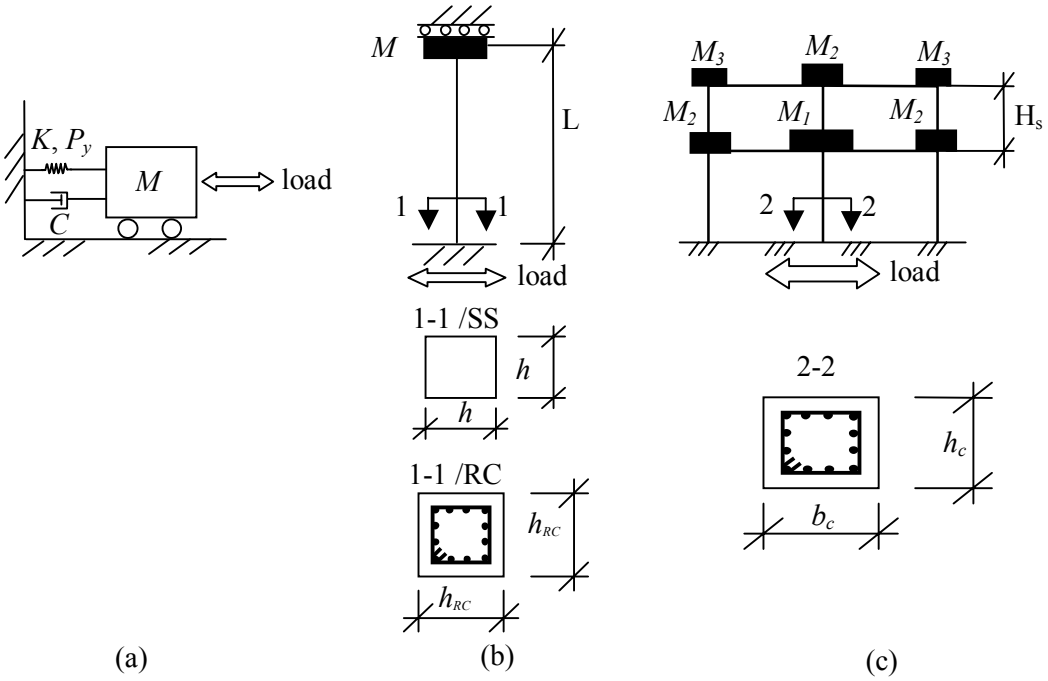

Figure 4.2: a) Basic single-degree-of-freedom (SDOF) structure; b) Single-degree-of-freedom structure with structural steel (SDOF-SS) and reinforced concrete sections (SDOF-RC); c) Multiple-degree-of-freedom (MDOF) structure with reinforced concrete section

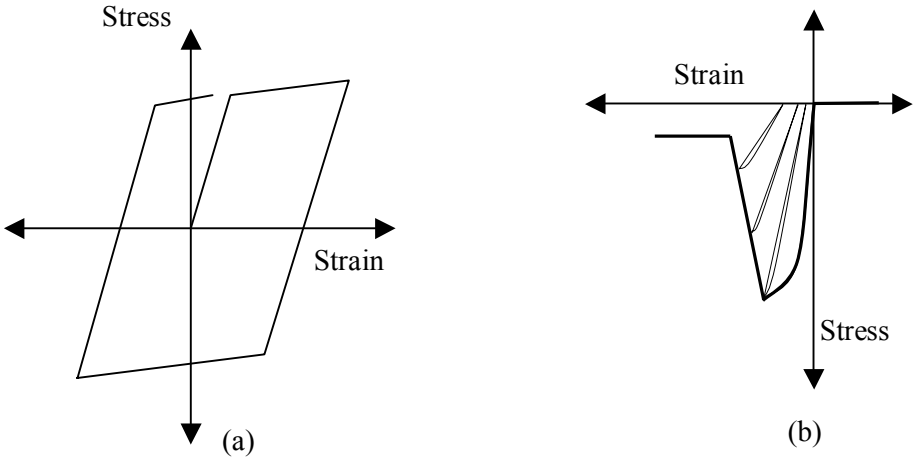

Figure 4.3: a) Stress-strain relationship of steel; b) Stress-strain relationship of concrete

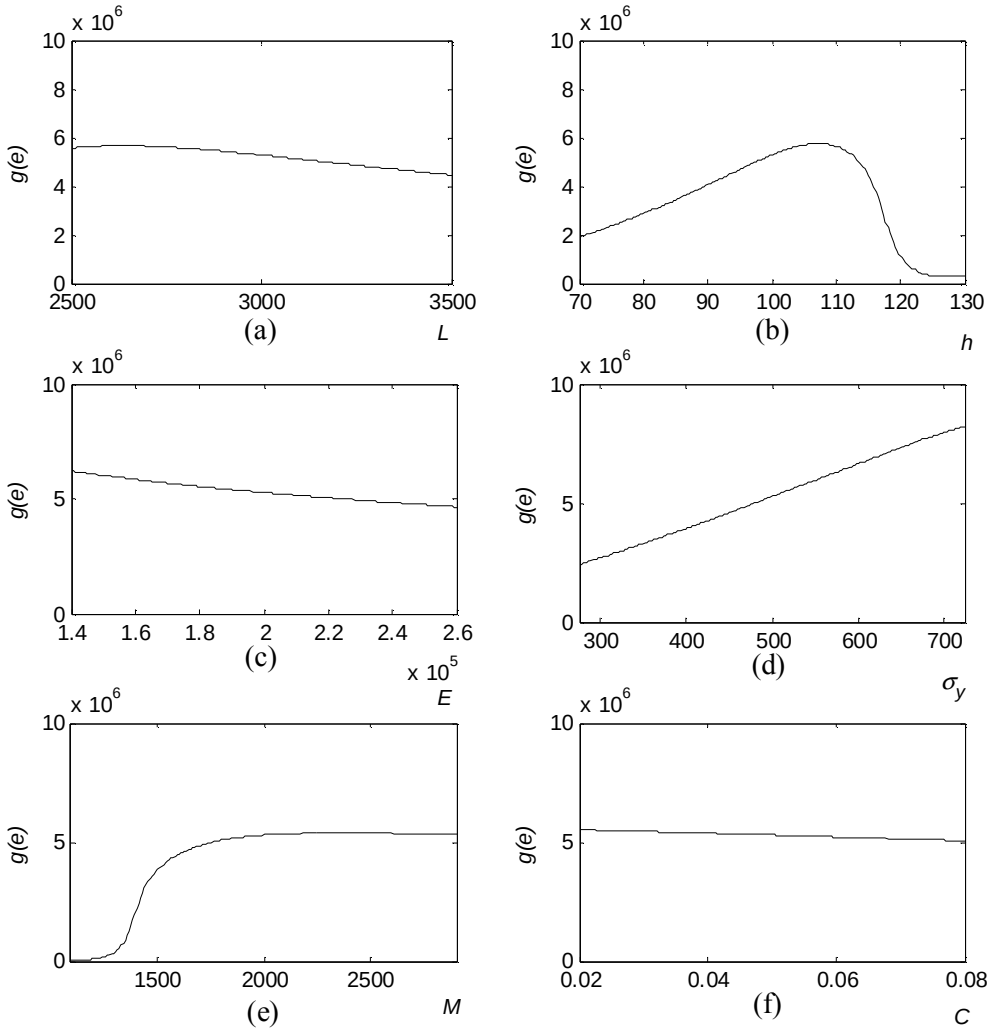

Figure 4.4: Behaviour of energy limit-state function (in Nmm) of the SDOF-SS, for the variation of (a) length (mm) ; (b) cross-section dimension (mm); (c) Young's modulus of steel, (N/mm^2); (d) yield stress of steel (N/mm^2); (e) mass (kg); (f) critical damping ratio

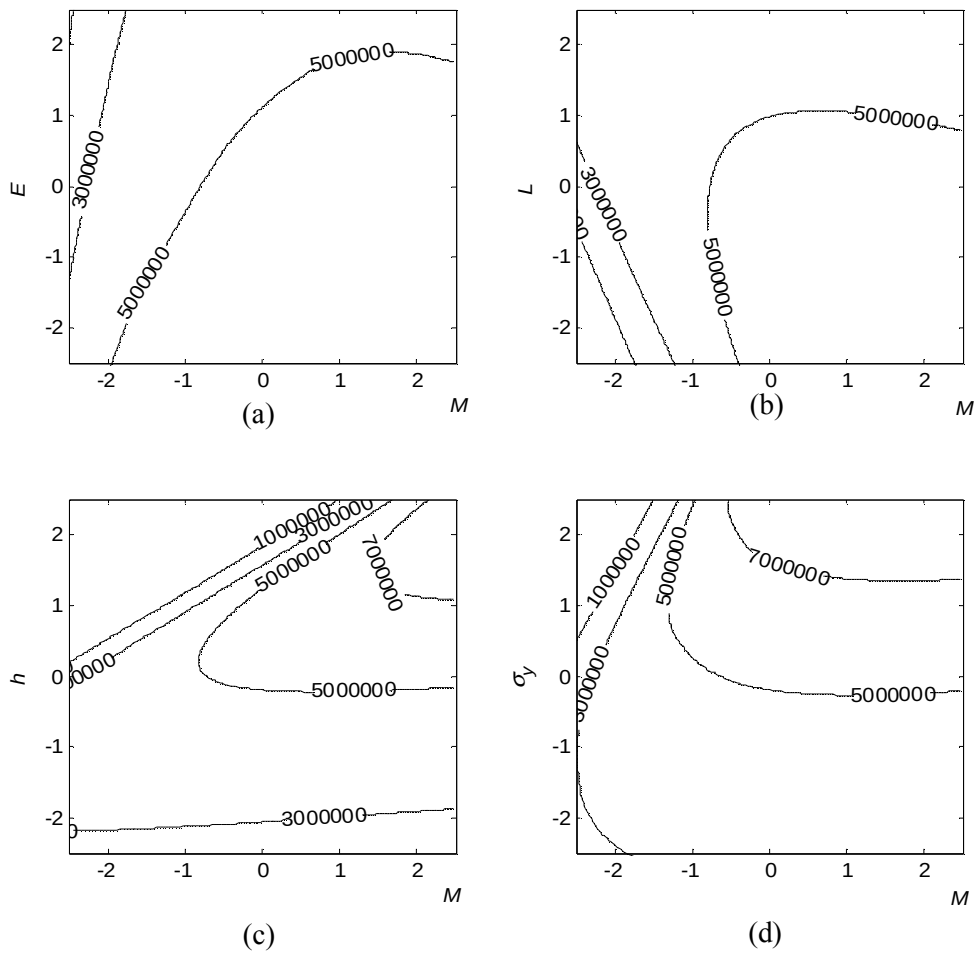

Figure 4.5: Behaviour of the energy limit-state surface (in Nmm) of the SDOF-SS in the standard normal space for the variation of the random variables; (a) mass and Young's modulus of steel, (b) mass and length, (c) mass and cross-section dimension, (d) mass and yield stress of steel.

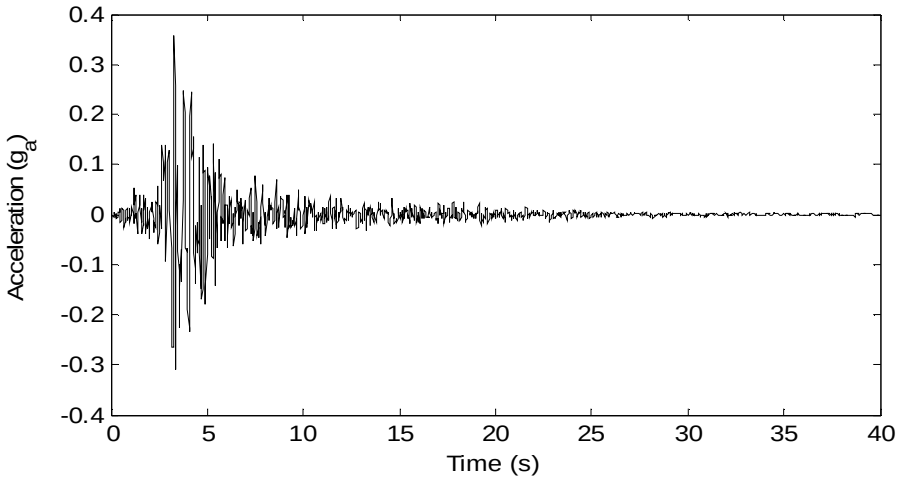

(a)

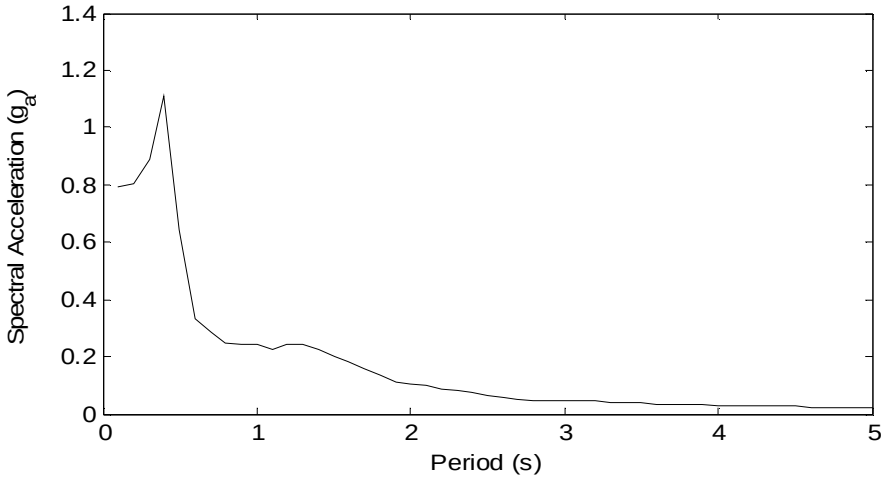

(b)

Figure 4.6: (a) Ground motion record; (b) Elastic response spectrum with 5% damping

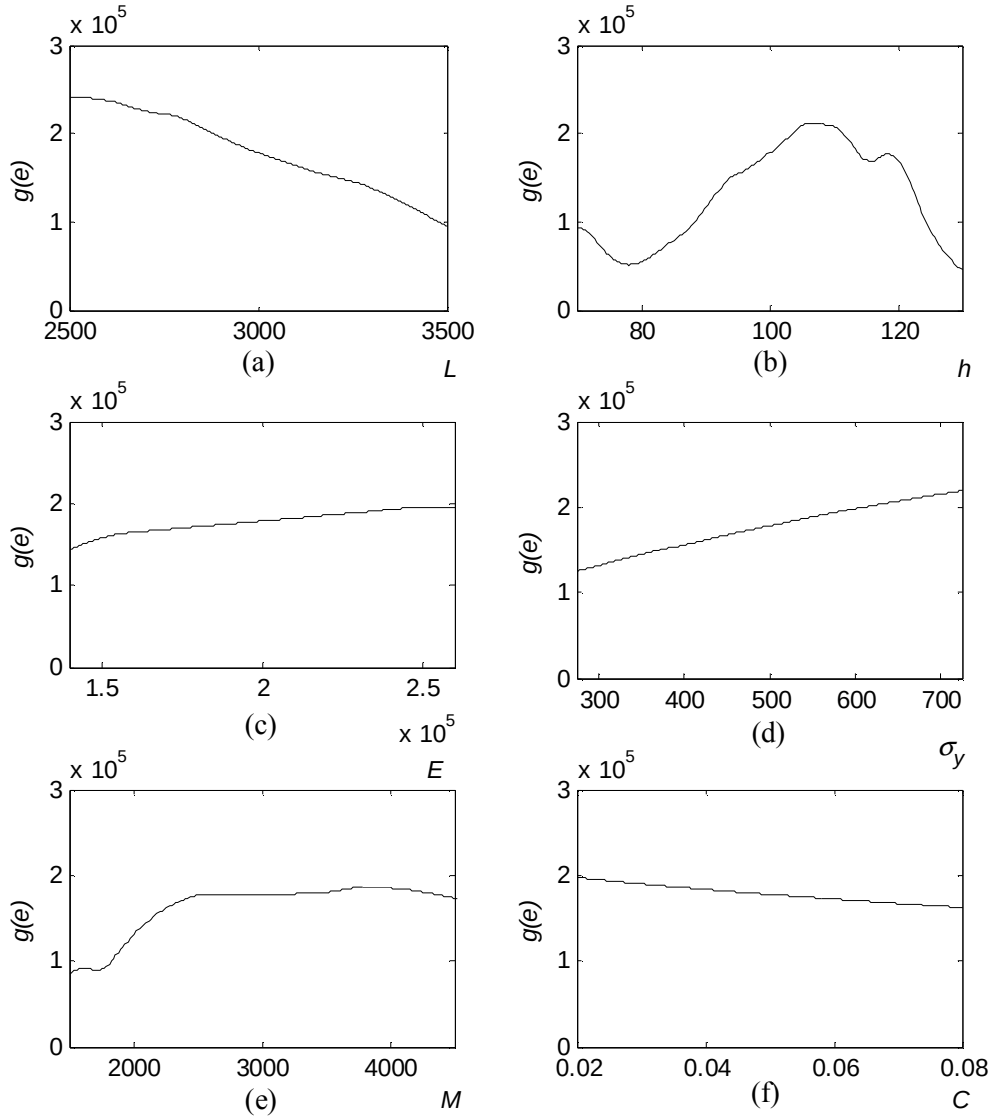

Figure 4.7: Behaviour of energy limit-state function (in Nmm) of the SDOF-SS for the ground motion loading, for the variation of (a) length (mm) ; (b) cross-section dimension (mm); (c) Young's modulus of steel, (N/mm^2); (d) yield stress of steel (N/mm^2); (e) mass (kg); (f) critical damping ratio

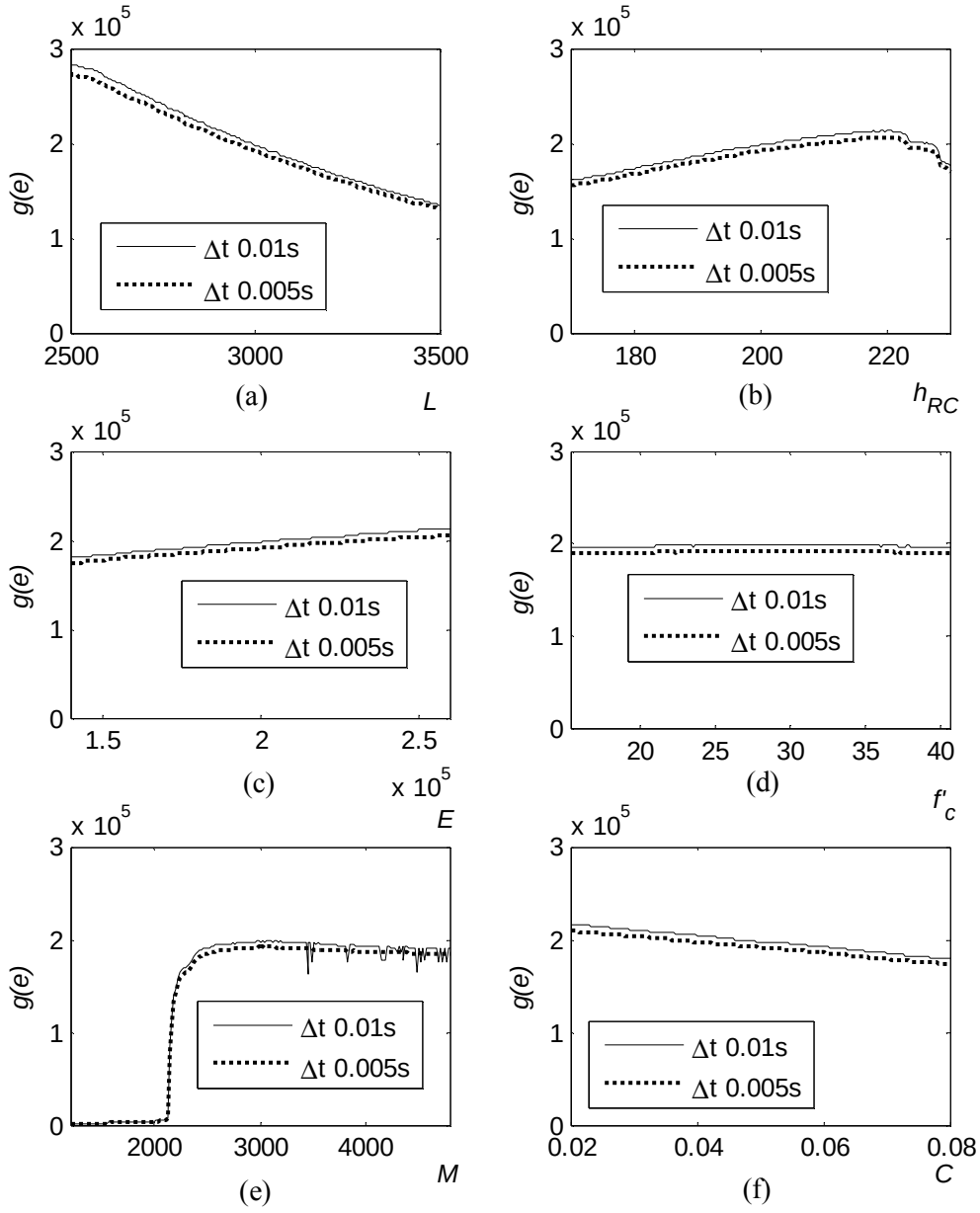

Figure 4.8: Behaviour of energy limit-state function (in Nmm) of the SDOF-RC, for the variation of (a) length (mm) ; (b) cross-section dimension (mm); (c) Young's modulus of steel, (N/mm^2); (d) compressive strength of concrete (N/mm^2); (e) mass (kg); (f) critical damping ratio

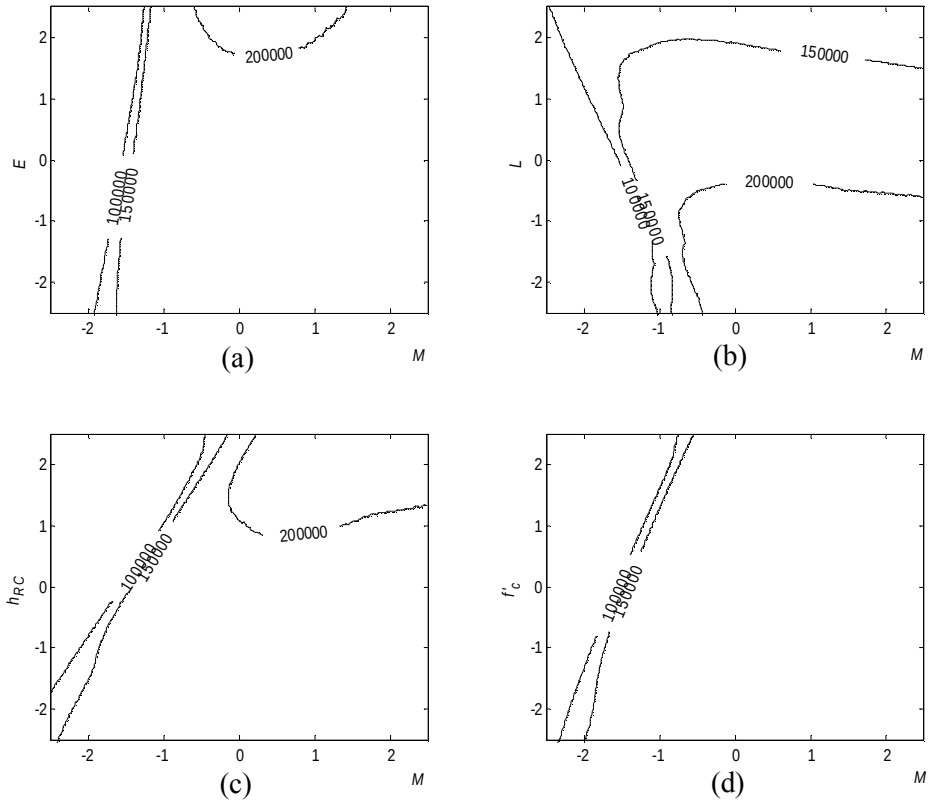

Figure 4.9: Behaviour of the energy limit-state surface (in Nmm) of the SDOF-RC in the standard normal space for the variation of the random variables; (a) mass and Young's modulus of steel, (b) mass and length, (c) mass and cross-section dimension, (d) mass and compressive strength of concrete

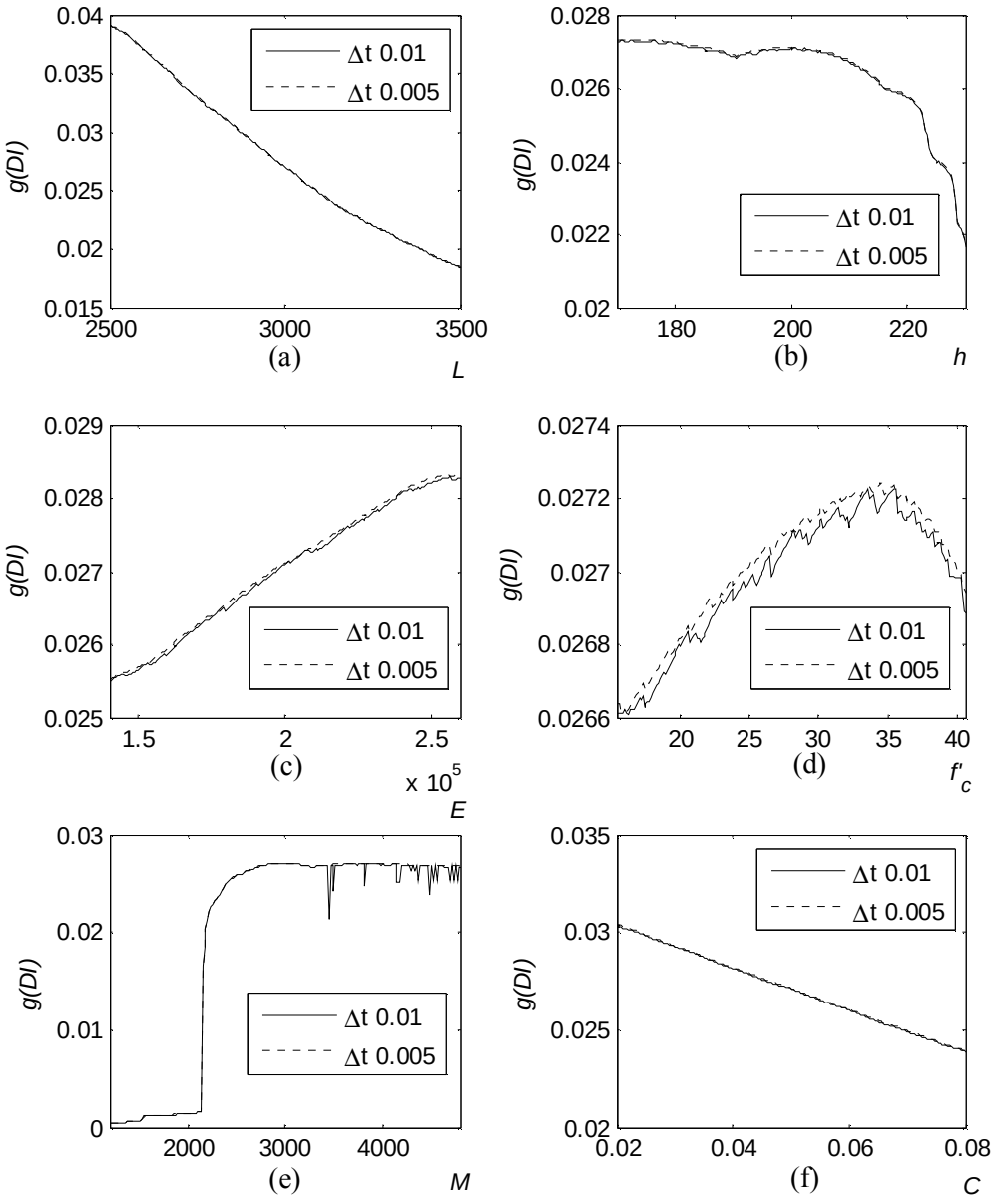

Figure 4.10: Behaviour of damage index limit-state function of the SDOF-RC, for the variation of (a) length (mm) ; (b) cross-section dimension (mm); (c) Young's modulus of steel, (N/mm^2); (d) compressive strength of concrete (N/mm^2) (e) mass, (kg); (f) damping ratio

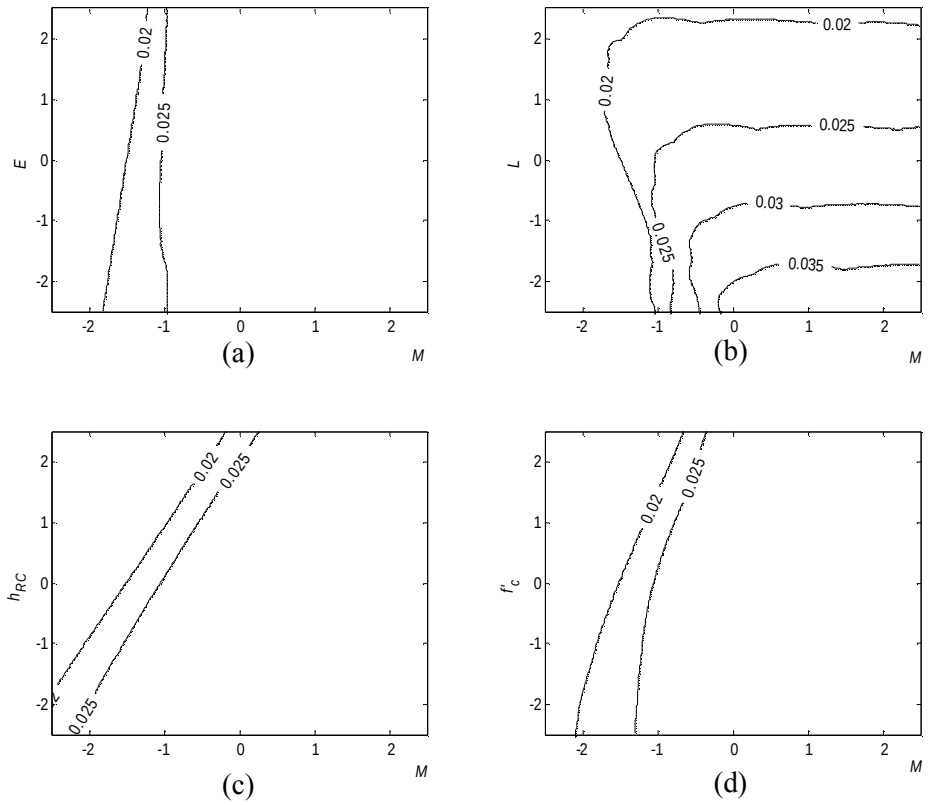

Figure 4.11: Behaviour of the damage limit-state surface of the SDOF-RC in the standard normal space for the variation of the random variables; (a) mass and Young's modulus of steel, (b) mass and length, (c) mass and cross-section dimension, (d) mass and compressive strength of concrete

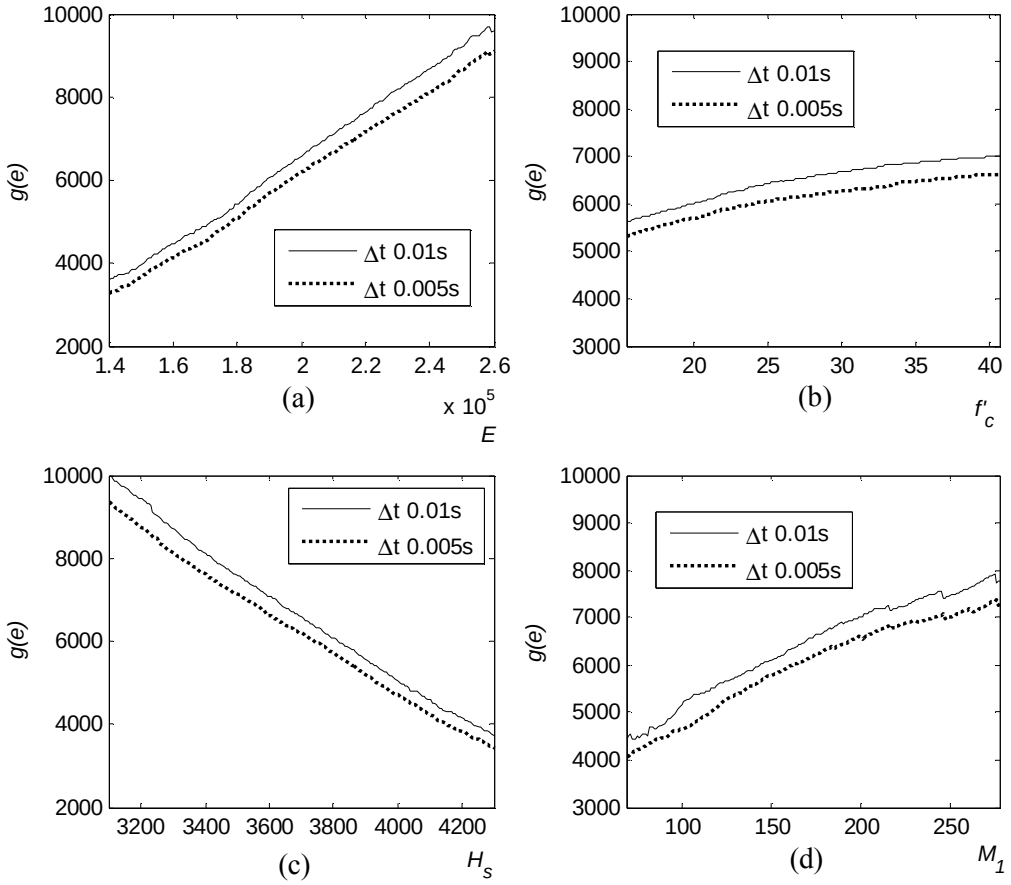

Figure 4.12: Behaviour of energy limit-state function (in Nmm) of the MDOF, for the variation of (a) Young's modulus of steel, (N/mm^2); (b) compressive strength of concrete (N/mm^2); (c) height of the top storey (mm); (d) mass on the center column in bottom storey (kg)

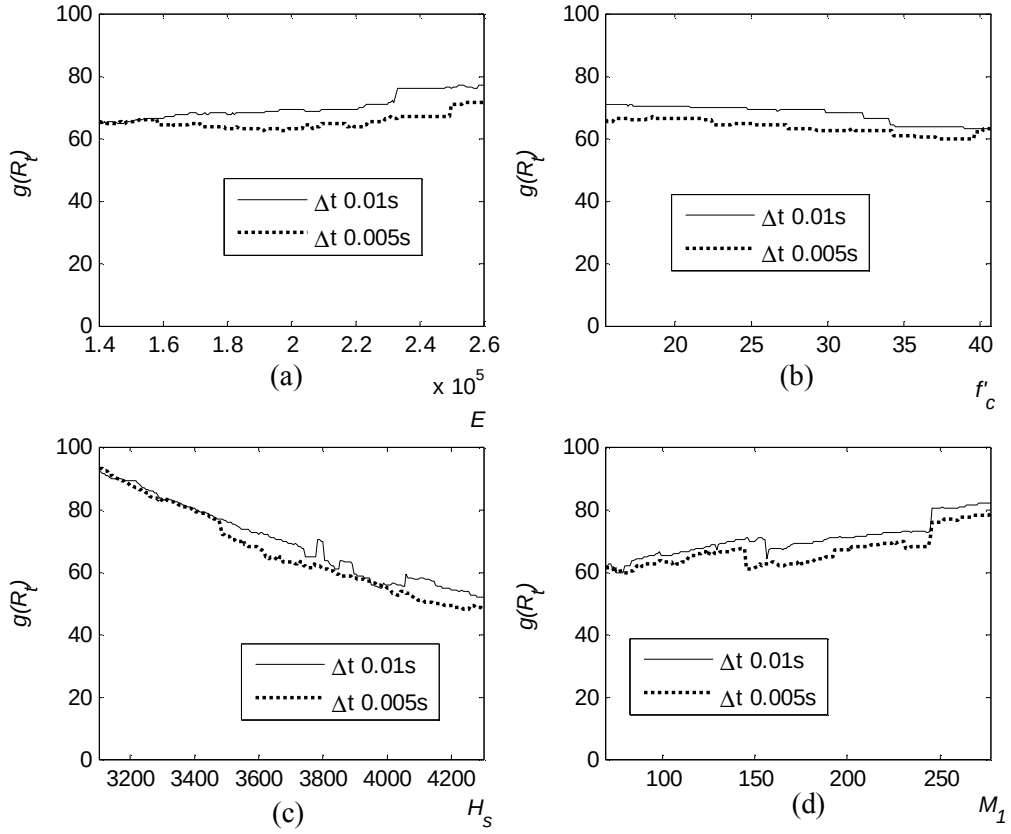

Figure 4.13: Behaviour of cost limit-state function (in $) of the MDOF, for the variation of (a) Young's modulus of steel, (N/mm^2); (b) compressive strength of concrete (N/mm^2); (c) height of the top storey (mm); (d) mass on the center column in bottom storey (kg)

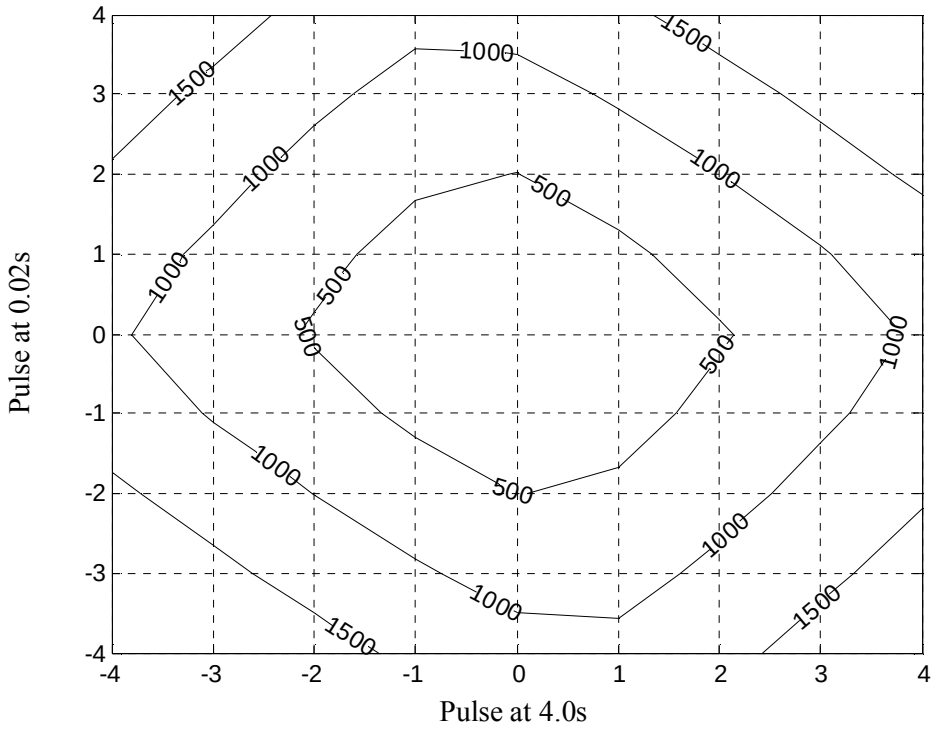

Figure 4.14: Behaviour of energy limit-state surface (in Nmm) of SDOF structure

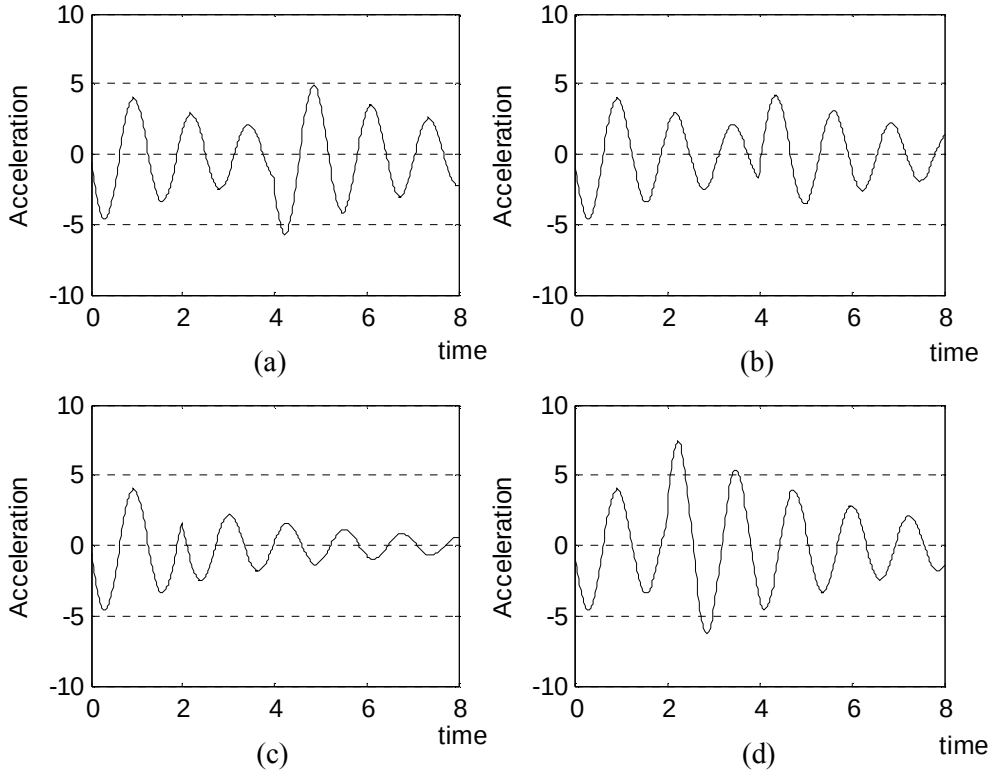

Figure 4.15: Variation in the amplitude of excitation with respect to the pulse spacing. Excitations with pulse spacing at 0.02s and 4.0s and a) amplitude of both the pulses 1.0, b) amplitude of the pulses 1.0 and -1.0, respectively. Excitations with pulse spacing at 0.02s and 2.0s with c) amplitude of both the pulses 1.0, and d) amplitude of the pulses 1.0 and -1.0, respectively.

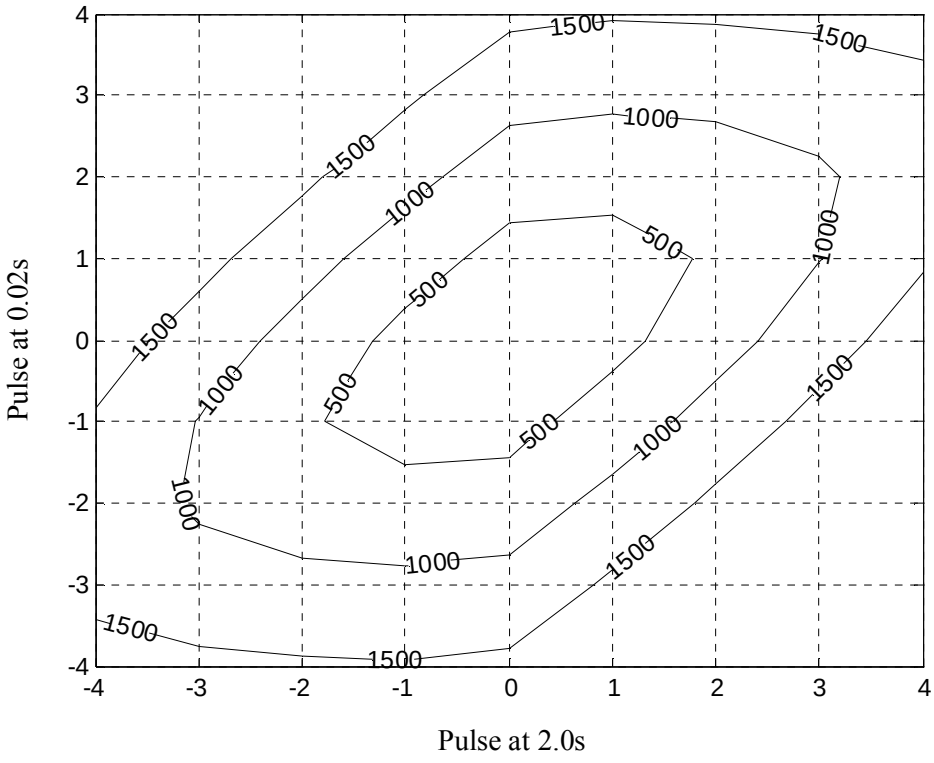

Figure 4.16: Behaviour of the energy limit-state surface (in Nmm) of the SDOF with random pulses in the loading spaced at 0.02s and 2.0s

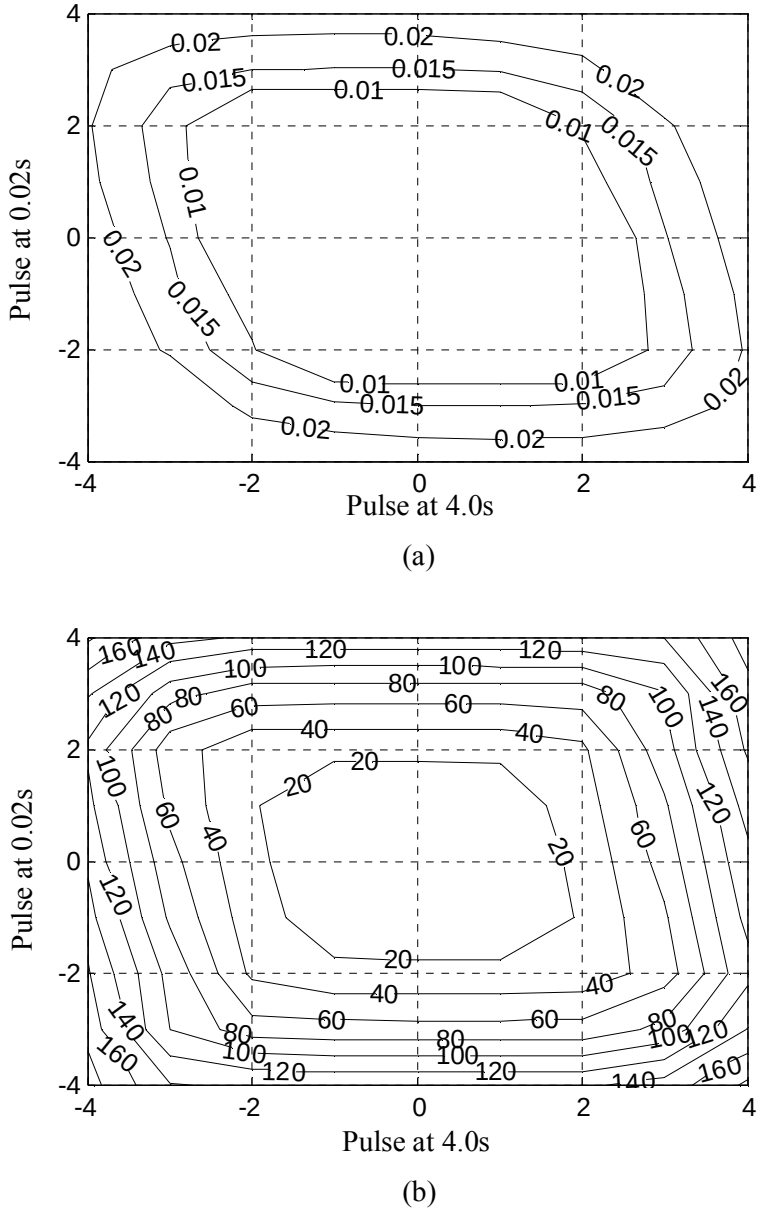

Figure 4.17: a) Behaviour of the damage index limit-state surface of the SDOF-RC structure; b) Behaviour of the cost limit-state surface (in $) of the MDOF structure

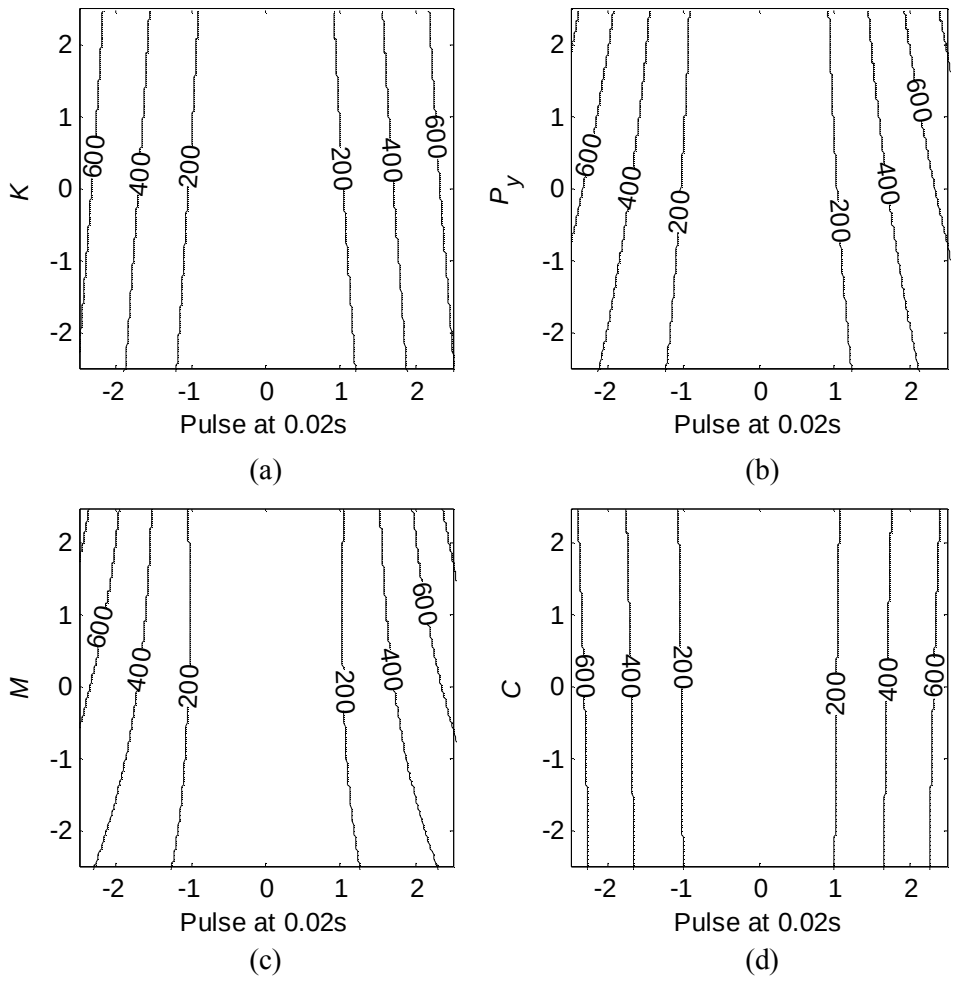

Figure 4.18: Behaviour of the energy limit-state surface (in Nmm) of the SDOF in the standard normal space with the random variables as, a) stiffness and loading pulse, b) yield strength and loading pulse, c) mass and loading pulse, d) damping ratio and loading pulse

REFERENCES

Au, S.K. and Beck, J.L. (2001), "First excursion probabilities for linear systems by very efficient importance sampling," *Probabilistic Engineering Mechanics*, 16, 193-207

Au, S.K., and Beck, J.L., (2003), "Subset simulation and its application to seismic risk based on dynamic analysis," *Journal of Engineering Mechanics*, 129 (8), 901-917

Bracci, J.M. Reinhorn, A.M. Mander, J.B. and Kunnath, S.K. (1989), "Deterministic model for seismic damage evaluation of RC structures," *Technical Report NCEER-89-0033*. National Center for Earthquake Engineering Research, State University of New York, Buffalo, NY

Breitung, K. (1984), "Asymptotic approximations for multinormal integrals," *Journal of Engineering Mechanics*, 110 (3), 357-366

Caughey, T.K. (1963), "Equivalent linearization techniques," *Journal of the Acoustical Society of America*, 35(11), 1706-1711

Ching, J., Beck, J.L., and Au, S.K. (2005), "Hybrid subset simulation method for reliability estimation of dynamical systems subject to stochastic excitation," *Probabilistic Engineering Mechanics*, 20, 199-214

Der Kiureghian, A. and De Stefano, M. (1991), "Efficient algorithm for second-order reliability analysis," *Journal of Engineering Mechanics*, 117 (12), 2904-2923

Der Kiureghian, A. (2000), "Geometry or random vibrations and solutions by FORM and SORM," *Probabilistic Engineering Mechanics*, 15 (1), 81-90

Ditlevsen, O. and Madsen, H.O. (1996), *Structural reliability methods*, John Wiley and Sons

Hagen, O. and Tvedt, L. (1991), "Vector out-crossing as parallel system sensitivity measure," *Journal of Engineering Mechanics*, 117(10), 2201-2220

Fiessler, B., Neumann, H.-J., and Rackwitz, R. (1979), "Quadratic limit states in structural reliability," *Journal of Engineering Mechanics*, 105 (4), 661-676

Fujimura, K., and Der Kiureghian, A. (2007), "Tail-equivalent linearization method for nonlinear random vibration," *Probabilistic Engineering Mechanics,* 22(1), 63-76

Katafygiotis, L.S., Moan, T., and Cheung, S.H., (2007), "Auxiliary domain method for solving multi-objective dynamic reliability problems for nonlinear structures," *Structural Engineering and Mechanics*, 25 (3), 347-363

Koo, H., A. Der Kiureghian (2003), *FORM, SORM and Simulation Techniques for Nonlinear Random Vibrations*, Report No. UCB/SEMM-2003/01, Department of Civil and Environmental Engineering, University of California, Berkeley, CA

Koo, H., Der Kiureghian, A., and Fujimura, K. (2005), "Design-point excitation for non-linear random vibrations," *Probabilistic Engineering Mechanics,* 20(2), 136-147

Kratzig, W.B., Meyer, I.F. and Meskouris, K. (1989), "Damage evolution in reinforced concrete members under cyclic loading," In A.H-S. Ang, M.Shizonuka and G.I. Schuller (Ed.s), *Structural Safety and Reliability: Proceedings of 5th International Conference on Structural Safety and Reliability (ICOSSAR '89), San Francisco, 7-11 Aug 1989*. New York: American Society of Civil Engineers.

Li, C.C. and Der Kiureghian, A. (1995), "Mean out crossing rate of nonlinear response to stochastic input," *Proceedings of 7th International Conference on Applications of Statistics and Probability in Civil Engineering*, Paris, France, July 10-13, 1995. A.A.Balkema

Lutes, L.D. and Sarkani, S. (2004), *Random Vibrations: Analysis of Structural and Mechanical Systems*, Butterworth-Heinemann.

Mason, A. B., Jr., and Iwan, W. D. (1983), "An approach to the first passage problem in random vibration," *Journal of Applied Mechanics, Transactions of ASME,* 50(3), 641-646

Mehanny, S.S., and Deierlein, G.G. (2000), *Modeling of Assessment of Seismic Performance of Composite Frames with Reinforced Concrete Columns and Steel Beams.* Report No. 135, The John A. Blume Earthquake Engineering Center, Department of Civil and Environmental Engineering, Stanford University.

McKenna, F., Fenves, G.L., and Scott, M.H. (2004), *OpenSees*: *Open system for earthquake engineering simulation*. Pacific Earthquake Engineering Research Center, University of California, Berkeley, CA

Naess, A. (1990), "Approximate first-passage and extremes of narrow-band Gaussian and non-Gaussian random vibrations," *Journal of Sound and Vibration,* 138(3), 365-380

Park, Y., and Ang, A. H. -S. (1985) "Mechanistic seismic damage model for reinforced concrete," *Journal of Structural Engineering,* 111(4), 722-739

Ruben, H. (1962), "Probability content of regions under spherical normal distributions, IV: The distribution of homogeneous and non-homogeneous quadratic functions of normal variables," *The Annals of Mathematical Statistics*, 33(2), 542-570

Vanmarcke, E. H. (1975), "On the distribution of the first-passage time for normal stationary processes," *Journal of Applied Mechanics, Transactions of ASME,* 42 Ser E(1), 215-220

Wen, Y.K. (1980), "Equivalent linearization for hysteretic systems under random excitation," *Journal of Applied Mechanics*, *Transactions of ASME,* 47(3), 150-154

Williams, M.S. and Sexsmith, R.G. (1995), "Seismic damage indices for RC structures: A state-of-the-art review," *Earthquake Spectra* 11(2): 319-349.

Yang, J.N., and Shinozuka, M. (1971), "On the first excursion probability in stationary narrow- band random vibration," *Journal of Applied Mechanics, Transactions of ASME*, 38 Ser E (4), 1017-22

Yao, T.H.-J. and Wen, Y.K., (1996), "Response surface method for time-variant reliability analysis," *Journal of Engineering Mechanics*, 122, 193-201.

Zhang, Y., and Der Kiureghian, A. (1994), "First-excursion probability of uncertain structures," *Probabilistic Engineering Mechanics,* 9(1-2), 135-143

Zhang, J. and Foschi, R.O., (2004), "Performance-based design and seismic reliability analysis using designed experiments and neural networks," *Probabilistic Engineering Mechanics*, 19, 259-267

Chapter 5. PROBABILISTIC EVALUATION OF COLLAPSE[1]

5.1. INTRODUCTION

The primary objective in this chapter is to apply probabilistic capacity models developed for individual members in global structural reliability assessments. Member degradation prior to global failure is included. The work is motivated by the emerging performance-based earthquake engineering approach, in which realistic simulation of structural behaviour is a key ingredient. This approach requires sophisticated structural models, as well as probabilistic analysis to account for uncertainties in loads, structural properties, and analysis procedures. Two short-term objectives are addressed in this chapter: 1) extension of the conventional nonlinear static seismic analysis procedure with reliability analysis, and 2) utilization of probabilistic capacity and post-failure response models based on experimental data for individual members. The result is a sophisticated structural reliability software that provides the probability of collapse subsequent to degradation of individual members. Notably, importance measures are available from the analysis to identify the most influential structural parameters.

The significance of the developments in this chapter is seen in light of the extensive use of nonlinear static analysis − often referred to as pushover analysis − in contemporary earthquake engineering practice. In this approach the capacity of structures to withstand a ground motion is evaluated by subjecting the structural model to gradually increasing lateral loads. The design is deemed satisfactory for the "collapse prevention" performance level if the structural integrity is maintained past the lateral displacement that is expected to be imposed by the design earthquake. Techniques such as the capacity spectrum method and the coefficient method are employed to determine this target displacement (FEMA 356 2000, ATC-40 1996, FEMA 440 2005, Chopra and Goel 2000, Fajfar 1999, Lin *et al*. 2004). This methodology is extended in the present study with uncertainty characterization of structural parameters and reliability

[1] A version of this chapter has been published. Koduru, S.D. and Haukaas, T. and Elwood, K.J.(2007), "Probabilistic evaluation of global seismic capacity of degrading structures," *Earthquake Engineering and Structural Dynamics*, 36(13), 2043-2058

analysis to determine the failure probability. In particular, commonly employed structural models are extended with probabilistic capacity models to allow degradation of individual members, and consequently the structure, prior to reaching the target displacement. The finite element models include nonlinear beam-column elements with fiber-discretized cross-sections with individual material models for concrete and reinforcing steel fibers.

It is emphasized that the methodology developed in this chapter is based on the assumption that one mode of vibration dominates the response, which is an inherent assumption in the classical pushover approach. The inclusion of additional vibration modes in nonlinear pushover analysis is an on-going and challenging research topic (Chopra and Goel 2002). In the present study improvements of the classical approach that include probabilistic results and parameter importance measures are suggested. However, similar to the challenging nature of combining the response from different pushover analyses, the issue of combining the associated probabilities is not addressed by this study.

The present study addresses the seismic capacity evaluation of existing reinforced concrete (RC) structures. In many buildings constructed before the advent of modern seismic code provisions the columns are lightly reinforced in the transverse direction. These are prone to brittle shear failures rather than ductile flexural failures and are often referred to as "shear critical" columns. After shear failure, a column may exhibit loss of axial load carrying capacity and, consequently, collapse of the structure is possible. Several models are developed to estimate the shear and axial capacity of shear critical columns, including those by Sugano (1996), Pujol (2002), Elwood and Moehle (2005a,b). However, these are deterministic models in which the uncertainty − a key issue for reliability assessments − is not explicitly accounted for. Recently, probabilistic capacity models have been developed based on a Bayesian methodology (Gardoni *et al*. 2002, Zhu *et al*. 2005). These models are ideally suited for the global seismic reliability analysis put forward in this chapter.

The merger between finite element analysis and reliability methods employed herein is termed "finite element reliability analysis." This methodology has been developed during the past two decades to

account for uncertainties in input parameters of the finite element model and to compute the probability of rare response events. Haukaas and Der Kiureghian (2004) implemented finite element reliability analysis in OpenSees, which is an open-source, object-oriented software developed specifically for earthquake engineering (McKenna *et al*. 2004). In the present study, OpenSees is further extended with probabilistic capacity models for individual elements and applied in the proposed probabilistic pushover analysis methodology. The developments in this chapter also extend the initial efforts presented by Haukaas and Elwood (2005), in which the concept of a target displacement was not incorporated and only shear failures of columns were considered.

In the following, the overall reliability analysis methodology is first presented, including the determination of the target displacement demand and the associated collapse limit-state formulation. The availability of parameter importance measures from the reliability analysis is emphasized. The probabilistic capacity and post-failure response models are then presented followed by potential problems and remedies in the reliability analysis. In particular, the problem with "gradient discontinuities" is discussed along with smoothing techniques to ensure convergence of the reliability analysis. Finally, a numerical example is presented to demonstrate a practical application of the methodology.

5.2. FINITE ELEMENT RELIABILITY ANALYSIS FOR SEISMIC CAPACITY EVALUATIONS

In the current engineering practice, nonlinear static pushover analysis is the predominant means of verifying a structure's capacity to withstand a ground motion. In this chapter the coefficient method in FEMA-440 (2005) is employed, in which the expected lateral displacement at the top of the structure relative to the base − here referred to as the "target displacement demand," u_t, − is given as

$$u_t = C_o C_1 C_2 S_a \frac{T_e^2}{4\pi^2} g_a \tag{5-1}$$

The coefficients C_j (j = 0,1,2) are given in FEMA-440 (2005), while S_a denotes the response spectral acceleration at the effective fundamental period T_e for the structure and g_a is the acceleration due to

gravity. It is noted that the target displacement computed by Eq. (5-1) is conditioned upon the occurrence of an earthquake with a specific return period. That is, the uncertainty in the ground motion is not explicitly accounted for. Rather, the aim of the presented methodology is to compute the probability of collapse prior to reaching a target displacement, such as that specified by Eq. (5-1). Subsequently, by varying the target displacement, the probability curve for the global structure is obtained, as demonstrated in the numerical example. This type of reliability analysis is also a valuable means of identifying the parameters of the structural model that should be addressed to improve the seismic capacity of the structure.

The reliability analysis to determine the probability of collapse prior to reaching u_t has three key ingredients: structural model, random variables, and limit-state function. As mentioned previously, a novelty in this study is the probabilistic member capacity and post-failure models employed in the structural model. The model parameters, as well as all material and geometry parameters of the structure, are characterized as random variables. It is emphasized that the uncertainty in the structural properties may be significant; considerable scatter is observed in the capacity of non-ductile RC members. The third ingredient, the limit-state function, g, is an implicit function of the random variables and is defined so that a negative outcome denotes the failure event. Hence, to compute the probability that the displacement at collapse is less than the target displacement demand is defined as

$$g(\mathbf{x}) = u_c(\mathbf{x}) - u_t \tag{5-2}$$

where $\mathbf{x}$ is the vector of random variables and u_c is the displacement response at which the structure collapses. For the moment it is assumed that collapse is defined as axial failure of a specific set of columns. This assumption is discussed later in this chapter. As a qualitative example of events that may take place during the analysis, consider the structure in Fig. 5-1. The schematic pushover curve for the building is shown to the right. The numbers in the curve correspond to events that occur during the pushover analysis. It is observed that the global stiffness exhibits a sudden degradation at shear failure of any column. Additional stiffness degradation is present due to the nonlinear response of the concrete and

the steel reinforcement. Upon axial failure of two columns a mechanism forms and collapse manifests. At this point the structural analysis terminates. In fact, singularity in the global stiffness matrix for the structure may be employed as a collapse indicator, as discussed later.

It is emphasized that the proposed methodology is anchored in the contemporary static pushover approach. This differs from the strategy that employs nonlinear dynamic analysis with suites of ground motions. It is important to realize that the pushover approach has unique advantages and disadvantages. Although the methodology put forward in this chapter enhances its value in several ways, a prudent approach must be applied by the analyst. For instance, for particular structures in which higher modes of vibration contribute significantly to the response, the dynamic analysis approach may reveal certain sequences of member failures that are not captured by the static pushover approach. It is, however, stressed that the probabilistic extension put forward in this chapter significantly improves the deterministic approach by indeed including the possibility for different failure modes (different column failure sequences) compared to the deterministic pushover approach currently utilized.

The probability p_f associated with the limit-state function in Eq. (5-2) is formulated as the multi-fold integral (Ditlevsen and Madsen 1996)

$$p_f = \int_{g(\mathbf{x})\le 0} \cdots \int f(\mathbf{x})\mathrm{d}\mathbf{x} \tag{5-3}$$

where $f(\mathbf{x})$ is the joint probability density function for the random variables. This problem cannot be solved analytically. Reliability methods such as the first- and second-order reliability methods (FORM and SORM), sampling, and response surface techniques are available to evaluate it in an approximate manner. These methods require repeated runs of the finite element analysis for different realizations of the random variables $\mathbf{x}$. As each finite element analysis is computationally costly, some reliability methods are unaffordable. This is for instance the case with mean-centered Monte Carlo sampling (MCS) analysis. In general, MCS requires thousands of runs of the finite element analysis, while FORM analysis requires only in the order of 10 to 20, albeit including the evaluation of response gradients. Efficient computation

of response gradients is already available in OpenSees through the implementation of the direct differentiation method (Haukaas and Der Kiureghian 2004). Moreover, FORM analysis renders available parameter importance measures to identify the most influential structural parameters. Based on these considerations FORM is employed in the finite element reliability analysis in this chapter. To facilitate the subsequent developments, this approach is briefly reviewed in the following.

In FORM, the integration boundary $g(\mathbf{x})=0$ in Eq. (5-3) − denoted the "limit-state surface" − is approximated by a hyper-plane. This approximation is not made in the space of the random variables $\mathbf{x}$ but in the transformed space of uncorrelated standard normal random variables, denoted $\mathbf{y}$. The hyper-plane is tangent to the limit-state surface at "the most probable failure point" (MPP), $\mathbf{y}^*$, which is the point on the limit-state surface closest to the origin. In FORM, the reliability index β is the distance from the origin to the MPP and is related to the probability by $p_f = \Phi(-\beta)$, where Φ is the standard normal cumulative distribution function.

The determination of the MPP constitutes a constrained optimization problem. This problem is most efficiently solved by gradient-based algorithms, that is, algorithms that require both the value of g and its gradient, $\partial g/\partial \mathbf{y}$ at trial points $\mathbf{y}_i$ towards the MPP $\mathbf{y}^*$. A schematic overview of the algorithm that iteratively searches for the MPP is shown in Fig. 5-2. The communication between the reliability algorithm and the finite element analysis is shown by dashed arrows. The finite element model repeatedly receives new realizations $\mathbf{x}_i$ of the random variables and returns the displacement response at collapse, $u_c(\mathbf{x}_i)$, along with the response sensitivities $\partial u_c/\partial \mathbf{x}$ computed by the direct differentiation method. In the expression for the gradient of the limit-state function it is noted that $\partial g/\partial u_c = 1$ for the limit-state function in Eq. (5-2), while $\partial \mathbf{x}/\partial \mathbf{y}$ is the Jacobian ($\mathbf{J}_{x,y}$) of the probability transformation, which is computed by the reliability algorithm in OpenSees.

An objective in this chapter is to identify the parameters that are most influential on the reliability of non-ductile RC structures. This is achieved by characterizing all structural parameters as random and utilizing

parameter importance measures from the reliability analysis to rank them. The three importance measures considered herein are $\boldsymbol{\gamma}$, $\boldsymbol{\delta}$, and $\boldsymbol{\eta}$ presented by Haukaas and Der Kiureghian (2005). The importance measure $\boldsymbol{\gamma}$ identifies the significance of the uncertainty in each random variable. To this end, consider the contribution of the variance of each random variable to the variance of the approximated hyper-plane g at $\mathbf{y}^*$. In FORM, the contribution of the variances of $\mathbf{y}$ to the variance of g at $\mathbf{y}^*$ is available by evaluating the well-known "alpha vector," which is the negative normalized gradient vector $\boldsymbol{\alpha} = -\nabla_y G(\mathbf{y}^*) / \| \nabla_y G(\mathbf{y}^*) \|$. Thus, the relative importance of the elements in $\mathbf{y}$ is obtained by ranking the values of corresponding elements in $\boldsymbol{\alpha}$. However, the importance ranking of $\mathbf{y}$ does not imply the same ranking of $\mathbf{x}$ when the random variables are correlated. Therefore, the variance of g is obtained by linearizing the probability transformation $\mathbf{y} = T(\mathbf{x})$ at the MPP. This enables the separation of the contribution from the variances of $\mathbf{x}$ and the contribution from the correlations between $\mathbf{x}$. Consequently, the normalized importance vector for the original random variables, $\mathbf{x}$, reads

$$\boldsymbol{\gamma} = \frac{\boldsymbol{\alpha}\mathbf{J}_{\mathbf{y}^*,\mathbf{x}^*}\hat{\mathbf{D}}}{\| \boldsymbol{\alpha}\mathbf{J}_{\mathbf{y}^*,\mathbf{x}^*}\hat{\mathbf{D}} \|} \tag{5-4}$$

where $\boldsymbol{\alpha}$ is the negative normalized gradient as defined above, $\mathbf{J}_{\mathbf{y}^*,\mathbf{x}^*}$ is the Jacobian of the probability transformation, and $\hat{\mathbf{D}}$ is the diagonal matrix of the standard deviations of the transformed random variables. The random variable with the largest absolute value of $\boldsymbol{\gamma}$ has the highest contribution to the uncertainty in u_c.

It is also of interest to estimate the influence of the probability distribution parameters on p_f. For this purpose, the importance rankings of the means and the standard deviations of $\mathbf{x}$ are obtained by employing the reliability sensitivity measures derived by Hohenbichler and Rackwitz (1986), and Bjeranger and Krenk (1989). These importance measures are

$$\boldsymbol{\delta} = \nabla_{\mu} \beta \mathbf{D} \tag{5-5}$$

and $$\boldsymbol{\eta} = \nabla_{\sigma}\beta\mathbf{D} \tag{5-6}$$

where $\nabla_{\mu}\beta$ and $\nabla_{\sigma}\beta$ are the gradient vectors of β with respect to the means and the standard deviations, respectively, and **D** is the diagonal matrix of the standard deviations of **x**. The importance vector $\boldsymbol{\delta}$ provides an importance ranking of the means of the random variables, whereas $\boldsymbol{\eta}$ provides an importance ranking of their standard deviations. The importance measures, $\boldsymbol{\gamma}$, $\boldsymbol{\delta}$, and $\boldsymbol{\eta}$ are utilized in the numerical example to illustrate the relative importance of the intervening parameters.

5.3. IMPLEMENTATION OF PROBABILISTIC CAPACITY AND POST-FAILURE RESPONSE MODELS

The failure mechanics of shear critical RC columns is different from that of ductile columns found in modern buildings. For the latter type of columns, the concept of plastic hinges is frequently employed to model the nonlinear response when subjected to lateral load. Conversely, the lateral load capacity of the shear critical columns degrades due to the formation of diagonal shear cracks, and subsequently these columns may experience degradation of axial load capacity due to sliding along the principal shear failure plane. These phenomena are captured by the novel probabilistic capacity and post-failure response models that are included in the reliability analysis in this chapter. Shear failure and subsequent axial failure of individual columns takes place prior to the attainment of the final failure state of the global structure. The capacity models are drift-based, which implies that each column is expected to undergo shear failure and subsequently axial failure depending on the drift ratio. (Drift ratio is defined as the net difference in lateral displacement of the end points divided by the length of the column.) Several approaches are possible to model this type of degradation. In this study the modeling technique presented by Elwood (2004) is adopted, in which "springs" are coupled in series to one end of the column. These springs monitor the drift ratio of the adjoining column and initiate the transition into the post-shear failure and post-axial failure response regimes.

The probabilistic capacity models utilized in this study are developed by applying a Bayesian updating procedure to an experimental database (Zhu *et al*. 2007). The shear capacity model for the shear spring has the form

$$\ln(\frac{\Delta_s}{L}) = \ln\left(\theta_1 \rho'' + \theta_2 \frac{s}{d} + (0.0069 - 0.26\theta_2) \frac{a}{d} + \theta_3 \frac{P}{A_g f_c'} \right) + \sigma\varepsilon \qquad (5\text{-}7)$$

where Δ_s/L is the shear capacity, $\rho'' = A_{st}/bs$ denotes the transverse reinforcement ratio; A_{st} denotes the area of transverse reinforcement; s is the hoop spacing; b is the width of column section; d is the depth to the centerline of the outermost tension reinforcement; a is the shear span; P is the axial load; $A_g = bD$ denotes the gross cross-sectional area of the column; D is the depth of column section and $f'c$ is the compressive strength of concrete. Notably, all these parameters are considered as random variables in the reliability analysis in this chapter. This is also the case with the model parameters θ_i (i = 1, 2, 3), and $\sigma\varepsilon$. These are the random variables that represent the model error in the shear capacity model. Table 5-1 lists the distribution types and the distribution parameters for the random variables θ_i and $\sigma\varepsilon$ as given by Zhu *et al*. (2007).

Once shear failure is detected, the force-deformation relationship for the shear spring is redefined. It is governed by two parameters: the degrading slope, K_{deg}, and the residual strength, F_{res} as shown in Fig. 5-3a. These parameters can be given by the user or computed in OpenSees according to formulae provided by Elwood (2004). Fig. 5-3 schematically shows the transition into the post-failure response at the failure deformation of the member, $\Delta_{t\text{-}fail}$. The total response of a member is governed by the response of the flexural element and the force-deformation relationship of the spring after the failure is detected at the failure strength, F_{fail}.

It is common to develop axial capacity models that are independent of the shear capacity. Examples are the deterministic shear and axial models developed by Elwood and Moehle (2004a, b) and the probabilistic shear and axial capacity models developed by Zhu *et al*. (2007). Unfortunately, the

assumption of independence between axial and shear failure is based on convenience and lack of data rather than physical insight. In fact, axial failure is conditioned upon shear failure for the models considered in this study. In normal structural analysis, the independence between shear and axial capacity models is not detrimental. However, the utilization of the models in the proposed reliability analysis may cause problems. As the realization of the random variables is altered to reach the MPP, as described previously, the outcome of the axial capacity of the columns that constitute a collapse mechanism is altered so that failure is reached exactly at the target displacement u_t; that is, so that $g(\mathbf{x}) = u_c(\mathbf{x}) - u_t = 0$. In effect, the realization of the axial capacity is altered while the shear capacity is not significantly affected. Consequently, when the shear and axial capacity models are independent, realizations where the shear capacity is greater than the axial capacity may occur.

To solve the problem of unphysical joint realizations of the shear and axial capacity models one would ideally develop correlated models or an axial capacity model that is conditioned upon shear failure. However, this is outside the scope of the present work and is addressed by ongoing research. Instead, the problem is remedied by modeling the axial capacity as the shear capacity plus a random variable h that is determined from the original probabilistic axial capacity model in Zhu *et al*. (2007):

$$\frac{\Delta_a}{L} = \frac{\Delta_s}{L} + h \tag{5-8}$$

where Δ_a/L is the axial capacity and Δ_s/L is the shear capacity in Eq. (5-7). The probability distribution parameters for h are dependent on the structural parameters of individual columns. Particular values presented in Table 5-1 correspond to the parameters of the columns in the subsequent numerical example.

Similar to the case of shear failure, degradation in the relationship between axial force and deformation is included, as shown in Fig. 5-3a. Furthermore, the axial deformation is coupled with the lateral deformation in a linear relationship to guide the degradation of axial force. This is adapted based on the observation that shortening of the column occurs with an increase in horizontal deformation, due to the

sliding along the shear failure plane. It is stressed that this heuristic axial force degradation model should be complemented by further experimental work on post-axial failure response of RC columns.

5.4. PROBLEMS AND REMEDIES IN THE CONVERGENCE OF THE RELIABILITY ANALYSIS

The convergence of the algorithm in Fig. 5-2 is conditioned upon a continuously differentiable limit-state function. That is, the gradient vector $\partial u_c / \partial \mathbf{x}$ must have continuous components in the space of random variables. This "gradient continuity" requirement is violated if any of the following conditions are present, 1) kinks in the stress-strain relationship of the material models; 2) kinks in the force-deformation models that govern the transition into the post-failure response regime; 3) numerical noise in the finite element response.

Examples of kinks in the stress-strain relationship are found in numerous material models. Consider the uniaxial bilinear material model that is characterized by an initial stiffness, a yield stress, and a hardening stiffness. When the material yields the stiffness abruptly changes into the second-slope stiffness. This kink in the stress-strain relationship leads to a kink in the limit-state function, thus violating the aforementioned continuity requirement. This problem is previously addressed by Haukaas and Der Kiureghian (2006) and Barbato and Conte (2006) with the implementation of "smooth" material models**.** For example, the uniaxial bilinear material model in OpenSees is smoothed with circular segments. Such smoothing proved efficient to remedy the convergence problems in the reliability analysis due to gradient discontinuities.

Similarly, if smoothing techniques are employed to avoid kinks in the force-deformation models governing the transition into the post-failure response, the smoothness of the limit-state function is preserved. In support of this smoothing approach, experimental results indicate a smooth transition of the member response into the post-failure regime (Sezen 2002). Thus, in the present study, the force-deformation models are smoothed to remove the kinks shown at F_{fail} and F_{res} in Fig. 5-3c. Trigonometric

functions are employed to ensure a smooth transition of the response from the detection of failure to the attainment of the residual capacity. The smoothed force–deformation relationship developed herein reads

$$F = \left(\cos\left(\left(\frac{\Delta - \Delta_{fail}}{\Delta_{res} - \Delta_{fail}} \right) * \pi \right) + 1 \right) * \frac{\left(F_{fail} - F_{res} \right)}{2} + F_{res} \tag{5-9}$$

where, F_{fail} is the force at detection of failure, Δ_{fail} is the deformation at F_{fail}, F_{res} is the residual force, and Δ_{res} is the deformation when the capacity degrades to F_{res}. Fig. 5-4 shows the smoothed post-failure response for the spring. In passing it is noted that reliability convergence problems due to the sudden transition into the post-failure response regime are not encountered if a particular column failure sequence is guaranteed in the entire outcome space of the random variables.

As mentioned previously, convergence problems also may occur due to numerical noise. Usually, these gradient discontinuities are at a significantly smaller scale than the discontinuities treated above. In fact, they are typically avoided by defining appropriate values of tolerance parameters. In this study, however, numerical noise could become significant depending on the manner in which the limit-state function is evaluated. Consider the limit-state function in Eq. (5-2) with u_c defined as the displacement at which a particular column undergoes axial failure. The displacement at detection of axial failure is not exactly the displacement at failure. This is due to the fact that failure is detected only after equilibrium is reached at each analysis step. Therefore, if u_c is taken as the displacement at *detection* of failure, a small perturbation in the realization of the random variables would not alter the value of u_c, while a larger perturbation would lead to detection of axial failure in a different analysis step. This leads to gradient discontinuities. This problem is remedied by either 1) employing the finite difference method with high perturbation values to evaluate the gradient of the limit-state function; this ensures that a change in u_c is observed with each perturbation in the realization of random variables and results in an "approximately continuous" gradient of the limit-state function; or 2) the calculation of the "exact" displacement at collapse by utilizing the displacements at the analysis steps prior to, and at, the detection of failure. The latter

approach is adopted in the current study, in which a linear interpolation is utilized, as described in the numerical example section.

In addition to the above conditions, the convergence of the reliability analysis is dependent on a sound definition of the limit-state function. According to Eq. (5-2), the limit-state function includes the displacement response, u_c, at which the structure collapses. However, a quantitative definition of structural collapse is not a trivial task. Typically, the following two approaches are employed to identify collapse in structural analysis; 1) failure of a set of elements and 2) non-convergence of the finite element analysis. Each approach presents its own challenges to the reliability analysis.

Consider the case in which structural collapse is defined as the failure of a specific set of elements. This is termed as a "failure mode." In the reliability analysis, it may not be possible to confirm a-priori that this is the failure mode at the MPP. Structural collapse may occur with the failure of a different set of elements resulting in a different failure mode. Therefore, all the failure modes must be considered to verify the structural collapse. This poses a system reliability problem. However, the number of failure modes increases exponentially as the complexity of the structure increases, resulting in an impractical task of enumerating all the failure modes. This renders the system reliability formulation impractical in the current work. Furthermore, consider the case when the failure mode at the MPP is easily identified. One would then define the limit-state function with that particular mode of failure. However, as the algorithm in Fig. 5-2 iteratively searches for the MPP, the structure may collapse in a different failure mode at a trial realization of the random variables. This renders the algorithm unable to evaluate both the value of g and its gradient, $\partial g/\partial \mathbf{y}$ at that trial realization. In effect, this characterization of g may lead to regions in the $\mathbf{y}$-space where it is unfeasible to evaluate g and thus, the ordinary gradient-based algorithms become ineffective. A potential solution to this problem is to employ a transformation into the $\mathbf{y}$-space such that a particular failure mode is guaranteed in the entire outcome space.

Alternatively, consider the failure of the finite element analysis algorithm to converge as an indicator of structural collapse. The non-convergence of this analysis generally is assumed to occur due to singularity

in the global stiffness matrix and is thus indicative of structural collapse. However, the analysis algorithm may also fail due to other reasons, such as non-convergence of the iterative algorithms in nonlinear problems and numerical instability caused by the improper modeling. Therefore, this approach requires careful structural modeling and a robust finite element analysis code. In the present study, these requirements are satisfied. However, it is emphasized that convergence problems in the reliability analysis may still occur due to gradient discontinuities caused by numerical noise and collapse in different failure modes. The gradient discontinuities caused by the numerical noise are similar in nature to those discussed above. That is, the response at collapse is indeed the value at the last converged analysis step and not exactly at collapse as defined by the capacity models. Again, the finite difference method with large perturbation values is a potential remedy to this problem. Another source of gradient discontinuity with this collapse definition is the presence of different failure modes. That is, consider a point in the **y**-space at which a small perturbation in the realization of the random variables changes the failure mode. This point represents a sudden transition of the response from one failure mode to another. This transition results in a "kink" in the limit-state surface, and consequently, a point of gradient discontinuity is present. In this work, this problem is resolved by ensuring a smooth transition of the response into the post-failure regime as described above in reference to Fig. 5-4.

5.5. NUMERICAL EXAMPLE

The two-bay single-storey RC frame in Fig. 5-5 is considered to demonstrate the probabilistic evaluation of its global seismic capacity. This frame is selected because the experimental data for the axial failure of central column and the analysis model are readily available in Elwood and Moehle (2003). The three columns have light transverse reinforcement to reflect the typical design of a number of existing buildings. The columns are modeled as nonlinear beam-column elements with fiber cross-sections, while the beams are modeled as elastic beam-column elements. Each spring that connects the top of each column with the beam (see Fig. 5-5) contains probabilistic capacity and post-failure models as previously described. The RC frame is subjected to the gravity loads G_1 = 95.6 kN, G_2 = 300 kN, and G_3 = 95.6 kN

shown in Fig. 5-5. A pushover analysis is performed for which the lateral loading scheme and model details are described by Elwood and Moehle (2003).

The material and geometric properties of each column are modeled as random variables with probability distribution parameters as shown in Table 5-2. The model uncertainty is accounted for by considering θ_i and $\sigma\varepsilon$ as individual random variables with distribution parameters as shown in Table 5-1.

The two-bay structure is assumed to collapse if any single bay fails to carry gravity loads due to axial failure of its columns. That is, two collapse mechanisms are considered for this structure; failure of the two rightmost columns resulting in the gravity collapse of right bay, and failure of the two leftmost columns resulting in the gravity collapse of left bay. However, the three columns have identical cross-section and the middle column carries almost three times the gravity load of the outer columns. Since the drift capacity at axial failure decreases with an increase in axial load (Zhu *et al*. 2007), and the fact that the lateral load produces an overturning moment, it is evident that the axial failure of the two leftmost columns is the prevailing failure mode.

As previously discussed, it is imperative that the displacement u_c that enters the limit-state function in Eq. (5-2) is the displacement exactly at collapse. That is, it cannot be the displacement at the analysis step before or after failure of the two leftmost columns. When an axial failure is detected the displacement at the previous and current analysis step is employed, along with the actual displacement capacity calculated from Eq. (5-8), to linearly interpolate and determine the global displacement u_c at which collapse occurs.

The target displacement u_t in the limit-state function in Eq. (5-2) is determined by employing the FEMA-440 (2005) guidelines as described in Eq. (5-1) and the spectral acceleration values for Vancouver, Canada. For the structure under consideration u_t = 30.64 mm is obtained, which represents about 2% global drift ratio. A finite element reliability analysis with this target displacement results in p_f = 0.0246 and a reliability index β = 1.97. In addition, to obtain a probabilitiy curve, the reliability analysis is performed with target displacements 44.20mm, 58.93mm, 73.66 mm, 88.39 mm, and 103.12 mm corresponding to 3%, 4%, 5%, 6%, and 7% drift ratios, respectively. Fig. 5-6 illustrates the resulting

probability curve for the displacement at collapse for various global drift ratios obtained by performing a sequence of reliability analyses.

The reliability analysis results, such as those in Fig. 5-6 provide insight into the expected performance of the structure. For example, consider the results from a regular finite element analysis for this structure, without the consideration of uncertainty in the model and structural parameters. From such an analysis, the global displacement at which the structure collapses is u_c = 78.23 mm. Initially, this indicates that the structure would be able to maintain its axial load without collapse at a displacement lower than the target displacement u_t = 73.66 mm, or drift ratios lower than 5%. However, the reliability analysis indicates that there is a probability of failure, p_f = 0.592 that the structure may fail at the drift ratios less than 5%. That is, there is only 41% probability that the structure will not collapse at a drift ratio of 5%. However, consider the displacement at collapse corresponding to 2% drift ratio. From the probability curve in Fig. 5-6 it is seen that p_f = 0.0246, which corresponds to 98% probability that the structure will not collapse at drift ratios less than or equal to 2%. Probabilities at other drift ratios may be extracted from Fig. 5-6.

One means of improving the reliability against collapse is to modify the distribution parameters of the random variables. This could be achieved either by gathering more data to reduce the uncertainty in the model parameters or by prescribing retrofit actions to change the structural properties. In this regard, the ranking from the importance measures is a valuable tool. Table 5-3 shows the values of the three importance measures $\boldsymbol{\gamma}$, $\boldsymbol{\delta}$, and $\boldsymbol{\eta}$ for the reliability analysis with u_t = 30.64 mm. In this table the parameters are ranked according to the $\boldsymbol{\gamma}$ vector. These results indicate that the model coefficients, θ_i, h and $\sigma\varepsilon$ of the capacity models have greater contribution to the uncertainty than the material and geometric parameters. Therefore, improving the probabilistic models would decrease the uncertainty of the structural performance and improve the collapse reliability estimate. Furthermore, the highest ranking parameter, $\sigma\varepsilon$ indicates that the variance of the shear capacity model error has the largest influence on p_f. This implies that an increase in the data utilized in the model development and an improvement in the model form would significantly improve the reliability estimates. The high ranking of h indicates that the

uncertainty associated with the axial capacity model is higher than all other parameters except $\sigma\varepsilon$. This is an expected result since h represents the combined uncertainty of all the model coefficients in the probabilistic axial capacity model. Furthermore, by comparing δ values it is observed that the mean value of h has a higher influence on the reliability than the mean value of $\sigma\varepsilon$. However, when comparing η values, it is evident that the standard deviation of $\sigma\varepsilon$ has a higher influence than that of h. Therefore, modifying the variance of $\sigma\varepsilon$ and mean of h would result in the largest improvement in the reliability estimates.

5.6. CONCLUSIONS

This study presents a methodology for probabilistic evaluation of global seismic capacity of non-ductile RC structures. The prevalent nonlinear static procedure is extended with finite element reliability analysis to perform global seismic reliability assessments. Probabilistic capacity models and the post-failure response models for individual columns are implemented in the structural model to capture the structural response following the member failures. Ongoing research aims at further extending this methodology with realistic, dynamic simulation of structural behaviour during seismic events.

In the present study, the post-failure response models are smoothed to better represent the observed structural behaviour and to prevent non-convergence of the reliability analysis. This study also identifies the challenges associated with the characterization and detection of structural collapse relative to the reliability analysis. The smoothing approach is emerging as a highly promising approach to address a number of these issues.

The presented numerical example demonstrates the feasibility of the proposed methodology by providing collapse probabilities summarized in a probability curve, as well as parameter importance measures to identify the most important sources of uncertainty. The results indicate that emphasis should be placed on further development of shear and axial capacity models to reduce the model error as much as possible.

Table 5.1: Distribution parameters of probabilistic model coefficients

Coefficients	Distribution	Mean	Standard deviation	Correlation coefficient		
				θ_1	θ_2	θ_3
θ_1	Normal	2.020	0.746	1.000	0.503	-0.707
θ_2	Normal	-0.025	0.008	0.503	1.000	-0.172
θ_3	Normal	-0.031	0.008	-0.707	-0.172	1.000
$\sigma\,\varepsilon$	Normal	0.000	0.410	0.000	0.000	0.000
h	Lognormal	0.022	0.026	0.000	0.000	0.000

Table 5.2: Uncertainty modeling of the material and geometric parameters

Parameter	Distribution	Mean	Standard deviation	Coefficient of variation	Correlation among columns
Concrete compressive strength (f'_c)	Lognormal	23.9 MPa	1.12 MPa	4.69%	0.6
Width of the column (b)[a]	Lognormal	0.23 m	$2.54 \cdot 10^{-3}$ m	1.10%	0.0
Depth of the column (D)[b]	Lognormal	0.23 m	$2.54 \cdot 10^{-3}$ m	1.10%	0.0
Depth to the centerline of the outermost tension reinforcement (d)[a,b]	Lognormal	0.20 m	$2.54 \cdot 10^{-3}$ m	1.27%	0.0
Hoop spacing (s)	Lognormal	0.15 m	$2.54 \cdot 10^{-3}$ m	1.69%	0.0
Shear span (a)	Lognormal	0.74 m	$2.54 \cdot 10^{-3}$ m	0.34%	0.0
Area of transverse reinforcement (A_{st})	Lognormal	0.10 m^2	$2.00 \cdot 10^{-3}$ m^2	2.00%	0.0

a – Correlated with a coefficient = 0.6
b – Correlated with a coefficient = 0.6

Table 5.3: Importance measures and ranking of the parameters

Ranking by γ value	Parameter	γ value	δ value	η value
1	Model error in shear capacity model ($\sigma\varepsilon$)	0.79767	0.79731	1.25677
2	Total uncertainty in axial drift capacity (h)	0.58350	1.65977	0.80970
3	Shear capacity model coefficient of (a/d) and (s/d) (θ_2)	0.10219	0.10214	0.02027
4	Shear capacity model coefficient of ρ'' (θ_1)	0.08810	0.08806	0.00851
5	Shear capacity model coefficient of ($P/A_g f'_c$) (θ_3)	0.05988	0.05986	0.01610
6	Depth to the centerline of outermost tension reinforcement of outer left column (d)	0.02533	0.02530	0.00093
7	Hoop spacing of outer left column (s)	0.02332	0.02330	0.00069
8	Concrete strength of outer left column	0.01128	0.01131	0.00078
9	Shear span of outer left column (a)	0.01080	0.01080	0.00027
10	Area of transverse reinforcement of outer left column (A_{st})	0.00465	0.00465	0.00014
11	Depth of outer left column (D)	0.00275	0.00275	0.00005
12	Concrete strength of center column	0.00029	0.00029	0.00002
13	Width of outer left column (b)	0.00021	0.00021	0.00000
14	Concrete strength of outer right column	0.00007	0.00007	0.00000
15	All other random variables	0.00000	0.00000	0.00000

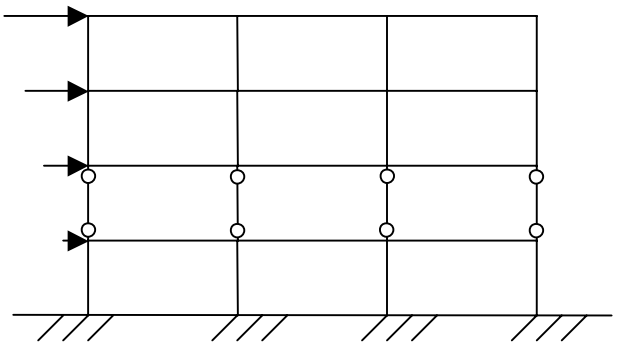

○ – Flexural yield

X – Shear failure

¦ – Axial failure

Event 1: Flexural yielding of second story columns

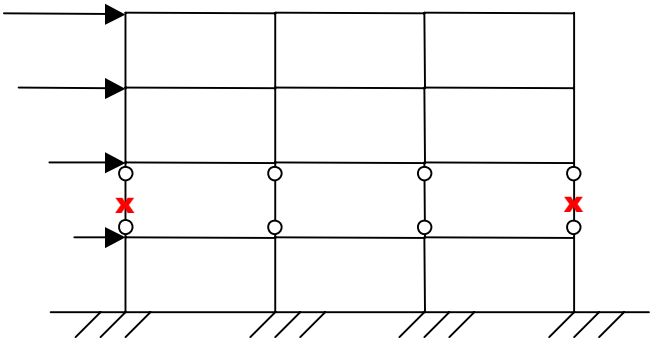

Event 2: Shear failure of exterior columns

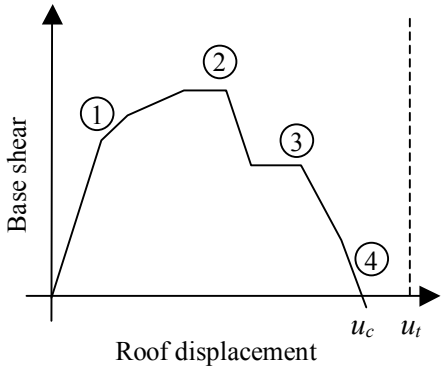

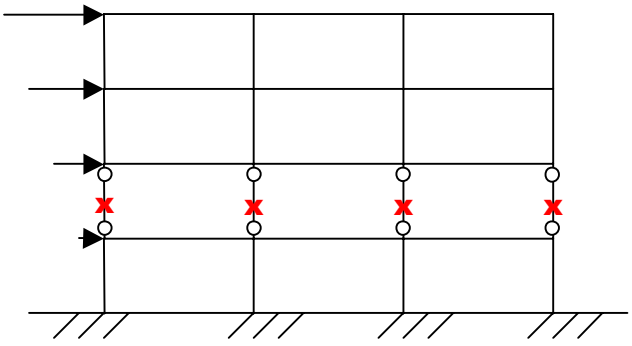

Event 3: Shear failure of interior columns

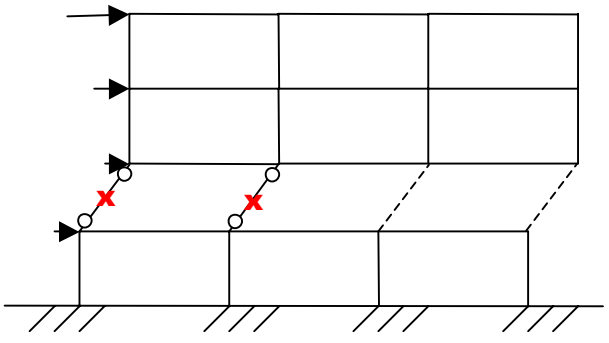

Event 4: Axial failure of two columns and collapse of structure

Figure 5.1: Possible structural events prior to attainment of the target displacement

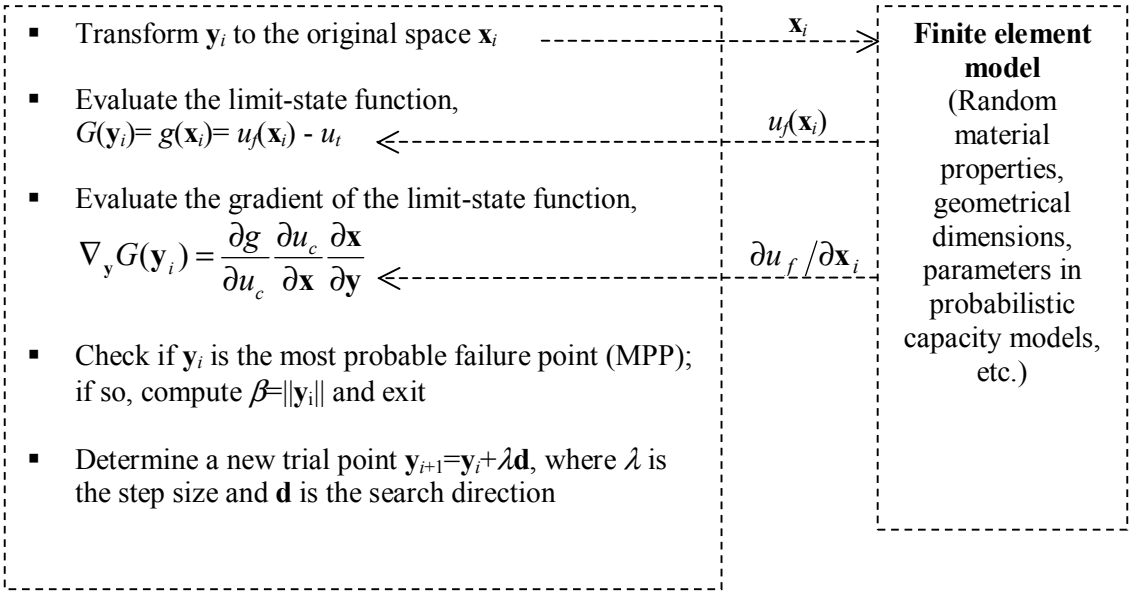

Figure 5.2: Key steps in finite element reliability analysis by FORM (*i*=1, 2, 3,)

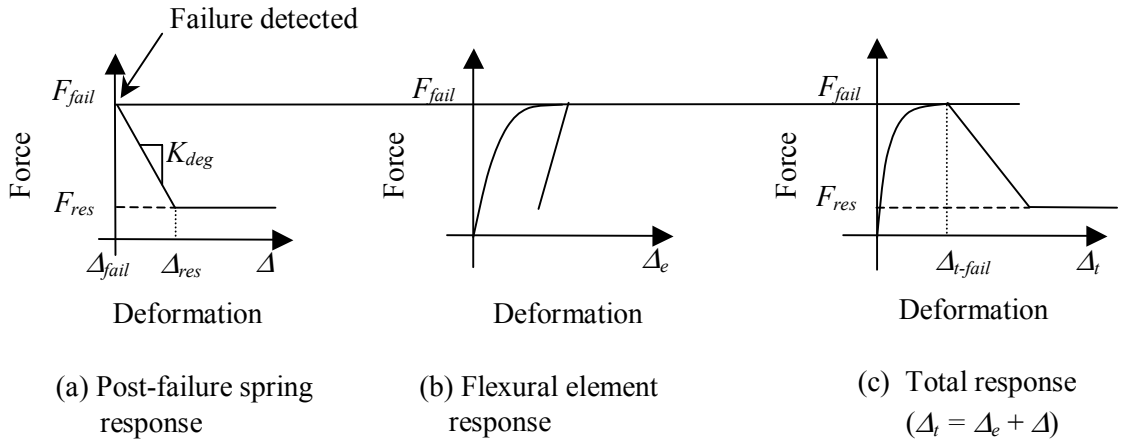

(a) Post-failure spring response

(b) Flexural element response

(c) Total response ($\Delta_t = \Delta_e + \Delta$)

Figure 5.3: Transition into post-failure response

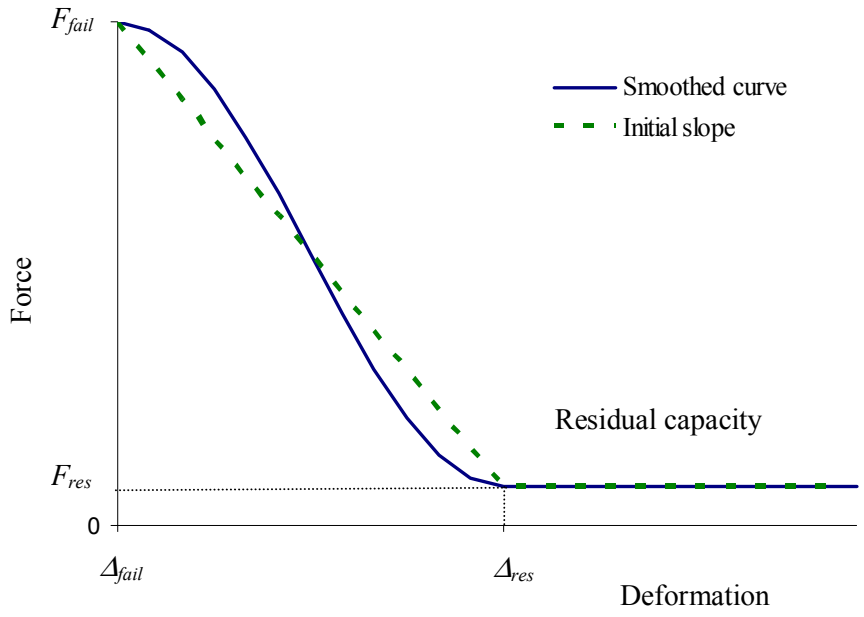

Figure 5.4: Smoothed post-failure response of springs

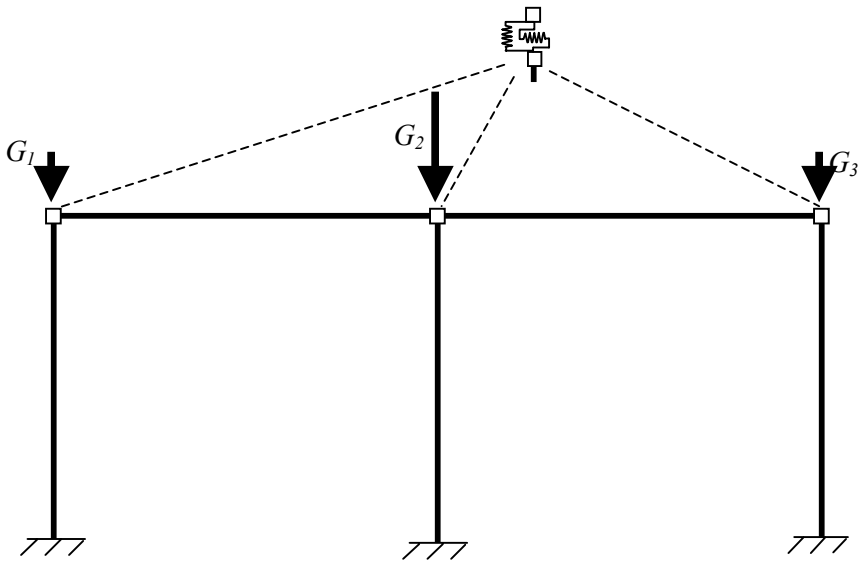

Figure 5.5: Finite element model of the RC frame

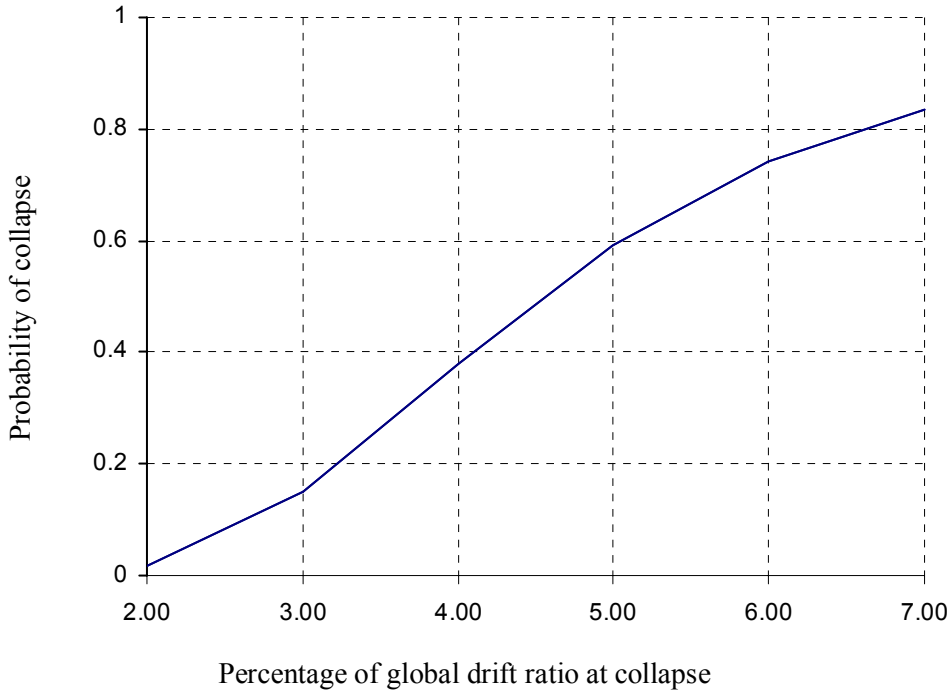

Figure 5.6: Probability curve of the displacement at global collapse

REFERENCES

American Society of Civil Engineers (ASCE) (2000). *Prestandard and Commentary for the Seismic Rehabilitation of Buildings*, *FEMA 356*, Federal Emergency Management Agency, Washington DC, November 2000.

Applied Technology Council (ATC - Project 55) (2005). *FEMA 440: Improvement of Nonlinear Static Procedures*, Department of Homeland Security, Federal Emergency Management Agency, Washington DC, June 2005.

Applied Technology Council (1996). *Seismic Evaluation and Retrofit of Concrete Buildings, Report ATC-40*, Applied Technology Council, Redwood City, CA

Bjerager, P., and Krenk, S. (1989). "Parameter sensitivity in first order reliability theory," *Journal of Engineering Mechanics*, 115 (7), 1577-1582

Chopra, A.K, and Goel, R.K. (2000). "Evaluation of NSP to estimate seismic deformation: SDF systems," *Journal of Structural Engineering,* 126(4), 482– 490

Chopra, A.K, and Goel, R.K.(2002), "A modal pushover procedure for estimating seismic demands for buildings," *Earthquake Engineering and Structural Dynamics*, 31, 561-582

Ditlevsen, O., and Madsen, H.O. (1996). *Structural Reliability Methods*, Wiley, Chichester, New York, NY

Elwood, K.J.,and Moehle, J.P. (2003). *Shake Table Tests and Analytical Studies on the Gravity Load Collapse of Reinforced Concrete Frames*, Report no. PEER 2003/01, Pacific Earthquake Engineering Research Center, University of California, Berkeley

Elwood, K.J. (2004). "Modelling failures in existing reinforced concrete columns," *Canadian Journal of Civil Engineering*, 31(5), 846-859.

Elwood, K.J., and Moehle, J.P. (2005a). "Drift capacity of reinforced concrete columns with light transverse reinforcement," *Earthquake Spectra*, 21(1), 71-89.

Elwood, K.J., and Moehle, J.P. (2005b). "Axial capacity model for shear-damaged columns," *ACI Structural Journal*, 102 (4), 578-587

Fajfar, P. (1999). "Capacity spectrum method based on inelastic demand spectra," *Earthquake Engineering and Structural Dynamics*, 28 (9), 979–993.

Gardoni, P., Der Kiureghian, A. and Mosalam K.M. (2002). "Probabilistic capacity models and fragility estimates for reinforced concrete columns based on experimental observations," *Journal of Engineering Mechanics*, 128, 1024-1038.

Haukaas, T., and Der Kiureghian, A. (2004). *Finite Element Reliability and Sensitivity Methods for Performance-Based Engineering*, Report no. PEER 2003/14, Pacific Earthquake Engineering Research Center, University of California, Berkeley

Haukaas, T., and Der Kiureghian, A. (2005). "Parameter sensitivity and importance measures in nonlinear finite element reliability analysis," *Journal of Engineering Mechanics*, 131(10), 1013-1026

Haukaas, T., Der Kiureghian, A. (2006) "Strategies for finding the design point in nonlinear finite element reliability analysis." *Journal of Probabilistic Engineering Mechanics*, 21 (2), 133-147.

Haukaas, T., and Elwood, K.J. (2005). "Finite element reliability analysis with degrading reinforced concrete columns," *Proceedings ICOSSAR 2005, International Conference on Safety and Reliability of Engineering Systems and Structures*, 3575-3581

Hohenbichler, M., and Rackwitz, R. (1986). "Sensitivity and importance measures in structural reliability," *Civil Engineering Systems*, 3 (4), 203-209

Lin, Y.-Y., Chang, K.-C., and Wang, Y.L. (2004). "Comparison of displacement coefficient method and capacity spectrum method with experimental results of RC columns," *Earthquake Engineering and Structural Dynamics*, 33(1), 35-48

McKenna, F., Fenves, G.L., and Scott, M.H. (2004). *OpenSees*: Open system for earthquake engineering simulation. Pacific Earthquake Engineering Research Center, University of California, Berkeley, C.A

Pujol, S. (2002). *Drift Capacity of Reinforced Concrete Columns Subjected to Displacement Reversals*, Ph.D. Dissertation, School of Civil Engineering, Purdue University.

Sezen, H. (2002). *Seismic Response and Modeling of Reinforced Concrete Building Columns*, PhD Dissertation, Department of Civil and Environmental Engineering, University of California, Berkeley.

Sugano, S. (1996). "Seismic Behavior of Reinforced Concrete Columns Which Used Ultra-High-Strength Concrete," *Proceedings of the 11th World Conference on Earthquake Engineering*, Pergamon, Elsevier Science Ltd., Paper No. 1383

Zhu, L., Elwood, K.J., Haukaas T., and Gardoni, P. (2006). "Application of a Probabilistic Drift Capacity Model for Shear-Critical Columns," *American Concrete Institute (ACI), Special Publication*, SP-236, 81-102.

Zhu, L., Elwood, K.J., and Haukaas, T. (2007), "Classification and seismic safety evaluation of existing reinforced concrete columns," *Journal of Structural Engineering*, 133, 1316-1330.

Chapter 6. PROBABILISTIC EVALUATION OF LOSS[1]

6.1. INTRODUCTION

The majority of the high-rise buildings in Vancouver, British Columbia, Canada are constructed with reinforced concrete (RC) and designed with shear wall systems to resist lateral seismic forces. The behavioural characteristics of these structures are dependent on the earthquake ground motions and vary for the different types of earthquakes that are possible in the Vancouver region. For a comprehensive assessment of seismic risk, the probable damage and loss suffered by high-rise RC structures under each distinct type of earthquake must be evaluated. The primary objective in this chapter is to evaluate the loss of a high-rise RC structure in a probabilistic manner, while accounting for different types of earthquakes generated in the Cascadia subduction zone.

The high-rise buildings, following the existing building codes, are designed to ensure life safety in a seismic event. That is, the limit-states in design codes provide safety against building collapse for a specific "design" intensity. The structures are designed to dissipate energy by undergoing inelastic deformations at controlled locations, such as plastic hinge regions. However, the damage suffered by the structure and the consequent monetary loss due to repair costs, loss of occupancy, and depreciation of value may be of significant concern to the owners, occupants, and other stakeholders in the buildings. Hence, the evaluation of monetary loss due to the damage of structural and non-structural elements is a key ingredient in the performance assessment of these structures. However, these assessments cannot be performed in a deterministic manner.

Any evaluation of monetary loss due to seismic events is not realistic without considering the significant uncertainties present in the earthquake ground motions, structural behaviour, damage, and loss. Structural reliability analysis provides a rational approach to consistently deal with all the uncertainties. In the

[1] A version of this chapter has been submitted for publication. Koduru, S.D. and Haukaas, T., "Probabilistic loss assessment of a Vancouver high-rise building,"

present study, the probabilistic loss assessment is performed based on a "unified reliability analysis" framework. The unified reliability methodology (Haukaas 2007) is based on combining the aforementioned models into one reliability formulation. Specifically, in this methodology the uncertainties arising in the loading parameters, structural properties, such as material and geometry parameters, structural damage models and monetary losses are comprehensively considered in a single analysis. Explicit probabilistic models are considered for earthquake ground motions, structural and non-structural damage, and monetary loss. In practical implementation, this differs from the Pacific Earthquake Engineering Research Center (PEER) methodology, originally proposed by Cornell and Krawinkler (2000), wherein the probability distribution for the total loss is obtained by a triple integral that includes conditional probabilities from each model. Recently, Moehle *et al*. (2005) and Yang (2006) presented a practical application to carry out the integration. The unified reliability approach adopted in the present study may be regarded as an extension of that work, particularly with respect to the comprehensive ground motion model. Also, the present study entails a state-of-the-art inelastic finite element model for a shear-wall-type high-rise building, instead of a moment frame structure.

The uncertainties in the earthquake ground motions are included by employing stochastic models with parameters calibrated to the Cascadia subduction zone. There are three distinct types of earthquakes generated from the Cascadia subduction zone; Crustal, Subcrustal, and Subduction. Due to the earthquake source characteristics, dispersion of earthquake sources, and other seismological parameters, the three types of earthquakes differ in their influence on the damage potential to high-rise buildings. Hence, the probable monetary loss to a high-rise building is evaluated separately for each type of earthquake, and then discounted to present cost and combined. In this chapter, the entire process is developed and demonstrated for an existing building in Vancouver, BC.

It is noted that the uniform hazard spectra in National Building Code of Canada (NBCC 2005) does not combine the earthquake hazard from Crustal, Subcrustal, and Subduction earthquakes probabilistically. Instead, a so-called robust method is applied to amalgamate the probabilistic hazard estimates of the

Crustal and Subcrustal earthquakes with those of the Subduction earthquakes (Adams and Halchuk 2003). In this approach, the under-estimation of the total hazard is likely to be in the order of 40% when all types of earthquakes contribute to same level of hazard (Adams and Atkinson 2003). In the present study, a more refined methodology for combination of probabilistic results is presented to avoid this under-estimation of the seismic risk.

A key objective in the current study is to present a methodology for performance assessment of tall shear wall buildings under the complex seismological setting of the Cascadia subduction zone. For this purpose, parameter calibration for a stochastic ground motion model is performed to enable the simulation of Crustal, Subcrustal and Subduction type ground motion excitations. Moreover, a detailed three dimensional finite element model of a building located in downtown Vancouver is created, including appropriate models for damage and loss estimation. Unified reliability analysis is performed for each type of earthquake separately and the results are probabilistically combined to obtain a total probabilistic loss curve. It is emphasised that this is the first application of the unified reliability methodology to a real-world building with structural and non-structural components subjected to a comprehensive, calibrated probabilistic model for the earthquake hazard.

In the subsequent sections the unified reliability methodology is first presented. It is followed by the stochastic ground motion model and its parameter estimation. The building description, and the structural, damage, and loss models are then presented. The issues pertaining to reliability analysis with full-scale finite element models and a high number of random variables are discussed. Finally, the results from the unified reliability analysis; the probability curve for the total loss, are presented.

6.2. UNIFIED RELIABILITY ANALYSIS

The unified reliability analysis represents a framework to account for uncertainties when obtaining performance probabilities. The flexibility of the framework allows the substitution of different model formulations to assess the damage and consequent monetary loss. For example, the structural damage in

reinforced concrete members may be assessed by employing alternative damage models; e.g. Park *et al*. (1985) and Kratzig *et al*. (1989). Essentially, the unified reliability analysis extends the traditional structural reliability analysis with the inclusion of explicit models for the hazard, the structural damage, and the monetary loss. As an introduction to the unified reliability analysis, consider the conventional reliability problem (Ditlevsen and Madsen 1996),

$$p_f = \int_{g(\mathbf{x})\le 0} \cdots \int f(\mathbf{x})\mathbf{dx} \tag{6-1}$$

where p_f is the probability sought, $f(\mathbf{x})$ is a joint probability distribution of the random variables $\mathbf{x}$, and $g(\mathbf{x})$ is the limit-state function that defines the performance event for which the probability is being assessed. The limit-state function includes the performance measure for which the probability is sought. In modern structural reliability analysis, the evaluation of the limit-state function requires a structural analysis that has the random variables as input parameters. Consequently, the limit-state function is an implicit – as opposed to explicit – function of the random variables. When a finite element model is involved in the structural analysis the reliability analysis is referred to as finite element reliability analysis (Der Kiureghian and Taylor 1983).

In the unified reliability approach the limit-state function is formulated as,

$$g(\mathbf{x}) = L(\mathbf{x}) - L_t \tag{6-2}$$

where $L(\mathbf{x})$ is the monetary loss as an implicit function of random variables and L_t is a threshold value. The evaluation of $L(\mathbf{x})$, and consequently $g(\mathbf{x})$, requires the evaluation of the monetary loss and damage under uncertain dynamic loading. Fig. 6-1 shows schematically the steps involved in the evaluation of the monetary loss, and thus obtaining the value of the limit-state function in Eq. (6-2). It is observed that the random variables may enter into any or all of the models. Herein lays one of the novelties of the unified reliability approach: flexibility. In addition to the unified reliability analysis being executed in a single analysis – rather than individual computation of conditional probabilities from each model – the analyst

has unlimited flexibility in using different models and introducing correlation by multiple use of one random variable, e.g., using a material property in both the structural model and the damage model.

It is emphasized that when the reliability problem in Eq. (6-1) is solved by means of the limit-state formulation in Eq. (6-2), the probability of monetary loss being less than or equal to L_t is obtained. The probability curve for the loss is attained by varying L_t within a range of values and performing the reliability analysis at each threshold value.

The reliability problem in Eq. (6-1) cannot be solved analytically. Several numerical methods are developed to address this problem. These include the first- and second-order reliability methods (FORM and SORM), sampling methods and response surface methods. These methods require repeated runs of the finite element analysis and the evaluation of the limit-state function in Eq. (6-2) for different realizations of the random variables **x**. Because each finite element analysis is computationally costly, the reliability methods that require a high number of evaluations of the limit-state function are computationally intractable. FORM is highly appealing from this viewpoint and is being carefully studied by the authors to determine its suitability for the type of applications under consideration (Chapter 4). However, this is a comprehensive academic study that is outside the scope of this work. Focus in this chapter is on the details of the probabilistic models utilized in the performance-based earthquake engineering analysis and the computation and interpretation of the results, for a real-world building. Hence, in the current study a straightforward sampling approach is selected for convenience for the evaluation of the multi-fold integral in Eq. (6-1).

6.3. GROUND MOTION MODEL

The characteristics of the ground motion of an impending earthquake represent a major source of uncertainty in the prediction of structural and non-structural damage. Consequently, a *stochastic* ground motion model is a vital ingredient in the unified reliability analysis. From a practical perspective, ground motion records are scarcely available within the earthquake magnitudes of engineering interest, and for

the seismological and geological settings at a particular location. Even when recorded ground motions are available from similar regions of the world, these records do not capture the uncertainty in the ground motion of a future event. This makes the exclusive use of recorded ground motions questionable in a reliability analysis setting. Conversely, when a stochastic model is employed, the reliability analysis includes the variability in various characteristics of the ground motion at a site, including frequency content and amplitude. The influence of different ground motion characteristics on damage is thus accounted for.

In the literature, considerable research is devoted to the development of stochastic ground motion models. Most of these models are based on filtering a windowed Gaussian white noise to simulate ground motions. The stochastic models developed by Amin and Ang (1968), and Iyengar and Iyengar (1969) are some of the first to identify the nonstationarity in the ground motions. Nonstationarity is the variation in the frequency content and amplitude of the excitation with time. However, those models were limited to addressing the nonstationarity in the amplitude (temporal nonstationarity) and did not include the nonstationarity in the frequency content (spectral nonstationarity). This shortcoming was initially addressed by the stochastic model developed by Saragoni and Hart (1974). This model includes the spectral nonstationarity by dividing the excitation along the time axis into three distinct parts, each with a different frequency characterization. However, the division of the excitation along time axis causes abrupt change in the earthquake characteristics. Hence, instead of a division along the time axis, a division with respect to the frequency axis is proposed by Der Kiureghian and Crempien (1989), and Yeh and Wen (1990). This method is further developed by Li and Der Kiureghian (1995) into a discretized random process in the time domain, without Fourier transforms into the frequency domain. On the other hand, Lin and Yong (1987) introduced spectral nonstationarity by employing a non-homogeneous Poisson process to generate shot noise instead of Gaussian white noise for simulating the ground motions. Fan and Ahmadi (1990) developed the nonstationary models by applying a filter with time-varying frequency characteristics to the white noise. A similar application of time-dependent variation of frequency

characteristics are employed in the development of stochastic models by Sabetta and Pugliese (1996). Conte and Peng (1997) developed fully nonstationary models based on the concept of evolutionary spectra and employing time-frequency decomposition of the recorded ground motions with short-time Fourier transform methods. Thrainsson and Kiremidjian (2002) modelled the spectral nonstationarity by developing a distribution of Fourier phase differences from a recorded set of ground motions. Therefore, these models include the effects of geological and physical parameters of the earthquake source and travel path of the seismic waves by fitting model parameters to a data set of recorded ground motions. Unfortunately, when the recorded ground motions at a particular site are scarce it is difficult to fit the parameters of these models.

Conversely, stochastic models are developed based on the characteristics of earthquake source, path of seismic waves, soil properties at the site and distance from the source (Boore 1983, Atkinson and Boore 1997, Beresnev and Atkinson 1998, Atkinson and Silva 2000, Motazedian and Atkinson 2005). However, most of these models are characterized by stationary frequency content. In reality, however, nonstationarity in the frequency content (spectral nonstationarity) occurs in a ground motion because the high frequency seismic waves travel faster and arrive at a location earlier than the low frequency waves. The spectral nonstationarity could have a significant impact on the nonlinear response of a structure. Specifically, in the nonlinear response range, the natural frequency of the structure decreases as its stiffness degrades. Then the arrival of low frequency excitation with high amplitude potentially increases the damage of the structure due to resonance effects. Thus, spectral nonstationarity must be included in simulation models as it may play a critical role in the seismic damage assessments, and consequently the monetary loss.

In the present study, the stochastic model proposed by Li and Der Kiureghian (1995) is extended to fit the seismological conditions in Vancouver. The model includes spectral nonstationarity effects and does not require Fourier transformations, which would have increased the computational effort to simulate ground motions. Essentially, it represents the ground motion as a summation of several filtered Gaussian white

noise processes. The term "white noise" is here interpreted as a series of pulses with uncertain amplitude represented by Gaussian random variables. These are physically interpreted as pulses that represent the earthquake rupture. These pulses are filtered so that certain frequencies prevail when the shockwaves travel to the building site. Mathematically, the discretized form of the horizontal, uni-directional ground motion, $z(t)$, is written as, (Li and Der Kiureghian 1995)

$$z(t) = \sum_{k=1}^{K} q_k(t) s_k(t) \tag{6-3}$$

where $q_k(t)$ is a modulating function that describes the variation of the amplitude of a stationary process $s_k(t)$ over time, t, and K is the number of such stationary processes considered. Each of the stationary processes is written

$$s_k(t) = \sum_{i=1}^{N} y_i h_k(t - t_i) \tag{6-4}$$

where y_i is a vector of standard normal random variables that represents the white noise pulses, N is the number random pulses, and $h_k(t\text{-}t_i)$ is a linear filter represented by an impulse response function with a specific dominant frequency, ω_k and damping ratio, ξ_k. The impulse response function is zero until time t_i. Thus, $s_k(t)$ represents a stationary process where the train of pulses y_i represents the Gaussian white noise, which in turn is filtered by $h_k(t\text{-}t_i)$.

As indicated above, the stochastic ground motion model in Eqs. (6-3) and (6-4) has a physical interpretation. Specifically, the arrival of different seismic waves is modeled by including several filters; each with a different dominant frequency ω_k. The modulating functions control the arrival time, amplitude, and duration of the seismic waves. In fact, each filter is associated with a distinct modulating function. Effectively, this introduces spectral nonstationarity in the ground motion $z(t)$. The modulating function can take any temporal shape, such as trapezoidal, piece-wise linear, gamma, and rectangular. In the present study, the modulating functions are considered to be triangular in shape.

Fig. 6-2 illustrates the initial steps involved in the generation of a sample ground motion. In the first step, the Gaussian white noise (series of random pulses) is generated as shown in Fig. 6-2a. The white noise is then filtered by an impulse response function with 5Hz dominating frequency and 10% damping. Fig. 6-2b shows the filtered white noise process, which represents the stationary process $s_k(t)$. Finally, a triangular modulating function is applied to the stationary process; resulting in a modulated and filtered process, $z_k(t)$ as illustrated in Fig. 6-2c. The summation of several modulated stationary processes that correspond to different filters and modulating functions results in the final realization of ground motion excitations.

It is noted that the calibration of two groups of parameters is required to calibrate the stochastic ground motion model in Eqs. (6-3) and (6-4) to a particular location. These are the filter parameters (dominant frequency and damping ratio) and the modulating function parameters corresponding to each filter. The filter parameters are dependent on the soil characteristics at the location of the structure. In the current study, the building is located in downtown Vancouver. The surface geology of this area is consolidated glacial till (Turner *et al*. 1997). The natural period of the soil layers at this site is estimated based on experimental measurements of site periods in Vancouver with similar surface geology (Ventura *et al*. 2004). For the ground motion model in the present study, two filters with frequencies of 1Hz and 5Hz, and damping ratios of 5% and 10%, respectively, are considered. The 1Hz frequency filter represents the site period of approximately 1s. The 5Hz filter with 10% damping represent broad band high frequency content in the earthquake ground motions.

Given the utilization of two filters, the parameters of two modulating functions are required. The parameters required for the triangular modulating functions are the arrival time (the time at which the process starts), the peak amplitude, the duration, and the location of the peak amplitude. The generic shape of the modulating function and the parameters are identified in Fig. 6-3. In the present study the arrival time parameter is set to zero for all modulating functions. The remaining three parameters depend on the earthquake local magnitude (M) and the epicentral distance from the earthquake source to the site

(R). These are considered as random variables that are estimated separately for the Crustal, Subcrustal and Subduction earthquakes. The Crustal earthquakes occur at shallow depths while the Subcrustal earthquakes are deep earthquakes in the earth's crust. These earthquakes are of lower magnitudes and occur frequently compared to the Subduction earthquakes. Therefore, the duration, the peak amplitude, and the occurrence rate of these three types of earthquakes vary significantly. In the following, a probabilistic model for each of these earthquake sources is established.

6.3.1. Crustal earthquakes

The peak amplitude of a modulating function corresponding to each filter is considered as a function of M and R. The peak amplitudes for the Crustal earthquakes are estimated from the empirical ground motion relations developed by Atkinson (2005). Therefore the peak amplitude of the modulating function corresponding to the filter with 1Hz frequency is (Atkinson 2005)

$$\log_{10} A_{1c} = 3.13 + 0.68(M-6) - 0.12(M-6)^2 - 1.09\log_{10} D - 0.002D + \log_{10} c_1 \qquad (6\text{-}5)$$

where A_{1c} is the peak amplitude of the modulating function, D is the hypo-central distance defined as $D=(R^2+h^2)^{0.5}$, $h=10^{(-0.05+015M)}$ is the depth of the earthquake source, and c_1=0.0056 is the normalizing constant introduced in this work. The normalizing constants depend on the filter properties. Similarly, the peak amplitude of the modulating function corresponding to the filter with 5Hz frequency is (Atkinson 2005)

$$\log_{10} A_{2c} = 4.04 + 0.44(M-6) - 0.063(M-6)^2 - 1.17\log_{10} D - 0.0028D + \log_{10} c_2 \qquad (6\text{-}6)$$

where A_{2c} is the peak amplitude of the modulating function and c_2=0.0035 is a normalizing constant incorporated in this study. The amplitudes are considered random variables to represent the variability in M and R. The distribution parameters are derived based on the functions in Eqs. (6-5) and (6-6), with the probability density function for M as (Der Kiureghian and Ang 1977)

$$f(M) = \frac{b'\exp(-b'(M - M_{\min}))}{1 - \exp(-b'(M_{\max} - M_{\min}))} \tag{6-7}$$

where b'=2.3b, b is the coefficient relating to the annual rate of occurrence of the number of earthquakes from a source, M_{min}=5, and M_{max}=8, are the minimum and maximum earthquake magnitudes of engineering interest respectively. The function is zero outside the bounds of M_{min} and M_{max} .The probability density function for R is considered as

$$f(R) = \frac{2R}{R_{\max}^2 - R_{\min}^2} \tag{6-8}$$

where R_{max}=90km, is the maximum radius and R_{min}=10km, is the minimum radius of the circular area around the building site. The numerical values are selected based on data employed for empirical evaluation of Eqs. (6-5) and (6-6). As there are no known fault sources for Crustal and Subcrustal earthquakes in Vancouver, the distribution for R is derived based on an area source. The area between the radii R_{max} and R_{min} is assumed to have equal probability for containing an earthquake source. For the area with radius below R_{min}, the behaviour of ground motions varies significantly due to the "near-source" effects. These effects are not included in the current stochastic model and hence, the distribution of R is derived with a lower limit R_{min}.

The duration of both the modulating functions is considered to be equal to the duration of the earthquake. The duration of Crustal earthquake is estimated based on the stochastic model by Boore (1983). It is defined as

$$T_c = \frac{M_o^{1/3}}{4.9 \cdot 10^6 \beta_s (\Delta\sigma)^{1/3}} \tag{6-9}$$

where T_c is the duration of Crustal earthquake, β_s is the shear wave velocity, $\Delta\sigma$ is the stress drop parameter and M_o is the moment magnitude such that M_o=$10^{1.5(M+10.7)}$ as stated by Hanks and Kanamori (1979). Appropriate parameters for Vancouver are assessed based on the numerical values presented by Atkinson (1995, 1996). The probability distribution parameters of T_c are derived based on the distribution

of M in Eq. (6-7). The locations of peak amplitudes, denoted as $t_{pc,1}$ and $t_{pc,2}$, for the two modulating functions are assumed to be approximately $0.3T_c$ and $0.1T_c$ respectively. This assumption is based on the general observation of peak amplitude locations in earthquake ground motions and the parameters of the function (Boore 2003). This heuristic model is due to the lack of the recorded data to assess the parameters $t_{pc,1}$ and $t_{pc,2}$, which depend not only on the earthquake source but also on the geology of the location. The numerical values, probability distribution types, and the correlation of all the parameters of modulating functions are listed in Table 6-1. The correlation between the amplitudes and the duration of the modulating functions is substantial. However, substantial uncertainty exists as well in the correlation coefficients derived solely based on the influence of M. Hence, a correlation coefficient of 0.6 is chosen to represent moderate correlation among these parameters.

6.3.2. Subcrustal earthquakes

The peak amplitudes for the Subcrustal earthquakes are estimated from the empirical ground motion relations developed by Atkinson and Boore (2003). Similar to the Crustal earthquakes, the peak amplitude of the modulating function corresponding to each filter is considered as a function of M and R. Furthermore, the ground motion relations are modified to include normalizing constants. The peak amplitude of the modulating function corresponding to the filter with 1Hz frequency is, (Atkinson and Boore 2003)

$$\log_{10} A_{1sc} = -0.98 + 0.88M - 0.0013h - d\log_{10} D - 0.0017D + \log_{10} c_1 \qquad (6\text{-}10)$$

where A_{1sc} is the peak amplitude of the modulating function, D is the hypo-central distance defined as $D=(R^2+\Delta^2)^{0.5}$, $\Delta=0.00724\cdot 10^{0.0507M}$, h=50km is the depth of the earthquake source, and $d=10^{(0.301-0.01M)}$. The normalizing constant c_1 is introduced as described for Crustal earthquakes. Similarly, the peak amplitude of the modulating function corresponding to the filter with 5Hz frequency is, (Atkinson and Boore 2003)

$$\log_{10} A_{2sc} = 0.40 + 0.69M + 0.0057h - d\log_{10} D - 0.0019D + \log_{10} c_2 \qquad (6\text{-}11)$$

where A_{2sc} is the peak amplitude of the modulating function and the rest of the parameters are as defined for Eq. (6-10), with c_2 as the normalizing constant for filter with 5Hz frequency. The distribution for M is as presented in Eq. (6-7) with M_{min}=5, and M_{max}=7. The probability density function for R is considered as

$$f(R) = \frac{4R\cos^{-1}(R_{\min}/R)}{R_{\max}^2(\theta_{\max} - \sin\theta_{\max})} \tag{6-12}$$

where R_{max}=90km, is the maximum radius, R_{min}=40km, is the minimum radius, and θ_{max}= $\cos^{-1}(R_{min}/R_{max})$ is the angle of the arc segment intersected by the source boundary. Eq. (6-12) is derived based on the formulation presented by Foschi and Lo (1988) to obtain the probability distribution of R in the presence of area sources at a distance from the site. The area source of Subcrustal earthquakes is considered beneath the Georgia Strait and Puget Sound (Adams and Halchuk 2003). The minimum radius is the distance between the edge of the area source and Vancouver.

The duration of the modulating functions is considered equal to the duration of the Subcrustal earthquakes, T_{sc}. Similar to the Crustal earthquakes, the duration of Subcrustal earthquakes is estimated based on Eq. (6-9). The locations of peak amplitudes, $t_{psc,1}$ and $t_{psc,2}$, are considered to be approximately $0.3T_c$ and $0.1T_c$ respectively. Table 6-2 lists the parameters of the modulating functions of Subcrustal earthquakes.

6.3.3. Subduction earthquakes

In contrast to the empirical relations employed for the Crustal and Subcrustal earthquakes, the amplitude parameters for the modulating functions of Subduction earthquake are based on the "finite-fault" stochastic model by Motazedian and Atkinson (2005). This choice is made for two reasons; 1) the empirical relations for Subduction earthquakes are based exclusively on the recorded ground motions from other subduction zones owing to the lack of such records in the Cascadia subduction zone, and 2) the fault source for Subduction earthquakes is known (Hyndman and Wang 1995), unlike the case of Crustal and Subcrustal earthquakes. The source characteristics and the detailed seismological parameters

are available for the Subduction earthquakes. The inclusion of these parameters in finite-fault stochastic model provides good estimates for the amplitude and duration parameters of the earthquakes.

A set of 20 Subduction ground motion records are simulated by employing the finite fault stochastic model with the source parameters as presented by Beresnev and Atkinson (2002). The modulating function parameters are estimated from each of the simulated record based on energy measures (Koduru and Haukaas 2007). An overview of the parameter estimation procedure from a ground motion record is presented next.

For a unit intensity white noise, the variance of the model in Eq. (6-3) is

$$Var[z(t)] = \sum_{k=1}^{K} q_k^2(t) \sum_{i=1}^{N} h_k(t - t_i)^2 = \sum_{k=1}^{K} Var[z_k(t)] \tag{6-13}$$

Since the model represents a non-stationary process, the variance is a function of time. From the equation above, it is evident that the variance of the modulated stationary process, $z_k(t)$, corresponding to each filter, is

$$Var[z_k(t)] = q_k^2(t) \sum_{i=1}^{N} h_k(t - t_i)^2 \tag{6-14}$$

Eq. (6-14) represents the variation of energy for a particular filter h_k with the dominant frequency ω_k. It is considered to be similar to the variation of the energy in the frequency band, ω_k-$\Delta\omega$ to ω_k+$\Delta\omega$, of the ground motion record, $a(t)$. For this reason, the Fourier transform of the record is evaluated as

$$\widetilde{F}(\omega) = \int_{-\infty}^{\infty} a(t) \exp(-i\omega t) dt \tag{6-15}$$

Next, the record is divided into components such as,

$$a_k(t) = \int_{D_k} \widetilde{F}(\omega) \exp(i\omega t) d\omega \tag{6-16}$$

where D_k, is the frequency band over the frequencies ω_k-$\Delta\omega$ to ω_k+$\Delta\omega$. Finally, the parameters of the modulating function are estimated by equating the energy content in $z_k(t)$ and $a_k(t)$ in discretized form such that

$$\sum_{i=1}^{n} a_{ki}^2 = \sum_{i=1}^{n} q_{ki}^2 \sum_{j=1}^{N} h_k (t_i - t_j)^2 \tag{6-17}$$

where n represents number of discrete points in the earthquake duration T_s such that $T_s=n\Delta t$ with a constant time interval Δt. It is noted that this procedure may result in underestimation of the amplitudes for certain frequencies depending on the filters employed. Furthermore, the finite fault stochastic model does not include explicit modelling of the spectral nonstationarity. The locations of the peak amplitude, denoted as $t_{ps,1}$ and $t_{ps,2}$, are evaluated from the simulated records of the finite fault stochastic model. As the model does not include the spectral nonstationarity explicitly, these estimates are approximate. As noted before, these parametric values are the best estimates given the lack of the recorded data. However, the methodology for fitting parameters to the stochastic model in Eq. (6-3) is applicable to any ground motion record. Table 6-3 represents the modulating function parameters for Subduction earthquakes.

6.4. BUILDING MODEL

The building selected for this study is a fifteen storey RC structure located in Vancouver. This building is employed as a reference for the mass and stiffness characteristics of the model. However, it is emphasized that numerous parameters, especially regarding the cost of damage, are assumed values that may not reflect the reality for this building. It is a mixed use building with commercial occupancy in the first storey and residential occupancy in the upper storeys. The building has 4 levels of underground parking below grade. The superstructure (the part of the building that is above grade) remains fairly regular with minor setbacks at the 4th storey and the 14th storey. The height of the first storey varies from 4.7m to 2.7m and the height of rest of the storeys is 2.7m. The shear walls in the staircase and the elevator core form the primary lateral force resisting system. The building is practically symmetrical along the North-South (N-

S) axis, but unsymmetrical along East-West (E-W) axis due to the projections of the underground structure and the superstructure up to the 4th floor.

In the current study, a three dimensional (3D) model of the superstructure is modelled with finite elements using the OpenSees software developed by McKenna *et al*. (2004). The underground structure was designed to be rigid compared to the structural members in the upper storeys. It is therefore unlikely that damage occurs in the parking structure and hence, it is not considered in the structural model. Instead, the ground motion is considered to be applied at the ground floor. The structural model consists of three distinct components: gravity support columns, header beams in the shear walls, and shear walls. The gravity support columns and the header beams are modelled as beam-column elements. Given the height-to-width ratio of the walls, flexural behaviour will be predominant in the shear walls. For this reason, the shear walls are also modelled as beam-column elements. The RC flat plate slabs, which are part of the gravity support system, are considered as rigid. Instead of explicit modelling of the RC slabs, their behaviour is included by means of the "rigid diaphragm" option in OpenSees. This constrains the nodes at each storey against relative lateral displacement and simulates the diaphragm behaviour of RC slabs. Figs. 6-4a and 6-4b show the 3D structural model of the building.

The shear walls were designed to yield and form plastic hinges between the first storey and the 4th storey. That is, the lateral support system is expected to respond primarily in the first mode and form a plastic hinge zone within the bottom four storeys. However, the structure may respond in higher modes depending on the excitation from the earthquake ground motion. Therefore, the shear walls are modelled with nonlinear elements up to the 10th storey. The upper storeys, from the 10th storey to the 15th storey, are expected to remain elastic because they experience considerably less axial and shear forces.

The nonlinear behaviour of the shear walls is modelled by fibre-discretized cross sections in the plastic hinge zone. The fibre-discretized sections account for the interaction between bending moments and axial forces in evaluating the sectional response of an element. Thus, these sections are employed in the plastic hinge zone where the shear walls experience maximum axial force. Each fibre in the cross-section is

characterized by different nonlinear uniaxial material models for the concrete and the reinforcing steel. Specifically, the inelastic "Concrete01" and "SmoothSteel01" material models in OpenSees are used to model the concrete and the steel reinforcement, respectively. The rest of the nonlinear elements of the shear walls, from the 4th storey to the 10th storey, are defined with sections that exhibit a hysteretic material model, which includes the force-deformation curve from section analysis and a stiffness degradation factor of 0.05. The shear force-deformation model is separately included in the section models of all the nonlinear elements.

As the shear walls undergo large lateral displacements after yielding, the gravity columns will also experience these displacements. In fact, excessive lateral displacements may cause considerable damage in the gravity columns. Furthermore, the gravity columns carry considerable axial loads at the bottom storeys. Hence, the gravity support columns are also modelled as nonlinear elements with fibre-discretized cross sections in the plastic hinge zone. Similar to the shear walls, the gravity columns are modelled as nonlinear elements with appropriate hysteretic material parameters from the 4th storey to the 10th storey and as elastic elements above the 10th storey. In contrast, all the header beams are modelled by means of nonlinear elements with hysteretic models for the moment-curvature relationship. Conversely, elastic models are employed for the axial and shear behaviour. The masses in the structural model are estimated based on the design-values of the dead and live loads of the structure.

Table 6-4 lists the first three fundamental periods of the structure based on the initial structural stiffness, as computed with OpenSees. The periods calculated from the model match fairly well with the periods of the real structure measured from ambient vibration tests (Dyck and Ventura 1998). The damping ratio for the first two fundamental periods is set to 3% on the basis that the damping in a typical RC structure varies from 2% to 5%. The Rayleigh damping parameters are selected such that the modal damping ratios for the first three fundamental periods are as shown in Table 6-4. Table 6-5 presents the numerical values of the selected structural parameters and their probability distribution parameters. The material properties in the plastic hinge zone of the structure and the structural mass are considered as random variables.

6.5. DAMAGE AND LOSS MODELS

The estimation of monetary loss is a complex task since it depends on several factors, such as the duration of non-functionality (downtime) of the building, the damage to the contents of the building, and the repair cost associated with damaged structural and architectural components. In the literature, models to comprehensively evaluate the monetary loss are scarce. In fact, the inclusion of losses due to damage of both structural and non-structural components adds to the comprehensive nature of the present study. The loss due to damage to structural elements is estimated based on a damage index described in the following. The loss due to damage to non-structural components is assessed based on their sensitivity to inter-storey drift ratios and floor accelerations.

6.5.1. Structural members

In the current study, the structural damage model developed by Mehanny and Deierlein (2000) is employed to assess the structural damage index. This damage model is based on inelastic deformations and is cumulative over the duration of loading. The cumulative nature of the damage index facilitates inclusion of the effect of the loading sequence, such as number of cycles and location of peak amplitude, on the damage accumulation. Therefore, the effects of the earthquake excitation characteristics on the structural damage are accurately modeled. In passing, it is noted that the use of a cumulative damage model is advantageous for the feasibility of the reliability analysis. Instead of employing limit-state functions that defines failure as the excursion of some non-monotonic response, e.g., displacement, above a selected threshold, the cumulative damage approach yields a monotonically increasing response. Effectively, this addresses the challenging time-variant reliability problem in earthquake engineering applications. Instead of dealing with a "first-excursion" problem the use of cumulative response measures simplifies the problem, as demonstrated in Chapter 4. In addition to this appealing reformulation of the problem, it is argued that cumulative damage measures represent a realistic and pragmatic approach when the limit-state function is defined in terms of monetary loss due to severe ground shaking.

The Mehanny-Deierlein damage model is employed to measure damage in the headers beams throughout the structure. These beams are expected undergo severe inelastic deformations compared to the other structural members. The damage model is also employed to measure damage in the gravity columns and the shear walls in the plastic hinge zone. Although the Mehanny-Deierlein damage model was calibrated to vary from 0.0 to 1.0 based on the experimental data for the frame members, such as beams and columns, it is also employed to assess damage of the shear walls in the present study. This indicates the need for future research to assess damage in shear walls; a topic that is current being subjected to several research efforts that are outside the scope of this work.

The structural damage index value is converted to monetary loss by assuming the relationship

$$L_m = \begin{cases} 0.5 \cdot \left(1 + \sin\left(\pi\left(D_s - 0.5\right)\right)\right) \cdot C_m & \text{for } D_s < 1 \\ C_m & \text{for } D_s \geq 1 \end{cases} \tag{6-18}$$

where L_m is the monetary loss due to the damage to structural member number m, D_s is the Mehanny-Deierlein damage index multiplied by $(1+\varepsilon_d)$, where ε_d is a zero-mean normal random variable with 0.05 standard deviation, that represents the model uncertainty in the damage model, and C_m is the replacement cost of structural member number m. The replacement cost of structural members is \$1500, \$9000 and \$14000 for the header beams, gravity columns, and shear walls, respectively. These values are estimates of the post-earthquake construction costs, which are assumed to be twice the current construction costs in Vancouver. All the cost values are considered to be in Canadian dollars.

The total loss due to structural damage is evaluated by summation over the monetary losses in each individual structural member. Consequently, the monetary loss due to structural damage, L_{ST}, reads

$$L_{ST} = (1 + \varepsilon_s) \cdot \sum_{m=1}^{M} L_m \tag{6-19}$$

where M here represents the number of structural members and ε_s is a zero-mean normal random variable with 0.3 standard deviation, that represents uncertainty in the estimation of structural replacement cost. In

the present study, a summation is employed in Eq. (6-19) because the seismically designed ductile structure is expected to experience mild to moderate level of damage. Conversely, if the structure under consideration is expected to experience near-collapse under seismic loads then it could be appropriate to calculate the monetary losses based on other formulations, such as a weighted sum of L_m.

6.5.2. Non-structural members

The non-structural components are divided into three categories: 1) window glazing and frames, 2) interior partition walls and exterior architectural elements, and 3) building equipment. The damage in categories 1 and 2 is sensitive to inter-storey drifts, while the damage in category 3 is considered to be sensitive to floor accelerations. The monetary loss is estimated based on summation of damage quantities from these categories. It is noted that, in the present study, the damage is estimated based on the peak inter-storey drifts and peak floor accelerations.

The non-structural damage is measured in terms of the quantity of the non-structural elements that has to be replaced to restore the functionality of the structure. In this work, this is quantified by means of a "damage quantity" (*DQ*), which is measured in square meters. Before the *DQ* can be computed, the damage ratio (*DR*) is required. The *DR* is defined as the fraction of the total quantity of non-structural elements that need replacement. Fig. 6-5 illustrates the steps involved in the estimation of the monetary loss due to non-structural damage. The inner box (dashed line) contains the steps involved in the estimation of the *DQ* for each category of the non-structural components. Once the damage quantity is estimated, the monetary loss corresponding to each category is evaluated. As stated previously, the total monetary loss due to the damage of non-structural components is a summation of the loss corresponding to each category, as shown in the outer box (solid line) in Fig. 6-5. The evaluation of the quantity in each gray-shaded box is presented in the following.

For each non-structural component type, a functional relationship is developed between the damage and the response parameter at each storey, based on data presented in Table 6-6 (Ferritto 1984). For Category 1

$$DR_{1,l} = -1.05\delta^3 + 3.62\delta^2 - 2.19\delta - 0.67\sin(-2.44\delta - 0.030), \quad \text{for} \quad 0.15 \le \delta \le 2.00 \qquad (6\text{-}20)$$

where $DR_{1,l}$ is the damage ratio for Category 1 at the l^{th} storey, and δ is the peak inter-storey drift ratio at that storey. Similarly, for Category 2

$$DR_{2,l} = -0.38\delta^3 + 1.20\delta^2 - 0.47\delta + 0.09\sin(-3.87\delta + 3.14), \quad \text{for} \quad 0.15 \le \delta \le 2.00 \qquad (6\text{-}21)$$

where $DR_{2,l}$ is the damage ratio for Category 2 at the l^{th} storey. The damage ratios in Eqs. (6-20) and (6-21) are zero for δ below 0.15 and 100% for δ above 2.0. In Category 3

$$DR_{3,l} = 2.63A^4 + 6.28A^3 + 4.05A^2 + 0.17A - 0.02842, \quad \text{for} \quad 0.07 \le A \le 1.4 \qquad (6\text{-}22)$$

where $DR_{3,l}$ is the damage ratio for Category 3 at the l^{th} storey, and A is the peak floor acceleration at that storey expressed in units of g_a (acceleration of gravity). The damage ratio is zero for values of A below 0.07 and the damage is 100% for values of A above 1.4.

The damage quantity for each category, i, is subsequently evaluated as

$$DQ_i = (1 + \varepsilon_n) \cdot \sum_{l=1}^{NL} DR_{i,l} \cdot TQ_{i,l} \qquad (6\text{-}23)$$

where ε_n is a zero-mean normal random variable with 0.1 standard deviation, that represents the model uncertainty in the non-structural damage model, NL is the number of storeys in the building, and $TQ_{i,l}$ is the total quantity of Category i at the l^{th} storey. The total quantity in each category is presented in Table 6-7. Finally, the monetary loss for each category is obtained from the damage quantity by means of the expression

$$L_i = C_i \cdot DQ_i \qquad (6\text{-}24)$$

where L_i is the monetary loss corresponding to category i, C_i is the monetary cost per unit damage quantity, and DQ_i is the damage quantity of the category. C_i is obtained by the relationship between damage quantities and losses as illustrated in Fig. 6-6. For each category, DQ_{min} and DQ_{max} are the

minimum and maximum damage quantities corresponding to the unit costs C_{min} and C_{max}. Specifically, C_{min} and C_{max} represent the repair costs per unit damage quantity. The minimum and maximum values for damage quantities and the corresponding costs for the three categories are listed in Table 6-7. Finally, the total loss due to the damage to non-structural components, L_{NS} is calculated as

$$L_{NS} = (1 + \varepsilon_{NS}) \cdot \sum_{i=1}^{3} L_i \tag{6-25}$$

where ε_{NS} is the zero-mean normal random variable with 0.30 standard deviation, to represent uncertainty in the estimation of cost of non-structural damage. Subsequently, the total monetary loss is computed by summation of structural loss from Eq. (6-19) and non-structural loss from Eq. (6-25), such that the total monetary loss is $L=L_{ST} + L_{NS}$. This monetary loss enters the limit-state function in Eq. (6-2).

6.6. EVALUATION OF THE TOTAL LOSS CURVE

The objective of the unified reliability analysis is to evaluate the performance of a structure in terms of monetary loss probabilities. One such result is the "loss curve," which represents the probability distribution for the total present value of the monetary loss within a time period. To achieve this result, it is necessary to establish intermittent probability distributions for the monetary loss given an earthquake at a specific source. In the present study, three such intermittent probability curves for the monetary loss are evaluated for the Crustal, Subcrustal and Subduction earthquakes. These curves are obtained separately by means of unified reliability analysis. These individual reliability analyses are carried out because each earthquake type is associated with a distinct earthquake source and is modelled with a separate set of ground motion parameters. The probability curve for each earthquake type represents the probability that the loss will be less than or equal to a particular dollar amount given the occurrence of that earthquake type. Consistent with the traditional notation for cumulative distribution functions (CDF), these probability curves are denoted $F(L|E_i)$, where L is the loss and E_i denotes the earthquake

type: $E_i \in \{\text{Crustal}, \text{Subcrustal}, \text{Subduction}\}$. The vertical bar denotes that the CDF is conditioned upon the occurrence of E_i.

The losses associated with an impending earthquake event will be incurred at some future time. To facilitate decision making at the present time, e.g., regarding retrofit actions, it is useful to discount the potential future loss to its present value. The reduction in present value is governed by the equation

$$L_{\text{present}} = L_{\text{future}} \cdot e^{-\gamma \cdot t} \tag{6-26}$$

where L_{present} is the discounted present value of the loss, L_{future} is the loss computed by the techniques presented previously, γ is the "real" interest rate (the interest rate minus the inflation rate), and t is the time of occurrence of the earthquake. This occurrence time is uncertain. By making the simplifying assumption that the occurrence of earthquakes are governed by the Poisson occurrence model it follows that the occurrence time t is a random variable with the exponential probability distribution. Consequently, the expected value of the present loss is obtained by the theorem of total probability (Ang and Tang 1975):

$$\mathrm{E}[L_{\text{present}}] = \int_0^T L_{\text{future}} \cdot e^{-\gamma \cdot t} \cdot f(t)\, dt \tag{6-27}$$

where $f(t)$ is the probability density function for t and T is the time period under consideration. When long time periods are considered, say, beyond 50 years, then the integral in Eq. (6-27) converges towards $\mathrm{E}[L_{\text{present}}]=L_{\text{future}}(\lambda/(\gamma+\lambda))$, where λ is the rate of occurrence in the Poisson model (Sexsmith 1983). Due to the variation in occurrence rate between the earthquake types, the aforementioned loss curves $F(L|E_i)$ for each type is discounted individually. In the following it is assumed that $F(L|E_i)$ is the conditional CDF for the discounted loss.

The final loss curve that considers all three types of earthquakes in Vancouver is obtained by invoking the theorem of total probability:

$$F(L) = \sum_{i=1}^{3} F(L \mid E_i) \cdot \mathrm{P}(E_i) \tag{6-28}$$

where $F(L)$ is the final loss curve, $F(L|E_i)$ represent the aforementioned conditional CDFs from the unified reliability analysis and $\mathrm{P}(E_i)$ represent the probabilities of occurrence of the three different types of earthquake. The probabilities $\mathrm{P}(E_i)$ are determined by means of the Poisson occurrence model. To this end, the average occurrence rate for the Crustal, Subcrustal and Subduction earthquakes are estimated to be 0.028, 0.015, and 0.0017, respectively. The values for the Crustal and Subcrustal earthquakes are derived based on the area of the source considered in the present study and the normalized values of occurrence rates of M>5.0 earthquakes (Adams and Halchuk 2003). The average occurrence rate for the Subduction type earthquake is based on an average of one Subduction earthquake per 590 years, as reported by Adams (1990). Normalization of the individual occurrence rate to obtain the relative probabilities of occurrence yields P(Crustal)=0.6264, P(Subcrustal)=0.3356, and P(Subduction)=0.0380. Subsequently, the substitution of the probabilities into Eq. (6-28) yields the final loss curve conditioned upon the occurrence of an earthquake of any type.

The average occurrence rate for earthquakes of any type is the summation of the average occurrence rates of the Crustal, Subcrustal, and Subduction events (Ang and Tang 1975). The numbers above yield the average occurrence rate of any earthquake is λ=0.0447. Consequently, the annual rate of exceedance of the loss L is the product $\lambda \cdot (1\text{-}F(L))$, where $F(L)$ from Eq. (6-28). Similarly, the probability of exceedance of a monetary loss during, say, a 50 year period is evaluated by rather multiplying $1\text{-}F(L)$ with the probability of occurrence of an earthquake in 50 years, given by the Poisson distribution. The resulting probability curve represents the probability that the monetary loss will exceed a dollar amount in present value, given the occurrence of an earthquake in 50 years.

6.7. ANALYSIS AND RESULTS

The uncertainty in the ground motion model for each of the these three cases include 500 random variables to represent the Gaussian white noise, as well as the random variables in the modulating

functions. Effectively, the white noise represents a random pulse at every 0.04s for the maximum duration of 20s. The random pulse spacing at 0.04s provides a versatile ground motion model with high fidelity. A closer spacing of the random pulses will compel a decrease in the time step size of the dynamic analysis and result in an unnecessary increase of the computational effort.

The probabilistic description of all the modulating function parameters are listed in Tables 6-1, 6-2 and 6-3, for the Crustal, Subcrustal and Subduction earthquakes, respectively. The intensity of the ground motions due to the Crustal and Subcrustal earthquakes is compared with the hazard curve from NBCC (2005). As mentioned earlier, the uniform hazard spectra from NBCC (2005) include only the hazard due to the Crustal and Subcrustal earthquakes. As illustrated in Fig. 6-7, the pseudo spectral acceleration at various return periods (inverse of occurrence rates) of the Crustal and Subcrustal earthquakes is considered for the spectral frequency of 1Hz. In general, the estimated pseudo spectral accelerations from the simulated Crustal and Subcrustal earthquakes are fairly close to the values of NBCC (2005) for the soil classification B. For the return period of 1 in 2500 years, corresponding to an occurrence probability of 2% in 50 years, the simulated value of pseudo spectral acceleration is $0.215g_a$ compared to $0.247g_a$ from the NBCC (2005). The discrepancies are primarily due to the number of earthquake sources considered for the Crustal earthquakes. In the present study, the earthquakes sources of the Crustal and Subcrustal earthquakes are restricted to within 90km radius from the location of interest. In contrast, the earthquake sources up to 200km radius are included in the NBCC (2005). The comparison in Fig. 6-7 validates the parameters calibrated to the stochastic ground motion model. Therefore, for the parameters in Tables 6-1, 6-2, and 6-3, the stochastic ground motion model results in the earthquake intensities similar to those proposed by current code level.

For the building under consideration, the lateral and torsional modes are coupled in the E-W direction. For a realistic evaluation of the structural behaviour, and the corresponding monetary loss, the dynamic analysis would ideally be performed with simultaneous ground motions in N-S and E-W directions. However, the state-of-the-art stochastic models of the ground motion utilized in this work simulate the

excitations in a single direction. In order to simulate the compatible excitations in N-S and E-W directions, the correlation among the peak accelerations, duration and other parameters of the ground motions in the two horizontal directions would have to be known. Given the absence of such information, which points to need for further research on bi-directional ground motions, the earthquake excitation is assumed to be at a 45 degree angle to the N-S and E-W directions. Hence, the components of the excitations in the N-S and E-W directions will be 70% of the intensity of the unidirectional excitation. It is argued that this is a reasonable assumption because the simultaneous application of 100% of the intensity in both directions will overestimate the seismic risk.

A unified reliability analysis for each of the three earthquake types is carried out. The choice of reliability method and the associated computational cost are discussed after the presentation of the results. First, the probability curves shown in Fig. 6-8 are obtained. As expected, the total monetary loss is highest given the occurrence of a Subduction earthquake. The probability of loss due to Crustal earthquakes is higher than that of Subcrustal earthquakes due to the proximity of the source of the Crustal earthquakes to Vancouver. Fig. 6-9 shows the probability curves for the monetary loss in terms of the expected present value based on the occurrence rate of each type of earthquake. The probability curves are estimated based on Eq. (6-27) considering the real interest rate as 3%. The discounted loss values provide an estimate for the investment in earthquake risk mitigation over a period of 50 years. Finally, Fig. 6-10 illustrates the total probability curve for monetary loss obtained by the evaluation of Eq. (6-28). The probability of loss below 1 million dollars is contributed primarily from the Subcrustal earthquakes. The Crustal earthquakes contribute significantly to the probability of loss above 1 million dollars. Though the monetary loss is significant given the occurrence of a Subduction earthquake, its contribution to the total probability of monetary loss is negligible. This is due to the small value of the probability of occurrence of the Subduction earthquakes compared to the Crustal and Subcrustal earthquakes.

Fig. 6-11 shows the annual probability of exceedance for the monetary loss. This curve acts as a decision-making tool for the annual investments, such as insurance premiums. It indicates that by paying

an annual insurance premium, a stakeholder is transferring the risk of incurring certain amount of monetary loss. For example, it is noted that the probability of monetary loss being greater than zero dollars is 4.5% while being greater than 1 million dollars is approximately 3.0%. If the stakeholder has no insurance there is 4.5% probability of suffering monetary loss. On the other hand, if the stakeholder invests in an insurance policy of 1 million dollars, then the probability of incurring a monetary loss decreases from 4.5% to 3.0%. This is due to fact that the insurance will cover the monetary losses below 1 million dollars. The annual probability is negligible for the monetary loss over 6 million dollars. Therefore, an insurance policy for more than 6 million dollars will not transfer any additional risk from the stakeholder to the insurance company.

Furthermore, Fig. 6-12 shows the probability of exceedance of the monetary loss in 50 years. It is observed that there is a 60% probability that the loss will exceed 0.5 million dollars in the next 50 years. Conversely, there is a negligible probability that the loss will exceed 3 million dollars in the next 50 years. The dollar amounts are in terms of present value, which implies that a maximum of 3 million dollars investment is justified at present in order to withstand the losses incurred due to the occurrence of an earthquake in the next 50 years.

In the present study, the mean-centered Monte Carlo sampling is employed for the reliability computations. One argument in favour of this approach is that the robustness of this method is independent of the behaviour of the limit-state surface. Specifically, another study by the authors has shown that the shape of the limit-state surface in the presence of stochastic ground motion and cumulative response measures is not directly amenable to traditional FORM analysis (Chapter 4). A drawback of the sampling approach is that the number of samples required for obtaining accurate results increases dramatically at low or high probabilities. For example, the sampling results have 9.5% coefficient of variation at probability of 0.1 for 1000 sampling points. This is the selected sample size in the present study; motivated by the tradeoff between accuracy and computational cost. Specifically, the computation time for a single finite element analysis in the present study is 20 minutes on a 2.66 GHz processor. Thus,

an increase in the sample size to achieve even a small decrement in the coefficient of variation involves a significant added computational effort. This indicates a need for future research on the behaviour of the limit-state function for complex structures, particularly in the context of efficient reliability methods, such as FORM (Chapter 4). Such knowledge would foster the development and application of sophisticated reliability methods in performance-based engineering.

6.8. CONCLUSION

In the present study, the methodology for unified reliability analysis is demonstrated by its application to an existing high-rise building in Vancouver, Canada. For this purpose, the earthquake ground motions for Crustal, Subcrustal and Subduction earthquakes of the Cascadia subduction zone are modelled separately. The parameters for the ground motion models are calibrated based on the ground motion relationships and simulated ground motions based on seismological models. The monetary loss due to the structural and non-structural damage in a 15 storey RC shear-wall structure is evaluated. The probability curves for the monetary loss for each type of earthquake are generated employing Monte Carlo sampling. Finally, the total probability of monetary loss in a high-rise RC structure due to the three types of earthquakes in the Cascadia subduction zone is estimated. The Crustal and Subcrustal earthquakes contribute substantially to the probability of monetary loss.

Table 6.1: Parameters of modulating functions – Crustal earthquakes

Parameter	Distribution Type	Mean	Standard Deviation	Correlation			
				A_{2c}	$t1_{pc}$	$t2_{pc}$	T_c
A_{1c}	Lognormal	4.91×10^{-3} m/s^2	6.35×10^{-3} m/s^2	0.6	0.0	0.0	0.6
A_{2c}	Lognormal	0.011 m/s^2	0.015m/s^2	1.0	0.0	0.0	0.5
$t_{pc,1}$	Uniform	2.80s	0.56s	0.0	1.0	0.0	0.3
$t_{pc,2}$	Uniform	0.95s	0.19s	0.0	0.0	1.0	0.3
T_c	Shifted Exponential	9.50s	3.85s	0.5	0.3	0.3	1.0

Table 6.2: Parameters of modulating functions – Subcrustal earthquakes

Parameter	Distribution Type	Mean	Standard Deviation	Correlation			
				A_{2sc}	$t1_{psc}$	$t2_{psc}$	T_{sc}
A_{1sc}	Lognormal	1.89×10^{-3} m/s^2	1.86×10^{-3} m/s^2	0.6	0.0	0.0	0.6
A_{2sc}	Lognormal	2.70×10^{-3} m/s^2	2.17×10^{-3} m/s^2	1.0	0.0	0.0	0.6
$t_{psc,1}$	Uniform	2.30s	0.46s	0.0	1.0	0.0	0.3
$t_{psc,2}$	Uniform	0.75s	0.15s	0.0	0.0	1.0	0.3
T_{sc}	Shifted Exponential	7.65s	3.80s	0.6	0.3	0.3	1.0

Table 6.3: Parameters of modulating functions – Subduction earthquakes

Parameter	Distribution Type	Mean	Standard Deviation	Correlation		
				A_{2s}	$t1_{ps}$	$t2_{ps}$
A_{1s}	Lognormal	0.081 m/s^2	0.332 m/s^2	0.3	0.0	0.0
A_{2s}	Lognormal	0.035 m/s^2	0.619 m/s^2	1.0	0.0	0.0
$t_{ps,1}$	Lognormal	5.00s	2.12s	0.0	1.0	0.0
$t_{ps,2}$	Lognormal	4.50s	1.70s	0.0	0.0	1.0
T_s	Deterministic	20.0s	0.0	0.0	0.0	0.0

Table 6.4: Fundamental periods and damping ratios

Mode	Period (s)	Frequency (Hz)	Damping ratio (%)
First mode (N-S)	0.90	1.10	3.0
Second mode (E-W + Torsion)	0.84	1.19	3.0
Third mode (Torsion + E-W)	0.25	4.01	5.7

Table 6.5: Distribution parameters of mass and material random variables

Parameter	Distribution Type	Mean	Coefficient of Variation
Mass (Storeys 1-4)	Lognormal	1806 Kg	0.10
Mass(Storeys 5-15)	Lognormal	1243 Kg	0.10
Maximum concrete compressive stress	Lognormal	35 MPa	0.06
Concrete strain at maximum compressive stress	Lognormal	0.002	0.15
Reinforcement steel yield stress	Lognormal	400 MPa	0.07
Reinforcement steel Young's modulus	Lognormal	200000 MPa	0.03
Reinforcement steel post-yield stiffness ratio	Lognormal	0.02	0.10

Table 6.6: Damage ratios for each category of non-structural elements

Category 1		Category 2		Category 3	
$\delta(\%)$	$DR_{1,l}$	$\delta(\%)$	$DR_{2,l}$	A (g_a)	$DR_{3,l}$
0.15	0.0	0.15	0.0	0.08	0.01
0.50	0.3	0.50	0.1	0.18	0.10
1.00	0.8	1.00	0.3	0.50	0.45
2.00	1.0	2.00	1.0	1.20	0.60
-	-	-	-	1.40	1.00

Table 6.7: Total quantity, damage quantity, unit loss ratios for each category of non-structural elements

Parameter	Category 1	Category 2	Category 3
TQ_1 (m^2)	311.56	467.34	1090.0
TQ_{2-3} (m^2)	178.98	268.47	1090.0
TQ_{4-13} (m^2)	136.22	204.33	634.41
TQ_{14-15} (m^2)	117.07	175.60	446.08
DQ_{min} (m^2)	9.29	46.45	92.90
DQ_{max} (m^2)	92.90	2322.58	1858.06
C_{min} ($/$m^2$)	861.00	129.00	32.00
C_{max} ($/$m^2$)	753.00	861.00	27.00

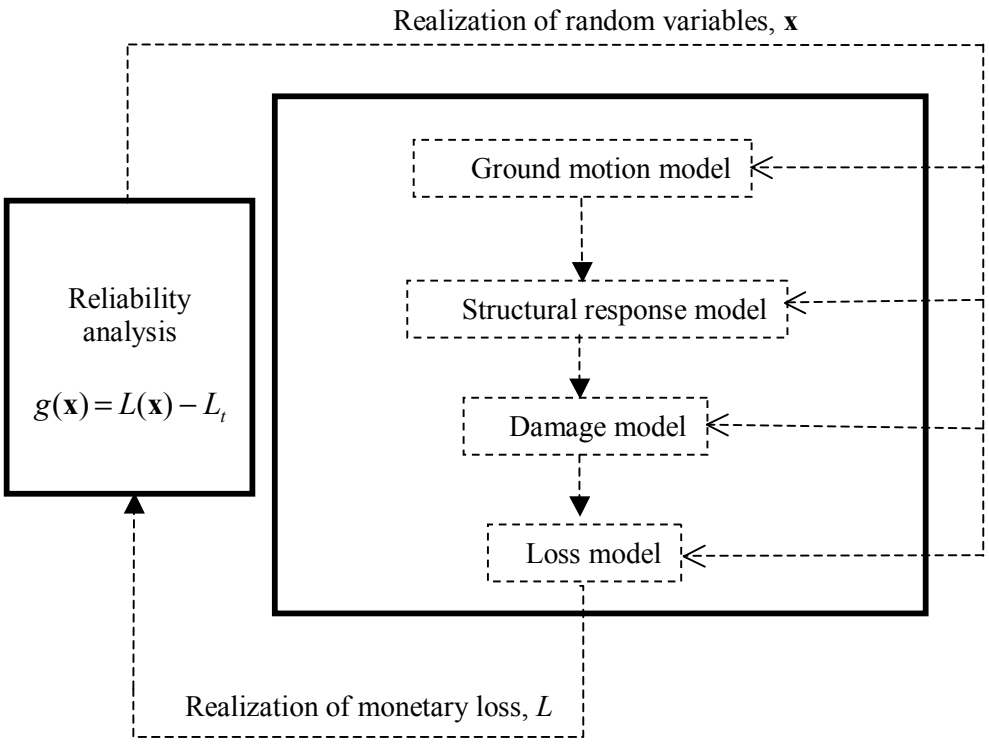

Figure 6.1: Evaluation of the monetary loss in unified reliability analysis.

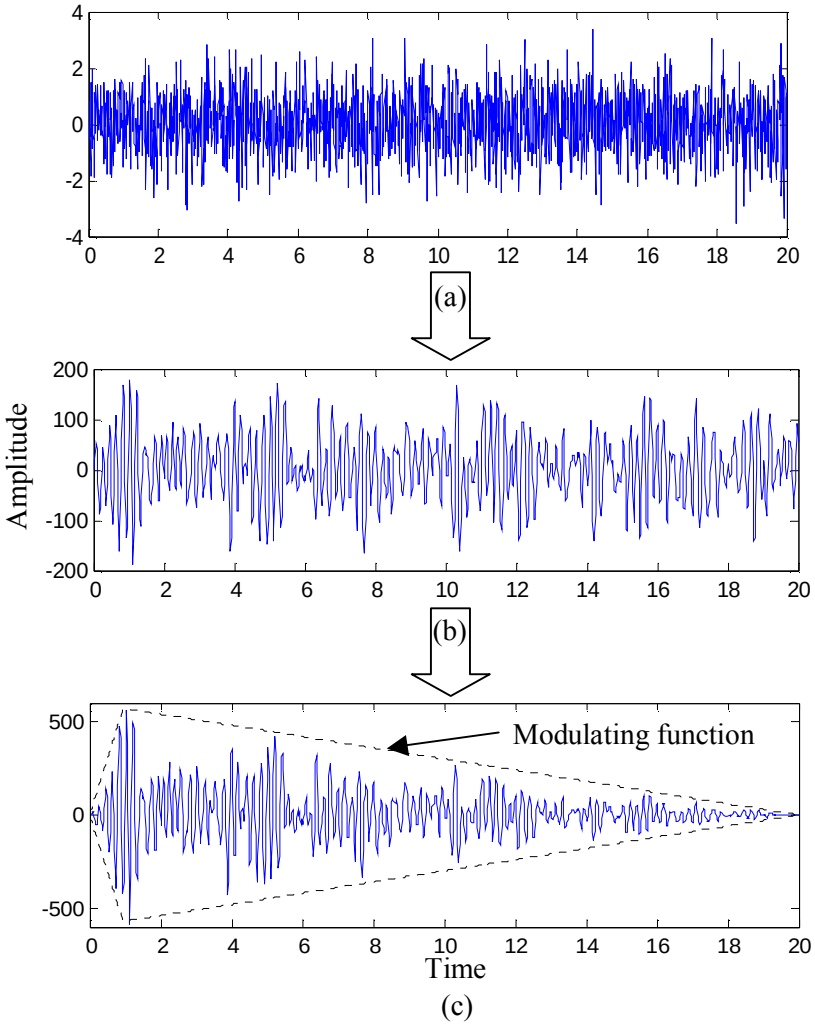

Figure 6.2: (a) White noise, y_i; (b) White noise filtered with 5Hz filter with 10% damping resulting in stationary process, s_k; (c) Modulated and filtered white noise, z_k

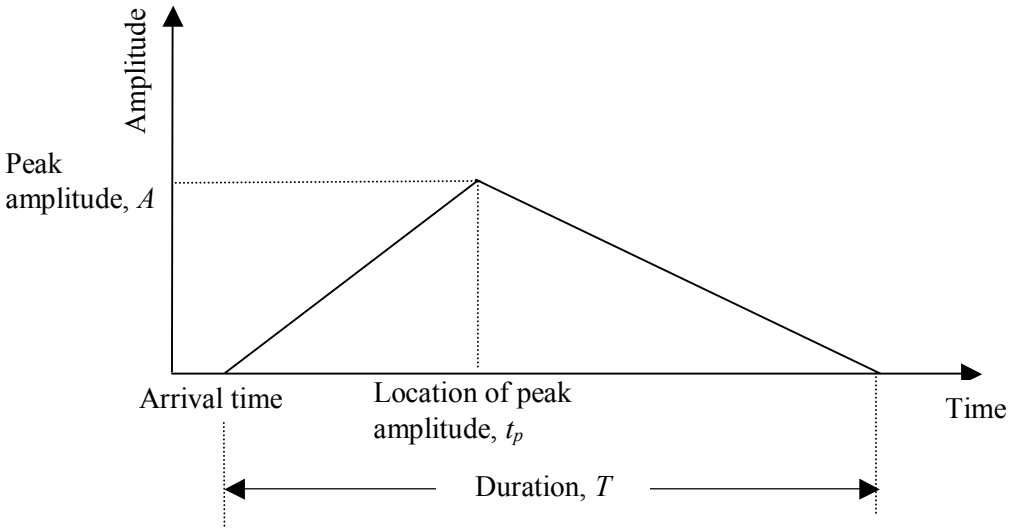

Figure 6.3: Parameters of a modulating function

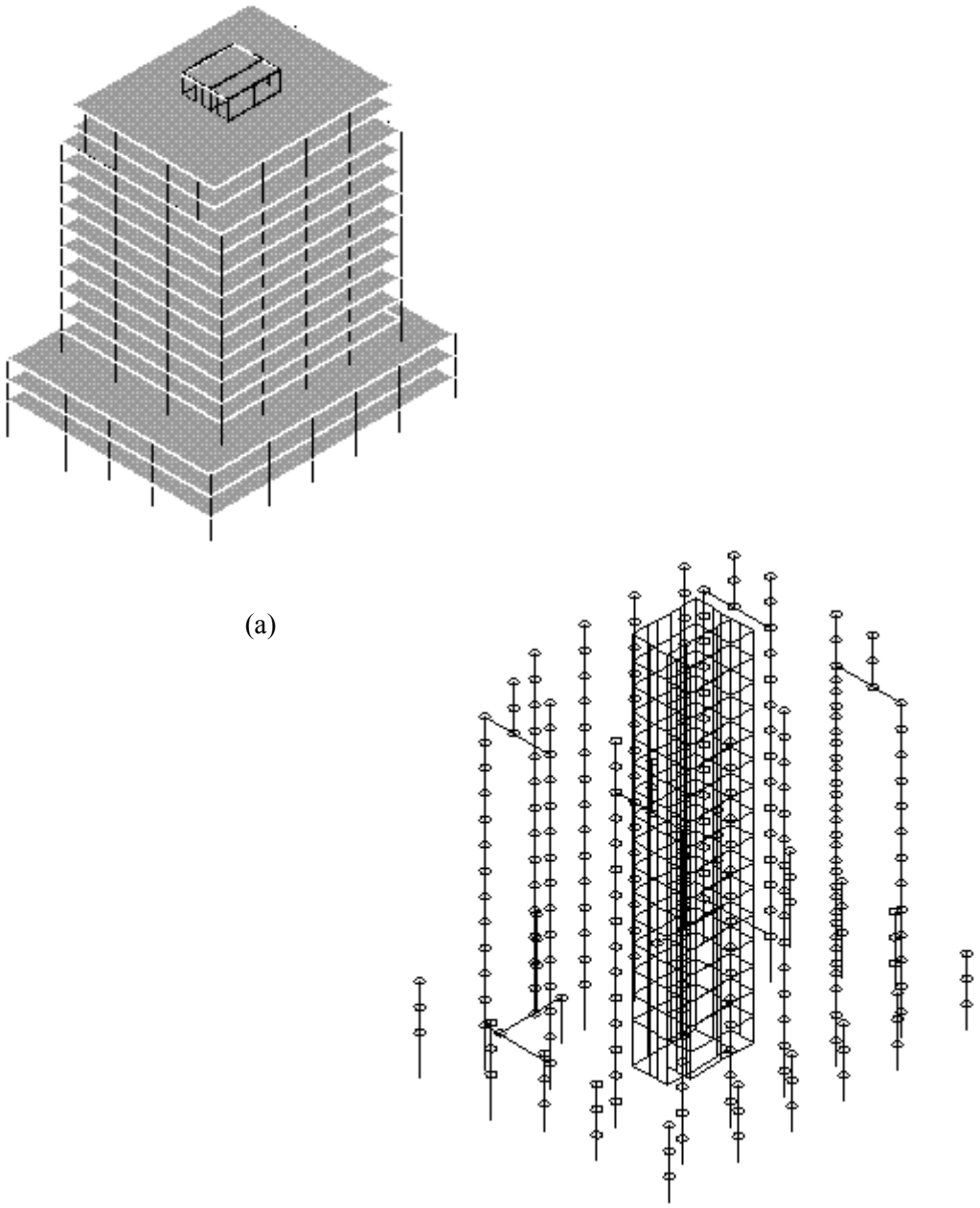

(a)

(b)

Figure 6.4: (a) 3D view of the analysis model of the building; (b) finite element model of the building (columns are constrained at each storey with rigid diaphragms).

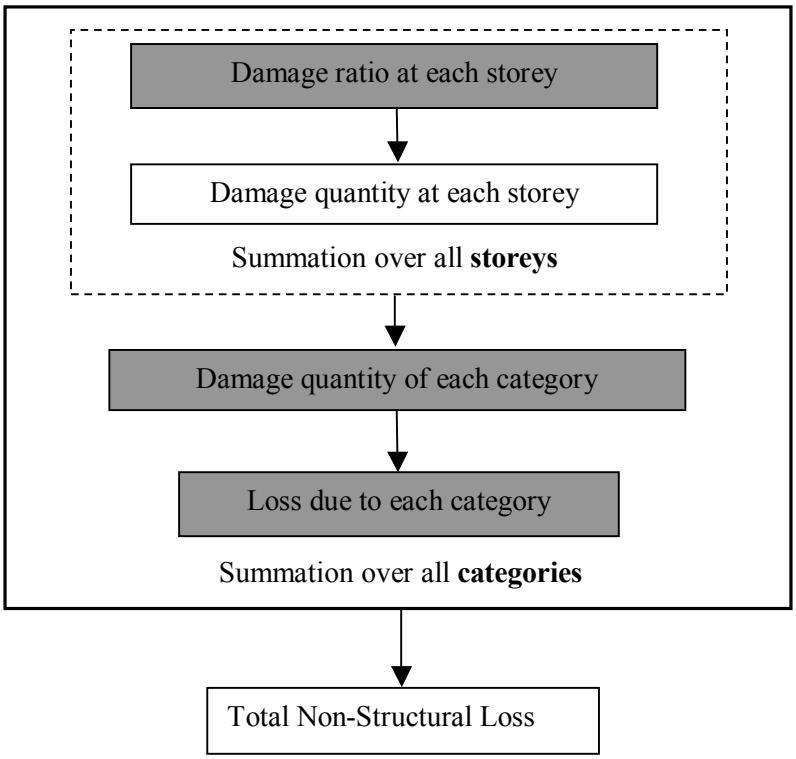

Figure 6.5: Steps involved in the evaluation of the monetary loss due to the damage of non-structural components

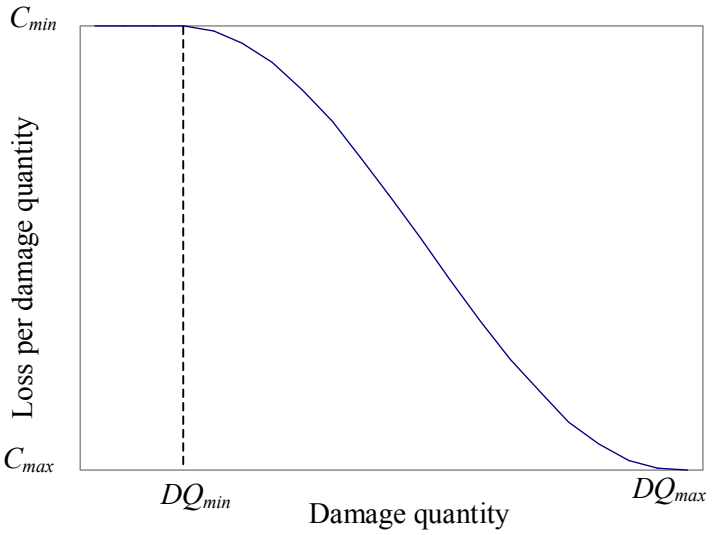

Figure 6.6: Damage quantity – loss relationship

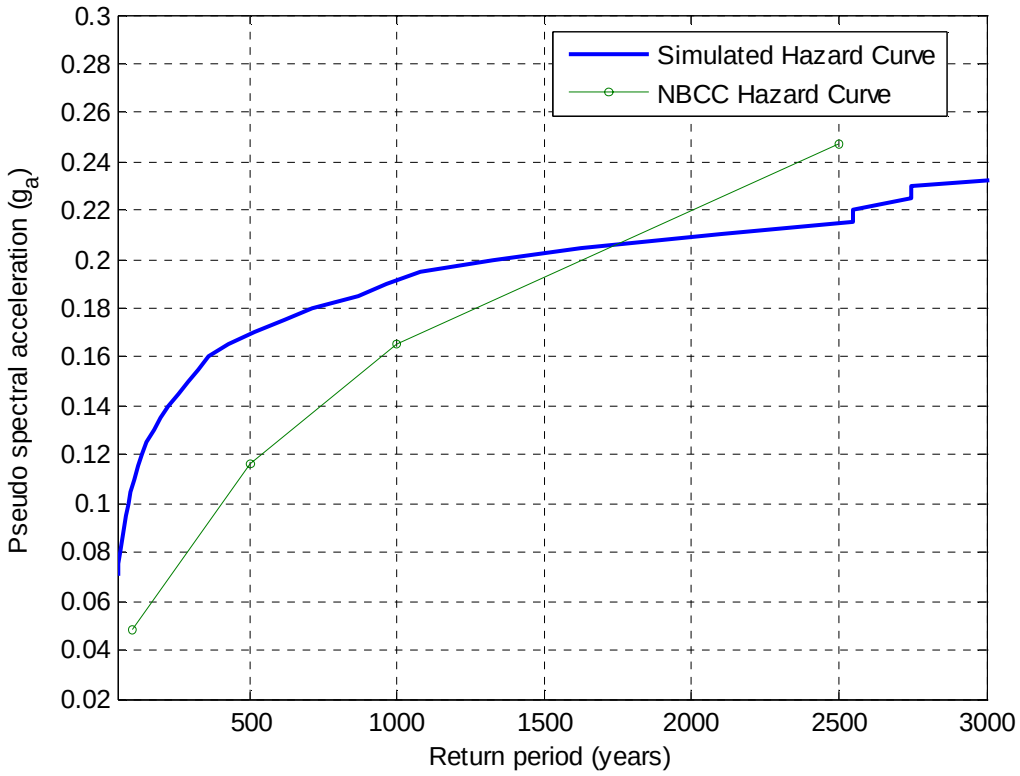

Figure 6.7: Comparison of hazard curves for spectral frequency of 1Hz

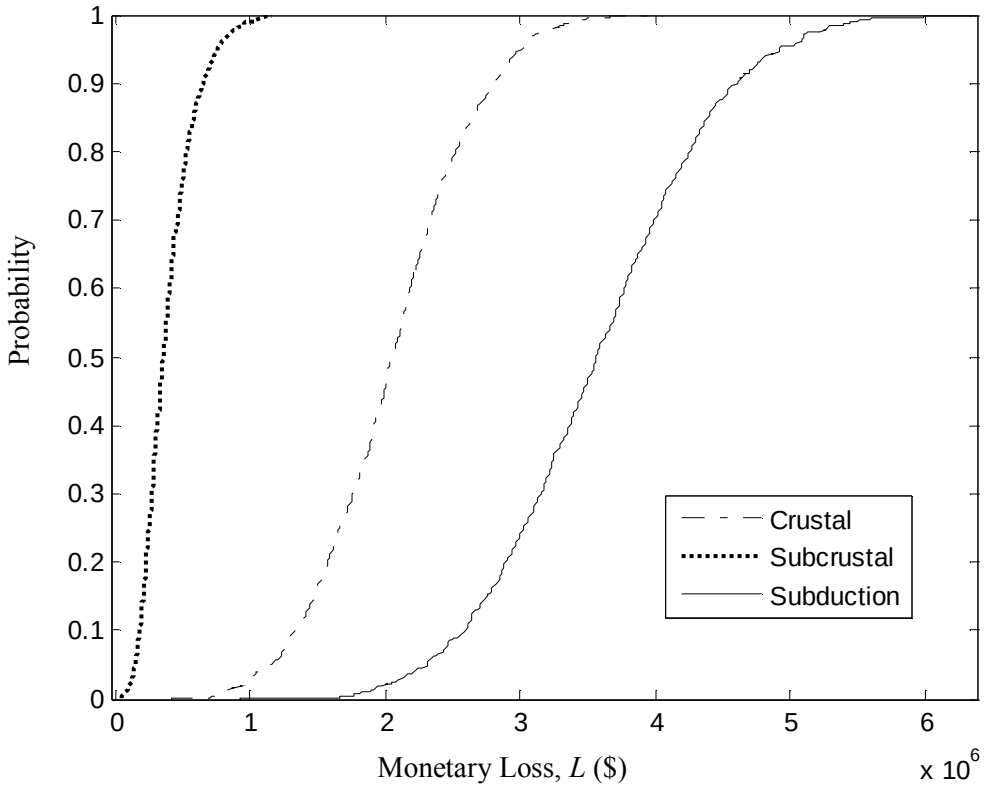

Figure 6.8: The probability curves of monetary loss conditioned on the occurrence of Crustal, Subcrustal and Subduction earthquakes

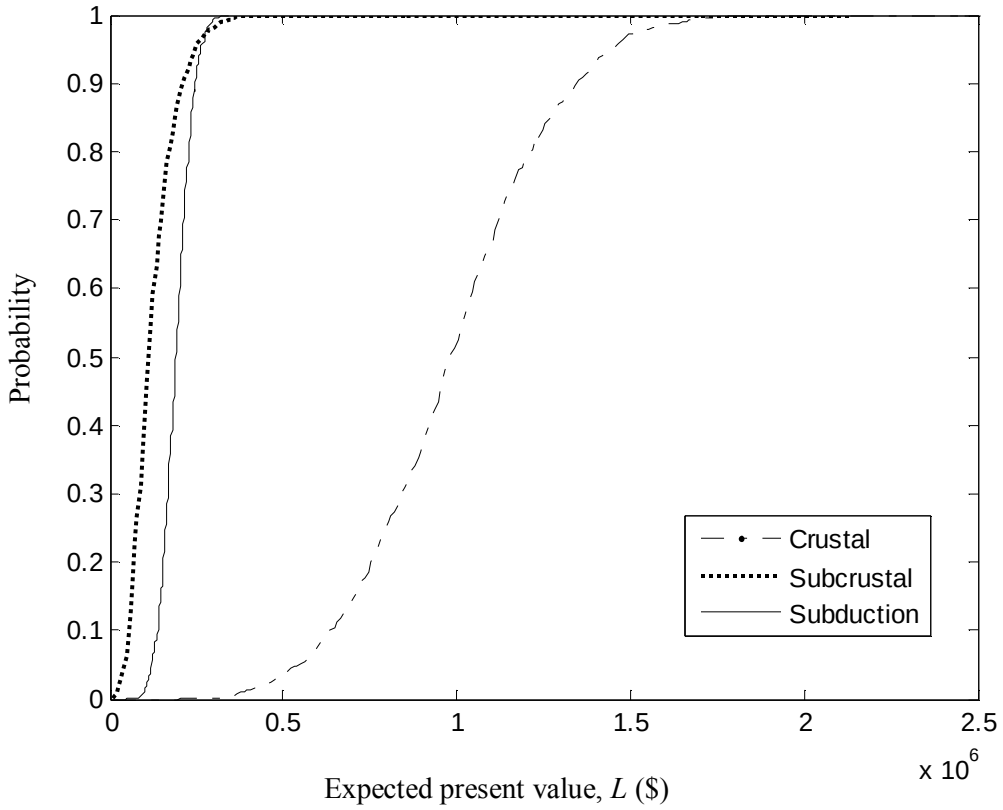

Figure 6.9: The probability curves for discounted monetary loss, *L* conditioned on the occurrence of Crustal, Subcrustal and Subduction earthquakes.

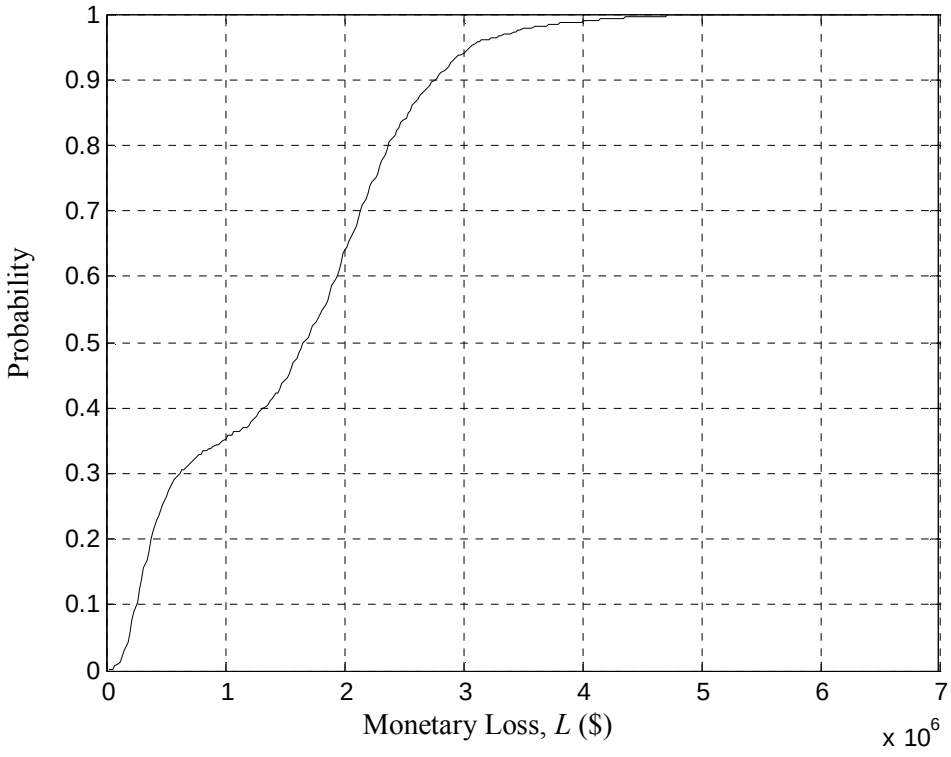

Figure 6.10: The combined total probability curve of monetary loss conditioned on the occurrence of an earthquake

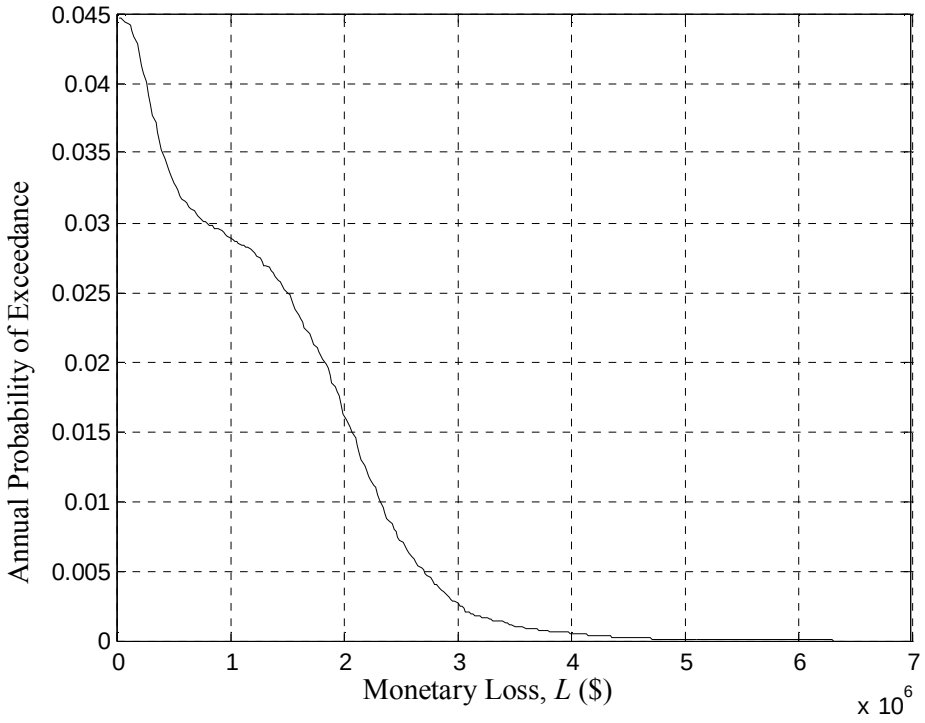

Figure 6.11: Annual probability of exceedance of monetary loss

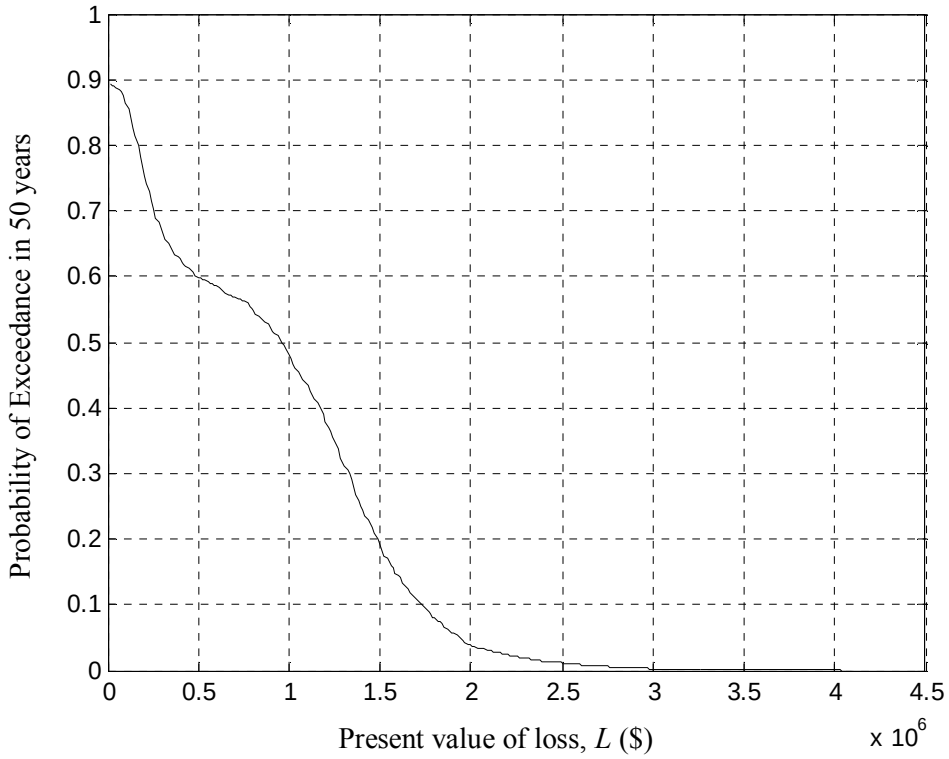

Figure 6.12: Probability of exceedance in 50 years of discounted loss

REFERENCES

Adams, J. (1990) "Paleoseismicity of the Cascadia subduction zone – evidence from the turbidites off the Oregon-Washington margin," *Tectonics,* 9(4), 569-583

Adams, J., and Atkinson, G.M. (2003), "Development of seismic hazard maps for the proposed 2005 edition of National Building Code of Canada," *Canadian Journal of Civil Engineering*, 30(2), 255-271

Adams, J. and Halchuk, S. (2003), *Fourth generation seismic hazard maps of Canada: Values for over 650 Canadian localities intended for the 2005 National Building Code of Canada*. Open File 4459, Geological Survey of Canada.

Amin, M. and Ang, A. H. S. (1968), "Nonstationary stochastic model of earthquake motions," *Journal of Engineering Mechanics Division,* 94 (EM2), 559-583

Ang, A.H.S. and Tang, W.H. (1975), *Probability concepts in engineering planning and design: Basic principles*.Wiley

Atkinson, G.M. (1995), "Attenuation and source parameters of earthquakes in the Cascadia region," *Bulletin of the Seismological Society of America,* 85 (5), 1327-1342.

Atkinson, G.M. (1996), "The high-frequency shape of the source spectrum for earthquakes in eastern and western Canada," *Bulletin of the Seismological Society of America,* 86 (1), 106-112

Atkinson, G.M. (2005), "Ground motions for earthquakes in South-western British Columbia and North-western Washington: Crustal, In-slab, and Offshore events," *Bulletin of the Seismological Society of America,* 95 (3), 1027-1044.

Atkinson, G.M. and Boore, D.M. (1997), "Stochastic point-source modeling of ground motions in the Cascadia region," *Seismological Research Letters*, 68 (1), 74-85

Atkinson, G.M. and Boore, D.M. (2003), "Empirical ground-motion relations for subduction-zone earthquakes and their application to Cascadia and other regions," *Bulletin of the Seismological Society of America,* 93 (4), 1703-1729.

Atkinson, G.M. and Silva, W. (2000), "Stochastic modelling of California ground motions," *Bulletin of the Seismological Society of America,* 90 (2), 255-274.

Beresnev, I.A. and Atkinson, G.M. (1997), "Modeling finite-fault radiation from the omega-n spectrum," *Bulletin of the Seismological Society of America,* 87 (1), 67-84

Beresnev, I. A. and Atkinson, G.M. (2002), "Source parameters of earthquakes in eastern and western North America based on finite-fault modeling," *Bulletin of the Seismological Society of America,* 92 (2), 695-710

Boore, D.M. (1983), "Stochastic simulation of high-frequency ground motions based on seismological models of the radiated spectra," *Bulletin of the Seismological Society of America,* 73 (6), 1865-1894

Boore, D.M. (2003), "Simulation of ground motion using stochastic method," *Pure and Applied Geophysics,* 160, 635-676

Conte, J.P. and Peng, B.-F. (1997), "Fully nonstationary analytical earthquake ground motion model," *Journal of Engineering Mechanics,* 123 (1), 15-24

Cornell, C.A. and Krawinkler, H. (2000), *Progress and challenges in seismic performance assessment*, PEER Center News, http://peer.berkeley.edu/news/2000spring.

Der Kiureghian, A. and Ang, H.-S. (1977) "A fault-rupture model for seismic risk analysis," *Bulletin of the Seismological Society of America,* 67 (4), 1173-1194

Der Kiureghian, A. and Crempien, J. (1989) "Evolutionary model for earthquake ground motion," *Structural Safety,* 6 (2-4), 235-246

Der Kiureghian, A. and Taylor, R.L. (1983), "Numerical methods in structural reliability," *Proceedings of the Fourth International Conference on Applications of Statistics and Probability in Civil Engineering, ICASP4*, *Florence, Italy June 13–17, 1983*. Pitagora Editrice, Bologna

Ditlevsen, O. and Madsen, H.O. (1996), *Structural reliability methods,* New York: J.Wiley and Sons.

Dyck, C. and Ventura, C.E. (1998), *Ambient vibration measurements of Heritage Court Tower*. EQ98-007, University of British Columbia Earthquake Engineering Research

Fan, F.G. and Ahmadi, G. (1990), "Nonstationary Kanai-Tajimi models for El Centro 1940 and Mexico City 1985 earthquakes," *Probabilistic Engineering Mechanics* 5 (4), 171-181

Ferritto, J.M. (1984), "Economics for seismic design for new buildings," *Journal of Structural Engineering,* 110(12), 2925-2938

Foschi, R.O. and Lo, R.C. (1988), "EQPROB: A PC-based, graphics-assisted program for seismic risk analysis," *Proceedings of 3rd International Conference on Computing in Civil Engineering, Vancouver, Canada, August 10-12 1988.* Canadian Society of Civil Engineering

Hanks, T.C. and Kanamori, H. (1979), "A moment magnitude scale," *Journal of Geophysical Research,* 84 (5), 2348-2350

Haukaas, T. (2007), "Unified reliability and design optimization in earthquake engineering," *Proceedings of the Risk Acceptance and Risk Communication Workshop, Stanford, California, March 26-27.*

Hyndman, R.D., Rogers, G.C., Dragert, H., Wang, K., Clague, J.J., Adams, J. and Bobrowsky, P.T. (1996), "Giant earthquakes beneath Canada's west coast," *Geoscience Canada,* 23 (2), 63-72

Hyndman, R.D. and Wang, K. (1995), "The rupture zone of Cascadia great earthquakes from current deformation and thermal regime," *Journal of Geophysical Research,* 100 (11), 22133-22154

Iyengar, R.N. and Iyengar, K.T.S.R. (1969) "A nonstationary random process model for earthquake accelerograms," *Bulletin of the Seismological Society of America,* 59 (3), 1163-1188

Koduru, S.D. and Haukaas, T. (2007), "Seismic reliability analysis with probabilistic models for ground motion and structure," *Proceedings of COMPDYN '07: ECCOMAS Thematic Conference on Computational Methods in Structural Dynamics and Earthquake Engineering, Rethymno, Crete, Greece, June 13–16 2007.*

Kratzig, W.B. Meyer, I.F. and Meskouris, K. (1989), "Damage evolution in reinforced concrete members under cyclic loading," In A.H-S. Ang, M.Shizonuka and G.I. Schuller (eds), *Structural Safety and Reliability: Proceedings of 5th International Conference on Structructural Safety and Reliability (ICOSSAR '89), San Francisco, 7-11 Aug 1989*. New York: American Society of Civil Engineers.

Li, C.C. and Der Kiureghian, A. (1995), "Mean out crossing rate of nonlinear response to stochastic input," *Proceedings of 7th International Conference on Applications of Statistics and Probability in Civil Engineering, Paris, France, July 10-13, 1995.* A.A.Balkema.

Lin, Y.K. and Yong, Y. (1987), "Evolutionary Kanai-Tajimi earthquake models," *Journal of Engineering Mechanics,* 113(8), 1119-1137

McKenna, F., Fenves, G.L., and Scott, M.H. (2004), *OpenSees*: *Open system for earthquake engineering simulation*. Pacific Earthquake Engineering Research Center, University of California, Berkeley, CA

Mehanny, S.S. and Deierlein, G.G. (2000), *Modeling of assessment of seismic performance of composite frames with reinforced concrete columns and steel beams*. Report No. 135, The John A. Blume Earthquake Engineering Center, Department of Civil and Environmental Engineering, Stanford University.

Moehle, J., Stojadinovic, B., Der Kiureghian, A. and Yang, T.Y. (2005), *An application of PEER performance-based earthquake engineering methodology*. Research Digest No. 2005-1, Pacific Earthquake Engineering Research Center, University of California, Berkeley, California

Motazedian, D. and Atkinson, G. M. (2005), "Stochastic finite-fault modeling based on a dynamic corner frequency," *Bulletin of the Seismological Society of America,* 95, 995-1010.

NBCC, (2005) *National Building Code of Canada*. Ottawa: National Research Council of Canada.

Park, Y.J. Ang, A.H-S. and Wen, Y.K. (1985), "Seismic damage analysis of reinforced concrete buildings," *Journal of Structural Engineering,* 111(4), 740-757

Sabetta, F. and Pugliese, A. (1996), "Estimation of response spectra and simulation of nonstationary earthquake ground motions," *Bulletin of the Seismological Society of America,* 86 (2), 337-352

Saragoni, G.R. and Hart, G.C. (1974), "Simulation of artificial earthquakes," *International Journal of Earthquake Engineering and Structural Dynamics,* 2 (3), 249-267

Sexsmith, R.G. (1983), "Bridge risk assessment and protective design for ship collision," Introductory Report. *International Association for Bridge and Structural Engineering (IABSE). Colloquium on Ship Collision with Bridges and Offshore Structures*, Copenhagen

Thrainsson, H. and Kiremidjian, A.S. (2002) "Simulation of digital earthquake accelerograms using the inverse discrete Fourier transform," *Earthquake Engineering and Structural Dynamics* 31, 2023-2048.

Turner, R.J.W, Clague, J.J., Groulx B.J., and Journeay J.M. (1997), *GeoMap Vancouver: Geological Map of the Vancouver Metropolitan Area.* Open File 3511, Geological Survey of Canada.

Ventura, C.E., Onur, T. and Hao, K.X.-S. (2004), "Site period estimations in the Fraser river delta using micrometer measurements – experimental and analytical studies," *Proceedings of 13th World Conference on Earthquake Engineering, Vancouver, Canada, August 1-6, 2004,* Canadian Association for Earthquake Engineering

Yang, T.Y. (2006), *Performance evaluation of innovative steel braced frames,* Ph.D. Dissertation, University of California, Berkeley, California

Yeh, C.H. and Wen, Y.K. (1990), "Modeling of nonstationary ground motion and analysis of inelastic structural response," *Structural Safety* 8 (1-4), 281-298

Chapter 7. CONCLUSIONS AND FUTURE WORK

7.1. SUMMARY OF RESEARCH CONTRIBUTIONS

In the present study, the primary objective has been to promote the utilization of structural reliability methods, such as FORM in the context of performance-based earthquake engineering. This objective is achieved by exploring two main areas; one focuses on the study of uncertainties and FORM in the context of finite element reliability analysis, the other involves performing the reliability analysis with performance limit-states, such as collapse and monetary loss, in reinforced concrete structures.

In the topic of uncertainty, at first, the identification, quantification, and separation of aleatory and epistemic uncertainties are presented. The reliability index, an outcome of FORM analysis, is considered to represent aleatory uncertainty. The presence of epistemic uncertainty introduces uncertainty in the reliability index itself. Two different methods; the Bayesian probabilistic approach and the fuzzy randomness approach, are presented to separate the aleatory and epistemic uncertainties. In the first approach, a probability distribution of the reliability index is obtained, while the second approach provides the reliability index as a fuzzy number. Software tools for the application of both approaches are developed by extending an open-source C++ software framework, OpenSees (McKenna *et al*. 2004).

The dispersion of the reliability index indicates the amount of epistemic uncertainty present. Confidence bounds on the reliability index and importance ranking of the various sources contributing to the epistemic uncertainty are additional outcomes of the methods implemented. As the epistemic uncertainty is reducible, these results are valuable to reduce the overall uncertainty in the estimation of the reliability and safety of the structure.

In the study of the feasibility of FORM in finite element reliability analysis, several case studies are performed with static and dynamic analysis. For the case of static analysis, FORM is found to provide accurate estimates of the probability with reasonable computational effort. However, several potential challenges exist for successful application of FORM, which are summarized under the categories of 1)

gradient discontinuities, 2) numerical noise, and 3) nonlinearity of the limit-state surface. Furthermore, solution strategies are presented to overcome the difficulties. A flow chart is provided to assess the applicability of FORM for a finite element reliability problem at hand.

In the case of dynamic analysis, the feasibility of FORM with cumulative response parameters is investigated. Cumulative response parameters are demonstrated to be particularly effective for the performance assessment of the structures. The study indicates that FORM is not amenable for the finite element reliability analysis with cumulative response parameters. This is due to the fact that the geometric shape of limit-state surface in the standard normal space violates the essential criterion for the application of FORM. From the study of the characteristics of the limit-state surface, strategies for estimation of probabilities are presented. Solution strategies with the approximation of the hyper-spheriod, and bounding by symmetric hyper-planes, provide bounds on the probability estimates. In conclusion, FORM is applicable to reliability analyses with static loading, while being inadequate for the application in reliability analyses with dynamic loading.

The contributions from the work in the area of uncertainties and feasibility of FORM are:

1. A framework to quantify epistemic uncertainty is presented. The uncertainty in the reliability index is a measure of confidence in the reliability result. It allows for distinction between reducible (aleatory) and irreducible (epistemic) uncertainties and provides a rational basis for collecting data to reduce the epistemic uncertainty.
2. Software tools are developed to perform epistemic reliability analysis, which provides a probability distribution of the reliability index.
3. FORM is found to be feasible for application in finite element reliability analysis with static loading. The limit-state surface in the static case exhibits moderate nonlinearity and is amenable to FORM to obtain reasonable estimates of the probability.

4. The hyper-plane approximation of the limit-state surface, which is a fundamental assumption in FORM, is found to be inadequate for finite element reliability analysis with dynamic loading and cumulative response measures. The study of the limit-state surface with cumulative responses and random dynamic loading indicates that it has a closed and symmetric geometric shape. This novel finding motivates the development of computationally efficient reliability methods that estimate the probability content of such geometric shapes in the multivariate standard normal space.

Following the above conclusions, FORM is applied in the context of nonlinear static analysis to assess the collapse probability of a reinforced concrete frame. A novelty in this application is the utilization of global response, as opposed to component response, for the seismic reliability assessment. Furthermore, probabilistic capacity and post-failure behaviour models, previously developed based on experimental data, are employed to include shear and axial failure of individual structural members before the final limit-state. The epistemic uncertainty present in the estimation of model parameters is included in the reliability analysis. The difficulties in the quantification of structural collapse and the associated challenges in performing a finite element reliability analysis with FORM are presented. Finally, a probability curve for the lateral displacement at global structural collapse, which includes the strength degradation of individual structural components, is obtained. Furthermore, importance measures are employed to identify the most influential random variables. The study indicates that the parameters of the probabilistic capacity models have the highest influence on the estimated probabilities. Therefore, in order to improve the confidence in the collapse predictions, it is most beneficial to reduce the epistemic uncertainty in the model parameters by gathering more data or improving the model form.

The final application of performance-based earthquake engineering is to assess the monetary loss due to impending earthquakes for an existing high-rise building located in Vancouver, Canada. The unified reliability analysis methodology is applied for this reinforced concrete building, which has a shear-wall core as the lateral load resisting system. The earthquake excitations are modelled in detail with a stochastic ground motion model. A novel approach is presented for the calibration of stochastic model

parameters to the seismological and geological characteristics of Vancouver region. Three different sets of model parameters are assessed based on the Crustal, Subcrustal and Subduction earthquake sources near Vancouver. Thus, ground motion excitations specific to the location of the buildings are modelled. A comprehensive three-dimensional finite element model of the buildings is created. Furthermore, damage and cost models are considered separately for the structural and non-structural components. As concluded above, FORM is not amenable for the reliability analysis with dynamic excitation. For convenience, the mean-centered Monte Carlo simulation method is applied to obtain probability curves for monetary loss.

The contributions from the work in the applications of performance-based earthquake engineering are:

5. Global structural response measures to detect structural collapse are developed and utilized in the finite element reliability analysis.
6. A set of parameters are estimated to simulate ground motions corresponding to Crustal, Subcrustal and Subduction earthquakes in Vancouver, Canada.
7. A procedure is developed to estimate the ground motion model parameters from recorded ground motions. With this approach, stochastic ground motion model parameters can be estimated if a ground motion record is available for any location of interest.
8. The unified reliability analysis methodology is successfully demonstrated by application to an existing real-world high-rise building.

7.2. FUTURE RESEARCH DIRECTIONS

Several topics that require further research are identified in the course of this study. These are listed as the following.

1. The current decision-making models include single probability estimates of discrete events. These probability estimates have lumped aleatory and epistemic uncertainties. Therefore, there is a need for the development of decision-making models that treat the epistemic and aleatory uncertainties separately.

2. The feasibility of the application of FORM is severely hampered when the finite element analysis fails to converge. A modification of the search algorithms, which find the design point, to accommodate non-convergence of finite element analysis may increase the ease of application of FORM.

3. The geometric shape of the limit-state surface when cumulative response parameters are included indicates that a second-order reliability method (SORM) with suitable approximation by quadratic shapes may produce accurate probability estimates.

4. Efficient methods for computation of gradients and curvatures of the limit-state functions are required to reduce the computational effort and promote the utilization of SORM in the reliability analysis with cumulative response parameters.

5. Research into the development of generalized measures for the quantification of structural collapse is required. This facilitates the automation of structural collapse recognition by analysis software and paves the way for the utilization of sophisticated reliability methods for structural performance assessments.

6. Parameter estimation methods to achieve spectral nonstationarity in stochastic ground motion models are scarce. Further research effort is required to investigate the importance of spectral nonstationarity on nonlinear structural response.

7. The stochastic ground motion models are limited to the simulation of uni-directional ground motion excitations (Boore 2003). Further studies are required to establish correlation among the ground motions in two horizontal directions.

8. Further investigations are required to develop computationally efficient models to account for axial, shear and moment interaction, and damage estimation in reinforced concrete shear walls. Experimental studies to calibrate the damage models are required for rigorous performance assessments.

9. Models to estimate the repair costs and monetary loss due to downtime need improvement for accurate estimation of economic losses. There is a requirement for explicit models to relate monetary losses and repair costs to the damage states of structural and non-structural components.

10. Efficient software tools facilitate the promotion of reliability analysis in performance-based earthquake engineering. Availability of software tools, which communicate between popular structural analysis programs and reliability methods, and provide graphical user interface, encourages the practicing engineers to employ reliability methods.

REFERENCES

Boore, D.M. (2003), "Simulation of ground motion using stochastic method," *Pure and Applied Geophysics,* 160, 635-676

McKenna, F., Fenves, G.L., and Scott, M.H. (2004), *OpenSees*: *Open system for earthquake engineering simulation*. Pacific Earthquake Engineering Research Center, University of California, Berkeley, CA